Harmonic Domain Modelling of Direct Connected Generator and HVDC Convertor units

Dinh Nhut-Quang, BE (Hons.)

A thesis presented for the degree of
Doctor of Philosophy
in
Electrical and Electronic Engineering
at the
University of Canterbury,
Christchurch, New Zealand.

January 1998

ABSTRACT

This thesis describes a new method of analysing the harmonic content of direct connected generator-HVdc convertor units. Existing analysis techniques are reviewed, and their strengths and weaknesses are discussed. A set of simultaneous equations that fully describes the harmonic interaction among the generators, convertors and the dc system is derived. The simultaneous equations are solved using Newton's method. By exploiting the sparse nature of the Jacobian matrix of partial derivatives, the solution is obtained quickly. The solution of a test system is verified by means of dynamic simulations. The developed unified solution is a significant improvement on existing harmonic analysis.

A harmonic model of the salient-pole generator is developed and validated against time domain simulations and harmonic measurement results obtained from the Benmore convertor station when being operated as a group connected unit. The relationship between the generator terminal voltages and currents in the presence of saliency can be represented by analytical expressions in sequence components, derived from normal machine parameters. The effect of generator saturation on the harmonic content is not significant. The effect of rotor angle on the commutation process in the presence of saliency is significant in direct connected units.

By choosing the generator terminal voltage as the firing angle reference, existing firing control for conventional HVdc schemes can be used for direct connected units with practically no modification. Provided that the nominal firing angles are kept within the restriction limits, imposed by the overlap angle, generator terminal power factor, equivalent continuous negative-sequence harmonic loading and the number of generators, practically no extra capacity for harmonic current loading is required in direct connected units. The generator harmonic ratings can be taken at the nominal speed and rated power output. Conventional tuned dc filters are ineffective in adjustable speed operation.

Finally, detailed three-phase harmonic information of the Benmore convertor station when being operated in the group connected mode is collected and discussed. The test results are used for validating the developed models, and they also provide valuable evidence of the feasibility of direct connected units.

ACKNOWLEDGEMENTS

Completion of this thesis marks the end of an invaluable, positive learning experience. The most sincere thanks must go to Professor Jos Arrillaga, whose knowledge, supervising experience and enthusiasm is invaluable. I am extremely grateful for his time, numerous advice and inspiration.

Many thanks are also due to Drs Alan Wood, Bruce Smith, Chris Arnold, Neville Watson, Dave Watson, Pat Bodger, and Mr Mike Dewe for countless discussions and advice; Ken Smart for being extra helpful all the time. I would like to thank the computing staffs who have courageously kept the computer systems up and running; my postgraduate colleages, particularly Drs Roger Brough, Shiun Chen, Wade Enright, Maria-Luiza Lisboa, Stu MacDonald, Du Zhen-Ping; Graeme Bathurst, Dave Hume, Thomas Keppler, Simon Todd and Andrew Ward for the many lively discussions and functions. Special thanks to my many other friends who have been providing valuable friendship and much needed distractions, especially Parapol Anusarnsunthorn, Michael Burns, Dr Felix Hartanto, Dr David Hawkins, Dr Matt Hebley, Jos Li, Paul Johnstone, Nu, Elwyn Smith, Sugar, and Tran Minh-Tri. Many thanks to Nu for proof-reading parts of this thesis.

The financial support from the University of Canterbury through the Doctoral scholarship; from the University of Canterbury Power Systems Research group; from Trans Power New Zealand, ECNZ, and the CHART development group for the Benmore convertor harmonic measurements are gratefully acknowledged.

I wish to express my deepest gratitude to my Mom, Dad, my brother Tan and the extended family in VietNam, whose invaluable life long encouragement and support have helped lighten the long term effort. Thank you so much.

And finally, I wish to extend the warmest thanks and gratitute to my sponsor families, especially Mr & Mrs Leo and Joan Clark; Michael, Susan and Bridget Coulter; Charlotte and Andrew Robb; Paul, Jenny and Kelly Clark; Mr & Mrs Macann, whose generosity and unassuming support have made this work possible.

CONTENTS

ABSTRACT iii

ACKNOWLEDGEMENTS v

GLOSSARY xix

CHAPTER 1 INTRODUCTION 1
- 1.1 HVdc Transmission 1
- 1.2 Main Objectives 2
- 1.3 Thesis Outline 3

CHAPTER 2 DIRECT CONNECTION SCHEMES AND HARMONIC MODELLING REVIEW 5
- 2.1 Introduction 5
- 2.2 Unit Connection Concept 5
- 2.3 Main Applications 8
- 2.4 A Review of Harmonic Analysis methods 8
  - 2.4.1 Time Domain Simulations 9
  - 2.4.2 Harmonic Domain Modelling 10
    - 2.4.2.1 Simplified Convertor Formulation 10
    - 2.4.2.2 Iterative Harmonic Analysis 11
    - 2.4.2.3 Method of Norton Equivalents 14
    - 2.4.2.4 Unified Solution using Newton's Method 14
- 2.5 Conclusions 15

CHAPTER 3 GENERATOR MODELLING IN THE HARMONIC DOMAIN 17
- 3.1 Introduction 17
- 3.2 The Process of Frequency Conversion 18
- 3.3 Generator Harmonic Impedances in Sequence Components 19
  - 3.3.1 Frame of Reference and Rotor Angle 19
  - 3.3.2 Negative-Sequence Harmonic Impedances 20
  - 3.3.3 Positive-Sequence Harmonic Impedances 21
  - 3.3.4 Zero-Sequence Harmonic Impedances 23
  - 3.3.5 Skin Effect 23
- 3.4 Synchronous Generator Harmonic Equivalents 24
- 3.5 Saturation Effects on Steady State Operation 26

3.5.1 Saturation Effects on Generator Harmonic Impedances 27
3.5.2 Generator Saturation Harmonics 30
3.6 Model Validation 32
3.7 Levels of Harmonic Impedances 33
3.8 Conclusions 39

CHAPTER 4 CONVERTOR ANALYSIS IN THE HARMONIC DOMAIN 41
4.1 Introduction 41
4.2 Commutation Analysis for a Unified Iterative Solution 41
4.2.1 Star Connection Analysis 42
4.2.2 Delta Connection Analysis 43
4.3 Convertor Control and Firing Process 45
4.3.1 Firing Process 45
4.3.2 Constant Current Control 45
4.3.3 Constant Power Control 46
4.4 Direct Voltage 47
4.4.1 Star Connection Voltage Samples 47
4.4.2 Delta Connection Voltage Samples 48
4.4.3 DC Voltage Construction by Convolution 50
4.5 Secondary Phase current 52
4.6 Transformer Modelling 53
4.7 Summary 57

CHAPTER 5 A HARMONIC DOMAIN UNIT CONNECTION MODEL 59
5.1 Introduction 59
5.2 System Variables 60
5.3 Generator-Convertor Interaction 62
5.3.1 Fundamental Frequency 62
5.3.2 Harmonic Frequencies 62
5.4 Convertor Interaction with dc System 63
5.5 Reactive Power and Voltage Control by Generator Excitation 63
5.5.1 Firing Angle Referenced to the Generator Terminal Voltage 63
5.5.2 Firing Angle Referenced to the Generator Internal Voltage E'' 64
5.6 Functional Description of a Unit Connection 65
5.6.1 Phase Components Formulation. 65
5.6.2 Sequence Components Formulation. 66
5.7 Newton's Solution 68
5.7.1 Jacobian of Partial Derivatives 69
5.7.2 Initialization 72
5.8 Model Validation and Performance 74

5.8.1 Validation 74
5.8.2 Convergence Properties 77
5.9 Conclusions 80

CHAPTER 6 HARMONIC BEHAVIOUR OF DIRECT CONNECTED UNITS 83
6.1 Introduction 83
6.2 Firing Angle References for Direct Connected Units 84
6.3 Overlap Angle Constraint 86
6.4 Generator Terminal Power Factor 86
6.5 Effects of Salient-Pole Generators 89
6.5.1 Effect of Generator Saliency on Harmonic Levels 89
6.5.2 Effect of Saliency on Generator Terminal Power Factor 92
6.5.3 Effect of Rotor Angle 95
6.5.4 Effect of Generator Saturation 95
6.6 Group Connection Implementation 97
6.6.1 Commutation Angle and Generator Power Factor in Group Connections 99
6.6.2 Harmonic Content in Group Connections 99
6.7 Effects of Adjustable Speed Operation 105
6.8 Effects of dc Side Resonances 106
6.8.1 On dc Side Harmonics 106
6.8.2 On ac Side Harmonics 113
6.9 Conclusions 114

CHAPTER 7 HARMONIC EVALUATION OF BENMORE CONVERTOR STATION WHEN OPERATED AS A DIRECT CONNECTED UNIT 115
7.1 Introduction 115
7.2 Testing Procedure 116
7.3 Fundamental Frequency Variation 117
7.4 Three-Phase Harmonic Information 117
7.5 Harmonic Variation with dc Current Order 121
7.5.1 DC signals 121
7.5.2 AC harmonics 123
7.6 Generator Harmonic Ratings 123
7.7 Conclusions 131

CHAPTER 8 CONCLUSIONS AND FUTURE WORK 133
8.1 Conclusions 133
8.2 Suggestions for future work 135
8.2.1 Transformer Saturation Modelling 135
8.2.2 Subsynchronous Resonances and Interharmonic Studies 136

APPENDIX A TEST SYSTEMS DATA 137
A.1 Hwang's Generator Parameters 137
A.2 Benmore's Generators and transformers 137

APPENDIX B SALIENT-POLE GENERATOR HARMONIC IMPEDANCE CALCULATION FROM MEASURED HARMONIC VOLTAGES AND CURRENTS 141

APPENDIX C CUBIC SPLINE INTERPOLATION 143

APPENDIX D HARMONIC PHASOR REPRESENTATION 145
D.1 Complex Fourier Series 145
D.2 Positive Frequency Harmonic Phasors 146
D.3 Convolution of Harmonic Phasors 147

APPENDIX E SIMPLIFIED CONVERTOR COMMUTATION ANALYSIS AND HARMONIC CALCULATION 149

APPENDIX F JACOBIAN OF PARTIAL DERIVATIVES 151
F.1 Voltage Control Equation Partial Derivatives 153
F.2 Terminal Voltage Partial Derivatives 153
F.2.1 With Respect to ac Voltage Variation 154
F.2.2 With Respect to dc Ripple Current Variation 157
F.2.3 With Respect to end of Commutation Variation 159
F.2.4 With Respect to Firing Instant Variation 161
F.3 Direct Current partial derivatives 162
F.3.1 With Respect to ac Voltage Variation 162
F.3.2 With Respect to dc Ripple Current Variation 164
F.3.3 With Respect to end of Commutation Variation 166
F.3.4 With Respect to Firing Instant Variation 167
F.4 End of Commutation mismatch Equation partial derivatives 168
F.4.1 With Respect to ac Voltage Variation 168
F.4.2 With Respect to dc Ripple Current Variation 169
F.4.3 With Respect to end of Commutation Variation 170
F.4.4 With Respect to Firing Instant Variation 170
F.5 Firing Instant mismatch Equation partial derivatives 171
F.6 Average delay angle partial derivatives 172
F.6.1 With Respect to ac Voltage Variation 172
F.6.2 With Respect to dc Ripple Current Variation 173
F.6.3 With Respect to end of Commutation Variation 173
F.6.4 With Respect to Firing Instant Variation 174

APPENDIX G PUBLISHED PAPERS 175

REFERENCES 177

LIST OF FIGURES

2.1 Conventional HVdc sending end arrangement. 6

2.2 Unit Connection configuration. 6

2.3 An example of a Group Connection arrangement. 7

2.4 Effects of arbitrary snubber capacitances on the harmonic levels in PSCAD2-EMTDC simulations. 10

2.5 Matched reactance pair method for six-pulse convertors. 12

2.6 Matched reactance pair method for twelve-pulse convertors. 13

3.1 Response of a salient pole generator to the presence of a harmonic current. 18

3.2 Phasor diagrams of an unsaturated salient-pole synchronous generator operating at a lagging power factor. 19

3.3 Generator Thevenin and Norton harmonic equivalents. 24

3.4 Structure of the generator impedance or admittance matrix in phase coordinate and sequence components. 25

3.5 Modified equivalent circuit. 26

3.6 Graphical construction for finding the components of armature voltage due to saturation E_s corresponding to Potier voltage E_p. 28

3.7 Determination of rotor angle under saturation for salient-pole synchronous generators operating at a lagging power factor. 29

3.8 Test system for model validation. 33

3.9 Model validation by comparison of time and harmonic domain solutions for harmonic current injections. 34

3.10 Generator harmonic impedances obtained from the measurement and calculation. 35

3.11 Generator harmonic impedances for a particular loading. 36

3.12 Magnitude and phase angle of cross coupling terms for various loadings. 37

3.13 Generator-transformer-convertor unit. 37

3.14 Variation of the 7th harmonic voltage in relation to the rotor angle and firing delay angle. 38

4.1 Circuit for star-g/star commutation analysis. 43
4.2 Circuit for star-g/delta commutation analysis. 44
4.3 Constant current controller. 45
4.4 Circuit for a conduction period with a delta connected source. 49
4.5 Sampling functions used in convolution. 50
4.6 Equivalent circuit for star-g/star transformer. 54
4.7 Equivalent circuit for star-g/delta transformer. 55

5.1 Twelve-pulse Unit Connection. 60
5.2 Dependency among system variables. 61
5.3 Phasor diagram of a salient-pole generator in direct connected units. 64
5.4 Sparsity structure of the Jacobian in sequence components for 13 harmonics. 71
5.5 Flow diagram for the unified harmonic solution. 73
5.6 Model intervalidation by comparison of time domain and unified harmonic solutions for generator voltage and current waveforms. 76
5.7 Model intervalidation by comparison of time domain and unified harmonic solutions for generator harmonic voltages and currents. 77
5.8 DC voltage waveforms reconstructed from 50 harmonics. 78

6.1 Phasor diagram of a non-salient generator in direct connected units. 84
6.2 Relationship between firing angles referenced to the generator fundamental terminal voltage and internal voltage $E"$. 85
6.3 Comparison of commutation periods for direct connected units and perfect ac filtering schemes. 86
6.4 Comparison of (a) internal displacement factors $\cos(\phi_e)$, and (b) generator terminal power factors $\cos\phi$ for direct connected units and perfect ac filtering schemes. 88
6.5 Phasor diagrams of saliency effect on harmonic voltages. 90
6.6 (a) Maximum and minimum limits for the 11th current harmonics of a salient-pole generator in direct connected units; (b) Voltage harmonics corresponded to the current limits. 93
6.7 Commutation angles limits for salient-pole generators in direct connected units. 94
6.8 Generator terminal power factor ($\cos\phi$) for salient-pole generators. 94
6.9 Effect of rotor angle on the commutation angle (a), and on 11th harmonic current level (b) in the presence of generator saliency. 96

6.10 Simplification of a Group Connection to the basic Unit Connection for harmonic analysis. 97

6.11 (a) Commutation angle and (b) generator terminal power factor in a Group Connection being operated with various number of generators. 100

6.12 Generator harmonic currents in a Group Connection being operated with various number of generators. 101

6.13 Generator harmonic voltages in a Group Connection being operated with various number of generators. 102

6.14 Generator equivalent negative-sequence currents for a Group Connection. 103

6.15 Relationship between firing angles referenced to E'' and to the generator terminal voltage V for a Group Connection. 103

6.16 Typical hydraulic turbine power-speed characteristic. 105

6.17 (a) Commutation angle and (b) generator terminal power factor variation with speed for various firing angle. 107

6.18 Harmonic current variation with speed for various firing angle. 108

6.19 Harmonic voltage variation with speed for various firing angle. 109

6.20 A typical dc side configuration with a dc filter, smoothing inductor and a simplified representation of a dc line. 110

6.21 (a) Harmonic impedance of the dc filter. (b) Harmonic impedances of a dc system consisting of a smoothing inductor (0.8 H), dc filter and a line inductance of 0.2 H. 111

6.22 Harmonic voltages at the dc filter point for adjustable speed operation. 112

6.23 Generator current harmonics at different generator speed in the presence of dc side resonances. 113

7.1 Benmore group connection and CHART measurement points. 116

7.2 Fundamental frequency variation during the test measurement. 118

7.3 Three-phase generator bus voltages and their harmonics in sequence components for a dc current of 1016 amps. 119

7.4 Three-phase generator currents and their harmonics in sequence components for a dc current of 1016 amps. 120

7.5 Variation of the zero-sequence voltage harmonics with respect to the fundamental 16 kV bus voltage. 121

7.6 DC voltage level for various dc current orders. 122

7.7 DC current and harmonics for the current order of 1016 Amps. 122

7.8 Variation of the measured generator terminal power factor angle (lagging), average firing angles (referenced to the measured generator terminal voltage) and commutation angles for a range of dc current. 124

7.9 Comparison of generator terminal voltage waveforms obtained from the test measurement and harmonic domain solution. 124

7.10 Variation of the generator current harmonics for a dc current range. 125

7.11 Variation of the generator voltage harmonics for a dc current range. 126

7.12 (a) Commutation angle and generator terminal power factor at the rated power output for the Benmore Convertor station operating as group connected units; (b) Relationship between E'' referenced and generator terminal voltage V referenced firing angles. 128

7.13 Generator harmonic current and voltage levels for the Benmore Convertor station operating as group connected units. Firing angles are referenced to the generator terminal voltage. 129

7.14 Generator equivalent negative-sequence currents for the Benmore Convertor station operating as group connected units. 130

7.15 Convertor transformer current THD for the Benmore Convertor station operating as group connected units. 130

A.1 Benmore generator open circuit saturation curve. 139

C.1 Cubic spline interpolation of the Benmore generator open circuit characteristic. 144

E.1 Star-star transformer primary current and its harmonic content, commutation period is 13 degrees. 150

F.1 Partial derivatives in the Jacobian. 152

LIST OF TABLES

2.1 Iterations to convergence for six-pulse unit connected IHA algorithms. 12

4.1 Construction of dc voltage and ac phase current samples. 48

4.2 Limits of convertor states for use in sampling functions. 51

5.1 Mismatch equations for a 12 pulse convertor in phase coordinates. 66

5.2 Mismatch equations for a 12 pulse convertor in sequence components. 67

5.3 The selection of the cut-off limit for Jacobian elements in order to maximize solution speed and preserving the robustness of the solution. 70

5.4 Iterations to convergence for the unified Unit Connection solution using Newton's method. 78

5.5 Solution speed and convergence factor in relation to the magnitude of generator subtransient reactances for solutions up to the fiftieth harmonic. 79

6.1 Minimum firing angles for various overlap angle limits. 87

6.2 Adjustment for the generator and convertor parameters of Group Connections operating with a reduced number of generators. 98

6.3 Nominal firing angle restriction limits for group connected units imposed by overlap angle, mis-firing, generator power factor and continuous equivalent negative-sequence harmonic loading constraints. 104

7.1 Generator harmonic ratings for different group connected configuration at the Benmore convertor station; *results from the 1993 measurement. 127

7.2 Adjustment of parameters for the Benmore system operating in group connected and unit connected mode. 127

A.1 Generator harmonic ratings for twelve-pulse group connected operation at the Benmore convertor station. 138

A.2 Benmore generator open circuit saturation characteristic. 138

F.1 The coefficient matrix $C_{\alpha\delta i}$ which specifies the dependency among commutation current i, terminal voltage phase, and ac current phase 155

F.2 Coefficient matrix E_i^{α} defining the contribution of the commutation currents to each phase current. i is the commutation number. 158

F.3 Construction of dc voltage partial derivatives. 164

F.4 Limits of convertor states for use in sampling functions. 166

GLOSSARY

Subscripts and Superscripts

+, -	phase connected to positive and negative dc rails respectively
0,+,-	Three sequence labels
a, b, c	Three phase labels
b	Phase beginning conduction
D	Associated with star-g/delta group
d	Associated with direct-axis
e	Phase ending conduction
g	Associated with generators
k	Harmonic order
i	Firing number, $i = 1...6$
n	Integer $n = 1, 2, 3...$
o	Phase not participarting in a commutation
p	Conduction interval number, $p = 1...12$
q	Associated with quadrature-axis
P	Primary side
S	Secondary side
S	Associated with star-g/star group

Symbols

$\otimes$	Convolution operator
$*$	Conjugation operator
$\mathcal{R}$	Real part of
$\mathcal{I}$	Imaginary part of
$\frac{\partial y}{\partial x}$	Partial derivative of y with respect to x
j	$\sqrt{-1}$
α	Firing angle
β	Equidistant timing reference
β	An arbitrary phase angle
δ	Rotor angle
δ_{sat}	Rotor angle under saturation condition
θ_i	Firing instants

λ	Convergence factor
μ, μ_0	Average commutation duration
ϕ	Power factor angle
ϕ	End of commutation instants
ω	Fundamental angular frequency
ψ	Flux linkage
χ	Crossings of generator fundamental terminal voltages
a_1, a_2	Off nominal tap ratios
D	Commutating current DC offset
E	Generator Thevenin voltage source harmonics
E_d	Constant DC voltage source
E_f	Generator excitation voltage
E_p	Potier voltage
$f(\lambda)$	Magnetic saturation function
F	Full mismatch vector in Newton's method
$F_{\alpha 0}$	Average delay angle mismatch
F_θ	Firing mismatches
F_ϕ	End of commutation mismatches
F_I	AC side harmonic current mismatches
F_{Id}	Direct current harmonic ripple mismatches
F_S	Rectified power mismatch
F_V	AC terminal harmonic voltage mismatches
F_{Vd}	DC side harmonic voltage mismatches
F_W	Sequence components ac side harmonic voltage mismatches
G	Current transducer gain
$i(t)$	Time domain current waveform
$i_c(t)$	Time domain commutating current waveform
i_d	Time domain generator direct-axis current
i_q	Time domain generator quadrature-axis current
I	Convertor three-phase ac side harmonic currents
I_c	Commutating current harmonics
I_d	Convertor dc side harmonic currents
I_d	(chapter 3) Generator direct-axis current
I_N	Norton harmonic current source
I_q	Generator quadrature-axis current
J	Jacobian Matrix
L	Commutating inductance
L_d	Generator direct-axis inductance
L_q	Generator quadrature-axis inductance

P	Current controller proportional gain
P	Real power
Q	Reactive power
R	Resistance
S	Complex power
T	Sequence transform matrix
T_I	Current controller integral time constant
$v(t)$	Time domain voltage waveform
V	Convertor three-phase ac side harmonic voltages
V_d	Convertor dc side voltage harmonics
V_{dp}	pth direct voltage sample harmonics
W	Convertor ac side terminal voltage in sequence components
X	Solution vector in Newton's method
X_c	Commutating reactance
X_d	Generator direct-axis reactance
X_d	DC side reactance
X_p	Potier reactance
X_q	Generator quadrature-axis reactance
$X"$	Generator subtransient reactance
$X_d"$	Generator direct-axis subtransient reactance
$X_q"$	Generator quadrature-axis subtransient reactance
Z_{gen}	Generator harmonic impedance

Abbrieviations

CIGRE	Conference Internationale de Grands Reseaux Electriques
HVdc	High Voltage direct current
IHA	Iterative Harmonic Analysis
MHLF	Multiphase Harmonic Load Flow

Chapter 1

INTRODUCTION

1.1 HVDC TRANSMISSION

DC transmission dated back from the dawn of electricity, when Marcel Deprez transmitted 1.5 kW at 2 kV for over 35 miles in 1882. As low voltage levels from generators limited the transmission distance, stepping up the voltage through transformers was necessary. This effectively eliminated the use of dc in power transmission until the advent of the mercury arc valves that enabled high voltage rectification, and thus HVdc (High Voltage Direct Current) transmission for longer distances. More reliable thyristor valves gradually took over the mercury arc valves since the mid-seventies, reducing costs and increasing reliability. Worldwide power transfer capacity has increased from a mere 20 MW in the first HVdc scheme connecting mainland Sweden and Gotland (in 1954) to over 46 000 MW in recent time [Narain 1996].

HVdc has several distinctive advantages over ac transmission systems, particularly when being used to transmit power over long distances, or interconnect large asynchronous ac systems operating at the same or at different frequencies. The asynchronous nature of a dc link does not appreciably increase the fault level, and subsequently the required ratings of existing equipment. Moreover dc links can be used to improve ac system stability as the power flow in a dc scheme can be controlled at high speed [Arrillaga 1983]. In the case of long submarine power transmission, HVdc is the only choice since the voltage rating of the submarine cables makes ac transmission infeasible.

When the generated power is supplied exclusively to a HVdc transmission link, such as in an isolated power station, it is advantageous to simplify the rectifier station, via a direct connection of each machine set to a separate convertor group with series-parallel combinations made on the dc side. In these schemes, ac harmonic filters, ac switching and protection gears, and a transformation step are dispensed with. The convertor valve halls and power station can be integrated into a HVdc Power Station, resulting in further reduction in land requirement, civil and construction works. Cost savings in HVdc direct connection schemes have been estimated at 30 to 40% in comparison with conventional schemes [CIGRE JWG 14/11-09, 1997].

1.2 MAIN OBJECTIVES

The absence of ac filters and close proximity of the generators and convertors lead to strong harmonic interactions in direct connected units. The convertor harmonic currents flowing into the generator stator windings cause additional thermal stresses, parasitic torques and produce harmonic voltage distortion at the convertor terminal, which increases the insulation requirement for both generators and convertor transformers. Large voltage distortion also influences the commutation process, and thus affecting ac harmonic currents. In addition, the frequency conversion nature of the salient-pole generator adds another dimension of complexity to the harmonic interaction.

So far, electromagnetic transient simulation of twelve-pulse direct connected convertor units to the steady state, based on the solution of differential equations using step by step integration technique [Dommel 1969], is the only satisfactory harmonic analysis method for such systems. However this is a very inefficient approach considering the long time constants of the synchronous generator, and the great number of simulations needed to fully describe the harmonic behaviour. When modelling convertor operation, extra snubber capacitance is often added to aid the numerical stability of such programs, however that artificial capacitance can introduce substantial errors in the harmonic calculation.

On the other hand, simplified convertor formulae [Kimbark 1971] can not represent the effect of harmonic distortion on ac and dc convertor terminal, and the frequency coupling caused by rotor saliency in the presence of current unbalance or distortion. Such effects can be adequately modelled in the Harmonic Domain [Semlyen *et al.* 1988]. There are essentially two types of solution techniques, sequential and unified, that have been developed for convertor harmonic analysis. Sequential solution techniques such as Iterative Harmonic Analysis (IHA), which solves the convertor and ac system interaction in two separate steps, have suffered convergence problems when being used to analyse harmonics in direct connected units. Non-convergence or divergence is caused by large ac terminal voltage distortion due to substantial generator harmonic impedances [Callaghan and Arrillaga 1990]. Convergence can be improved when all the non-linearities are solved together in a unified solution [Smith *et al.* 1996]. But so far, unified solutions for direct connected units have not been developed.

The research effort described in this thesis was motivated by the desire to improve the harmonic analysis techniques as well as the understanding of the harmonic interaction in direct connected schemes. The principal goal was to develop a fast and accurate harmonic model of direct connected generator-HVdc convertor units using a unified solution technique as a suitable tool for harmonic analysis of these schemes. The developed model provides a platform for investigating the harmonic behaviour of direct connected units under the influence of generator saliency and saturation, adjustable speed operation, dc system resonances, etc.

A detailed harmonic generator model which takes into account the rotor angle effects on saliency and saturation is also developed since the present Harmonic Domain generator model [Medina and Arrillaga 1994] does not include these critical factors. The generator model is expressed as a harmonically coupled impedance matrix with elements derived from the normally available generator parameters such as subtransient reactances.

Detailed three-phase harmonic information of the Benmore convertor station when being operated in the group connected mode, collected in November 1995, is presented. The test results are used to assess the accuracy of the developed generator and direct connected models, and they also provide valuable evidence of the feasibility of direct connected schemes.

1.3 THESIS OUTLINE

Chapter 2 summarizes the direct connection concept, and critically reviews the advantages and disadvantages of existing methods for harmonic analysis of direct connected units.

Chapter 3 derives a salient-pole generator harmonic model in sequence components. Sequence components formulation is more desirable than phase components as the generator converts harmonics from one sequence to another in the steady state, thus gives insight understanding into the harmonic couplings. The derived model is validated by means of time domain simulations. The harmonic measurement results obtained from the Benmore convertor station when being operated as a group connected unit is also used to validate the developed generator model.

Chapter 4 summarizes a harmonic domain convertor model developed recently by Smith *et al.* [1995], expressed in terms of simultaneous equations that fully describe the convertor in the steady state.

The generator and convertor models are integrated into a twelve-pulse Unit Connection harmonic model in Chapter 5. The generator, convertor and dc system harmonic interaction are formulated and solved in a unified algorithm using Newton's method. Since unbalance is accounted for in the commutation process, the distorted generator voltage can be chosen as a *pseudo-commutation voltage*. The voltage control by generator excitation in the absence of convertor transformer on-load tap-changers is also modelled. The solution of a test system is verified against a time domain simulation.

In Chapter 6, the developed model is used to investigate the effects of generator saliency, rotor angle and saturation, the number of generators in Group Connections, adjustable speed operation, and dc side resonances on the harmonic levels. The firing angle references, generator terminal power factor rating, and overlap angle constraints in direct connected units are also examined.

Chapter 7 reports on the three-phase harmonic measurement of a HVdc Group Connection, containing four 112.5 MVA hydro generators at the Benmore end of the New Zealand HVdc link. The test measurement results, procedures, setup and configuration of the CHART (Continuous Harmonic Analysis in Real-Time) harmonic monitoring instrumentation are described. The results include measured waveforms and their harmonic content in sequence components for a range of dc line current. Using the developed direct connected model, generator harmonic levels are derived for the unit connected mode, which has not been operated at the Benmore terminal, to provide evidence in terms of harmonic ratings for the viability of this mode of operation. Finally, the overall conclusions are drawn in Chapter 8.

Chapter 2

DIRECT CONNECTION SCHEMES AND HARMONIC MODELLING REVIEW

2.1 INTRODUCTION

Since the steady state performance is critical in the operation of direct connected units, it is necessary to be able to predict and quantitatively assess the harmonic behaviour of such systems at the design stages. Existing methods of harmonic analysis applied to large convertor installations are critically reviewed in this chapter, with particular attention paid to the ability of the techniques to evaluate the strong harmonic interaction in direct connected units.

The basic direct connection concept, typical configuration, main advantages, disadvantages, and possible applications of direct connected schemes are also summarized in this chapter.

2.2 UNIT CONNECTION CONCEPT

In the conventional HVdc systems, generators are allocated to a common ac bus which feeds all the convertors, as illustrated in Figure 2.1. The ac harmonic filters on the convertor bus prevent characteristic convertor harmonics from penetrating into the generators or further into the ac network. However the presence of filters also imposes steady state operation at a fixed electrical frequency. The large filter capacitances can cause generator self-excitation on the occurrence of load rejection, resulting in substantial dynamic overvoltages.

The possibilities of gaining efficiency and reducing cost by using adjustable speed operation and simplifying the sending terminal are the main motivations behind the direct connection concept [Calverley *et al.* 1973]. In its simplest form, the concept takes the form of a "one-to-one" configuration, or a Unit Connection, in which the ratings of the individual components are matched, as shown in Figure 2.2. The basic feature is that the generator transformers and all the ac filters are removed and the generators are directly connected to twelve-pulse convertors.

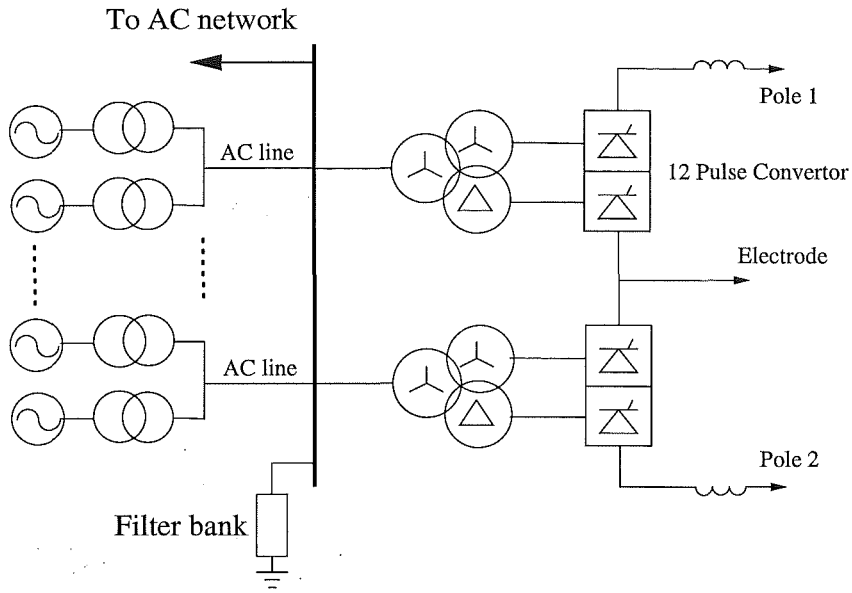

Figure 2.1 Conventional HVdc sending end arrangement.

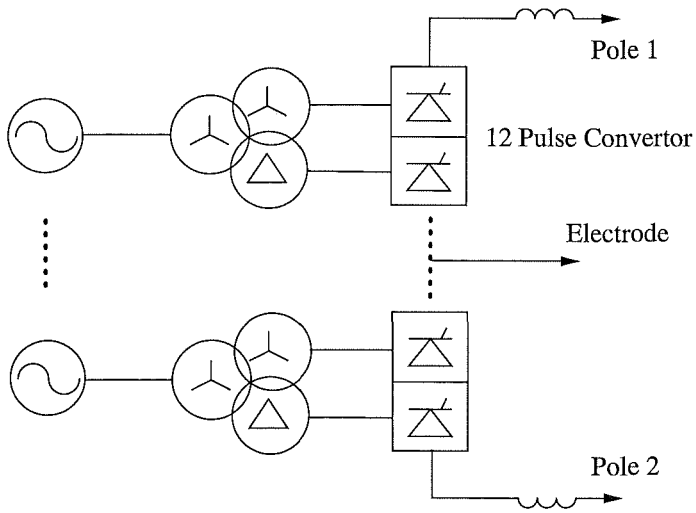

Figure 2.2 Unit Connection configuration.

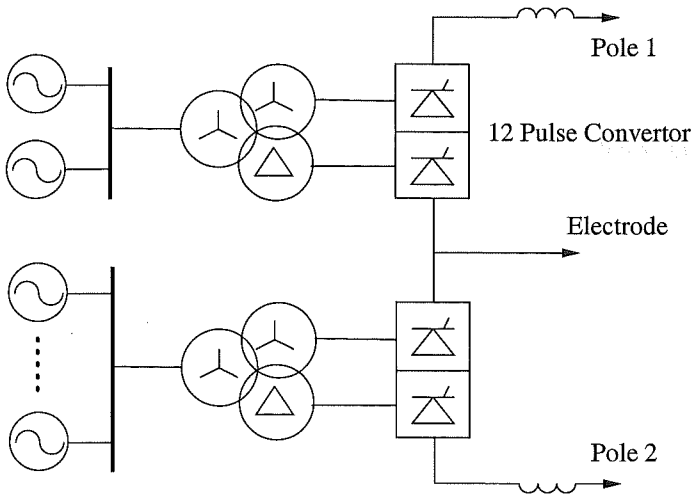

Figure 2.3 An example of a Group Connection arrangement.

The absence of tuned ac filters enables the generating units to operate within an adjustable speed/frequency band, rather than at a fixed speed. Since hydro turbines are intrinsically adjustable speed machines, net energy generation, unit reliability and service life duration of turbine can all be increased. Furthermore, the simplified layout with substantially reduced equipment requirement leads to less land requirement at the HVdc sending end. Operating and maintenance costs will lessen accordingly. The saving in capital costs for the convertor station is conservatively evaluated at 30 to 40% in comparison with the conventional schemes [CIGRE WG 11/14-09, 1993]. Substantial overvoltages due to the large filter capacitance during faults or power swing is eliminated, leading to reduced insulation over-rating factors. In addition, current and power flow are unaffected by ac system disturbances from major faults or oscillations. It is also proposed that the voltage and reactive power control be exercised entirely by the generator excitation. As a result, the sending end transformers on-load tap changers are no longer required. This control action is taken into account in the developed formulation in Chapter 5.

Without ac filters the convertor harmonic currents flow through the generator stator windings, causing additional thermal stresses and ripple torques. In the event that generators are operated at frequencies other than power frequency, a separate source of power for station auxiliaries must be arranged. The basic one-to-one arrangement however, lacks flexibility on the account that each individual generating unit is dedicated to a single convertor. In the case of a series connection on the dc side, for instance, dc transmission voltage has to be reduced with loss of efficiency if one or more units are down. Additional equipment will be required for the station to cope with outages. For this reason, one-to-one arrangement is not recommended in general. It may however, be possibly suitable for stations with only a few very large units and for small, compact and isolated stations.

A variation of the basic one-to-one arrangement that offers more flexibility of operation and of maintenance is the Group Connection [Uhlman 1975], in which more than one generator can be connected to a twelve-pulse convertor. When there are a large number of generating units involved, a combination of parallel Group Connection could be used, as illustrated in Figure 2.3. The generator transfer bus and ac switchgear are required. The Group Connection can maintain a constant dc voltage at reduced dc power levels which keeps the transmission efficiency high [Arrillaga *et al.* 1993b]. The matching of generator and convertor ratings is no longer required. Adjustable speed operation is still allowed although the group of synchronized generators will require some form of joint speed control.

Nevertheless, the basic one-to-one arrangement is ideal for harmonic studies as other configuration can be simplified to this arrangement with various modifications to power plant ratings. This is further investigated in Chapter 6.

2.3 MAIN APPLICATIONS

Potential applications of direct connected HVdc schemes are in cases when the whole output of the generating station can be transmitted via HVdc, such as:

- Transmission of large power from remote sources of generation, such as hydro and low grade coal fields, when the new development requires little or no local load.
- Variable frequency operation such as pump storage schemes and wind power.
- Connection of large generating stations to load centres using back-to-back HVdc schemes. This practically eliminates the stability and short circuit level problems associated with equivalent ac interconnections.

2.4 A REVIEW OF HARMONIC ANALYSIS METHODS

Harmonic analysis of the convertor can be divided into two broad categories: time domain and frequency domain analysis. Although time domain has been developed primarily for transient studies, it can be used for harmonic analysis when systems are simulated to reach steady state. On the other hand, frequency domain techniques have been designed for, rather than being applied to harmonic analysis.

The simplified convertor formulae [Kimbark 1971] cannot take into account the effects of harmonics and frequency couplings due to generator saliency, thus is inadequate for harmonic analysis of direct connected units. More detailed convertor models in the Harmonic Domain, a frame of reference which consists of the fundamental and its harmonic frequencies [Semlyen *et al.* 1988], are iterative and can be categorized into two types based on the solution techniques: sequential and unified solution models. A

sequential solution model, the Iterative Harmonic Analysis (IHA), has been primarily developed for analysing harmonic interaction between convertor and ac system, in which harmonic impedances are usually small. When extending IHAs to model direct connected units, they suffer from convergence problems due to large ac voltage distortion in the absence of harmonic filters. Convergence can be improved when a unified solution is used, in which all the non-linearities around the convertor are solved together.

2.4.1 Time Domain Simulations

Time domain or dynamic simulation is the solution of differential equations to determine circuit voltages and currents at each time step. Electrical circuit simulation programs based on the trapezoidal integration technique [Dommel 1969] such as PSCAD-EMTDC [Woodford *et al.* 1983] and EMTP [Dommel *et al.* 1980] are widely available, and they have evolved primarily to investigate the response of the systems to transient disturbances.

Basic to the EMTP method is the representation of each inductor and capacitor as a resistor in parallel with a time dependent and a history dependent current source. A thyristor switch is modelled as a resistor branch, and the switching is accomplished by changing the resistor value, i.e. large values for non-conduction and small values during conduction. Consequently, a network of lumped R, L and C components is built up as an equivalent circuit of resistive branches and current sources. The trapezoidal rule is used for integrating the ordinary differential equations of lumped inductors and capacitors. Due to the switching action, the conductance matrix must be updated at each switching instant. The node voltages are then calculated using nodal analysis, and the current source values for the next time step are calculated from the history terms. Harmonic information can be obtained by simulating the desired systems to reach the steady state, a process that is computationally intensive. Nevertheless, the modular and general purpose nature of these programs simplify the network construction process considerably.

In PSCAD2-EMTDC simulations, it is necessary to include an artificial snubber capacitance across each thyristor to improve numerical stability. The artificial capacitance used does not represent the actual snubber capacitance in the circuit. Numerical instability occurs when the rate of change of the voltages in the switching process are large. However the often required large capacitance value can affect the harmonic results. Simulations with various values of snubber capacitance were carried out to study the extent of the harmonic variation in a Unit Connection. Figure 2.4 shows the variation of the 11th and 13th ac current harmonics with respect to snubber capacitance values for a particular loading condition. It is observed that the magnitudes of the harmonics vary by up to 12% for various values of the snubber capacitance. An interpolation algorithm applied to switching devices has been developed which could eliminate the need for using

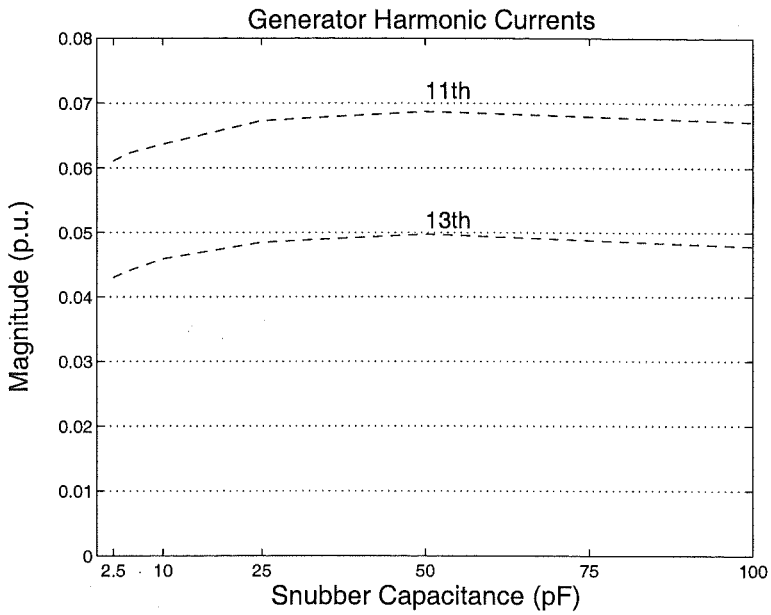

Figure 2.4 Effects of arbitrary snubber capacitances on the harmonic levels in PSCAD2-EMTDC simulations.

the artificial capacitance [Gole *et al.* 1997]. This interpolation algorithm is going to be incorporated into the 3.0 future releases of PSCAD-EMTDC.

The duration of time steps also influences the harmonic results. Ideally, switching instants should fall exactly on one of the solution points. But in order to accomplish this, the simulation step size may need to be changed, requiring a network reformation. Alternatively the switching may be assumed to occur at the nearest solution point at the expense of introducing a small error. It has been found that for small time steps, i.e. 5μs or smaller, the effect on harmonics is minimal.

In summary, provided that the snubber capacitance value and the time step size are carefully selected, harmonic analysis may be performed by running dynamic simulations to the steady state. Although frequency dependent components can be included as a combination of R, L and C, the selection of these elements is a difficult and tedious process.

2.4.2 Harmonic Domain Modelling

2.4.2.1 Simplified Convertor Formulation

The simplified convertor analysis assumes that the dc current is ripple free and the commutation voltage is sinusoidal and balanced. The generator is simply represented by a Thevenin equivalent with the impedance based on the subtransient reactance. Under these ideal conditions, analytic expressions can be written for the transfers across the convertor [Kimbark 1971].

A rigorous investigation by Sankar [1991] concluded that the simplified formulation is inadequate for harmonic analysis of direct connected units, particularly in the presence of generator saliency. Nevertheless it does provide a quick estimation of the harmonic content and can be used as a starting point for an iterative solution.

2.4.2.2 Iterative Harmonic Analysis

As the terminal voltages are distorted in the absence of ac filters, an iterative solution is necessary. Iterative Harmonic Analysis (IHA), a general technique for assessing the harmonic generation of non-linear devices, was first used to investigate the harmonic interaction between convertor and ac system by Reeve and Baron [1971]. In this simple algorithm, the convertor and ac system interaction was solved in two steps at each iteration. Given the terminal voltages as pseudo-commutation voltages, ac currents were derived from the convertor solution while the direct current was assumed to be flat. The corresponding ac current harmonics, obtained by using a Fourier analysis, were then impressed upon the ac system representation to obtain updated terminal voltages. More detailed convertor models with dc system and control representation were developed by Eggleston [1985] and Yacamini and de Oliveira [1980] [1986].

Since the convertor, ac and dc system non-linearities are solved sequentially, IHA algorithms are essentially Gauss-Seidel, or fix point iteration in nature. Although accurate results can be obtained when convergence occurs [Arrillaga *et al.* 1987], IHAs frequently suffer from non-convergence due to the Gauss-Seidel nature of the algorithm.

Yacamini and de Oliveira [1986] claimed that instability of an actual system was characterized by divergence of the iterative algorithm. Rigorous investigation of IHA algorithms applied to convertor analysis which was carried out by Callaghan and Arrillaga [1990] has proved that divergence of IHA need not be representative of true harmonic instability. Sufficient criteria for convergence was also derived analytically. Non-convergence occurs when the ac system is weak and the commutating reactance is small, leading to large variation of terminal voltage harmonics in consecutive iterations.

In the case of six-pulse convertors without ac filters, non-convergence of IHA has been shown to occur when the generator impedance is 0.1 p.u. or more at fundamental frequency, and the commutating reactance is 0.1 p.u. or less for a formulation containing the first 50 harmonics. The iterations to convergence for a six-pulse IHA algorithm are given in Table 2.1 [Callaghan and Arrillaga 1990]. The convergence threshold is very low since typical values for generator subtransient and transformer leakage reactance are 0.2 and 0.1 p.u. respectively. Thus with no modification, IHA cannot be used to analyse the harmonic interaction in six-pulse direct connected units.

Callaghan also showed that convergence could be improved by inserting a pair of equal and opposite reactances, so called *inserted reactance pair*, between the transformer primary and generator bus so that their series combination is equivalent to a 'piece of

X_{gen}	X_c	Iterations to convergence
0.05	0.15	8
0.07	0.13	14
0.08	0.12	20
0.09	0.11	36
0.10	0.10	Stagnated
0.12	0.08	Stagnated
0.15	0.05	Diverged
0.18	0.02	Converged to nonsense solution

Table 2.1 Iterations to convergence for six-pulse unit connected IHA algorithms; firing angle is 20 degrees and the number of harmonics considered is 50.

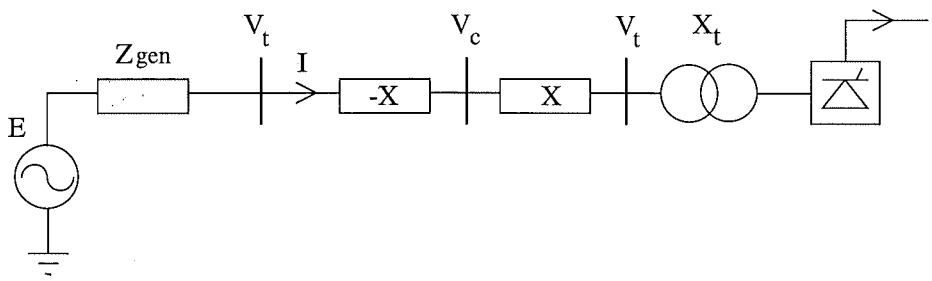

Figure 2.5 Matched reactance pair method for six-pulse convertors.

wire', as depicted in Figure 2.5. The positive reactance is then absorbed into the commutating reactance, while the negative reactance is absorbed into the generator impedance. As a result, the effective commutating reactance is increased and the reactive component of the generator impedance is decreased without effecting the physical system. Therefore by adjusting the parameters of the simulation, the same physical situation may be made to converge or diverge at will.

However this method is not effective for systems consisting of more than one convertor bridge such as twelve-pulse or higher pulse systems, since the harmonic currents are phase shifted among the bridges. Considering a twelve-pulse convertor with an inserted reactance pair as shown in Figure 2.6, the new commutation voltages are V_S and V_D for the star-star and star-delta valve group respectively. Although the terminal voltage V_t is common to both valve groups, V_S and V_D take on different values:

$$V_S = V_t + j2I_S X \tag{2.1}$$

$$V_D = V_t + j2I_D X. \tag{2.2}$$

By injecting the currents into the generator representation, the terminal voltage is

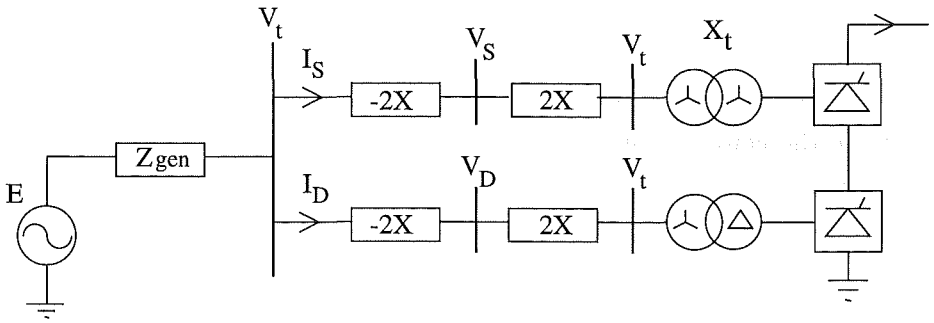

Figure 2.6 Matched reactance pair method for twelve-pulse convertors.

expressed as:

$$V_t = -(I_S + I_D)Z_{gen} + E. \tag{2.3}$$

Assuming for simplicity that $Z_{gen} = X$, equations 2.1 and 2.2 become:

$$V_S = j(I_S - I_D)X + E \tag{2.4}$$

$$V_D = j(I_D - I_S)X + E. \tag{2.5}$$

As a result, the $12n \pm 1$ characteristic harmonics are eliminated in the commutation voltages V_S and V_D due to the difference terms $(I_S - I_D)$ and $(I_D - I_S)$, but the 5, 7, 17,..., $6(2n-1) \pm 1$ harmonics are introduced. Since the distortions due to the $6(2n-1) \pm 1$ harmonics are higher than those from the $12n \pm 1$ harmonics, no improvement is gained by using the inserted reactance pair method for twelve-pulse or higher pulse convertor systems.

Most recent works have been directed toward improving the solution method itself, rather than improving the fix point iteration of IHAs. By solving the convertor and the interaction with the ac and dc system in a unified manner, convergence is improved. The improvement lies in the fundamentally different solution techniques of the two analyses. The unified solution is solved by Newton's method, in which all variables are related to each other via the Jacobian matrix. For example, some variation from the set dc current level affects all the other variables such that the required value is eventually restored. On the other hand, IHA convertor variables are solved sequentially with a purely unilateral relationship between the input and output variables. A large change in those variables regarded as input could lead to divergence.

2.4.2.3 Method of Norton Equivalents

A variation of the IHA is the method of Norton equivalents. The convergence can be improved when the convertor is represented in the ac system solution at each iteration by a Norton equivalent instead of a constant current source. The Norton admittance represents a linearisation of the convertor response to variation in terminal voltage.

Convertor and generator models have been developed for the Multiphase Harmonic Load Flow (MHLF) program by Xu *et al.* [1990][1991][1994]. The harmonic load flows are obtained from iterations between the Norton equivalent circuits of the nonlinear elements and the linear network solutions at harmonic frequencies. The convertor model in MHLF assumes a predetermined firing angle and dc current. Only the contribution of the commutation current to the phase currents is linearised. The problem with modelling the convertor and ac system by Norton equivalents is that the convertor is simply an interface between the ac and dc systems, with only the ac system represented in the overall solution process. If the convertor controller is modelled, a separate iterative procedure is required to solve the convertor interaction with the dc system at each iteration.

Harmonic studies in MHLF so far have only included filtered systems. While in theory, the algorithm can be extended to model direct connected units, it has not been attempted.

2.4.2.4 Unified Solution using Newton's Method

The first Newton type solution of the interaction of the convertor with the ac system is the Harmonic Power Flow developed by Xia and Heydt [1982]. The load flow, harmonic interaction between nonlinear loads, and firing angle for convertors are linearised together in a unified Jacobian. This single phase program was extended to three phases by Valcarcel and Mayordomo [1993]. However the described solution method is a fixed point iteration of three separate Newton procedures; one each for the load flow, ac system harmonic interaction, and commutation angles. The direct current is assumed ripple free, and in common with Xia, the convertor operating point is specified in terms of real and apparent power, rather than current order or dc power. Moreover the models exclude the linearisation of an important interaction between the convertor and the load flow, which may not be solvable by a fixed point iteration.

A full linearisation of the convertor requires that variables other than electrical quantities, such as switching angles and control variables, are linearised in the same Jacobian matrix. Since the variables are a mixture of real and complex quantities, the solution is formulated in positive harmonics and real variables only. A system of mismatch equations describing the interaction among the convertor, ac and dc system is solved in a unified algorithm developed by Smith *et al.* [1995]. The harmonic transfer

across the convertor is modelled using convolution analysis, leading to a reduced set of variables. The Jacobian is an estimation of the behaviour of the nonlinear system in response to small perturbations, thus it gives insights into the transfer of distortions around the convertor. The solution has been accelerated by employing sparsity methods, and the convergence has been found to be robust and fast. However harmonic models of direct connected units have not been developed.

2.5 CONCLUSIONS

In the absence of filters, detailed harmonic analysis is required to predict and evaluate the strong interaction that exists between the generator and convertor. Such interaction can be analysed using electromagnetic transient programs on reaching steady state. However this is a very inefficient approach, considering the long time constants of the synchronous generator. Moreover the large snubber capacitance value across each thyristor often required to improve numerical stability can introduce a large error in the ac current harmonics.

Although the simplified convertor formulae in the Harmonic Domain give direct harmonic solution, they have been found to be inadequate for harmonic analysis of direct connected units. Iterative Harmonic Analysis of the harmonic interaction between convertor and an ac system has been found to give accurate results when convergence is obtained. However due to the Gauss-Seidel or fix point iteration nature of the algorithms, IHAs suffer from instability when being used to model the strong harmonic interaction in direct connected units. This is caused by large ac harmonic voltage distortion due to large generator harmonic impedances and the absence of harmonic filters. IHAs' convergence can be improved in six-pulse convertor systems by inserting a matched reactance pair between the generator terminal and the convertor transformer. However this method is not applicable for twelve-pulse convertors since the harmonic currents are phase shifted among the bridges due to the transformer connection.

Alternatively, convergence is improved when all the interactions around the convertor are formulated and solved in a unified algorithm, as implemented for direct connected units in Chapters 3, 4 and 5.

Chapter 3

GENERATOR MODELLING IN THE HARMONIC DOMAIN

3.1 INTRODUCTION

A salient-pole generator acts as a harmonic convertor due to saliency and as a voltage harmonic source due to saturation, generator slot and winding distribution. With the increased size of modern generating plant and greatly improved synchronous machine designs, the voltage distortion due to slot and winding distribution have become less significant and will rarely need to be taken into account in system studies. It is also assumed that the generator dc excitation current is ripple free. As a result, only accurate representation of saliency and saturation is required in a generator model.

The harmonic representation of the synchronous machine as an emf in series with kX_d'' or the average of kX_d'' and kX_q'' [Clarke 1950] can not take into account the process of harmonic conversion. The more advanced generator model in the harmonic domain was formulated in phase components, and took the rotor saliency and saturation into account [Medina and Arrillaga 1994]. This model however, did not include the important effects of rotor angle on saliency and saturation. The transformer saturation formulation was used to model generator saturation, but because of the difference in the nature of saturation in generators and transformers, transformer saturation formulation is not applicable to generator saturation modelling. Section 3.5 investigates the unsuitability of this saturation model, and examines the generator saturation phenomenon in detail.

This chapter describes the derivation of a generator model in the harmonic domain that takes into account the effects of rotor angle on the stator-rotor frequency conversion phenomenon due to saliency and saturation. Since generators convert harmonics from one sequence to another in the steady state, it is desirable to develop the model in sequence components, thus greatly simplifying the formulation and increasing the intuitive understanding of the model.

The proposed model is validated against a time domain simulation using the PSCAD2-EMTDC program [Woodford *et al.* 1983]. From the results of three-phase harmonic measurements at the Benmore convertor station when being operated as a group connected unit, described in Chapter 7, the generator impedances at the charac-

teristic harmonics $(12n \pm 1)$ are obtained and compared with those calculated using the proposed formulation.

3.2 THE PROCESS OF FREQUENCY CONVERSION

In a cylindrical rotor machine, a negative-sequence current of order k injected to the stator will create a flux of order $k+1$ in the rotor, which in turn will induce a negative-sequence voltage of order k. For the case of a positive-sequence current of order k injected to the stator, a flux of order $k-1$ is produced, which in turn produces a positive-sequence voltage of order k.

In a salient-pole machine, a negative-sequence current of order k produces two counter rotating fluxes of order $k+1$ in the rotor; one inducing a negative-sequence voltage of order k and the other a positive-sequence voltage of order $k+2$ in the stator. Similarly, a positive-sequence current of order k in the stator produces counter rotating fluxes of order $k-1$, which in turn induce a positive-sequence voltage of order k and a negative-sequence voltage of order $k-2$. The same process is repeated for a current injection of order $k-2$ and of higher harmonic orders in the stator. This is illustrated in Figure 3.1 for cases where the stator current contains either positive or negative fifth harmonic content.

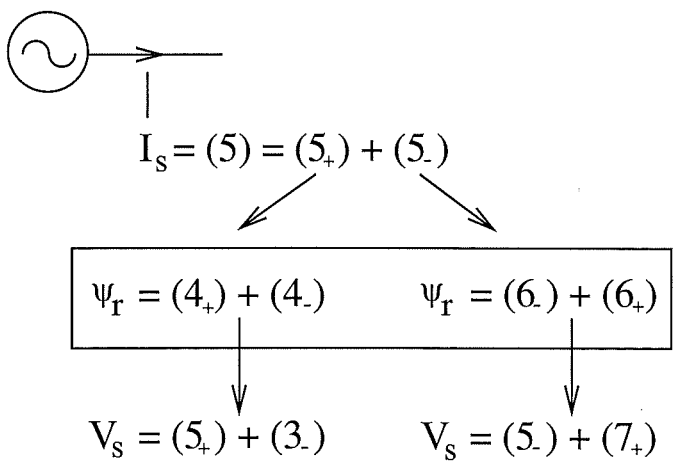

Figure 3.1 Response of a salient pole generator to the presence of a harmonic current.

In general terms, it can be noted that an unbalanced harmonic current of order k injected in the stator will produce harmonic voltages of orders $k-2, k$ and $k+2$.

3.3 GENERATOR HARMONIC IMPEDANCES IN SEQUENCE COMPONENTS

3.3.1 Frame of Reference and Rotor Angle

A positive frequency domain representation of a time domain quantity is equal to the real or imaginary part of a rotating phasor. The real part yields a cosine referenced waveform, whereas the imaginary part yields a sine referenced waveform. The cosine referenced phase a voltage is chosen as the phase angle reference in this analysis.

The effects of saliency can be taken into account by the two-reaction theory proposed by Blondel [1923] and extended by Doherty and Nickle [1926] and Park [1929]. The armature current $\mathbf{I}$ is resolved into two components: $\mathbf{I}_d$ in time quadrature with, and $\mathbf{I}_q$ in time phase with the excitation voltage $\mathbf{E}_f$.

Under steady state operation, the excitation voltage is

$$\mathbf{E}_f = \mathbf{V}_t + \mathbf{I}R_a + j\mathbf{I}_d X_d + j\mathbf{I}_q X_q \,, \tag{3.1}$$

where

$$\mathbf{I}_d = \mathbf{I}\sin(\delta+\phi)\; e^{j(\delta+\phi-\pi/2)}, \tag{3.2}$$

$$\mathbf{I}_q = \mathbf{I}\cos(\delta+\phi)\; e^{j(\delta+\phi)}, \tag{3.3}$$

and X_d and X_q are the direct and quadrature axis synchronous reactances, and the variation of air gap inductance is approximated by a second harmonic term.

The corresponding phasors are shown in Figure 3.2 for an unsaturated salient-pole generator operating with a lagging power factor angle ϕ. The *rotor angle* δ can be expressed as

$$\tan\delta = \frac{I(X_q\cos\phi - R_a\sin\phi)}{V_t + I(X_q\sin\phi + R_a\cos\phi)}\,. \tag{3.4}$$

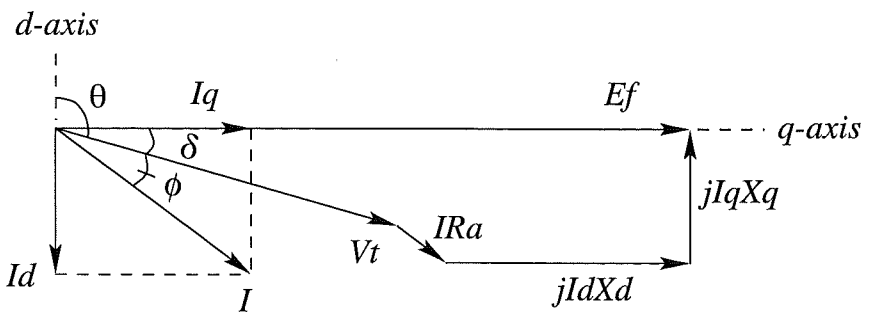

Figure 3.2 Phasor diagrams of an unsaturated salient-pole synchronous generator operating at a lagging power factor.

3.3.2 Negative-Sequence Harmonic Impedances

Generator negative-sequence harmonic impedances are derived by injecting negative-sequence currents into the generator Park's equations and taking the ratios of the terminal voltages and currents at each harmonic. For a harmonic k, the current injections are

$$\begin{bmatrix} i_{ak} \\ i_{bk} \\ i_{ck} \end{bmatrix} = \mathcal{R} \left\{ \begin{matrix} Ie^{j(kwt-\beta)} \\ Ie^{j(kwt+2\pi/3-\beta)} \\ Ie^{j(kwt-2\pi/3-\beta)} \end{matrix} \right\} = I \begin{bmatrix} \cos(kwt-\beta) \\ \cos(kwt+2\pi/3-\beta) \\ \cos(kwt-2\pi/3-\beta) \end{bmatrix} \tag{3.5}$$

where β is an initial angle.

The field circuit is shorted, since it is not excited at harmonic frequencies, i.e.

$$v_{fk} = 0\,. \tag{3.6}$$

The field rotates at synchronous speed with the d-axis leading phase a positive-sequence fundamental voltage as shown in Figure 3.2. The instantaneous position of the rotor is

$$\theta = wt + \pi/2 + \delta\,. \tag{3.7}$$

Park's transformation from three-phase to dq coordinates is

$$\begin{bmatrix} i_{dk} \\ i_{qk} \\ i_{0k} \end{bmatrix} = \frac{2}{3} \begin{bmatrix} \cos\theta & \cos(\theta-2\pi/3) & \cos(\theta+2\pi/3) \\ -\sin\theta & -\sin(\theta-2\pi/3) & -\sin(\theta+2\pi/3) \\ \frac{1}{2} & \frac{1}{2} & \frac{1}{2} \end{bmatrix} \begin{bmatrix} i_{ak} \\ i_{bk} \\ i_{ck} \end{bmatrix} \tag{3.8}$$

Substituting the injected harmonic currents expressed in equation 3.5 into equation 3.8 and simplifying yields:

$$\begin{bmatrix} i_{dk} \\ i_{qk} \\ i_{0k} \end{bmatrix} = I \begin{bmatrix} \cos[(k+1)wt-\beta+\pi/2+\delta)] \\ -\sin[(k+1)wt-\beta+\pi/2+\delta)] \\ 0 \end{bmatrix}. \tag{3.9}$$

The Park's flux linkages are [Kimbark 1968]:

$$\begin{bmatrix} \psi_{dk} \\ \psi_{qk} \\ \psi_{0k} \end{bmatrix} = \begin{bmatrix} L_d'' i_{dk} \\ L_q'' i_{qk} \\ 0 \end{bmatrix}, \tag{3.10}$$

where $L_d^{"}$ and $L_q^{"}$ are the direct and quadrature axis subtransient inductances respectively. Using the dq to abc transformation the flux linkage in phase a is

$$\begin{aligned}\psi_{ak} &= \psi_{dk}\cos\theta - \psi_{qk}\sin\theta + \psi_{0k} \\ &= \frac{1}{2}(L_d^{"}+L_q^{"})I\cos(kwt-\beta) + \frac{1}{2}(L_d^{"}-L_q^{"})I\cos[(k+2)wt-\beta+\pi+2\delta)]\,. \quad (3.11)\end{aligned}$$

Phase a voltage is then derived:

$$\begin{aligned}v_{ak} &= R_a i_{ak} + \frac{d\psi_{ak}}{dt} \\ &= \mathcal{R}\left\{\left[R_a + jk\left(\frac{X_d^{"}+X_q^{"}}{2}\right)\right]Ie^{j(kwt-\beta)}\right\} \\ &\quad +\mathcal{R}\left\{(k+2)\left(\frac{X_q^{"}-X_d^{"}}{2}\right)Ie^{j[(k+2)wt-\beta+2\delta+\pi/2]}\right\} \quad (3.12)\end{aligned}$$

Although the applied negative-sequence current is of order k, the armature flux linkages, and subsequently the armature voltages, consist of harmonics of order k and $k+2$. Calculating phase b and c indicates that the voltage harmonic k is of negative-sequence, and voltage harmonic $k+2$ is of positive-sequence. The ratios of voltages and currents at the same harmonic order are the harmonic self impedances

$$Z_{-k,-k} = R_a + jk\left(\frac{X_d^{"}+X_q^{"}}{2}\right) \quad (3.13)$$

The generator cross couplings from negative-sequence harmonic currents k to positive-sequence harmonic voltages $k+2$ are

$$Z_{+(k+2),-k} = (k+2)\left(\frac{X_q^{"}-X_d^{"}}{2}\right)e^{j(2wt+2\delta+\pi/2)} \quad (3.14)$$

It is observed that the harmonic impedances are independent of the initial phase β of the applied harmonic currents. The self terms, $Z_{-k,-k}$, are also independent of the rotor angle, whereas the cross coupling terms are not.

3.3.3 Positive-Sequence Harmonic Impedances

The generator positive-sequence fundamental impedance can be found by deriving the excitation voltage in terms of the terminal voltage and load current. Substituting equa-

tion 3.2 and 3.3 into 3.1 yields

$$Z_{+1,+1} = \left[R_a + \frac{1}{2}(X_d - X_q)\sin 2(\delta+\phi)\right] + j\left[X_q + (X_d - X_q)\sin^2(\delta+\phi)\right] \quad (3.15)$$

In a load flow or harmonic study, the value of the internal emf is not required, thus $Z_{+1,+1}$ can be assigned arbitrary.

For harmonic frequencies, injecting positive-sequence harmonic currents to the armature windings yields:

$$\begin{bmatrix} i_{dk} \\ i_{qk} \\ i_{0k} \end{bmatrix} = I \begin{bmatrix} \cos[(k-1)wt - \beta - \pi/2 + \delta)] \\ \sin[(k-1)wt - \beta - \pi/2 + \delta)] \\ 0 \end{bmatrix} \quad (3.16)$$

The flux linkage and voltage of phase a are:

$$\begin{aligned} \psi_{ak} &= \psi_{dk}\cos\theta - \psi_{qk}\sin\theta + \psi_{0k} \\ &= \frac{1}{2}(L_d'' + L_q'')I\cos(kwt - \beta) + \frac{1}{2}(L_d'' - L_q'')I\cos[(k-2)wt - \pi + 2\delta - \beta)] \quad (3.17) \\ v_{ak} &= R_a i_{ak} + \frac{d\psi_{ak}}{dt} \\ &= \mathcal{R}\left\{\left[R_a + jk\left(\frac{X_d'' + X_q''}{2}\right)\right] Ie^{j(kwt-\beta)}\right\} \\ &\quad + \mathcal{R}\left\{(k-2)\left(\frac{X_q'' - X_d''}{2}\right) Ie^{j[(k-2)wt-\beta-2\delta+\pi/2]}\right\} \quad (3.18) \end{aligned}$$

Thus the positive-sequence harmonic parameters are:

$$Z_{+k,+k} = Ra + jk\left(\frac{X_d'' + X_q''}{2}\right) \quad (3.19)$$

$$Z_{-(k-2),+k} = (k-2)\left(\frac{X_q'' - X_d''}{2}\right)e^{j(-2wt-2\delta+\pi/2)} \quad (3.20)$$

The harmonic self impedance terms for positive and negative-sequence are found to be the same. This is apparent as both sequences would have the same leakage path at a particular harmonic frequency. Note the phase angle of the cross coupling terms is now $\pi/2 - 2\delta$. The cross coupling term is zero for an applied second harmonic positive-sequence current.

For a different phase angle reference, modifications to the mathematical expressions for the cross couplings are needed. For instance, if the phase a armature current is

chosen as reference, the instantaneous rotor position becomes

$$\theta = wt + \pi/2 + \delta + \phi \tag{3.21}$$

The self terms and the magnitude of the cross coupling terms are unchanged, whereas the phase angles of the cross coupling terms become

$$\angle Z_{+(k+2),-k} = e^{j(2wt+2\delta+2\phi+\pi/2)} \tag{3.22}$$

$$\angle Z_{-(k-2),+k} = e^{j(-2wt-2\delta-2\phi+\pi/2)} \tag{3.23}$$

3.3.4 Zero-Sequence Harmonic Impedances

There is no cross coupling between the zero-sequence and other sequences in Park's differential equations. Thus the generator zero-sequence can simply be represented by an impedance at each harmonic frequency, i.e.

$$Z_{0k} = R_{0k} + jX_{0k} \approx R_{01} + jkX_{01} \tag{3.24}$$

where R_{01} and X_{01} are the fundamental zero-sequence resistance and reactance respectively.

3.3.5 Skin Effect

A constant armature winding resistance value has been assumed so far. However due to the skin effect the frequency dependence of the resistance accounts for the increased winding losses with frequency. A skin effect correction factor can be directly incorporated into the model by changing the resistance value at each harmonic. A commonly accepted resistance characteristic is [CIGRE Joint Task Force 36.05.02/14.03.03, 1996]:

$$R_k = R_1\sqrt{k} \tag{3.25}$$

where R_1 is the fundamental frequency resistance. Nevertheless, the contribution of the armature resistance in the generator impedance remain small at harmonic frequencies as the generator ratio $X"/R$ is typically 40 at the fundamental, and decreases with higher harmonic order.

3.4 SYNCHRONOUS GENERATOR HARMONIC EQUIVALENTS

The generator can be represented as a Thevenin or Norton harmonic equivalent, as shown in Figure 3.3, and the terminal harmonic voltages are thus given as

$$V_t = E - [Z_g]I\,, \tag{3.26}$$

where E is the excitation voltage and Z_g is the generator harmonic impedance matrix.

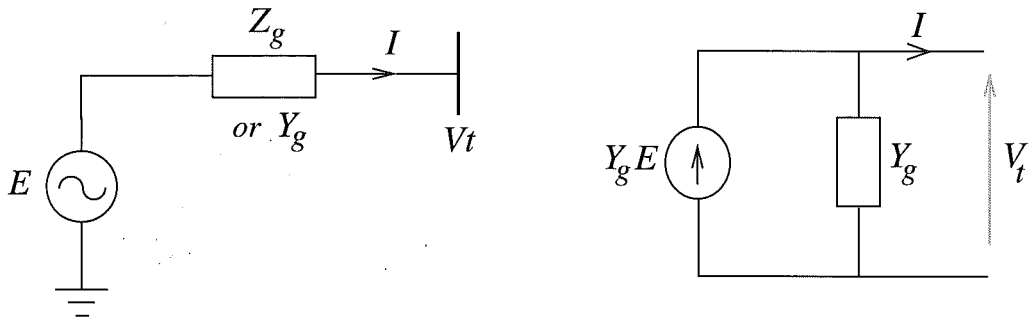

Figure 3.3 Generator Thevenin and Norton harmonic equivalents.

V_t and I contain all the relevant voltage and current harmonic phasors in sequence components, i.e.

$$V_t = [V_{01,01}, V_{-1,-1}, V_{+1,+1}, ..., V_{0k,0k}, V_{-k,-k}, V_{+k,+k}] \tag{3.27}$$

$$I = [I_{01,01}, I_{-1,-1}, I_{+1,+1}, ..., I_{0k,0k}, I_{-k,-k}, I_{+k,+k}] \tag{3.28}$$

For salient-pole generators, the impedance matrix consists of three diagonals as shown in equation 3.29. The main diagonal contains the self terms and the other diagonals contain cross coupling terms between the harmonics.

$$Z_{gen} = \begin{bmatrix} Z_{g\,1,1} & & Z_{g\,1,3} & & & \\ & Z_{g\,2,2} & & Z_{g\,2,4} & & \\ Z_{g\,3,1} & & Z_{g\,3,3} & & \ddots & \\ & Z_{g\,4,2} & & \ddots & & Z_{g\,k-2,k} \\ & & \ddots & & \ddots & \\ & & & Z_{g\,k,k-2} & & Z_{g\,k,k} \end{bmatrix} \tag{3.29}$$

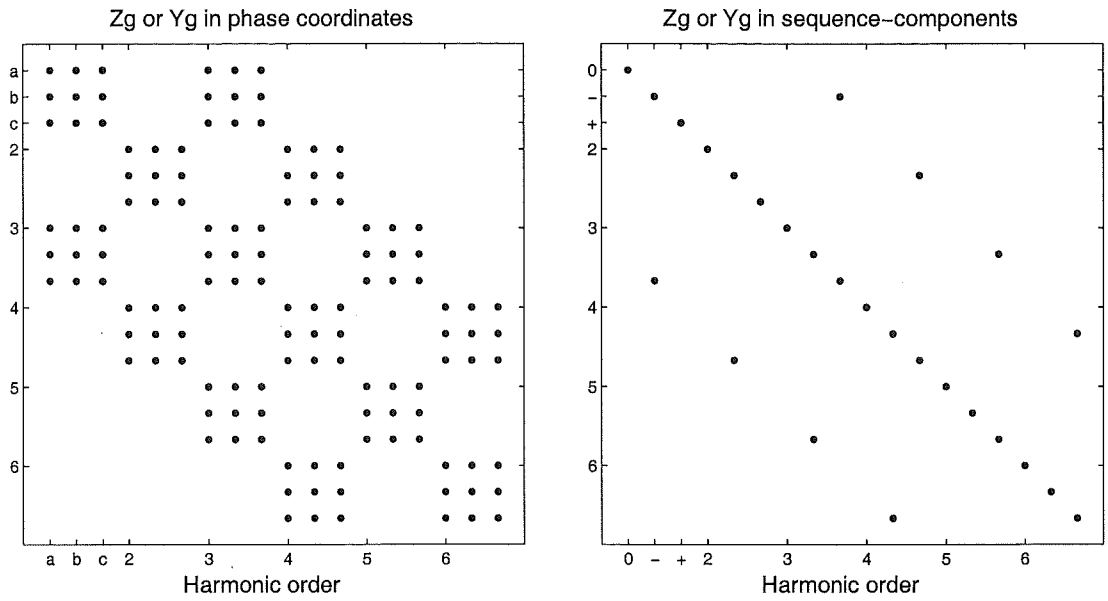

Figure 3.4 Structure of the generator impedance or admittance matrix in phase coordinate and sequence components.

The elements of Z_g are themselves sparse three-by-three matrices:

$$Z_{g\,k,k} = \begin{bmatrix} Z_{0k,0k} & 0 & 0 \\ 0 & Z_{-k,-k} & 0 \\ 0 & 0 & Z_{+k,+k} \end{bmatrix} \tag{3.30}$$

$$Z_{g\,k,k+2} = \begin{bmatrix} 0 & 0 & 0 \\ 0 & 0 & Z_{-k,+(k+2)} \\ 0 & 0 & 0 \end{bmatrix} \tag{3.31}$$

$$Z_{g\,k,k-2} = \begin{bmatrix} 0 & 0 & 0 \\ 0 & 0 & 0 \\ 0 & Z_{+k,-(k-2)} & 0 \end{bmatrix} \tag{3.32}$$

where the harmonic impedances are given in equations 3.13, 3.14, 3.19, 3.20 and 3.24. Z_g is always invertible, thus Y_g can be obtained by inverting Z_g.

Figure 3.4 illustrates the structure of an unsaturated generator impedance or admittance matrix in both phase coordinate and sequence components form. It is clear that the sequence components formulation provides more sparsity, leading to reduced storage space and increased speed in system studies. More significantly, the sequence components formulation is defined by simple analytical expressions obtained directly from normally available machine parameters, whereas a transformation involving complex numbers is required in obtaining phase component formulation.

The Norton shunt admittance will have a different value for each loading as the cross

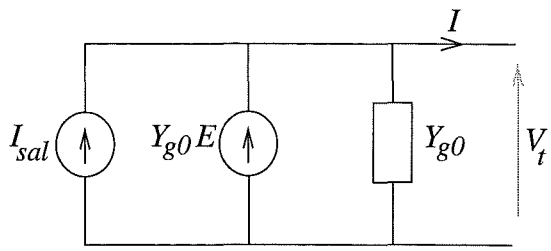

Figure 3.5 Modified equivalent circuit.

couplings are dependent on rotor angle. However a constant admittance matrix can be used, provided that the injected current is suitably modified to retain the accuracy of the Norton equivalent. The constant admittance, Y_{g0}, consists of only the main diagonal (self impedance terms) and the saliency is taken into account by current injections, as shown in Figure 3.5.

The armature current is:

$$I = Y_g(E - V) = Y_{g0}(E - V) + I_{sal} \tag{3.33}$$

and hence

$$I_{sal} = (Y_g - Y_{g0})(E - V) = Y_{sal}(E - V) \tag{3.34}$$

where I_{sal} is the current injection due to saliency and Y_{sal} consists of the cross coupling terms only.

Using this approach, it is not necessary to update the Y_g matrix at each step of an iterative algorithm. Instead, changes in the rotor angle and consequently in saliency terms are taken into account by the current injections.

3.5 SATURATION EFFECTS ON STEADY STATE OPERATION

The effects of magnetic saturation on the generator steady state behaviour is investigated in this section. As the flux across the air gap increases, the core and teeth of the rotor and stator saturate. Subsequently, the reluctance of the magnetic circuit increases, leading to a decrease in the generator reactances, and thus an increase in the dc excitation level. Based on the assumption that saturation is a function of the total air-gap flux only, there are essentially three main effects on the generator steady state behaviour:

- An increase in dc excitation level
- Decreases in generator reactances lead to changes in rotor angle, and thus changes in generator harmonic cross couplings.

- The production of harmonics due to non-linear magnetising characteristic.

In a steady state system study, the excitation requirement is not required to be included in the formulation. The calculation of the generator dc excitation is readily available in literature, where the excitation can be calculated from the terminal voltages and currents obtained from the system study. The second and third effects are to be examined in the following sections.

3.5.1 Saturation Effects on Generator Harmonic Impedances

As the subtransient reactances X_d'' and X_q'' of a synchronous machine with damper windings are associated with fast transient flux that flows mostly in air, they remain constant for a wide range of terminal voltage under saturation condition [Kilgore 1935]. Consequently, the self impedances at harmonic frequencies are unchanged according to equation 3.13 and 3.19.

With saturation, the rotor angle is decreased [Kilgore 1935], regardless of motor or generator action, or of power factor, leading to changes in the harmonic cross coupling terms for all harmonics according to equation 3.14 and 3.20. The calculation of rotor angle from the terminal voltage, load current and generator magnetic characteristics has been developed using various techniques such as Potier reactance [Kimbark 1968], saturation factors for d- and q-axis [Harley *et al.* 1980], etc.

The Potier reactance technique uses a saturation correction voltage E_s, obtained from the open-circuit saturation curve and the Potier voltage E_p, to determine the excitation voltage E_f. E_f indicates the position of the q-axis under saturation, and the adjusted rotor angle is readily obtained since the terminal voltage is known. Although it is assumed that saturation is the same on the d-, q-axis and between the axes, the level of saturation will vary in practice. However this is a reasonable assumption in the context of the steady state rotor angle calculation for large salient-pole generators with damper windings, where the error obtained would be small. The significant advantage of this technique is that the Potier reactance and open-circuit saturation curve are readily available.

Calculation of rotor angle using Potier Reactance

Given terminal voltage V_t, armature current I, load angle ϕ, Potier reactance X_p and the open-circuit saturation curve, the rotor angle with saturation taken into account can be calculated as follow:

- Determine rotor angle δ using unsaturated synchronous reactances, and E_q, which is the unsaturated E_f, as previously described in Section 3.3.1.

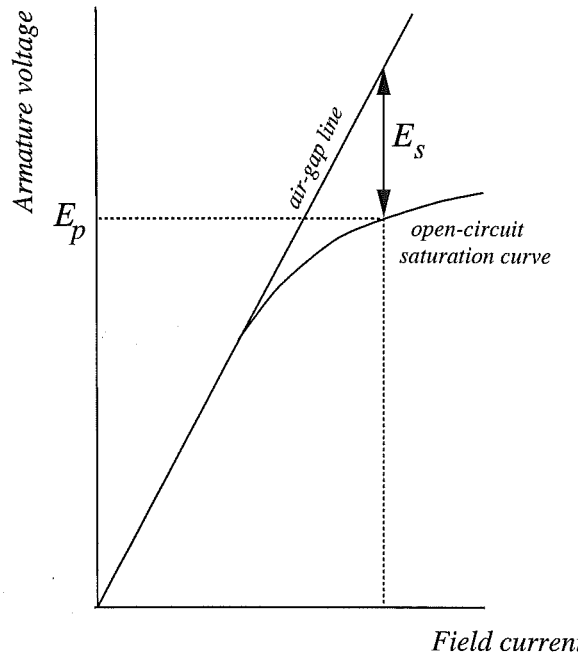

Figure 3.6 Graphical construction for finding the components of armature voltage due to saturation E_s corresponding to Potier voltage E_p.

- Find the Potier voltage as a vector sum of the terminal voltage and the voltage drop across the Potier reactance, i.e. $E_p = V_t + jX_pI$

- Calculate the magnitude of the saturation correction voltage E_s using the open-circuit saturation curve and the Potier voltage E_p, as illustrated in Figure 3.6. In order to eliminate the manual calculation of E_s, the saturation curve is represented by a mathematical expression that can be obtained by using the *cubic spline* curve fitting technique, summarized in Appendix C. Thus E_s is directly expressed as a function of E_p.

- The saturated E_f is the sum of phasors E_q and E_s, i.e. $\mathbf{E}_f = \mathbf{E}_q + \mathbf{E}_s$, where E_s is in phase with E_p.

- The saturated rotor angle δ_{sat} is obtained by subtracting the unsaturated δ with a correction angle $\Delta\delta$, where $\Delta\delta$ is obtained from the phasors relationship in Figure 3.7, as to be described below.

With reference to Figure 3.7, the angle β can be found from:

$$\begin{aligned} \tan\beta &= \frac{E_{p_d}}{E_{p_q}} \\ &= \frac{I(X_q - X_p)\cos(\delta+\phi)}{V_t\cos\delta + IR\cos(\delta+\phi) + IX_p\sin(\delta+\phi)} \end{aligned} \tag{3.35}$$

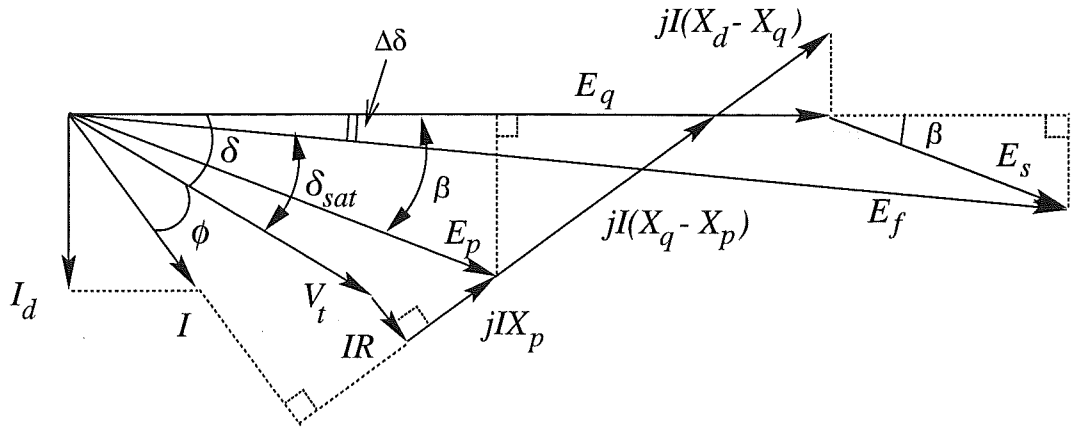

Figure 3.7 Determination of rotor angle under saturation for salient-pole synchronous generators operating at a lagging power factor.

The variation of rotor angle $\Delta\delta$ can be obtained from E_s and β:

$$\Delta\delta = \tan^{-1} \frac{E_s \sin\beta}{E_q + E_s \cos\beta} \tag{3.36}$$

The adjusted rotor angle δ_{sat} is therefore:

$$\delta_{sat} = \delta - \Delta\delta, \tag{3.37}$$

where δ and $\Delta\delta$ are given in equation 3.4 and 3.36.

This completes the calculation of rotor angle under saturation using the Potier reactance and the open-circuit (i.e. d-axis) saturation curve.

In general, regardless of calculation methods, rotor angle can be directly expressed as a function of the terminal voltage, load current and generator magnetic characteristics, $f(\lambda)$, i.e.

$$\delta_{sat} = f(V_t, I, \phi, f(\lambda)) \tag{3.38}$$

and hence the rotor angle is readily incorporated into equation 3.14 and 3.20.

On the other hand, any rotor angle calculation technique using saturation factors for d- and q-axis requires saturation curves for both d- and q-axis. However the q-axis saturation characteristic is not often available, and it is also necessary to make an assumption that the saturation characteristic can be interpolated between the axes. Since superposition of individual magnetic circuit is not valid in the presence of saturation, it is not clear at this time which of the many methods of interpolation is closest to the practical test measurements. Nevertheless, generator saturation characteristic is usually close to the air-gap line, thus changes in rotor angle due to saturation is relatively small.

3.5.2 Generator Saturation Harmonics

There are two kinds of space harmonic flux-waves exist in generators. The space harmonic, which has been treated extensively in literature, is generated by the harmonic content of the magnetising mmf wave and by the slot openings. The other type of space harmonic is the result of magnetic saturation in the machine. The first space harmonic is normally referred to simply as space harmonic and the second has been named saturation harmonic. Although all harmonics should be considered together in the determination of the air-gap flux distribution, saturation and space harmonics can be examined separately without appreciable error.

The saturable portion of the generator magnetic circuit consists of stator teeth, rotor teeth, stator core and rotor core. When a sinusoidal magnetising mmf is applied, the resultant air gap flux wave may be either flat-topped or peaked depending upon whether the teeth or cores are more saturated. Saturation of stator and rotor teeth causes the air gap flux wave to be flat-topped, and saturation of the cores makes the wave to be peaked. The flux in the cores is the space integral of the flux in the air gap; that is, the air gap flux density is proportional to the space derivative of the core flux. If the core is saturated and the teeth are not, the core flux distribution along the circumference is a flat-topped wave. Since the derivative of a flat-topped wave is a peaked wave, the air gap flux distribution is therefore peaked [Lee 1961].

In all practical machines, however, teeth are more saturated than cores. Air gap flux waves in saturated machines are always flat-topped. Since tooth saturation and core saturation have different effects on the shape of air gap flux wave, highly saturated machines do not necessarily have high saturation harmonics. The saturation harmonic content is high only when the teeth are highly saturated but the cores are not saturated.

As saturation harmonics are produced by the redistribution of the flux density in the air gap when part of the magnetic circuit saturates, i.e. changing the *shape* of the flux waves, the determination of generator saturation harmonics is extremely difficult and requires a knowledge of the paths dimensions and the magnetic characteristics of the material at every point in the circuit. The direct and quadrature saturation curves, which are normally used to calculate the excitation requirement and values of saturated reactances, cannot be used to determine the harmonics produced by saturation. This is because these saturation curves only indicate the rms values of the terminal voltages (and thus also of air gap flux), but not the shape of the flux waves.

A couple attempts have been carried out to model saturation harmonics in the synchronous generator by Xu *et al.* [1991] and Medina and Arrillaga [1994]. However as the d-, q-axis, or both axes saturation curves are used to derive the harmonic content, these models will give inaccurate results. Moreover in the latter model, the harmonic currents produced are assumed to be proportional to a fundamental magnetising current on the stator (analogous to transformer saturation modelling) which is virtually non-existent

since most, if not all, of the magnetising current is flowing in the rotor electrical circuit. This is because the dc resistance of the rotor circuit is much lower than the impedance of the stator circuit at fundamental frequency, and the amount of magnetising current in each circuit is inversely proportional to the impedance of the circuit. Consequently, these approaches are unsuitable for generator saturation harmonics modelling.

Although it is not straightforward to model saturation harmonics, it is possible to estimate them and examine their effects.

Stator harmonic voltages due to saturation

Since the waveform of the air gap flux is repeated pole after pole, saturation harmonics are odd-order harmonics, and the generator acts as harmonic voltage sources under saturation. When a flat-topped air gap flux wave rotates in a machine, its shape remains unchanged because of the symmetry of the magnetic structure. This means that there is no relative motion among the fundamental and all harmonic flux waves. In other words, all the harmonic flux waves rotate at the same speed and in the same direction as the fundamental. The harmonic fluxwaves induce odd harmonic voltages in the stator winding and harmonic currents on the line if there is a path for them to flow. Note that there are no harmonic currents on the rotor due to saturation directly since rotor harmonic currents would produce pulsating mmfs rather than space (or stationary) harmonic waves, and the rotor is rotating at the same speed as the armature mmf wave. In the induction motor case, harmonic currents are induced in the rotor due to the slip speed differential.

Rigorous analysis of saturation harmonics of polyphase induction machines by Lee [1961] concluded that the saturation harmonic content is low even though its magnetic circuit is highly saturated, and it is because the saturation of the cores partly offsets the flattening effect of teeth saturation. Quantitatively, the 3rd, 5th and 7th harmonic components of a flat-topped flux-wave in the highly saturated 18kVA induction machine are approximately 6-8%, 4% and 3% of the fundamental respectively [Lee 1961], [Zagradisnik and Hribernik 1988].

Since an accurate analysis of generator harmonics required machine physical characteristics and in the absence of information on synchronous generator saturation harmonics, the induction motor case is used here as the worst case for synchronous generators in terms of saturation harmonics. Synchronous generators are usually larger in physical size, thus normally saturate less than induction motors.

In synchronous generators, the distributed winding and slot pitch factors (k_d and k_p respectively), which are used to suppress space harmonics (particularly the 5th and 7th) [Say 1983] [McPherson and Laramore 1990], will also suppress saturation harmonics since they both are of the same type of harmonics that rotate at the same speed as the fundamental. Harmonic voltages are therefore only a fraction of the harmonic fluxes.

A typical value of k_d and k_p for 5th harmonics is 0.259 for a coil pitch of 150^o, thus the 5th harmonic voltage is only 6.7% ($= k_d k_p$) of the 5th harmonic component of the flat-topped flux wave, i.e. $V_5 = 0.0027$ p.u. in this case.

The third and triplen voltage harmonics are of zero-sequence, thus regardless of whether the machine is connected in wye or delta, no third harmonic voltage will appear at the line terminals. In normal system connections, the stator connection is wye-grounded and the generators are connected to the transmission system through a delta-star/grounded transformer, and thus no third harmonic current can flow. Consequently, the only effect of the triplen voltage harmonics is an increase in the generator insulation requirement.

For the 5th, 7th, 11th, 13th, etc. harmonic orders, the amount of harmonic current flowing in the stator due to saturation is dependent on the external network connections and harmonic impedances of the circuit. They can be obtained from a harmonic penetration study. However given the small harmonic voltage levels involved, the stator harmonic currents due to saturation are insignificant. Therefore, the harmonics produced by generator saturation can be ignored in synchronous generator steady state studies.

3.6 MODEL VALIDATION

The proposed formulation for the generator harmonic impedances is validated against a time domain simulation for the test system of Figure 3.8 using the PSCAD2-EMTDC program [Woodford *et al.* 1983]. The generator parameters, based on Hwang [1969] and saturation characteristics are listed in Appendix A. The salient-pole generator in the PSCAD2 program takes into account the direct-axis saturation, but does not include the cross saturation effects where the direct-axis saturation changes quadrature-axis parameters. As a result, the quadrature-axis synchronous reactance and thus the rotor angle are unchanged under saturation. In this case, equation 3.38 can be used to calculate rotor angle under saturated condition. Due to the insignificant effect of saturation harmonics, they are not modelled in the PSCAD2 program, thus are neglected in the validation process.

10% of negative-sequence harmonic currents of fundamental, 5th and 9th order were injected simultaneously to the generator bus. Due to the generator saliency, positive-sequence 3rd, 7th and 11th voltages are produced. Having run the simulation to steady state, an FFT was performed over one fundamental cycle of the voltage and current waveforms to obtained their harmonic contents, and the results were compared with those calculated in the harmonic domain.

The time domain solution serves to verify the harmonic analysis if upon comparison a close agreement is found in the terminal voltages. This is clearly the case, as illustrated

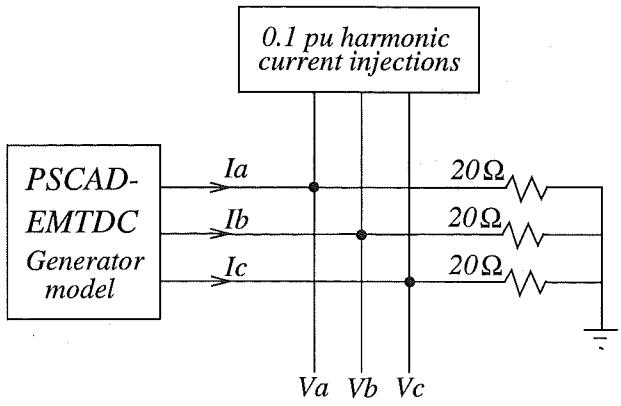

Figure 3.8 Test system for model validation.

by the results in Figure 3.9. Close agreement of phase angles as well as magnitudes indicates that the generator impedances, including the saliency effect, have been accurately modelled. It was found necessary to use a time step of 5μs, and to simulate for 700 fundamental frequency cycles to allow transients to decay. Therefore the analytical generator model in the harmonic domain is very efficient computationally in comparison with the time domain for analysing harmonic behaviour.

One of the objectives of the harmonic measurements carried out at the Benmore convertor station in 1995 when being operated as a group connected unit was to provide information for possible validation of the generator harmonic model. Three-phase harmonic measurements of a generator currents and its terminal voltages were obtained. From measured harmonic voltages and currents, generator harmonic impedances at the characteristic harmonics $12n \pm 1$ such as self terms and cross-coupling terms are obtained by using the developed saliency formulation. The derivation of the harmonic impedances in the presence of saliency from the measured harmonic voltages and currents is described in Appendix B. The results are shown in Figure 3.10 together, for comparison, with those derived from the model using the given generator parameters, listed in Appendix A2. At the 11th and 13th harmonic orders which have the largest harmonic voltages and currents (thus the data is most reliable), close agreement has been obtained. The harmonic impedance trends are also consistent, particularly the cross-coupling terms due to saliency. Thus the harmonic measurements also serve to validate the developed generator saliency formulation.

3.7 LEVELS OF HARMONIC IMPEDANCES

An indication of the relative importance of the self and cross coupling harmonic impedances is given in Figure 3.11 for a test machine, using the parameters given in Appendix A1. The rotor angle is 2^o for the circuit shown in Figure 3.8. Since the

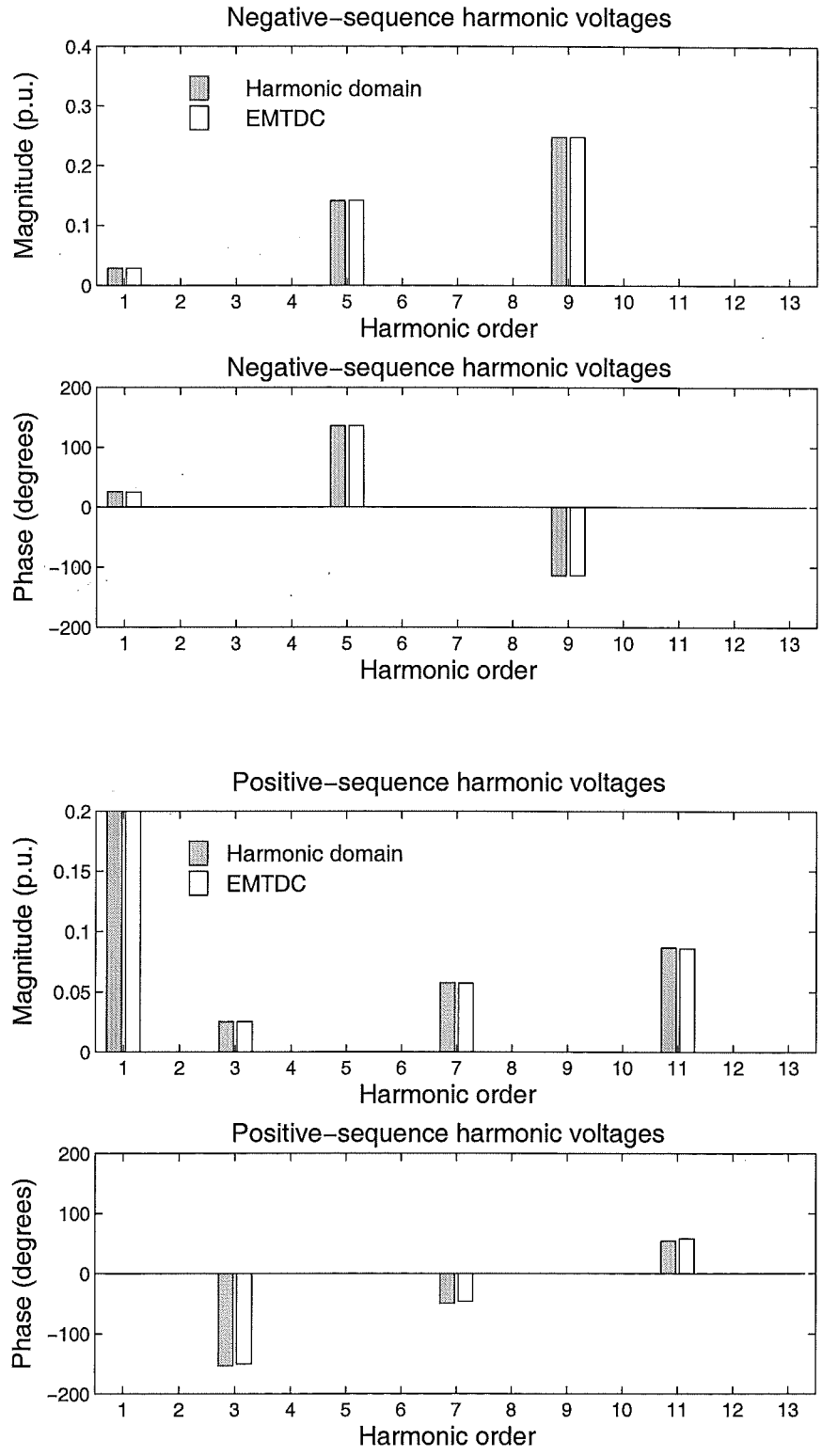

Figure 3.9 Model validation by comparison of time and harmonic domain solutions for harmonic current injections.

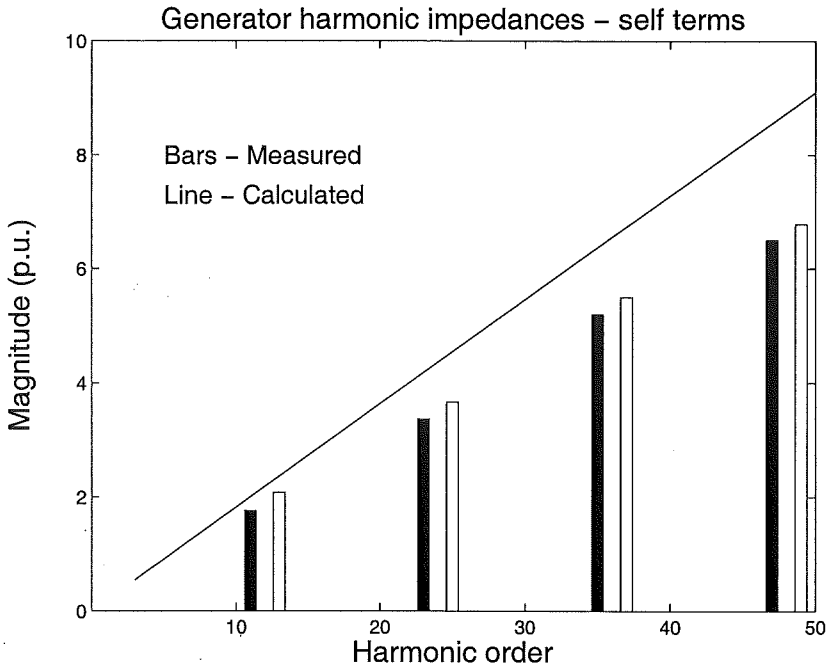

(a)

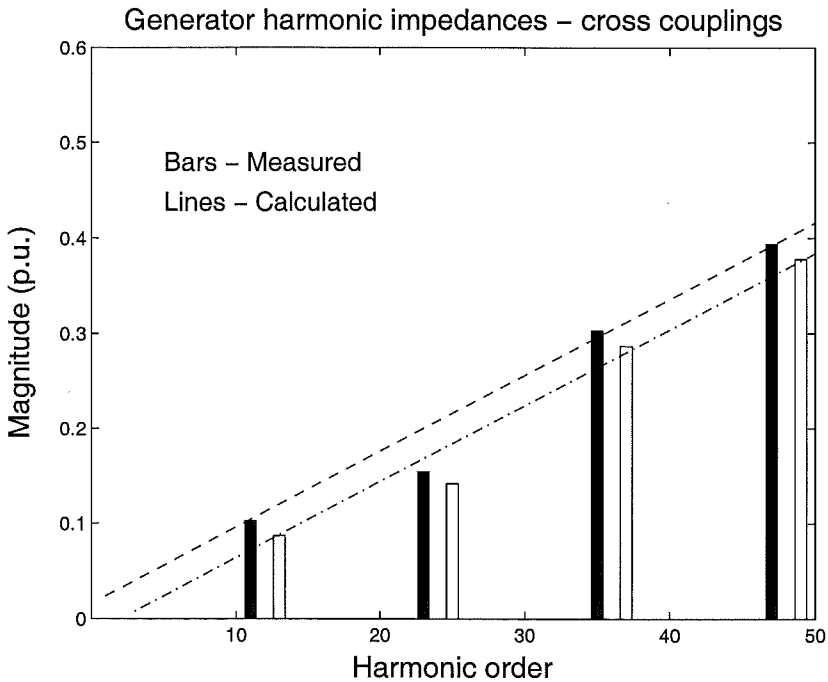

(b)

Figure 3.10 Generator harmonic impedances obtained from the measurement and calculation. (a) Self harmonic impedance terms, (b) *Dashed-dashed* line and filled bars are the cross coupling terms from negative-sequence k to positive-sequence $k+2$, and *dashed-dotted* line and unfilled bars are the cross coupling terms from positive-sequence k to negative-sequence $k-2$.

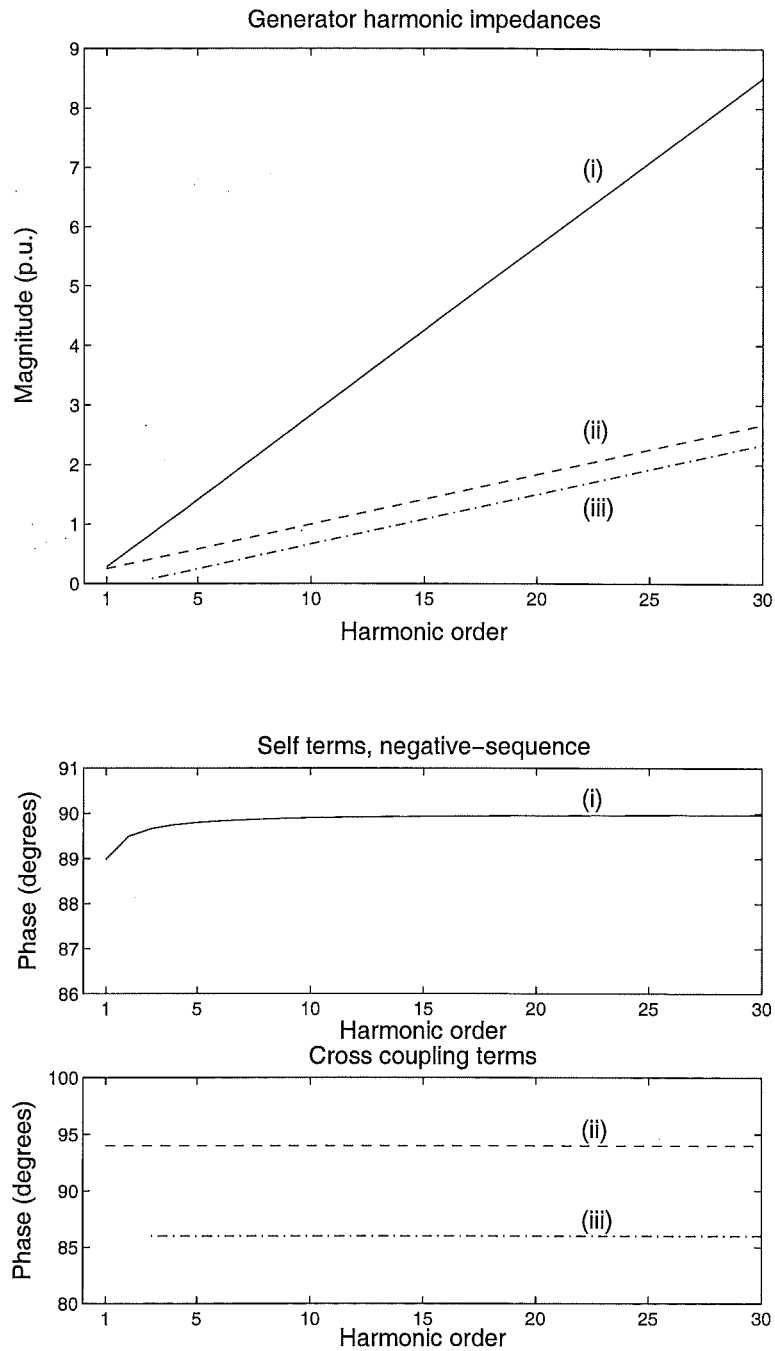

Figure 3.11 Generator harmonic impedances for a particular loading, $\delta = 2$ electrical degrees, where (i) Self terms - Negative-sequences; (ii) Cross couplings - Negative to positive-sequences; (iii) Cross couplings - Positive to negative-sequences.

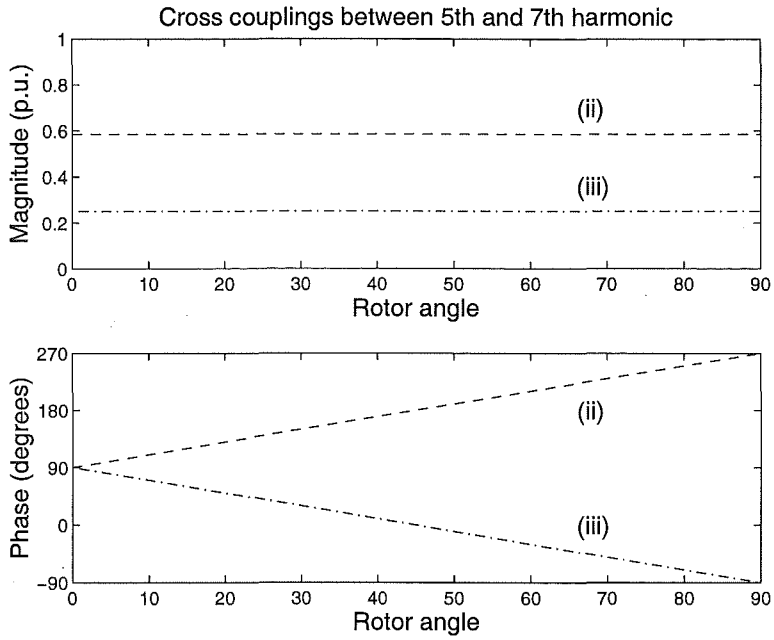

Figure 3.12 Magnitude and phase angle of cross coupling terms for various loadings, where (ii) Negative to positive-sequences couplings; (iii) Positive to negative-sequences couplings.

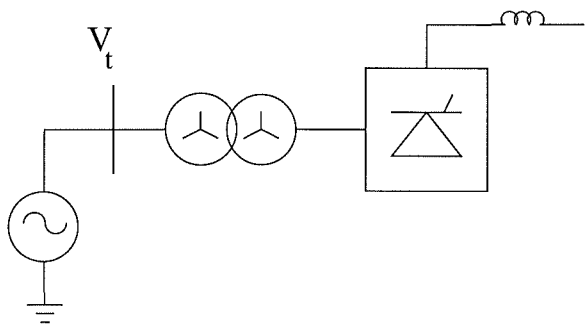

Figure 3.13 Generator-transformer-convertor unit.

magnitudes and phase angles of the harmonic self impedances, apart from the fundamental frequency, are the same for both positive and negative-sequence, only the latter is shown. The contribution of the resistance is negligible in comparison with the reactance at high harmonic orders. The magnitude of the cross coupling terms due to saliency are roughly 30% of the self impedances for this test generator.

Under a steady state operating condition, the phase angles of the cross couplings from one sequence to another are the same for all harmonics. However these will vary as a function of the rotor angle δ for various loadings, as illustrated in Figure 3.12. On the other hand, the magnitude of a particular cross coupling term does not change with the rotor angle.

The effect of rotor angle on the cross couplings is emphasized in the case of a direct connection of generators to HVdc convertors. In a simple system consisting of a

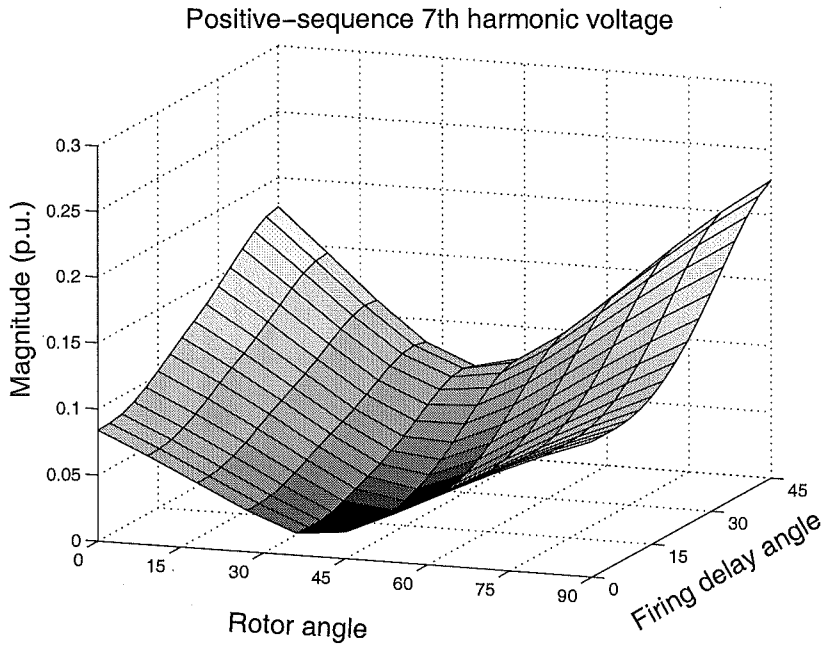

Figure 3.14 Variation of the 7th harmonic voltage in relation to the rotor angle and firing delay angle.

single generator-transformer-convertor unit, shown in Figure 3.13, an approximate direct solution for harmonic voltages can be obtained by modelling the convertor as a fixed injection of characteristic harmonic currents, and the dc current is assumed to be ripple free. Under these conditions, the commutation angle and harmonic currents can be calculated using the simplified convertor formulation [Arrillaga 1983]. The calculation is shown in Appendix E and the results are used here.

Because of saliency, each $6k+1$ positive-sequence voltage is made of two components due to the corresponding positive-sequence $6k+1$ and negative-sequence $6k-1$ currents. Thus the harmonic voltages are dependent on the phase angle difference between the currents as well as the rotor angle. Given the fundamental terminal voltage, dc current, commutation reactance and firing angle, characteristic harmonic currents can be calculated.

As an example to illustrate the rotor angle effect on saliency, the 7th harmonic voltage can be approximated by injecting negative-sequence 5th and positive-sequence 7th currents, calculated using the simplified convertor formulation, into a salient-pole machine with varying rotor angle. The machine parameters are listed in Appendix A1. With 1 p.u. terminal voltage, fundamental current and 5% transformer leakage reactance, the 7th voltage variation is shown in Figure 3.14. The commutating reactance was estimated as the sum of transformer leakage and the average of the direct and quadrature axis subtransient reactances. It is clear that the position of the rotor and the firing delay angle do have significant effects on the harmonic voltages. It is observed that for rotor angle less than 45^o, the 7th voltage is reduced with increasing rotor angle.

Consequently, any harmonic model for saliency that does not take into account the rotor angle (i.e. zero rotor angle is assumed) will likely to over-estimate the 7th harmonic voltage levels.

In practice, ac voltage harmonics and dc current ripple do influence harmonic currents, thus detailed harmonic interaction around a convertor is required to accurately predict the commutation periods as well as ac and dc terminal harmonic distortions. More detailed investigation of the saliency effect is carried out in Chapter 5 and 6.

3.8 CONCLUSIONS

A synchronous generator model in the Harmonic Domain has been developed. The model uses a harmonically coupled impedance matrix which takes into account the effects of saturation and the stator-rotor frequency conversion phenomenon due to saliency. It has been found that the harmonic cross couplings vary as a function of the generator rotor angle, whereas the generator harmonic self impedances, except the fundamental positive-sequence impedance, are independent of rotor angle. The importance of rotor angle in the saliency effect has been highlighted in the case of a direct connection of generators to AC/DC convertors in which harmonic voltages vary not only with the firing angle but also the rotor angle.

Without saturation effects, the relationship between the generator terminal voltages and currents in the presence of saliency can be represented by analytical expressions in sequence components. The expressions are derived from normally available machine parameters such as direct and quadrature-axis subtransient reactances. As a result, this analytical model is a powerful tool for a fast and accurate prediction of the harmonic levels on the generator terminals in the presence of saliency and distortion.

Saturation in the machine air gap flux reduces the rotor angle which leads to changes in the cross coupling terms for all harmonics. The self impedance terms are not affected by saturation as they are solely dependent upon the subtransient reactances which are constant since they are associated with fast transient flux that flows mostly in air. Magnetic saturation also produces odd order harmonics due to the distortion of the airgap flux wave. However saturation harmonics are small and can be ignored from synchronous generator steady state studies.

The variation of generator air gap subtransient inductance has been approximated by a second harmonic term described by Park's equations, which have also been used extensively in other computer models. Alternatively, generator impedance can be obtained by using a more rigorous analysis such as Finite Element Analysis. However this is a computationally intensive and labourious process. The subtransient inductance has also been assumed to be invariant for harmonic frequencies. Accurate inductance values at harmonic frequencies can be obtained through test measurements and they can be

readily taken into account at each interested harmonic in the harmonic domain model.

The generator harmonic model has been validated against time domain simulations and results from harmonic measurements of a group connected unit.

Chapter 4

CONVERTOR ANALYSIS IN THE HARMONIC DOMAIN

4.1 INTRODUCTION

Essential to the Unit Connection model is the analysis of harmonic transfers across the convertor. Of all the available convertor models in the Harmonic Domain, reviewed in Chapter 2, the harmonic transfer analysis most suitable for a unified iterative solution was developed by Smith *et al.* [1995].

This model consists of a general set of non-linear equations that fully describes the harmonic transfers through the convertor in the steady state. The formulation convolves periodic sampled quantities in the harmonic domain with their sampling functions, so that no Fourier transform is required. The sampling functions are defined in terms of the exact switching instants, which are obtained as part of the overall iterative procedure that accurately models the effect of ac voltage and dc current distortion on the valve conduction periods. Distortions and unbalance are taken into account in the analysis of the switching instants.

As thorough understanding of the convertor is neccessary to the overall Unit Connection, the convertor harmonic domain model is summarized in this chapter.

4.2 COMMUTATION ANALYSIS FOR A UNIFIED ITERATIVE SOLUTION

In the absence of ac harmonic filters at the generator terminal in the case of direct connected units, the ideal sinusoidal commutation voltage moves inside the generator and the commutating reactance consists of the transformer leakage reactance and generator subtransient reactance. However since generator subtransient reactance varies with rotor angle due to saliency, an iterative solution for the commutation process is necessary. By choosing the generator terminal voltages as *pseudo-commutation voltages*, which can be unbalanced or contain harmonic distortion, the effect of the varying generator subtransient reactance and transformer leakage reactance can be considered separately in the iterative solution. Given the generator terminal voltage as a pseudo-commutation

voltage, the convertor harmonic currents can be obtained from the commutation analysis, to be described in Sections 4.2.1 and 4.2.2, in which the reactances are solely the transformer leakage reactances. The generator terminal voltages are then updated by injecting the convertor harmonic currents into the generator harmonic impedance as derived in Chapter 3.

In general, the ac terminal voltages and convertor transformer reactance are no longer the ideal sinusoidal commutation voltages and commutation reactance in the presence of distortion on the ac terminal. The commutation reactance consists of the transformer leakage and a portion of the ac system reactance, which may contain phase-dependent or frequency-dependent components. In such cases, the following commutation analysis can also be used, and the ac terminal voltages can be chosen as pseudo-commutation voltages in the iterative solution so that the reactance in the commutation analysis consists of solely the transformer leakage reactance.

Two separate analyses of the commutation process are given in this section. One for a bridge connected to a star/star transformer, and the other for a bridge connected to a star-g/delta transformer. Commutation reactances can be unbalanced between the phases. The result of this commutation analysis is a set of non-linear equations that can be solved to find the exact end of commutation angles given distortions on the ac and dc terminals. The presence of resistance in the commutation circuit complicates the analysis, however when the interaction of the convertor with generators or ac system is solved, the effect of commutation resistance can be accounted for by placing it between the ac system terminal and the convertor transformer primary windings.

4.2.1 Star Connection Analysis

The commutation circuit is shown in Figure 4.1, where V_a, V_b, I_c and I_d are sums of harmonic phasors. In this diagram phase a is commutating off, while phase b is commutating on. The commutation ends when $I_c = I_d$.

Summing voltage drops around the commutating current loop at harmonic order k yields

$$V_{ak} + jkX_aI_{ck} - jkX_aI_{dk} + jkX_bI_{ck} - V_{bk} = 0, \tag{4.1}$$

from which the commutation current can be obtained:

$$I_{ck} = \frac{jkX_aI_{dk} - V_{abk}}{jk(X_a + X_b)}, \tag{4.2}$$

where $V_{abk} = V_{ak} - V_{bk}$.

Using the harmonic coefficients derived in 4.2, the periodic commutation current in

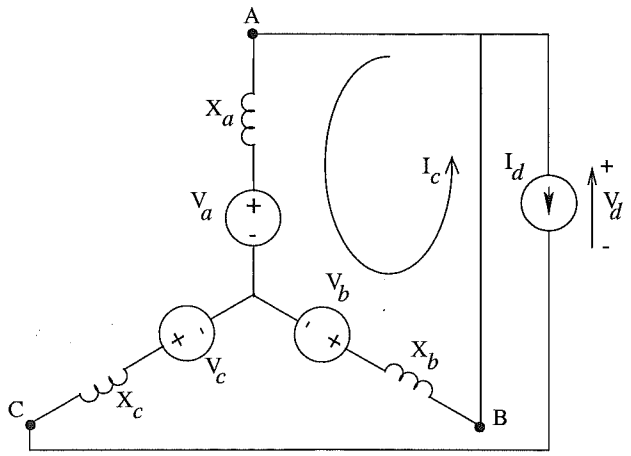

Figure 4.1 Circuit for star-g/star commutation analysis.

the time domain is expressed as

$$I_c(t) = D + \mathcal{I}\left\{\sum_{k=1}^{n_h} I_{ck} e^{jkwt}\right\}, \tag{4.3}$$

where

$$D = -\mathcal{I}\left\{\sum_{k=1}^{n_h} I_{ck} e^{jk\theta_i}\right\}. \tag{4.4}$$

D ensures that the steady state commutation current is zero at the instant of firing, θ_i. For incorporation into Newton's method, equation 4.3 is written as a steady state mismatch equation. The mismatch is the current in the valve that is commutating off, which at the end of the commutation should be zero. This is obtained by substituting $wt = \phi_i$ into equation 4.3 and taking the difference between the dc and commutation current. For the ith commutation

$$F_{\phi i} \stackrel{\text{def}}{=} \mathcal{I}\left\{j(I_{d0} - D) + \sum_{k=1}^{n_h}(I_{dk} - I_{ck}) e^{jk\phi_i}\right\} = 0. \tag{4.5}$$

I_{d0} and I_{dk} denote dc and harmonic components of the dc current respectively. It is evident from this analysis that the dc current ripples do affect the duration of the commutation.

4.2.2 Delta Connection Analysis

The objective is to solve for the commutation current I_c in terms of the voltage and current sources, as shown in Figure 4.2. Using phasor analysis, the following nodal and

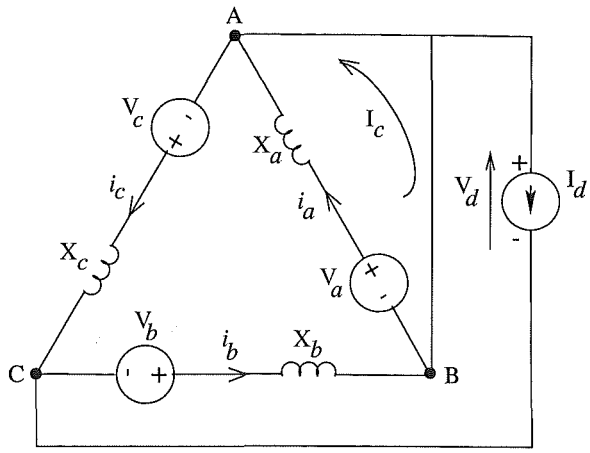

Figure 4.2 Circuit for star-g/delta commutation analysis.

mesh equations can be obtained for this circuit at each harmonic k:

$$\begin{aligned} I_{dk} - I_{ck} + i_{ck} - i_{ak} &= 0 && (4.6)\\ I_{ck} + i_{ak} - i_{bk} &= 0 && (4.7)\\ I_{dk} + i_{ck} - i_{bk} &= 0 && (4.8)\\ V_{ak} - ji_{ak}X_{ak} &= 0 && (4.9)\\ V_{bk} - ji_{bk}X_{bk} - V_{dk} &= 0 && (4.10)\\ V_{ck} - ji_{ck}X_{ck} + V_{dk} &= 0, && (4.11) \end{aligned}$$

where $X_k = kX_1$. The commutation current is obtained by combining equations 4.6, 4.8, 4.9 and 4.10

$$I_{ck} = -\frac{V_{ak}}{jX_{ak}} + \frac{V_{bk} - V_{dk}}{jX_{bk}} \tag{4.12}$$

The dc voltage during the commutation is obtained from equations 4.6, 4.7, 4.10 and 4.11

$$V_{dk} = \frac{V_{bk}X_{ck} - V_{ck}X_{bk} - jI_{dk}X_{bk}X_{ck}}{X_{bk} + X_{ck}} \tag{4.13}$$

A similar analysis holds for every separate commutation, with appropriate modifications to the phase subscripts, and the direction of the dc current. The end of commutation mismatch equation for the star-g/delta connection is obtained as for the star-g/star connection above.

4.3 CONVERTOR CONTROL AND FIRING PROCESS

4.3.1 Firing Process

Equi-distant firing control is normally employed in modern HVdc scheme. The firing controller consists of a phase locked oscillator (PLO) tracking the fundamental component of the terminal voltage and generating essentially equi-spaced timing references. A well designed PLO is unaffected by harmonics in the terminal voltage as its time constant should be in the same order as the fundamental. Consequently, the PLO is not modelled, and the timing pulses are assumed perfectly equidistant, spaced by 60^o. The effect of a non-ideal PLO would be to introduce uncharacteristic ac current harmonics [Arrillaga 1983].

4.3.2 Constant Current Control

The result of this analysis is a set of non-linear equations that can be solved to find the exact firing instant given distortions on the dc terminals.

The controller described here is a PI constant current control, as shown in Figure 4.3, which will response to harmonics in the dc current.

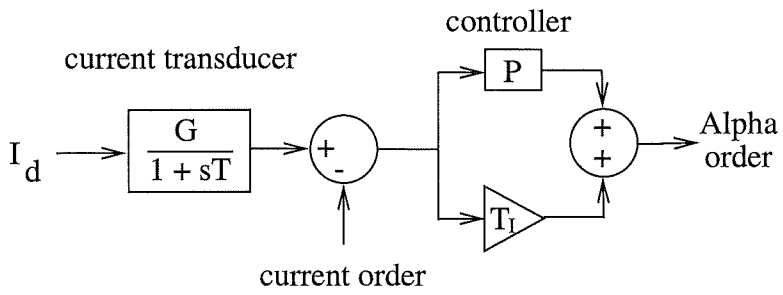

Figure 4.3 Constant current controller.

The alpha order can be expressed as a sum of harmonic phasors

$$\alpha = \mathcal{I}\left\{ j\alpha_0 + \sum_{k=1}^{n_k} \alpha_k e^{jkwt} \right\}, \tag{4.14}$$

where

$$\alpha_k = \frac{G}{1 + jkwT}\left(P + \frac{1}{jkwT_I}\right) I_{dk}. \tag{4.15}$$

A firing instant occurs when the elapsed angle β from a timing pulse is equal to the

instantaneous value of the alpha order:

$$\begin{aligned}\theta_i &= \alpha + \beta_i \\ &= \beta_i + \alpha_0 + \mathcal{I}\left\{\sum_{k=1}^{n_k} \alpha_{ik} e^{jk\theta_i}\right\}. \end{aligned} \tag{4.16}$$

The mismatch equation for the firing instants are therefore:

$$F_{\theta i} \stackrel{\text{def}}{=} \mathcal{I}\left\{j(\alpha_0 + \beta_i - \theta_i) + \sum_{k=1}^{n_k} \alpha_{ik} e^{jk\theta_i}\right\} = 0. \tag{4.17}$$

In the steady state, the dc component of the alpha order, α_0, takes on a value that causes the dc component of the dc current to be equal to the current order. Thus the constant current control mismatch equation is defined as

$$F_{\alpha 0} \stackrel{\text{def}}{=} (V_{d0} - E_d)Y_{d0} - I_{d0} = 0. \tag{4.18}$$

4.3.3 Constant Power Control

The constant power controller calculates and passes a current order to the current controller that leads to the rectified power being the power order for the link. The time constant of the power controller is assumed to be long enough that it is unresponsive to harmonics in the instantaneous dc power. The power controller is therefore modelled as

$$P_{measured} - P_{order} = 0. \tag{4.19}$$

The measured power is the constant component of the convolution of the measured dc voltage with the measured dc current, where the measured quantity is a harmonic weighting of the actual quantity due to the linear frequency response of the measurement transducer:

$$I_{dk}^m = C_{Ik} I_{dk}, \tag{4.20}$$

$$V_{dk}^m = C_{Vk} V_{dk}, \tag{4.21}$$

and

$$P_{measured} = \mathcal{I}\left\{\frac{1}{2} j \left[\sum_{l=0}^{n_k} (V_{dl}^m I_{dl}^{m*} - 2j(V_{d0}^m I_{d0}^m)\right]\right\}. \tag{4.22}$$

Normally the harmonics contribute little to the real power, and the measured power

can be simplified to:

$$P_{measured} = V_{d0} I_{d0}. \tag{4.23}$$

For a 12-pulse convertor, phasor analysis results in 25 simultaneous non-linear mismatch equations in the same number of variables that fully specify the state of the convertor as a function of the terminal harmonics. The 25 variables are the 12 firing instants, the 12 end of commutation instants and the dc component of the alpha order, α_0. Although perfect equidistant firing is assumed, the actual firing instants are not equi-spaced due to the current controller response to dc ripple. The end of commutation angles are also unbalanced as a result of ac voltage and dc ripple harmonics.

4.4 DIRECT VOLTAGE

A six pulse bridge has twelve states per cycles. Six of these are commutation states and six are normal conduction states. During normal conduction the positive and negative rails of the dc side are connected to the ac side via two conducting thyristors.

Each state can readily be modelled by a linear circuit which has no initial transient. For instance, during phase a to phase b commutation, the circuit is as shown in Figure 4.1.

The result is 12 harmonic spectra, one for each state and valids for the appropriate conduction interval only. In order to obtain a single spectrum which is valid for one complete cycle of dc voltage, the harmonic spectra are convolved with the spectrum of a periodic square pulse that has value of one during the corresponding conduction interval, and a value of zero everywhere else. The sum of generated spectra resulted from the convolution is the spectrum of dc voltage across the convertor.

4.4.1 Star Connection Voltage Samples

During normal conduction the dc voltage is readily obtained as the appropriate phase to phase voltage minus the voltage drops across the commutating reactances. Thus for a harmonic k

$$V_{dpk} = V_+ - V_- - jwk(L_+ + L_-)I_{dk}. \tag{4.24}$$

where p is the conduction interval number.

During a commutation on the positive rail, analysis of Figure 4.1 yields

$$V_{dpk} = \frac{L_e V_{bk} + L_b(V_{ek} - jkwL_e I_{dk})}{L_e + L_b} - V_{ok} - jkwL_o I_{dk}, \tag{4.25}$$

and

$$V_{dpk} = +V_{ok} - jkwL_oI_{dk} - \frac{L_eV_{bk} + L_b(V_{ek} - jkwL_eI_{dk})}{L_e + L_b} \tag{4.26}$$

for a commutation on the negative rail, where e refers to phase ending conduction, b to a phase beginning conduction, and o to the other phase.

From the know conduction pattern in each of the twelve states, equations 4.24, 4.25 and 4.26 are used to assemble the twelve samples of the dc voltage. These samples are summarized in table 4.1.

sample (p)	Phase currents			DC Voltage V_{dp}					
	A	B	C	b	e	o	+	-	eqn
1	I_{c1}	$-I_d$	$I_d - I_{c1}$	A	C	B			4.25
2	I_d	$-I_d$	0				A	B	4.24
3	I_d	$-I_{c2} - I_d$	I_{c2}	C	B	A			4.26
4	I_d	0	$-I_d$				A	C	4.24
5	$I_d - I_{c3}$	I_{c3}	$-I_d$	B	A	C			4.25
6	0	I_d	$-I_d$				B	C	4.24
7	I_{c4}	I_d	$-I_d - I_{c4}$	A	C	B			4.26
8	$-I_d$	I_d	0				B	A	4.24
9	$-I_d$	$-I_{c5} + I_d$	I_{c5}	C	B	A			4.25
10	$-I_d$	0	I_d				C	A	4.24
11	$-I_d - I_{c6}$	I_{c6}	I_d	B	A	C			4.26
12	0	$-I_d$	I_d				C	B	4.24

Table 4.1 Construction of dc voltage and ac phase current samples.

4.4.2 Delta Connection Voltage Samples

The dc voltage during a particular commutation has been derived in section 4.2.2. The general result is

$$V_{dpk} = P_{apk}V_{ak} + P_{bpk}V_{bk} + P_{cpk}V_{ck} + P_{dpk}I_{dk}, \tag{4.27}$$

where $p = 1, 3, 5, 7, 9, 11$. The coefficient matrix P is constant, and need only be calcu-

lated once. During a commutation on the positive rail

$$P_{epk} = \frac{X_{co}}{X_{co} + X_{ce}} \tag{4.28}$$

$$P_{opk} = \frac{-X_{ce}}{X_{co} + X_{ce}} \tag{4.29}$$

$$P_{bpk} = 0 \tag{4.30}$$

$$P_{dpk} = \frac{-jkX_{co}X_{ce}}{X_{co} + X_{ce}}, \tag{4.31}$$

where if $i \in \{1 \cdots 6\}$ is the number of a commutation on the positive rail, $p = 2i - 1$, then the subscripts $\{b, e, o\}$ are permutation of $\{a, b, c\}$ according to i. A similar result holds for a commutation on the negative rail.

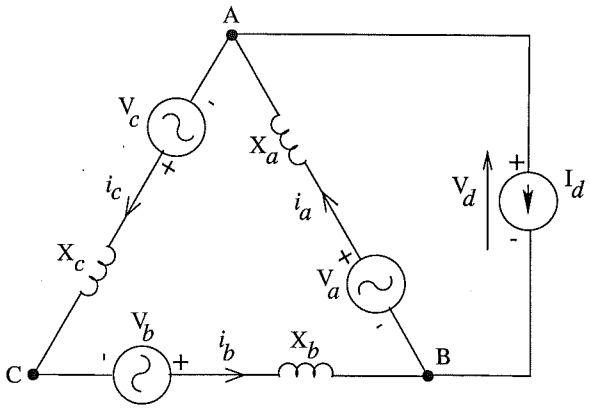

Figure 4.4 Circuit for a conduction period with a delta connected source.

During a normal conduction period all three phases of the voltage source contribute to the dc voltage, as illustrated in Figure 4.4 for a particular conduction period. This circuit is analysed by writing nodal and loop equations at harmonic k:

$$i_{ak} - i_{ck} - I_{dk} = 0 \tag{4.32}$$

$$I_{dk} - i_{ak} + i_{bk} = 0 \tag{4.33}$$

$$i_{ck} = i_{bk} \tag{4.34}$$

$$V_{ak} - ji_{ak}X_{ak} - V_{dk} = 0 \tag{4.35}$$

$$V_{bk} - ji_{bk}X_{bk} + V_{dk} + V_{ck} - ji_{ck}X_{ck} = 0, \tag{4.36}$$

then the dc voltage sample at harmonic k is solved:

$$V_{dk} = \frac{(V_{ak} - jX_{ak}I_{dk})(X_{bk} + X_{ck}) - X_{ak}(V_{bk} + V_{ck})}{X_{ak} + X_{bk} + X_{ck}}. \tag{4.37}$$

As for the star connected source, the solution for the dc voltage samples is generalized

over all twelve conduction periods into a matrix of coefficients of the ac and dc sources, i.e.

$$V_{dlk} = P_{alk}V_{ak} + P_{blk}V_{bk} + P_{clk}V_{ck} + P_{dlk}I_{dk}, \tag{4.38}$$

where $l = 2, 4, 6, 8, 10, 12$.

4.4.3 DC Voltage Construction by Convolution

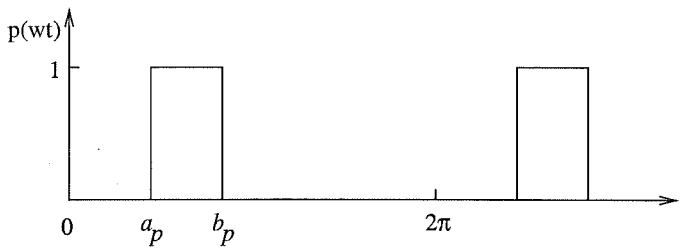

Figure 4.5 Sampling functions used in convolution.

The dc voltage spectrum is constructed by convolving each of the twelve voltage samples (expressed as a function of dc and ac sides sources) with a square pulse sampling function, as illustrated in Figure 4.5. The square pulse is periodic at the fundamental frequency and delimited alternatively by the firing and end of commutation angles as listed in table 4.2. The convolution described here is of positive frequency only, thus generates phase conjugated terms.

The Fourier coefficients of the sampling function are:

$$\begin{aligned} a_k &= \frac{1}{\pi}\int_0^{2\pi} p(wt)\cos(kwt)dwt \\ &= \frac{1}{\pi}\int_{a_p}^{b_p} \cos(kwt)dwt \\ &= \frac{1}{k\pi}\sin(kwt)\Big|_{a_p}^{b_p} \\ &= \frac{1}{k\pi}[\sin(kb_p) - \sin(ka_p)], \end{aligned} \tag{4.39}$$

and

$$\begin{aligned} b_k &= \frac{1}{\pi}\int_0^{2\pi} p(wt)\sin(kwt)dwt \\ &= -\frac{1}{k\pi}\cos(kwt)\Big|_{a_p}^{b_p} \\ &= \frac{1}{k\pi}[\cos(ka_p) - \cos(kb_p)] \end{aligned} \tag{4.40}$$

The complex Euler coefficient for the sampling function at harmonic k is

$$\begin{aligned}\Psi_{pk} &= b_k + ja_k \\ &= \frac{1}{k\pi}[cos(ka_p) - cos(kb_p)] + j\frac{1}{k\pi}[sin(kb_p) - sin(ka_p)], \qquad (4.41)\end{aligned}$$

$$\Psi_{po} = \begin{cases} j\frac{b_p - a_p}{2\pi} & b_p > a_p \\ j\left[1 - \frac{a_p - b_p}{2\pi}\right] & otherwise \end{cases} \qquad (4.42)$$

sample (p)	a_p	b_p
1	θ_1	ϕ_1
2	ϕ_1	θ_2
3	θ_2	ϕ_2
4	ϕ_2	θ_3
5	θ_3	ϕ_3
6	ϕ_3	θ_4
7	θ_4	ϕ_4
8	ϕ_4	θ_5
9	θ_5	ϕ_5
10	ϕ_5	θ_6
11	θ_6	ϕ_6
12	ϕ_6	θ_1

Table 4.2 Limits of convertor states for use in sampling functions.

Since the end of one conduction interval is the beginning of the next, all of the trigonometric evaluations are used in two consecutive sampling functions, thus halving the number of calculations. The dc voltage can now be expressed as

$$V_d = \sum_{p=1}^{12} V_{dp} \otimes \Psi_p. \qquad (4.43)$$

The convolution of two phasors is given by

$$A_k \otimes B_l = \begin{cases} \frac{1}{2}j(A_k B_l^*)_{(k-l)} - \frac{1}{2}j(A_k B_l)_{(k+l)} & if\ k \geq l \\ \frac{1}{2}j(A_k B_l^*)^*_{(l-k)} - \frac{1}{2}j(A_k B_l)_{(k+l)} & otherwise \end{cases} \qquad (4.44)$$

as described in Appendix D.

The conjugate operator makes the convolution non-analytic, and so not differentiable in the complex form. It avoids the need for negative harmonics however, and it is still possible to obtain partial derivatives by decomposing into real and imaginary parts. the

sampling function spectra must be evaluated up to $2n_h$ as is required to calculate voltage harmonics up to n_h. Since the convolution operator is linear, the twelve convolutions in equation 4.43 can be decomposed into convolutions of the component phasors:

$$V_{dp} \otimes \Psi_p = \sum_{k=1}^{n_h} \sum_{l=0}^{2n_h} V_{dpk} \otimes \Psi_{pl}. \tag{4.45}$$

This equation generates voltage harmonic components of order above n_h which are discarded. By using equations 4.43, 4.44 and 4.45, the kth harmonic phasor component of V_d is

$$V_{dk} = \frac{1}{2} j \sum_{p=1}^{12} \left\{ \sum_{l=k}^{n_h} (V_{dp_l} \Psi^*_{p_{l-k}}) + \sum_{l=0}^{n_h} (V_{dp_l} \Psi^*_{p_{l+k}})^* - \sum_{l=0}^{n_h} (V_{dp_l} \Psi^*_{p_{k-l}}) \right\} , k > 0 \tag{4.46}$$

$$V_{d0} = \frac{1}{2} j \sum_{p=1}^{12} \left\{ \sum_{l=0}^{n_h} (V_{dp_l} \Psi^*_{p_l}) - 2j(V_{dp_0} \Psi_{p_0}) \right\} \tag{4.47}$$

This completes the derivation of the dc voltage harmonics in terms of a dc side harmonic source and a three phase ac side voltage source connected in star or delta, with source inductance.

4.5 SECONDARY PHASE CURRENT

The derivation of the dc voltage involves the convolution of twelve different dc voltage samples, so by using the same sampling functions, 36 convolutions would be required to obtain the three phase currents. However referring to table 4.1, and using the linearity of the convolution, the phase a secondary current can be written as:

$$\begin{aligned} I_a = \; & I_d \otimes \{\Psi_2 + \Psi_3 + \Psi_4 + \Psi_5 - \Psi_8 - \Psi_9 - \Psi_{10} - \Psi_{11}\} \\ & + I_{c1} \otimes \Psi_1 - I_{c3} \otimes \Psi_5 + I_{c4} \otimes \Psi_7 - I_{c6} \otimes \Psi_{11}, \end{aligned} \tag{4.48}$$

and similarly for one of the other two phases. The third phase must always be the negative sum of the first two, since there is no path for zero sequence into a bridge. This leads to a total of 10 convolutions to calculate the three phase currents. As evident in equation 4.48, the periodic samples for the phase current calculation are just the dc side current, and the commutation currents derived in section 4.2. Thus the secondary phase current can be expressed as a function of the dc current and its harmonics, terminal voltage harmonics and the convertor switching angles. The calculation of the phase current flowing into the transformer primary is addressed in the transformer modelling section.

4.6 TRANSFORMER MODELLING

The convertor transformer is an essential element in a HVdc convertor as it simultaneously performs several useful tasks such as:

- Enabling efficient energy transmission by increasing the potential levels.
- Voltage control and minimization of reactive power consumption by means of tap changer control of the secondary voltage.
- Cancelation of six-pulse characteristic harmonics in a twelve-pulse unit by phase shifting through a star or delta connection.
- Reduction of characteristic harmonics as transformer leakage reactance lengthens the commutation period.

However, unbalance in the tap changer setting between two six-pulse groups will lead to imperfect cancelation of six-pulse harmonics on the ac and dc sides of the convertor. If the impedance in each phase of a three-phase bank is not equal, the convertor will generate positive and negative-sequence odd triplen harmonics. The unbalanced star-g/delta connected transformer also acts as a sequence transformer, causing the convertor to both respond to, and generate zero sequence harmonics. The transformer model is thus required to take into account these non-ideal operation.

The transformer is modelled as a series connection of ideal tap changing transformers on the primary and secondary sides, a resistance, a leakage reactance, and a star/delta connection. Although it is proposed that tap changers can be eliminated in direct connected units, they are included here for generalisation of the model. The resistance and reactance may be unbalanced, the tap settings are assumed to be the same on all phases although it can be unbalanced between the valve groups. The tap change controller is not modelled as it does not respond to harmonics. The magnetising current injection is approximated by a shunt to ground at the primary terminal. No attempt is made to model non-linear transformer effects such as core saturation or hysteresis.

The result of this analysis is a transfer model of the transformer that relates the primary currents to the secondary currents, and the secondary voltages to the primary voltages. For a star-g/star transformer with off-nominal taps, shown in Figure 4.6, the transformer and thyristor resistances are referred to an equivalent primary resistance, R_{ac}:

$$R_{ac} = a_1^2 \left(\frac{R_t}{a_2^2} + R_c \right). \tag{4.49}$$

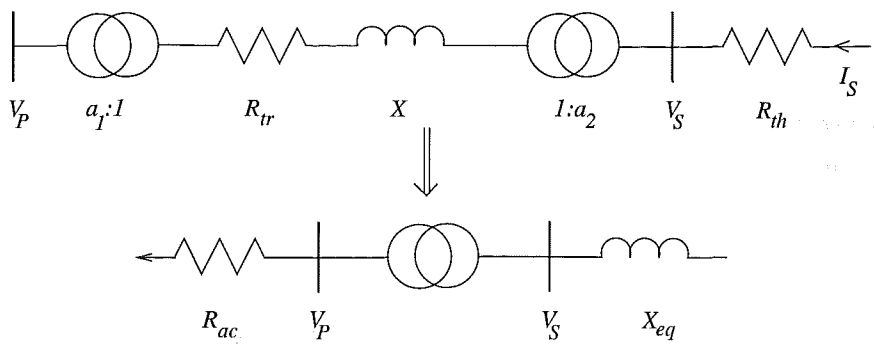

Figure 4.6 Equivalent circuit for star-g/star transformer.

The leakage reactance is referred to an equivalent on the secondary side:

$$X_{eq} = a_2^2 X. \tag{4.50}$$

The secondary voltage becomes independent of the current through the transformer since all impedances have been removed from the transformer, i.e.

$$V_S = \frac{a_2}{a_1} V_P, \tag{4.51}$$

and similarly for the phase current:

$$I_P = \frac{a_2}{a_1} I_S. \tag{4.52}$$

These equations are repeated for all phases and all harmonics.

In the case of a star-g/delta transformer, two separate analyses are required for transfers from the star to delta side and vice versa since part of the circulating zero-sequence current in the delta winding would appear as a positive or negative-sequence current on the primary side if the transformer is unbalanced.

The voltage transfer from star to delta is primarily concerned with setting up the delta connected source for the voltage sampling and commutation analysis, as shown in Figure 4.7. The delta connected source is scaled by a factor of $\sqrt{3}$, i.e.

$$V_S = \sqrt{3}\frac{a_2}{a_1} V_P, \tag{4.53}$$

and the equivalent reactance is:

$$X_{eq} = 3a_2^2 X. \tag{4.54}$$

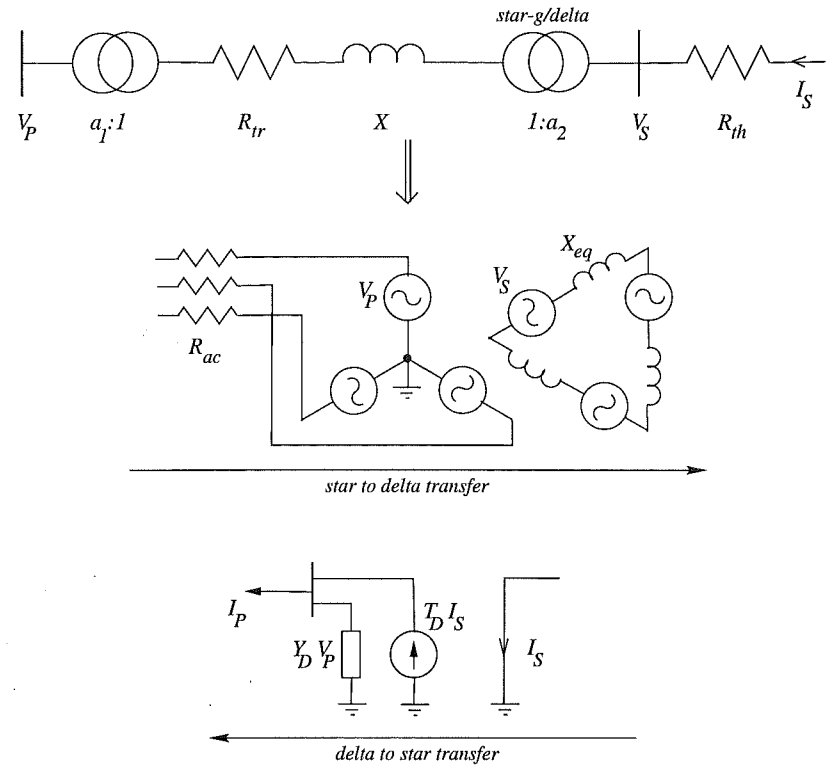

Figure 4.7 Equivalent circuit for star-g/delta transformer.

The transfer of thyristor resistance through the transformer is not affected by the $\sqrt{3}$ scaling since it is not connected in delta. Thus the referred ac system resistance is the same as described in equation 4.49.

In the current transfer from delta to star, the zero-sequence needs to be taken into account separately. The admittance matrix for an unbalanced star-g/delta transformer is readily obtained:

$$\begin{bmatrix} I_{Pa} \\ I_{Pb} \\ I_{Pc} \\ I_{Sa} \\ I_{Sb} \\ I_{Sc} \end{bmatrix} = \begin{bmatrix} \alpha^2 Y_a & 0 & 0 & -\alpha\beta Y_a & \alpha\beta Y_a & 0 \\ 0 & \alpha^2 Y_b & 0 & 0 & -\alpha\beta Y_b & \alpha\beta Y_b \\ 0 & 0 & \alpha^2 Y_c & \alpha\beta Y_c & 0 & -\alpha\beta Y_c \\ -\alpha\beta Y_a & 0 & \alpha\beta Y_c & \beta^2(Y_a + Y_c) & -\beta^2 Y_a & -\beta^2 Y_c \\ \alpha\beta Y_a & -\alpha\beta Y_b & 0 & -\beta^2 Y_a & \beta^2(Y_a + Y_b) & -\beta^2 Y_b \\ 0 & \alpha\beta Y_b & -\alpha\beta Y_c & -\beta^2 Y_c & -\beta^2 Y_b & \beta^2(Y_b + Y_c) \end{bmatrix} \begin{bmatrix} V_{Pa} \\ V_{Pb} \\ V_{Pc} \\ V_{Sa} \\ V_{Sb} \\ V_{Sc} \end{bmatrix} \tag{4.55}$$

where

$$Y = \frac{1}{R_c + jX} \tag{4.56}$$

$$\alpha = \frac{1}{a_1} \tag{4.57}$$

$$\beta = \frac{1}{\sqrt{3}a_2} \tag{4.58}$$

Equation 4.55 is used to calculate the primary current, by assuming that V_P and I_S are known, and eliminating V_S. The admittance matrix in equation 4.55 is not invertible, as the delta winding is floating. Thus there are infinite number of possible potentials of the delta winding which are consistent with a given current injection into the transformer. One such potential is that obtained by grounding phase c on the secondary so that $V_{Sc} = 0$. This permits the removal of the last row and column from equation 4.55, i.e.

$$\begin{bmatrix} I_{Pa} \\ I_{Pb} \\ I_{Pc} \\ I_{Sa} \\ I_{Sb} \end{bmatrix} = \begin{bmatrix} A & B \\ C & D \end{bmatrix} \begin{bmatrix} V_{Pa} \\ V_{Pb} \\ V_{Pc} \\ V_{Sa} \\ V_{Sb} \end{bmatrix}, \tag{4.59}$$

where

$$A = \begin{bmatrix} \alpha^2 Y_a & 0 & 0 \\ 0 & \alpha^2 Y_b & 0 \\ 0 & 0 & \alpha^2 Y_c \end{bmatrix}, \tag{4.60}$$

$$B = \begin{bmatrix} -\alpha\beta Y_a & \alpha\beta Y_a \\ 0 & -\alpha\beta Y_b \\ \alpha\beta Y_c & 0 \end{bmatrix}, \tag{4.61}$$

$$C = \begin{bmatrix} -\alpha\beta Y_a & 0 & \alpha\beta Y_c \\ \alpha\beta Y_a & -\alpha\beta Y_b & 0 \end{bmatrix}, \tag{4.62}$$

$$D = \begin{bmatrix} \beta^2(Y_a + Y_c) & -\beta^2 Y_a \\ -\beta^2 Y_a & \beta^2(Y_a + Y_b) \end{bmatrix}. \tag{4.63}$$

Eliminating V_S, the primary phase currents are:

$$I_P = [A - BD^{-1}C]V_P + BD^{-1}I_S, \tag{4.64}$$

$$\stackrel{\text{def}}{=} Y_D V_P + T_D I_S. \tag{4.65}$$

Y_D is a shunt admittance to ground at the convertor terminal that is added to the filter shunt. T_D is a transfer matrix across the transformer, of size 3×2, indicating that there is no zero-sequence current on the secondary side, and that only the phase a and b currents need to be calculated. If the transformer is balanced, the Y_D is a zero-sequence shunt, and so is not invertible. This also implies that if the transformer is nearly balanced, Y_D has a high condition number, and should not be inverted into an impedance without first being combined with an admittance that offers a path for positive and negative-sequence currents.

4.7 SUMMARY

Harmonic transfers around a twelve-pulse convertor unit in the presence of distortion and unbalance on the ac and dc terminal have been described. In the presence of distortion on the ac terminal, the ac terminal voltages and convertor transformer reactance are no longer the ideal sinusoidal commutation voltages and commutation reactance. The commutation reactance consists of the transformer leakage and a portion of the ac system reactance, which could contain phase-dependent or frequency-dependent components. As a result, an iterative solution for the commutation process is necessary. By choosing the ac terminal voltage as a *pseudo-commutation voltage*, which can be unbalanced or contain harmonic distortion, the effect of the ac system reactance and transformer leakage reactance can be considered separately in the iterative solution. Given the ac terminal voltage as a pseudo-commutation voltage, the convertor harmonic currents can be obtained from the described commutation analysis, in which the reactances are solely the transformer leakage reactances. The ac terminal voltage harmonics are then updated by injecting the convertor currents into the ac system harmonic impedance. Transformer transfer models for star-g/star and star-g/delta connection as well as the convertor constant current, constant power control, the effects of the distortions on the firing process have also been taken into account. Convolution in the harmonic domain is employed to construct the dc voltage and ac currents in terms of the switching angles, ac voltage harmonics and dc current harmonics. Thus the analysis is completely in the harmonic domain.

The convertor model is formulated in terms of a set of non-linear mismatch equations suitable for a unified iterative solution using Newton's method. These equations are incorporated with the generator equations and solved simultaneously, as described in

the next chapter, for individual convertor switching angles and the interaction between the convertor with both the generators and dc system.

Chapter 5

A HARMONIC DOMAIN UNIT CONNECTION MODEL

5.1 INTRODUCTION

In this chapter, the generator model developed in Chapter 3 combined with the convertor model described in Chapter 4, is solved in a unified algorithm to analyse the harmonic interaction between the generators, convertors and the dc system.

A minimal set of variables is selected to fully represents the system in the steady state. The variables are generator terminal voltage harmonics, dc current harmonics, firing instants, end of commutation instants and a control variable. A set of equations specifying the interaction between generator and convertor are developed and expressed in terms of these variables using functional description in both phase and sequence components, as detailed in section 5.6.

In the absence of the convertor transformer on-load tap-changers, the reactive power control by minimizing firing angle has been proposed to be maintained by varying the generator excitation [CIGRE JWG 14/11-09, 1997]. The use of sequence components greatly simplifies the inclusion of this control action in the formulation as generator excitation only controls positive-sequence fundamental voltage. Moreover the generator-convertor harmonic interaction is best explained in this frame of reference as both the generator and convertor convert harmonics from one sequence to another in the steady state.

As there is a mixture of real (eg. firing instants) and complex variables, the variables and equations must be decomposed into real quantities. The set of non-linear equations is solved by using Newton's method and a Jacobian matrix of partial derivatives, whose sparse nature is exploited to accelerate the solution. Initial solution estimates are obtained from the simplified convertor formulation [Arrillaga 1983], and convergence properties as well as the performance of the unified algorithm are examined, especially for difficult systems with high levels of distortion. Convergence threshold for the unified solution method is also compared with IHA algorithms. Finally, the Unit Connection formulation is validated against time domain simulations using the PSCAD2-EMTDC program [Woodford *et al.* 1983].

5.2 SYSTEM VARIABLES

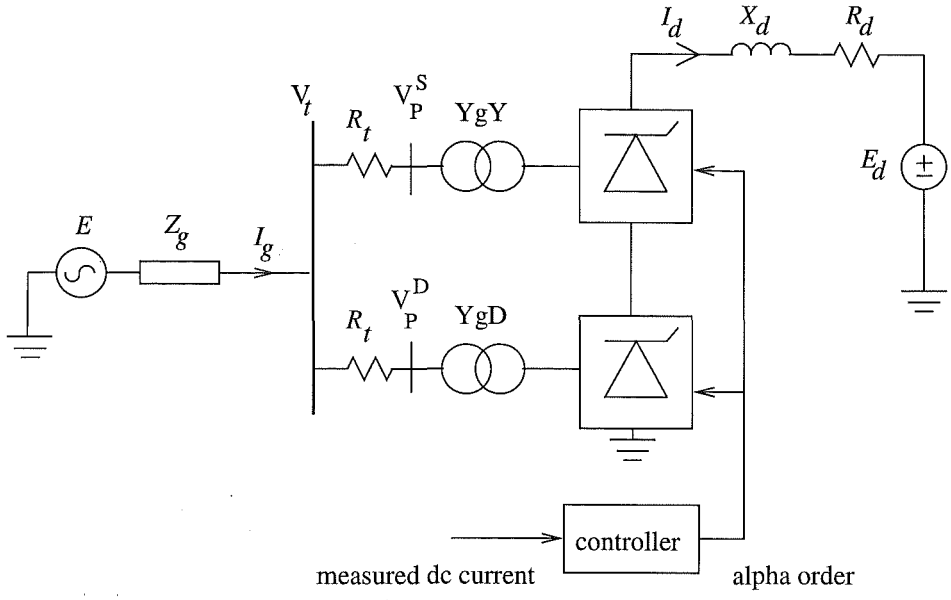

Figure 5.1 Twelve-pulse Unit Connection.

The basic Unit Connection to be solved, shown in Figure 5.1, consists of a twelve-pulse controlled rectifier, and Thevenin equivalents for the generator and dc system. The generator's harmonically coupled impedance matrix is that derived in Section 3.4. The rectifier is under constant current or constant power control, and the phase a terminal voltage is chosen as the phase angle reference.

The transformer and thyristor resistances are lumped into an equivalent resistance, R_t, and placed between the generator bus and transformers' primary. To eliminate the resistive element from the commutation circuit, the voltages on the primary side of the transformers V_P^S and V_P^D are used as commutation voltages. With this arrangement, one set of commutation voltage is required for each six-pulse bridge, doubling the number of variables. However by relating the primary voltages directly to the generator bus voltage through the voltage drops across the equivalent resistance, i.e.

$$\begin{aligned} [V_P^S]_k &= [V]_k - [R_t][I_P^S]'_k \\ [V_P^D]_k &= [V]_k - [R_t][I_P^D]'_k, \end{aligned} \tag{5.1}$$

the generator terminal voltages and their harmonics can be chosen as variables.

Figure 5.2 illustrates the inter-dependency amongst the system variables. The convertor operation in the steady state can be completely defined in terms of the ac terminal voltages, dc current harmonics and the switching angles. The ac currents and dc voltage harmonics are expressed in terms of the chosen variables using convolutions as described

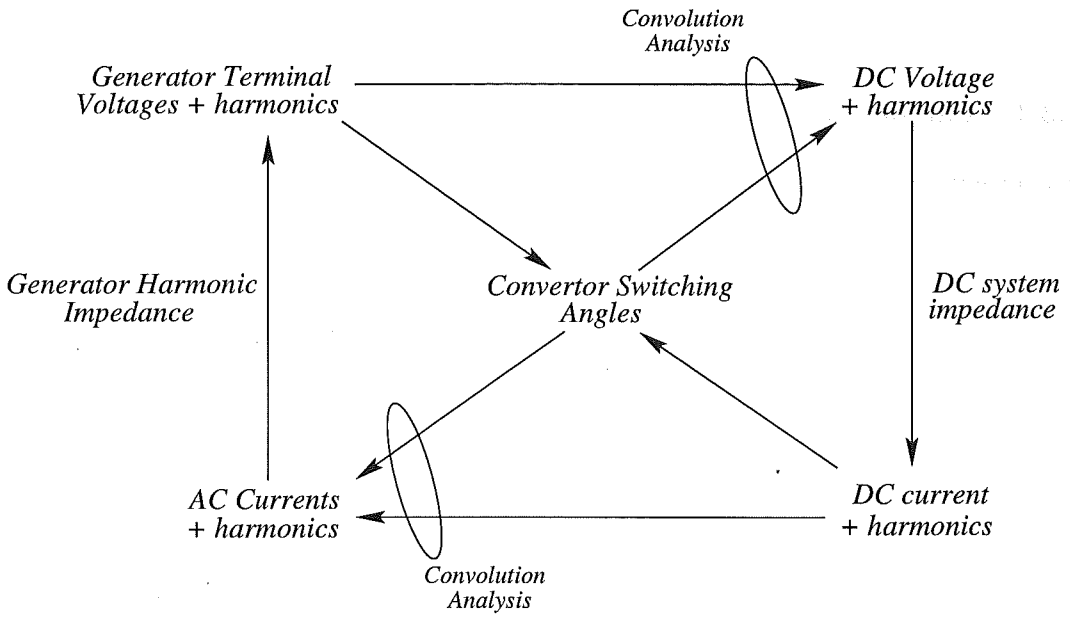

Figure 5.2 Dependency among system variables.

in Chapter 4. The solution method uses estimates of the variables to calculate those same quantities. The difference between the estimated and calculated values is zero or smaller than a preset tolerance at the solution.

For an analysis of a 12 pulse convertor up to the *nth* harmonic, there are $8n + 25$ variables:

- $3 \times 2 \times n$ ac voltage harmonics (Three-phase real and imaginary parts).
- $2 \times n$ dc current harmonics (Real and imaginary parts).
- 12 firing instants.
- 12 end of commutation instants.
- A control variable, for instance, constant current control.

A set of equations is to be developed to fully specify the generator-convertor interaction, and the interaction between generator-convertor unit and the dc system in the steady state. The effects of the distortions on the firing and commutation process are represented implicitly in the equations used for the calculation of the switching angles.

5.3 GENERATOR-CONVERTOR INTERACTION

5.3.1 Fundamental Frequency

In conventional power systems, the AVR action varies the excitation to keep the positive-sequence fundamental terminal voltage at a set value. Thus in fundamental frequency load flow studies, the generator internal positive-sequence emf E is not required to be calculated. The positive-sequence terminal voltage can be specified, which makes it a slack bus ("V, θ" bus where θ is the voltage angle) in the load flow.

Alternatively, when the firing angle instead of the voltage magnitude is specified, the generator bus becomes a "θ, α" bus. This implies that both the excitation and fundamental positive-sequence voltage magnitude are not specified, but they will take on values that satisfy the firing angle setting, as further explained in section 5.5.

Since the machine excitation acts symmetrically on the three phases, positive-sequence voltage only is present at the internal busbar. Consequently, the fundamental negative- and zero-sequence voltages are not influenced by the excitation or positive-sequence impedance. They behave similarly to the harmonic voltages and can be modelled in the same manner as these in the next section.

5.3.2 Harmonic Frequencies

The convertor harmonic currents flowing into the ac system will produce harmonic voltages on the convertor terminal. The harmonic voltages in turn influence the commutation and firing process. Given the transformer primary phase currents, the terminal voltage can be found as

$$[V]_k = [E]_k - [Z_g]_{k,k}[I_g]_k - [Z_g]_{k,k+2}[I_g]_{k+2} - [Z_g]_{k,k-2}[I_g]_{k-2}\,, \tag{5.2}$$

where the square brackets denote a three-phase quantity. The third and fourth terms on the right hand side of equation 5.2 are due to generator saliency which causes cross couplings between harmonics. Equation 5.2 is represented for all harmonics and expressed in the mismatch form suitable for Newton's solution as

$$F_{Vk} \stackrel{\text{def}}{=} V_k - [E]_k + [Z_g]_{k,k}[I_g]_k + [Z_g]_{k,k+2}[I_g]_{k+2} + [Z_g]_{k,k-2}[I_g]_{k-2} = 0. \tag{5.3}$$

Since the generator dc excitation is assumed ripple free, the harmonic component of E is zero. Note that E is different from the ideal sinusoidal commutation voltage E", which relates to the subtransient response of generators.

5.4 CONVERTOR INTERACTION WITH DC SYSTEM

The mismatch equations derived so far are functions of the dc current harmonics, which are required to be solved in the overall solution. The harmonic components of the dc ripple can be found by solving the equations describing the interaction between the convertor and the dc system. Impressing the calculated dc voltage upon the dc system admittance leads to

$$F_{Ik} \stackrel{\text{def}}{=} V_{dk} Y_{dk} - I_{dk} = 0, \tag{5.4}$$

where

$$Y_{dk} = \frac{1}{R_d + jkX_d}. \tag{5.5}$$

5.5 REACTIVE POWER AND VOLTAGE CONTROL BY GENERATOR EXCITATION

5.5.1 Firing Angle Referenced to the Generator Terminal Voltage

In conventional HVdc schemes, the tap changers on the convertor transformers are used to control the reactive power by adjusting the taps to keep the firing angle, α, within a limit while the ac terminal voltage is kept at a constant nominal level.

In the Unit Connection case, the terminal ac voltage magnitude becomes irrelevant due to the absence of local loads. The generator excitation control could be used to take over the function of on-load tap changers to keep the firing angle, α, within the predetermined range. This control action is expressed as

$$F_{\alpha set} \stackrel{\text{def}}{=} \alpha_{set} - \frac{1}{12} \sum_{i=1}^{12} (\theta_i - \chi_i) = 0\,, \tag{5.6}$$

where α_{set} is the desired firing angle referenced to the generator fundamental terminal voltage, θ_i and χ_i are the firing instant and terminal voltage fundamental crossings respectively. In order to minimize the reactive power consumption, the firing angle would be set to the minimum allowable value and the generator excitation varies the internal emf to give the desired dc line voltage, which is set by the invertor control.

In a frame of reference that uses real and imaginary components, it is necessary to specify the angle of the fundamental positive-sequence terminal voltage which, being used as a reference, is zero, i.e.

$$\mathcal{I}\{F_{V1\,ps}\} \stackrel{\text{def}}{=} \mathcal{I}\{V_{1\,ps}\} = 0\,. \tag{5.7}$$

where subscript $V1\ ps$ denotes the fundamental positive-sequence voltage.

The firing angle can be referenced to the generator terminal voltage, voltage behind subtransient reactance $E"$ or any other voltages in the unified iterative solution. As firing angles are normally referenced to a sinusoidal commutation voltage, the formulation of firing angles referenced to $E"$ is to be described in the next section.

5.5.2 Firing Angle Referenced to the Generator Internal Voltage $E"$

In the absence of ac filters, the sinusoidal commutation voltage is the voltage $E"$ behind generator subtransient reactance as shown in Figure 5.3. Since $E"$ leads the generator fundamental terminal voltage V_1 for a lagging power factor of less than 90^o, the valves can be fired before the crossings of the terminal voltages provided that they are fired after the crossings of $E"$ to avoid mis-firing.

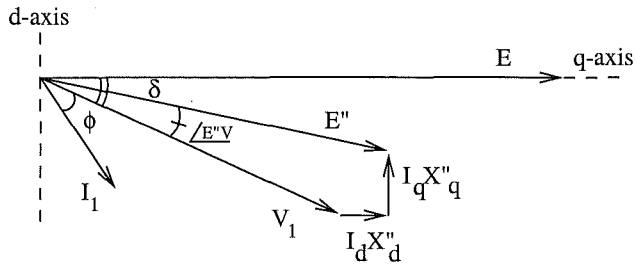

Figure 5.3 Phasor diagram of a salient-pole generator in direct connected units.

With reference to Figure 5.3, the phase angle $\angle E"V$ between $E"$ and V_1 can be calculated as:

$$\begin{aligned} \angle E"V &= \delta - tan^{-1}\left\{\frac{E"_d}{E"_q}\right\} \\ &= \delta - tan^{-1}\left\{\frac{V_1 \sin\delta - I_1 \cos(\delta+\phi)X"_q}{V_1 \cos\delta + I_1 \sin(\delta+\phi)X"_d}\right\}, \end{aligned} \tag{5.8}$$

The firing angle referenced to $E"$ is the sum of the firing angle referenced to V_1 and the phase angle $\angle E"V$, i.e.

$$\alpha_{set\ E"} = \alpha_{set\ V_1} + \angle E"V, \tag{5.9}$$

and the $E"$ referenced firing angle can replace the V_1 referenced firing angle in equation 5.6.

Since accurate measurements of the generator currents as well as voltages are required for the control system to calculate $E"$, the firing control of direct connected units can be simplified considerably by using the generator terminal voltage as the reference.

However it is necessary to use E'' as the reference for comparison between direct connected units and conventional HVdc schemes.

5.6 FUNCTIONAL DESCRIPTION OF A UNIT CONNECTION

5.6.1 Phase Components Formulation.

From the commutation analysis in Section 4.2, the equations for end of commutation instants can be expressed in terms of the commutation voltage, dc current harmonics, and the corresponding firing instants:

$$F_{\phi_i} = f_1(V_P^S, V_P^D, I_{dk}, \alpha_i, \phi_i) \tag{5.10}$$

As the convertor current controller is responsive to dc current harmonics, the equation for firing instants is a function of those harmonics:

$$F_{\theta_i} = f_2(I_{dk}, \theta_i, \alpha_0) \tag{5.11}$$

By means of convolution analysis in the Harmonic Domain, the generator current and dc voltage of a Unit Connection scheme can be expressed in terms of the ac terminal voltage harmonics, dc current harmonics and the switching angles, i.e.

$$\begin{aligned} I_g &= f_3(V_P^S, V_P^D, I_{dk}, \theta_i, \phi_i) \\ V_d &= f_4(V_P^S, V_P^D, I_{dk}, \theta_i, \phi_i) \end{aligned} \tag{5.12}$$

The relationship between the commutation and generator terminal voltages described by equation 5.1 can be rewritten as:

$$\begin{aligned} V_P^S &= f_5(V) \\ V_P^D &= f_6(V) \end{aligned} \tag{5.13}$$

The primary voltages can be dropped from the formulation by combining equations 5.12 and 5.13:

$$\begin{aligned} I_g &= f_3(f_5(V), f_6(V), I_{dk}, \theta_i, \phi_i) \\ &= f_7(V, I_{dk}, \theta_i, \phi_i) \end{aligned} \tag{5.14}$$

$$V_d = f_8(V, I_{dk}, \theta_i, \phi_i) \tag{5.15}$$

The derived equation 5.3 for the generator-convertor interaction is combined with

Equation	No. of Vars.	Function of
F_V	$2\times 3n$	$V - f_9(V, I_{dk}, \theta_i, \phi_i)$
F_{Id}	$2n$	$I_d - f_{10}(V, I_{dk}, \theta_i, \phi_i)$
F_ϕ	12	$f_{11}(V, I_{dk}, \theta_i, \phi_i)$
F_θ	12	$f_2(I_{dk}, \theta_i, \alpha_0)$
F_{α_0}	1	$f_{12}(V, I_{dk}, \theta_i, \phi_i, \alpha_0)$

Table 5.1 Mismatch equations for a 12 pulse convertor in phase coordinates, where n is the number of evaluated harmonics.

equation 5.14 to give

$$F_V \stackrel{\text{def}}{=} V - f_9(V, I_{dk}, \theta_i, \phi_i) = 0. \tag{5.16}$$

Similarly, the convertor-DC system interaction is expressed as

$$F_{Id} \stackrel{\text{def}}{=} I_d - f_{10}(V, I_{dk}, \theta_i, \phi_i). \tag{5.17}$$

The primary voltages are also eliminated in the end of commutation instant equations, i.e.

$$F_{\phi_i} = f_{11}(V, I_{dk}, \alpha_i, \phi_i) \tag{5.18}$$

The convertor constant current control equation F_{α_0}, a function of the dc voltage and current, can be expressed as

$$F_{\alpha_0} = f_{12}(V, I_{dk}, \theta_i, \phi_i, \alpha_0), \tag{5.19}$$

and the equations in terms of the selected variables are summarized in Table 5.1.

It is difficult to incorporate the voltage control by generator excitation in the phase component formulation since only the positive-sequence fundamental is controlled. On the other hand, this control action is easily integrated into the sequence components formulation to be described in the next section.

5.6.2 Sequence Components Formulation.

It has been necessary to model the convertor in phase coordinates since individual conduction intervals, related to switchings between the three phases, must be modelled explicitly. However when interfacing with generators, the sequence components solution

Variable	No. of Vars.	Function of
F_W	$2\times 3n-1$	$W - Tf_9(T^{-1}W, I_{dk}, I_{d0}, \theta_i, \phi_i)$
F_{Id}	$2n$	$I_d - f_{10}(T^{-1}W, I_{dk}, I_{d0}, \theta_i, \phi_i)$
F_ϕ	12	$f_{11}(T^{-1}W, I_{dk}, \theta_i, \phi_i)$
F_θ	12	$f_2(I_{dk}, I_{d0}, \theta_i, \alpha_0)$
F_{α_0}	1	$f_{12}(T^{-1}W, I_{dk}, I_{d0}, \theta_i, \phi_i)$
$F_{\alpha_{set}}$	1	$f_{13}(T^{-1}W, \theta_i)$

Table 5.2 Mismatch equations for a 12 pulse convertor in sequence components, where n is the number of evaluated harmonics. The reactive power control by generator excitation is also included.

is more suitable as only the positive-sequence is controlled by the generator excitation. This also enables the modelling of the convertor reactive power control by generator excitation in the absence of the convertor transformer on-load tap-changers. An additional advantage of sequence components is a substantial improvement in the sparsity of the Jacobian, since the harmonic cross couplings are from one sequence to another. Sequence to phase transformation is therefore required so that the equations can be written in sequence components.

Using the sequence transform matrix, T, sequence components formulation in terms of phase coordinates is

$$\begin{bmatrix} V_0 \\ V_- \\ V_+ \end{bmatrix} = \begin{bmatrix} 1 & 1 & 1 \\ 1 & a^2 & a \\ 1 & a & a^2 \end{bmatrix} \begin{bmatrix} V_a \\ V_b \\ V_c \end{bmatrix}, \tag{5.20}$$

where $a = e^{j2\pi/3}$. Setting

$$W = \begin{bmatrix} V_0 \\ V_- \\ V_+ \end{bmatrix} \tag{5.21}$$

as the sequence components voltage yields $V = T^{-1}W$. The existing phase coordinates equations can now be written as sequence component mismatches, in terms of the sequence components terminal voltage, using the sequence transformation. Table 5.2 summarizes the equations in sequence components. In order to model the reactive power control by generator excitation, the equation relating to the positive-sequence terminal voltage is replaced by the control equation $F_{\alpha set}$, in which the desired firing angle is specified.

If a three phase quantity has been decomposed in real rectangular components, a

real components sequence transform matrix, $\bar{T}$, can be constructed:

$$\bar{W}=\begin{bmatrix} V_0^R \\ V_0^I \\ V_-^R \\ V_-^I \\ V_+^R \\ V_+^I \end{bmatrix} = \begin{bmatrix} 1 & 0 & 1 & 0 & 1 & 0 \\ 0 & 1 & 0 & 1 & 0 & 1 \\ 1 & 0 & \mathcal{R}a^2 & -\mathcal{I}a^2 & \mathcal{R}a & -\mathcal{I}a \\ 0 & 1 & \mathcal{I}a^2 & \mathcal{R}a^2 & \mathcal{I}a & \mathcal{R}a \\ 1 & 0 & \mathcal{R}a & -\mathcal{I}a & \mathcal{R}a^2 & -\mathcal{I}a^2 \\ 0 & 1 & \mathcal{I}a & \mathcal{R}a & \mathcal{I}a^2 & \mathcal{R}a^2 \end{bmatrix} \begin{bmatrix} V_a^R \\ V_a^I \\ V_b^R \\ V_b^I \\ V_c^R \\ V_c^I \end{bmatrix} = \bar{T}\bar{V} \tag{5.22}$$

The chain rule readily yields the modifications that must be made to the phase coordinates partial derivatives, to yield the sequence components partial derivatives:

$$\begin{aligned} \left[\frac{\partial F_W}{\partial W}\right] &= I - \bar{T}\left[\frac{\partial f_9}{\partial V}\right]\bar{T}^{-1} \\ \left[\frac{\partial F_W}{\partial x}\right] &= -\bar{T}\left[\frac{\partial f_9}{\partial x}\right], x \in \{I_{dk}, \theta_i, \phi_i\} \\ \left[\frac{\partial F_x}{\partial W}\right] &= \left[\frac{\partial F_x}{\partial V}\right]\bar{T}^{-1}, x \in \{I_{dk}, \theta_i, \phi_i\} \end{aligned} \tag{5.23}$$

5.7 NEWTON'S SOLUTION

Since the ac voltage and dc current mismatch equations are not differentiable in complex form, the Newton solution is formulated in terms of real functions and variables. The variables are assembled into a real vector X as

$$X = [\mathcal{R}\{V\}, \mathcal{I}\{V\}, \mathcal{R}\{I_d\}, \mathcal{I}\{I_d\}, \theta, \phi, \alpha_0]^T, \tag{5.24}$$

where $\mathcal{R}$ and $\mathcal{I}$ denote the real and imaginary components respectively. The mismatch equations are likewise assembled into a real vector:

$$F(X) = [\mathcal{R}\{F_V\}, \mathcal{I}\{F_V\}, \mathcal{R}\{F_{Id}\}, \mathcal{I}\{F_{Id}\}, F_\theta, F_\phi, F_{\alpha 0}, F_{\alpha set}]^T. \tag{5.25}$$

Newton's method is an iterative process for finding a solution X_s that causes the mismatch vector to be zero, i.e.

$$F(X_s) = 0. \tag{5.26}$$

Given an initial estimate of the solution, X_0, the iterative process is described

as [Burden *et al.* 1981]

$$X^{N+1} = X^N + \Delta X^N \tag{5.27}$$

$$J(X^N)\Delta X^N = -F(X^N), \tag{5.28}$$

with convergence deemed to have occurred when some norm of the residual vector $F(X^N)$ is less than a preset tolerance, and J is the Jacobian matrix of partial derivatives of the equation set $F(X)$. The convergence tolerances selected are listed below:

$$\begin{aligned} \frac{|F_{V_k}|}{|V_k|} &< 0.001 \\ \frac{|F_{I_{dk}}|}{|I_{dk}|} &< 0.001 \\ |F_{\theta i}| &< 5e-8 \\ |F_{\phi_i}| &< 5e-8 \end{aligned} \tag{5.29}$$

As the convergence tolerance for the complex mismatches, F_V, F_{Id} is expressed in terms of the magnitude of the mismatch, the error in an estimated value for a variable, for instant V_{+11}, is smaller than 0.1% of its own magnitude. Thus all harmonics are treated equally. This convergence test is only applied to harmonics that have a size larger than $1e-5$ per unit in order to prevent any attempt to converge to an absolute error of zero for harmonics that are not present.

5.7.1 Jacobian of Partial Derivatives

By linearization around an operating point using the Jacobian of partial derivatives, Newton's method effectively reduces a set of non-linear equations to linear equations, which are solved to improve the accuracy of the solution estimates. Equation 5.28 represents a set of linear equations that must be solved at each iteration. This represents the majority of the processing required to obtain a solution. By introducing sparsity into the Jacobian matrix the Newton's solution can be accelerated.

If a mismatch equation is only weakly dependent upon one of the variables, then the partial derivative with respect to this variable will be small. Thus setting the corresponding Jacobian element to zero still represents an accurate linearization of the equation in terms of that variable. For a solution up to the fiftieth harmonic, the Jacobian is typically 91% sparse with elements smaller than 0.005 per unit set to zero. The cut-off limit of 0.005 per unit was selected to maximize the solution speed while preserving the robustness of the solution, as demonstrated in Table 5.3. Although more sparsity can

Cut-off Limit (p.u.)	Number of elements	Sparsity (%)	CPU time (seconds)	Number of iterations
0.05	15126	91.6	21.1	21
0.01	16564	90.8	24.3	21
0.007	16753	90.7	21.2	16
0.005	**16964**	**90.6**	**11.9**	**7**
0.001	18151	90.0	13.1	6
1e-4	22041	87.8	16.9	6
1e-6	40642	77.5	30.2	6

Table 5.3 The selection of the cut-off limit for Jacobian elements in order to maximize solution speed and preserving the robustness of the solution. Subtransient reactances = 1.0 p.u., transformer leakage reactance = 0.05 p.u., Idc = 1.0 p.u., 50 harmonics.

be obtained by setting larger elements to zero, the convergence rate is slower and more iterations are required.

The asymmetric sparse linear solver [Zlatev 1991], y12m, is used to solve equation 5.28 as the Jacobian is neither symmetric nor diagonally row dominant. Instead of inverting the Jacobian, it is factorized to LU components and equation 5.28 is solved by back substitution. The pivoting in the y12m solver is selected to compromise for both sparsity and numerical stability. The y12m solver computer program was extensively tested at the University of Copenhagen [1].

Symmetric bifactorization methods, such as by Zollenkopf [1970], require the Jacobian to be diagonally row dominant since it was designed to solve admittance matrix systems, in which the diagonal elements, i.e. self-admittance terms, are sums of other terms in the corresponding rows. Consequently, the symmetric bifactorization method has been found to be unsuitable as the Jacobian is not diagonally row dominant although it has a large diagonal.

The Jacobian elements can be obtained by using numerical partial differentiation or by evaluating analytical expressions of the partial derivatives. In the numerical approach, the elements are approximated by calculating the function with a small perturbation ($\triangle x_j$) to each of the variables sequentially [Gerald and Wheatly 1985], i.e.

$$\frac{\partial F_i}{\partial x_j} \simeq \frac{F_i(x_j + \triangle x_j, x_o) - F_i(x_j, x_o)}{\triangle x_j} \tag{5.30}$$

where x_o denotes the variables besides x_j. Numerical calculation of the Jacobian is

[1] FORTRAN codes are available on the World Wide Web at http://www.netlib.org/y12m/

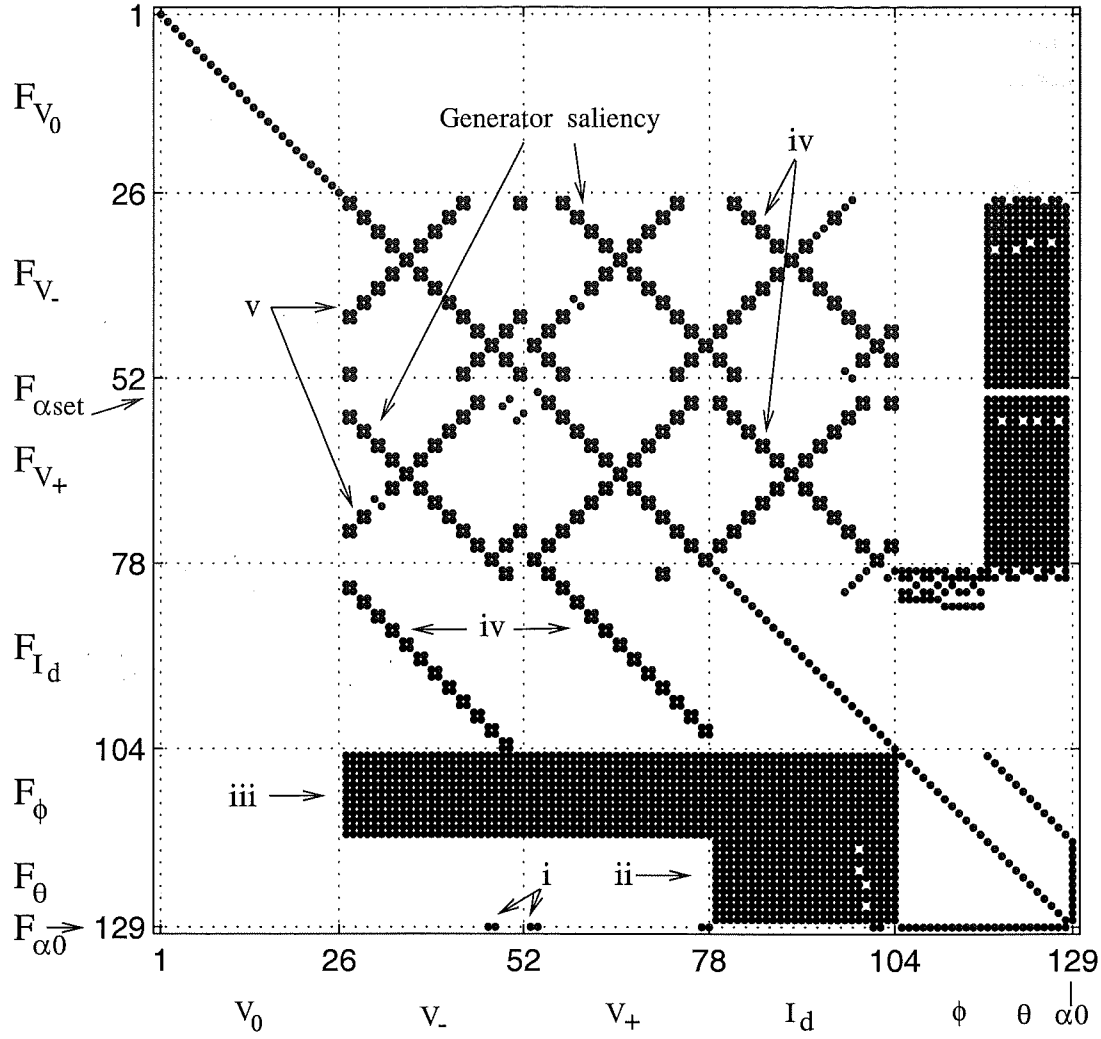

Figure 5.4 Sparsity structure of the Jacobian in sequence components for 13 harmonics.

a powerful method that is easy to apply, and programs are widely available [Press *et al.* 1992]. However it is approximately twenty times slower than the analytical approach for a formulation of 13 harmonics, since each column of the numerical Jacobian requires a computation of all the mismatch equations. Although the analytical method requires considerable effort to obtain the partial derivatives in analytic form, the gain in solution speed is substantial. Detailed derivation of the analytical Jacobian is given in Appendix F, and the obtained partial derivatives have been verified against the numerical solution.

For a formulation of 13 harmonics, the Jacobian is 129 elements square, as illustrated in Figure 5.4. In this example, there is no coupling between the zero and other sequences as the transformer phase impedance are assumed to be balanced, which is usually the case in a Unit Connection. Due to generator saliency, the elements representing the harmonic cross couplings are shifted up by two harmonics from negative-sequence k to

positive-sequence $k+2$, and down by two harmonics from positive to negative-sequence, as indicated in Figure 5.4. Moreover the Jacobian also gives insights to the harmonic transfers across the convertor through its structural features such as:

i The average delay angle mismatch is related to the average dc current, thus it is sensitive to changes in the fundamental terminal voltage and the harmonics coupled to the fundamental, such as 11th and 13th ac voltages.

ii The firing instants are sensitive to the dc current, its harmonics, and the constant current controller parameters.

iii The end of commutation mismatches are very sensitive to harmonics in the ac voltage and dc current. They are also sensitive to the firing instants.

iv A change in harmonic k on the dc side affects positive-sequence harmonic $k-1$ and negative-sequence harmonic $k+1$ on the ac side, and vice versa for the ac to dc conversion. The dc current harmonics are sensitive to the ac voltage harmonic variation as they are obtained by impressing the dc voltage on dc side admittance, where dc voltage harmonics are essentially ac voltage harmonics transfered through the convertor. These are called three-port terms by Larson *et al.* [1989].

v The elements in rows that are parallel and perpendicular to the main diagonals are the result of the commutation period modulation process [Wood and Arrillaga 1995]. Convolutions of the dc current harmonics with the sampling functions produce sum and difference harmonic terms; the sum terms give rows parallel with the main diagonal, and the difference terms give rows perpendicular to the diagonal.

5.7.2 Initialization

The simplified convertor analysis [Arrillaga 1983] is employed to calculate the first estimation of the system variables. An initial estimate of the convertor delay angle is obtained using equation 5.31,

$$V_{d0} = \frac{2 \times 3\sqrt{2}}{\pi}|V_1| \cos\alpha - \frac{3X}{\pi} I_{d0}, \tag{5.31}$$

where V_1 is the phase to phase rms fundamental voltage referred to the secondary of the convertor transformers. Since there are two six-pulse valve groups, multiplication factor of 2 is required in the first term on the right hand side of equation 5.31.

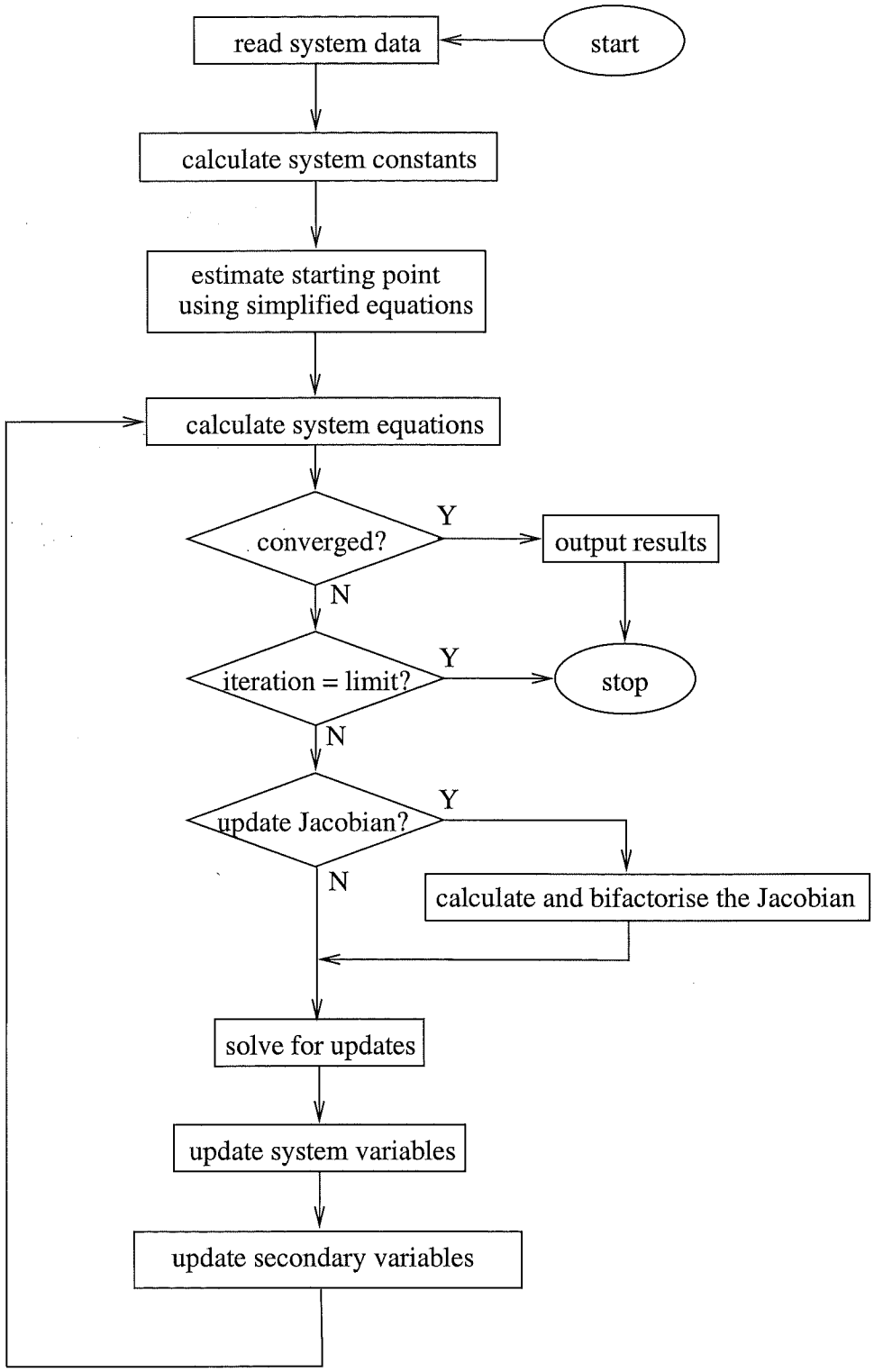

Figure 5.5 Flow diagram for the unified harmonic solution.

The dc voltage is estimated from the voltage drop through the dc system and the dc voltage source:

$$V_{d0} = E_d + I_{d0}R_d \tag{5.32}$$

The average commutation angle μ is obtained from:

$$V_{d0} = \frac{3\sqrt{2}}{\pi}|V_1|[\cos\alpha + \cos(\alpha+\mu)] \tag{5.33}$$

These angles are then used to assemble rough estimates of the individual firing and end of commutation angles:

$$\theta_i = \beta_i + \alpha \tag{5.34}$$

$$\phi_i = \theta_i + \mu \tag{5.35}$$

Figure 5.5 illustrates the steps of the unified harmonic solution in which the Newton's method is implemented in the main loop. The secondary variables are dc voltage harmonics and ac current harmonics, which are calculated using equations derived in Section 4.4 and 4.5 respectively.

5.8 MODEL VALIDATION AND PERFORMANCE

5.8.1 Validation

Using the developed formulation, the system of Figure 5.1 is solved and compared with the results obtained from a time domain simulation using the PSCAD2-EMTDC program. The unit connected mode of a Group Connection containing 4 generators has been selected to provide a high level of harmonic distortion for validating purpose. The Group Connection implementation is to be described in Section 6.6. The firing angle referenced to the generator fundamental terminal voltage is 15^o. The generator and convertor transformer parameters are listed in Appendix A2.

Despite the high level of distortion, close agreement in both magnitudes and phase angles has been obtained for the ac voltage, current harmonics and dc voltage as shown in Figure 5.6, 5.7 and 5.8. It was found necessary to use a time step of 5μs, and to simulate for 700 fundamental frequency cycles to allow transients to decay.

It has been found that large values of the snubber capacitance (across thyristors), which is required to aid numerical stability in the time domain simulations, can give inaccurate harmonic results. The ac harmonic currents vary by upto 12% for various value of the snubber capacitance. In order to minimize the effect of the snubber capacitances,

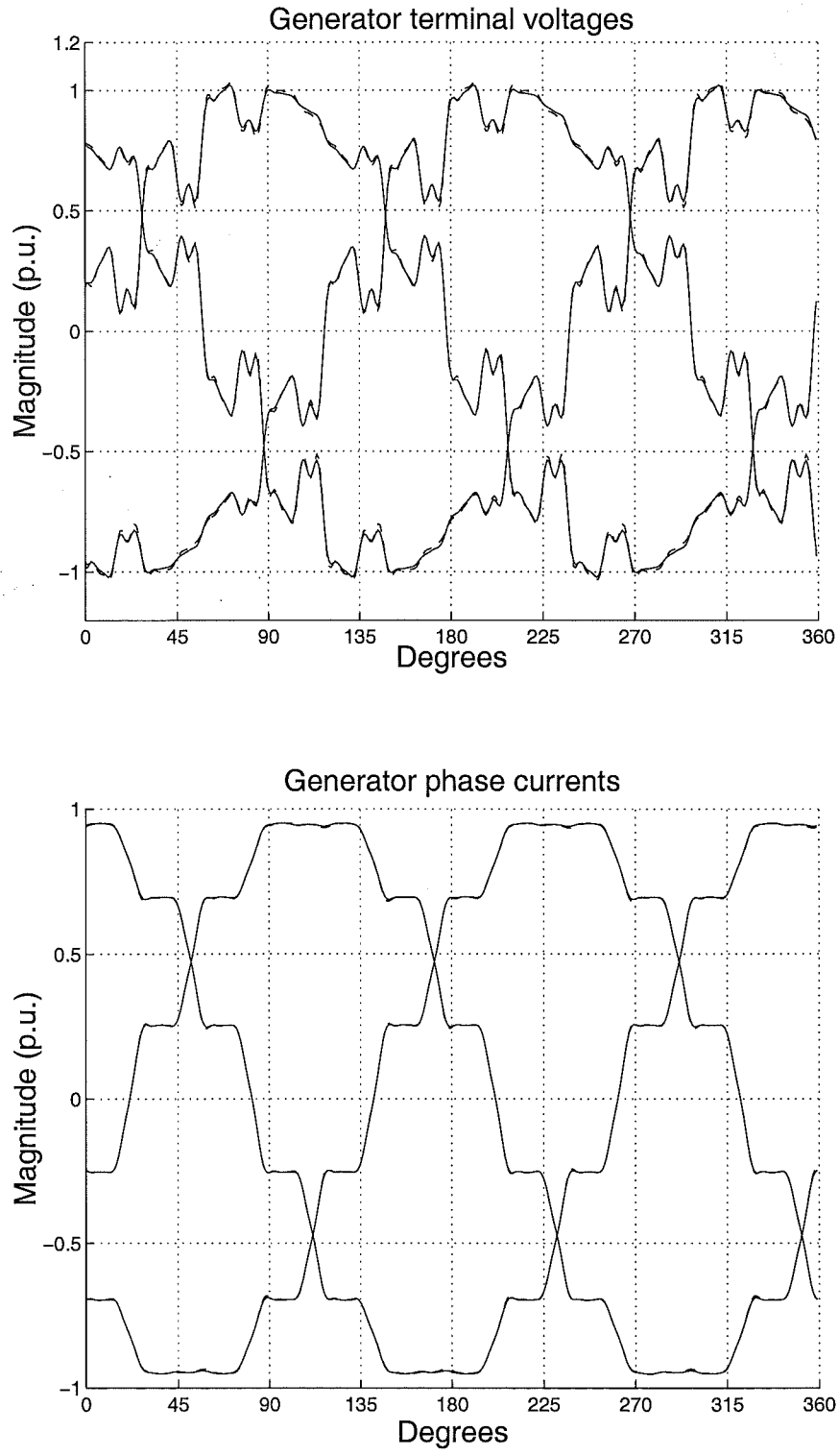

Figure 5.6 Model intervalidation by comparison of time domain and unified harmonic solutions for generator voltage and current waveforms, reconstructed from 50 harmonics. *Harmonic domain: solid, PSCAD: dashed.*

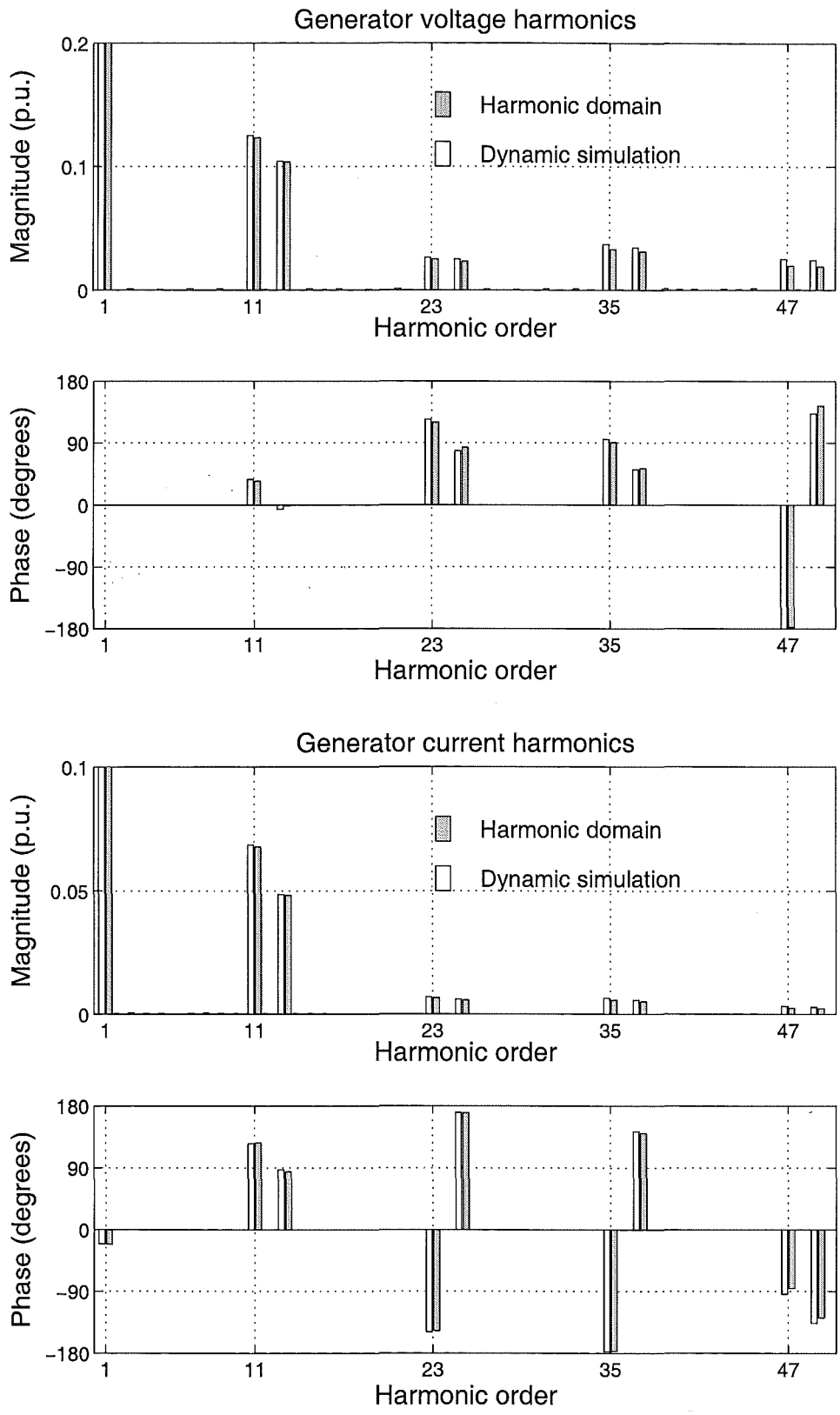

Figure 5.7 Model intervalidation by comparison of time domain and unified harmonic solutions for generator harmonic voltages and currents. PSCAD: left; Harmonic domain: right.

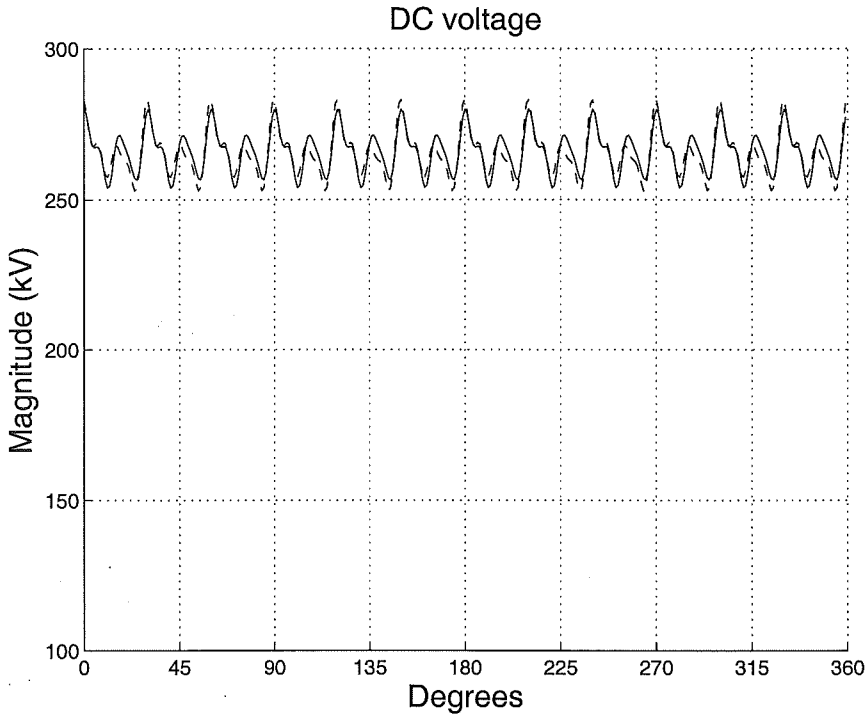

Figure 5.8 DC voltage waveforms reconstructed from 50 harmonics. *Harmonic domain: solid, PSCAD: dashed.*

a small capacitance value of $2pF$ was used. This introduced high frequency spikes in the time domain waveforms due to numerical oscillations. However, the harmonic content closely matched those from the harmonic domain solution. For comparison purpose, the waveforms were reconstructed from their first 50 harmonics.

5.8.2 Convergence Properties

If the initial estimation is sufficiently close to the final solution, the convergence of the Newton's method is quadratic [Gerald and Wheatly 1985]. However the convergence is slower, or in some cases divergence can occur, when the initial estimation is considerably far from the solution. The convergence of Newton's method is also dependent upon the gradient of the iterating function $F(X)$. The gradient is given by the magnitudes of the Jacobian elements. Divergence occurs when the gradient exceeds some "norm" value.

The iterations to convergence for various values of commutation reactance and generator subtransient reactance is listed in Table 5.4. The formulation consists of the first 50 harmonics and firing angle is set at 15°. For typical systems consisting of 0.1 p.u. commutation reactance (which is the transformer leakage reactance in the developed formulation), the convergence is obtained within 5 iterations for a wide range of generator subtransient reactance up to 0.5 p.u.. In comparison with sequential IHA algorithms, the unified solution is much more robust since IHA algorithms diverge when the commutation reactance is less than 0.1 p.u. and generator subtransient reactances

Generator	Transformer leakage reactance (p.u.)		
X'' (p.u.)	0.02	0.03	0.1
0.0	2	2	2
0.1	5	5	3
0.2	-	5	4
0.3	-	6	5
0.5	-	6	5

Table 5.4 Iterations to convergence for the unified Unit Connection solution using Newton's method. Hyphen denotes divergence.

are larger than 0.1 p.u., as reviewed in Chapter 2. The improvement lies in the unilateral relationship of the variables in the unified solution.

For smaller leakage reactance values, the convergence threshold is lower due to a substantial increase in gradient of the iterating function. Divergence occurs frequently when the commutation reactance is less than 0.02 p.u.. As time domain simulations of these systems give valid operating condition, divergence of the unified solution does not indicate harmonic instability.

The factors that significantly affect the gradient are the commutation reactance and generator subtransient reactances. Their influence on the Jacobian magnitude can be examined by considering a term on the Jacobian main diagonal for phase a at harmonic k. This term can be obtained by differentiating the voltage mismatch, represented by equation 5.3, with respect to ac voltage variation. Generator saliency is neglected for simplicity, and the differential is:

$$\frac{\partial \mathcal{R}\{F_{Vk}\}}{\partial \mathcal{R}\{V_m\}} = \mathcal{R}\left\{1 + Z_{k,k}\frac{\partial I_k}{\partial \mathcal{R}\{V_m\}}\right\} \tag{5.36}$$

The ac current I is made of commutation currents during commutation periods that involve phase a, and of dc current during normal conduction period. Since dc current harmonics are chosen as independent variables, they are held constant when differentiating other variables with respect to ac terminal voltages. Thus only contribution of the commutation current is required to be considered. The commutation current for commutation period i is given by:

$$I_{ci}(t) = D + \mathcal{I}\left\{\sum_{k=1}^{n_h} I_{cik} e^{jkwt}\right\}, \tag{5.37}$$

Generator subtransient reactance (p.u.)	CPU time (seconds)	Number of iterations	λ_c
0.0	1.6	2	1.2 e-5
0.2	6.3	4	2.8 e-3
0.4	6.6	5	5.1 e-3
0.6	8.6	5	1.0 e-2

Table 5.5 Solution speed and convergence factor in relation to the magnitude of generator subtransient reactances for solutions up to the fiftieth harmonic.

where

$$D = -\mathcal{I}\left\{\sum_{k=1}^{n_h} I_{cik} e^{jk\theta_i}\right\}, \tag{5.38}$$

$$I_{cik} = \frac{jkwL_c I_{dk} - V_{abk}}{jkwL_{ab}}, \tag{5.39}$$

and phase a and b are the phase ending and beginning conduction respectively.

Differentiating I_{cik} with respect to ac voltage yields:

$$\frac{\partial I_{cik}}{\partial \mathcal{R}\{V_{ab}\}} = -\frac{1}{jkwL_{ab}} \tag{5.40}$$

The firing instants, θ_i, are also independent variables, thus are held constant when differentiating with respect to ac voltage. Consequently, the differential of ac voltage mismatch with respect to ac voltage can be expressed in terms of generator harmonic impedance and commutation reactance:

$$\frac{\partial \mathcal{R}\{F_{Vk}\}}{\partial \mathcal{R}\{V_k\}} = 1 + \mathcal{R}\left\{A\, Z_{k,k} \frac{1}{jkwL_{eb}}\right\} \tag{5.41}$$

where A is a constant coefficient. The derivation of $\frac{\partial \mathcal{R}\{F_{Vk}\}}{\partial \mathcal{R}\{V_k\}}$ for all harmonics is described in Appendix F.

It is apparent from equation 5.41 that the gradient of $F(X)$ is directly proportional to the generator harmonic impedance and inversely proportional to the commutation reactance. Hence for large generator subtransient reactance and small commutation reactance values, the gradient is large which can lead to divergence. However it has been shown that convergence is fast and robust for typical reactance values and thus the developed formulation is sufficient for analysing the harmonic interaction in direct connected units.

A convenient measure of the rates of convergence is the sum of the magnitudes of all the mismatch equations, which is called *1-norm* [Gerald and Wheatly 1985]. At each iteration the *1-norm* is reduced by an approximately constant *convergence factor*, λ_c, depending upon the difficulty of the system, and whether the Jacobian is updated. The smaller λ_c, the faster the convergence. Table 5.5 shows the solution speed and convergence factors for various generator subtransient reactance values. The transformer leakage reactance is 10%. Clearly, the convergence is rapid when there is no voltage distortion, i.e. with perfect ac filtering (generator harmonic impedance is set to zero). For typical subtransient reactances of 0.15 to 0.25 per unit, the convergence is fast and robust, taking only 4 iterations and roughly 7 seconds on an UltraSparc processor. The solution speed will no doubt be reduced significantly as computer processing power improves, whereas the robustness of the algorithm, implicitly represented in the small convergence factor λ_c, is the most significant advantage of the unified solution using Newton's method.

Although the implemented Newton's method is quite powerful for solving sets of non-linear equations, obtaining the analytical Jacobian is a formidable task which requires detailed understanding of the formulation. On the other hand, numerical evaluation of the Jacobian is simple, but computationally intensive. Alternatively, there are quasi-Newton methods that provide computationally inexpensive approximations to the Jacobian for solution finding. The best of these methods is the Broyden's method [Broyden 1965].

Broyden's method converges superlinearly once the solution estimate is close enough to the solution, and it has been claimed that it is almost as robust as Newton's method [Press *et al.* 1992]. The solution speed would be slower than the Newton's method employing the analytical Jacobian approach, but faster than the numerical Jacobian approach. However, as the Jacobian approximation matrix used in the Broyden's method is not always close to the true Jacobian at the solution, the insights into the harmonic interaction would be compromised. Further work is required to implement Broyden's method for direct connected units to determine the convergence threshold as well as to further substantiate those claims on the robustness and speed of Broyden's method when being applied to direct connected systems.

5.9 CONCLUSIONS

A twelve-pulse Unit Connection harmonic model has been developed using a unified algorithm, in which all of the system variables and equations are solved simultaneously. The effects of the convertor control, generator saliency and saturation, ac terminal voltage and dc current harmonics are formulated using a set of mismatch equations which is solved by using Newton's method. The reactive power control by minimizing firing angle

is maintained by varying generator excitation in the absence of convertor transformer on-load tap-changers. The mixture of real and complex variables as well as equations has been decomposed into real quantities, and the Newton's solution is formulated using real values in positive harmonics only. By setting the small elements of the Jacobian of partial derivatives to zero and exploiting its sparsity, the solution is greatly accelerated while preserving the robustness of Newton's solution.

The initial estimation based on the simplified fundamental frequency formulation has been shown to provide a good starting point for the Newton's solution. The gradient of the iterating function of the Newton's solution, represented by the Jacobian of partial derivatives, is proportional to the generator subtransient reactance, and inversely proportional to the commutation reactance. Thus the gradient is large for large generator subtransient reactance and small commutation reactance values, which can lead to divergence. However the unified solution has been found to be fast and robust for typical reactance values and no modification is needed for harmonic analysis of direct connected units. This is a significant improvement in comparison with sequential IHA algorithms, in which divergence occurs when the commutation reactance is smaller than 0.1 p.u. and generator impedance is larger than 0.1 p.u..

The unified solution has been intervalidated with time domain simulations using the PSCAD2-EMTDC program. For the first time, it is possible to intervalidate dynamic simulations with a harmonic domain analysis for direct connected units. It has been found that the large snubber capacitance used in time domain simulations to aid numerical stability does have significant influence on the harmonic levels.

Chapter 6

HARMONIC BEHAVIOUR OF DIRECT CONNECTED UNITS

6.1 INTRODUCTION

In the absence of ac harmonic filters, the generator terminal voltages are distorted and the commutation voltages are the sinusoidal voltages E'' behind generator subtransient reactance. However as E'' is not physically accessible and varying with the generator terminal voltages as well as currents, the determination of firing angles in direct connected units are more complex than in conventional HVdc schemes. Alternatively, firing angles can be referenced to the generator terminal voltages, leading to a simpler firing control mechanism since generator currents are not required in the determination of firing angles. Section 6.2 discusses the advantages and disadvantages of using E'' and the generator terminal voltage as firing angle references.

Since the absence of ac filters also leads to a longer commutation period (also called overlap angle), firing angle limits due to overlap angle constraints are examined in Section 6.3. As transmitting power from remote hydro generating stations is one of the most suitable applications for the direct connected concept, the involved generators are usually of salient-pole type, and they would normally be connected in a Group Connection arrangement. The effects of generator saliency, rotor angle and saturation, and the number of generators in Group Connections on the harmonic levels are investigated in this chapter, with particular attention paid to the generator harmonic ratings. The generator terminal power factors in direct connected units are also compared with those in perfect ac filtering HVdc schemes in Section 6.4.

In the absence of ac filters and local load, generator speed can be adjusted to suit the optimal operation of the turbines. The economic advantages of the adjustable speed operation of Unit Connections have been well documented [Naidu and Mathur 1989]. However since the transformer leakage and generator subtransient reactance vary with speed, the harmonic content on the ac and dc side of the convertor are also varied with speed. Moreover the dc side harmonics will be varied over a wide range of frequency, and consequently direct connected units are more likely to be operated under resonance conditions on the dc side of the convertor than conventional schemes. Sections 6.7

and 6.8 examine the impact of adjustable speed operation on the ac and dc harmonic levels, particularly in the presence of dc side resonances.

6.2 FIRING ANGLE REFERENCES FOR DIRECT CONNECTED UNITS

In the presence of perfect ac filtering, the generator terminal voltages are the sinusoidal commutation voltages to which the firing angles are commonly referenced. On the other hand, the generator terminal voltages are distorted in direct connected units and the sinusoidal commutation voltage is the voltage $E"$ behind subtransient reactance as shown in Figure 6.1 for a non-salient generator. The valves must be fired after the crossings of $E"$ to avoid mis-firing, but can be fired before the crossings of the terminal voltages as $E"$ leads the terminal voltage V for a lagging power factor angle of less than 90^o, which is common in direct connected schemes. The *cosine* of the angle ϕ_e, measured from $E"$ and I_1, is defined as the internal fundamental displacement factor; $\cos\phi$ is the generator terminal power factor.

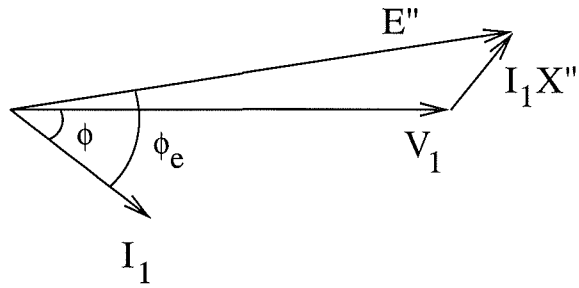

Figure 6.1 Phasor diagram of a non-salient generator in direct connected units.

The advantage of using the ideal sinusoidal voltage behind subtransient reactance $E"$ as the firing angle reference is that the limit for mis-firing is simply zero degree. However since $E"$ is not physically obtainable, accurate measurements of the currents as well as generator terminal voltages are required to calculate $E"$. The extra monitoring signals required can lead to errors in the determination of firing angles in the control system. The determination of firing angles referenced to $E"$ is further complicated in the presence of saliency, as depicted in Figure 5.3, since $E"$ varies with the generator terminal voltages, currents as well as rotor angle. On the other hand, by choosing the generator terminal voltage as the reference for firing angles, firing control process is simplified considerably as the currents are no longer required to be monitored. Moreover the existing firing control for conventional HVdc schemes, in which the reference is the generator terminal voltage, can then be used for direct connected units with practically no modification.

Figure 6.2 shows the relationship between firing angles referenced to the generator

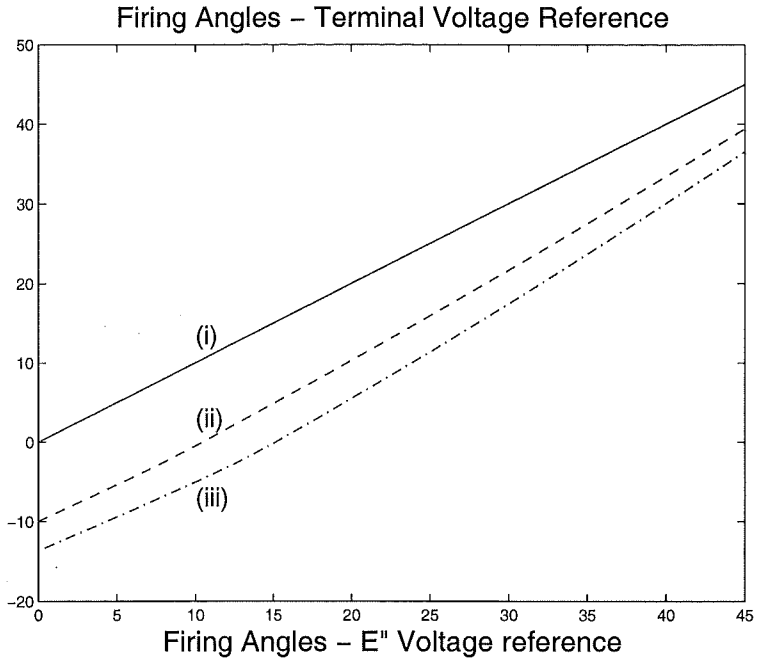

Figure 6.2 Relationship between firing angles referenced to the generator fundamental terminal voltage and internal voltage $E"$; (i) Perfect ac filtering, (ii) and (iii) direct connected units with non-salient generators with $X" = 0.2$ and 0.3 p.u. respectively.

fundamental terminal voltage and internal voltage $E"$ for typical $X"$ values of 0.2 and 0.3 per unit at generator rated power. As $E"$ typically leads V_1 by 5^o to 15^o, a zero firing angle referenced to the terminal voltage implies a firing angle of 5^o to 15^o with reference to $E"$ at rated power.

For comparison between direct connected units and conventional HVdc schemes which are assumed to have perfect ac filtering, it is necessary to use $E"$ as the reference. But for the operation of direct connected units, it is simpler to use the generator terminal voltage as the reference. Thus both references are used where appropriate. Firing angles referenced to $E"$ are simply referred to as firing angles (which has been conventionally defined in textbooks), whereas firing angles referenced to the terminal voltage would be clearly indicated.

It should be noted that the firing angle must be referenced to the sinusoidal commutation voltage $E"$ in the simplified convertor formulae [Kimbark 1971] since the generator terminal is an intermediate node and inaccessible when using the simplified formulation. On the other hand, the firing angle can be arbitrarily referenced, for instance to the terminal voltage or any other voltage, in the unified iterative solution. This is possible because the effects of generator subtransient reactance and the transformer leakage reactance on the commutation process can be considered separately in the iterative solution by allowing for distortion on the pseudo-commutation voltages, which have been chosen as the generator terminal voltages in the described model.

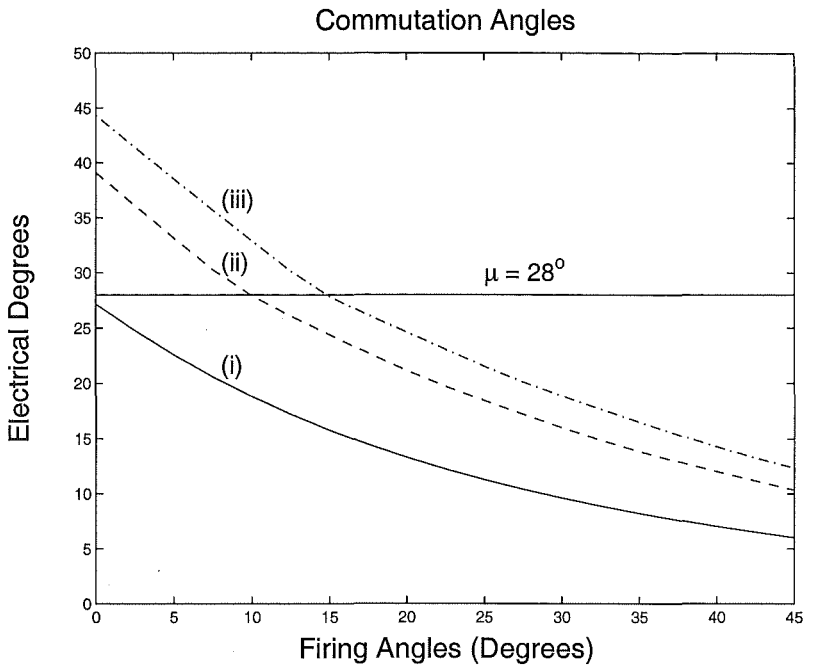

Figure 6.3 Comparison of commutation periods for direct connected units and perfect ac filtering schemes; (i) Perfect ac filtering, (ii) and (iii) direct connected units with non-salient generators with $X"$ = 0.2 and 0.3 p.u. respectively.

6.3 OVERLAP ANGLE CONSTRAINT

The absence of ac filters lengthens the commutation period since the generator subtransient reactance is also part of the commutating reactance. This is illustrated in Figure 6.3 for generators with typical $X"$ of 0.2 and 0.3 per unit, and transformer with typical leakage of 10%. The firing angle in the perfect filtering case is referenced to the sinusoidal terminal voltage whereas the internal voltage $E"$ is the reference in direct connected units. In order to keep the commutation process of the two bridges forming the twelve-pulse convertor group independent from each other, the overlap angle should be kept under 30^o. The usual practice is to base the system design on a maximum overlap angle between 26^o and 28^o. For a $\mu = 28^o$ limit, the minimum firing angles are 10^o and 14.9^o, as shown in Figure 6.3, for direct connected units containing non-salient generator with $X"$ of 0.2 and 0.3 per unit respectively. The minimum firing angles for other overlap angle limits are listed in Table 6.1. The overlap angle limit is not a problem in the presence of perfect ac filtering for the same system.

6.4 GENERATOR TERMINAL POWER FACTOR

The $\cos\phi$ (or fundamental frequency displacement factor between the generator terminal voltage and current) is commonly used by generator manufacturers as power factor. By comparing the power factors of generators used in direct connected units and in perfect

μ	α_{min}	
	$X"$ = 0.2 p.u.	$X"$ = 0.3 p.u.
26^o	12.7^o	17.8^o
27^o	11.3^o	16.3^o
28^o	10^o	14.9^o

Table 6.1 Minimum firing angles for various overlap angle limits. Transformer leakage is 10%.

ac filtering schemes, this section investigates if any extra capacity in terms of generator terminal power factor is required for direct connected units.

Figure 6.4(a) shows the internal fundamental displacement factors $\cos(\phi_e)$ measured between the ideal sinusoidal commutation voltage behind subtransient reactance and the generator current. It is apparent that the larger the subtransient reactance, the longer the commutation period and thus the smaller the internal displacement factor. On the other hand, the generator terminal fundamental power factors, shown in Figure 6.4(b), do not follow the same trend. Although more total reactive power is required by the convertor for the larger subtransient reactance, the machine own internal reactive power (the amount corresponding with the subtransient reactance) is larger, leading to a higher generator terminal power factor for commutation angles of 30^o or less. Both of the internal displacement factor and generator terminal power factor increase with smaller firing angles for commutation angles of 30^o or less, but decrease when the commutation angles exceed 30^o.

For $\mu < 30^o$, the generator terminal power factor in direct connected units is higher than in perfect ac filtering schemes for a given firing angle. Thus for a generator with the rated terminal power factor of 0.915 at a typical 15^o firing angle in the presence of perfect ac filtering as indicated by the line *iv* in Figure 6.4(b), the same generator can be used in direct connected units with a higher nominal firing angle, for instance, 22^o or 26^o for $X"$ of 0.2 or 0.3 per unit respectively. It is assumed that the reactive power contributed by the ac filters are not taken into account when calculating the reactive power capacity of generators in the perfect ac filtering case. However, this gain in power factor capacity could be offset by the need to have a higher nominal firing angle to keep the overlap angle under 30^o in direct connected units. For instance, the nominal firing angle should be within $16.3^o < \alpha_{nominal} < 26^o$ to keep the overlap angle under 27^o and generator terminal power factor greater than 0.915 (obtained from the nominal 15^o firing angle in the presence of perfect ac filtering). As long as the firing angle is kept within the limits corresponding to the overlap angle and power factor constraints, practically no de-rating of generators in terms of power factor for direct connected operation is required.

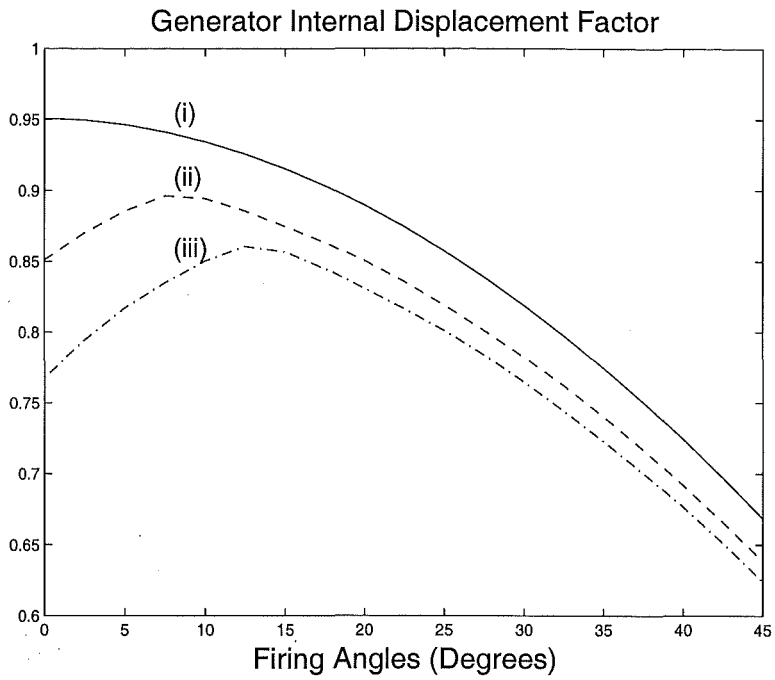

(a)

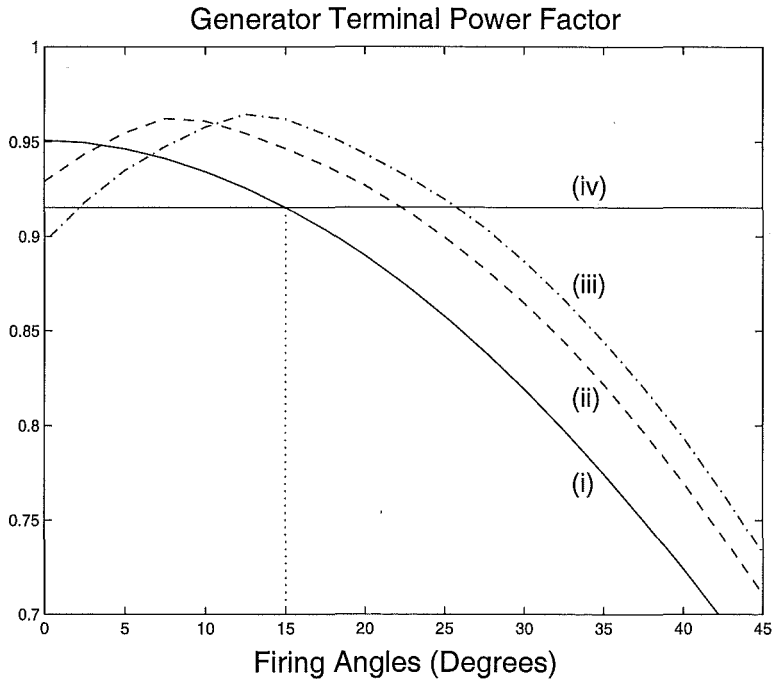

(b)

Figure 6.4 Comparison of (a) internal displacement factors $\cos(\phi_e)$, and (b) generator terminal power factors $\cos\phi$ for direct connected units and perfect ac filtering schemes; (i) Perfect ac filtering, (ii) and (iii) direct connected units with non-salient generators with $X^{"} = 0.2$ and 0.3 p.u. respectively; (iv) Terminal power factor rating in the presence of perfect ac filtering for a typical 15^o nominal firing angle.

6.5 EFFECTS OF SALIENT-POLE GENERATORS

6.5.1 Effect of Generator Saliency on Harmonic Levels

In a salient-pole machine the $12n-1$ negative-sequence voltages are made of two components due to the corresponding negative-sequence $12n-1$ and positive-sequence $12n+1$ convertor currents. This can be expressed in matrix form for the 11th and 13th harmonics as:

$$\begin{bmatrix} V_{11} \\ V_{13} \end{bmatrix} = \begin{bmatrix} Z_{g\,11,11} & Z_{g\,11,13} \\ Z_{g\,13,11} & Z_{g\,13,13} \end{bmatrix} \begin{bmatrix} -I_{11} \\ -I_{13} \end{bmatrix} \tag{6.1}$$

where the minus sign indicates that the currents are flowing into the generator. Expanding equation 6.1 using the saliency cross coupling terms derived in Chapter 3 yields (resistive terms are neglected):

$$\begin{aligned} V_{11} &= V_{11,11} + V_{11,13} \\ &= -Z_{g\,11,11} I_{11} - Z_{g\,11,13} I_{13} \\ &= -jA|I_{11}|e^{j\angle I_{11}} - Be^{j(\frac{\pi}{2}-2\delta)}|I_{13}|e^{j\angle I_{13}} \end{aligned} \tag{6.2}$$

where

$$\begin{aligned} A &= 11\frac{X_q'' + X_d''}{2} \\ B &= 11\frac{X_q'' - X_d''}{2}. \end{aligned} \tag{6.3}$$

Let P be the difference in phase angles between the harmonic current pair $12n \pm 1$, i.e.

$$P = \angle I_{11} - \angle I_{13}, \tag{6.4}$$

then the 11th harmonic voltage components caused by the 11th and 13th currents can be expressed in terms of the 11th current phase angle as:

$$V_{11,11} = -jA|I_{11}|e^{j\angle I_{11}} \tag{6.5}$$

$$V_{11,13} = -jB|I_{13}|e^{j\angle I_{11}}e^{j(-P-2\delta)}. \tag{6.6}$$

Thus the cross coupling term ($V_{11,13}$) is lagging the self-term ($V_{11,11}$) by an angle of $P+2\delta$.

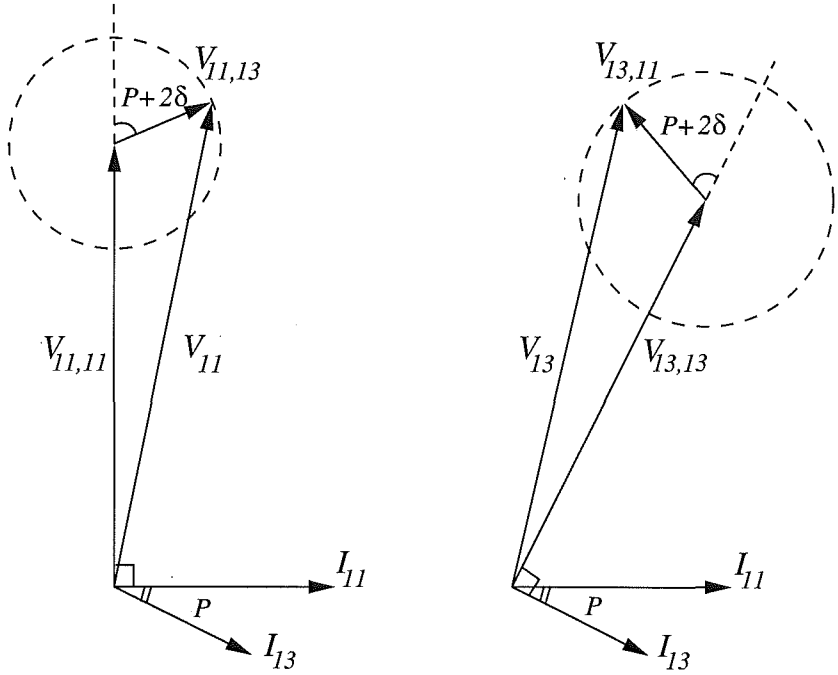

Figure 6.5 Phasor diagrams of saliency effect on harmonic voltages.

Similarly for the 13th voltage

$$\begin{aligned} V_{13} &= V_{13,13} + V_{13,11} \\ &= -jC|I_{13}|e^{j\angle I_{13}} - jD|I_{11}|e^{j\angle I_{13}}e^{j(2\delta+P)} \end{aligned} \tag{6.7}$$

where

$$\begin{aligned} C &= 13\frac{X_q'' + X_d''}{2} \\ D &= 13\frac{X_q'' - X_d''}{2}, \end{aligned} \tag{6.8}$$

and the cross coupling term ($V_{13,11}$) is leading the self-term ($V_{13,13}$) by an angle of $P+2\delta$.

It is easier to visualize equations 6.2 to 6.8 by using phasor relationships, shown in Figure 6.5, with all phase angles referenced to the generator fundamental terminal voltage phase angle. The addition of the two voltage components for each harmonic will result in larger or smaller voltage levels depending on the rotor angle and the difference between the harmonic current phase angles P. The rotor angle is dependent on the power output, synchronous reactances, terminal voltage, and generator saturation. The phase angle difference P is dependent on the firing and commutation angles, the later being in turn a function of the ac terminal voltages and their harmonics, dc current and its harmonics, firing angle and commutation reactance. As the ac terminal harmonic

voltages depend on generator saliency, all these quantities are inter-dependent. Therefore, an accurate harmonic solution in the presence of saliency can only be obtained by solving all the non-linearities in a unified iterative solution as described in Chapter 5.

However it is possible to estimate the worst effects due to saliency on the harmonic current levels by using the derived saliency formulation in Chapter 3. Consider the harmonic voltages in the case where the total phase angle $2\delta + P$ is 180^o. With reference to Figure 6.5, the 11th harmonic voltage can be obtained from equations 6.2 and 6.3 as:

$$\begin{aligned} |V_{11}| &= 11\frac{X_q'' + X_d''}{2}|I_{11}| - 11\frac{X_q'' - X_d''}{2}|I_{13}| \\ &= \frac{11}{2}X_d''(|I_{11}| + |I_{13}|) + \frac{11}{2}X_q''(|I_{11}| - |I_{13}|). \end{aligned} \tag{6.9}$$

Since typically $|I_{11}| \simeq \frac{13}{11}|I_{13}|$, and $\frac{1}{3}X_q'' \leq X_d'' \leq X_q''$, $|V_{11}|$ can be approximated as

$$|V_{11}| \simeq 11X_d''|I_{11}| \tag{6.10}$$

with upto 5% error only. Similarly,

$$|V_{13}| \simeq 13X_d''|I_{13}|. \tag{6.11}$$

As a result, the salient-pole generator can be considered as a non-salient generator with its subtransient reactance equal to the direct-axis subtransient reactance of the salient-pole generator. As the direct-axis subtransient reactance is smaller than the quadrature-axis subtransient reactance, the commutation period is the shortest and thus harmonic current levels are the largest. It is noted that this observation is valid only for direct connected systems in which no other harmonic besides the characteristic harmonics is produced by generator saliency.

On the other hand, when the angle $2\delta + P$ is 0^o, the harmonic voltage levels are:

$$|V_{11}| \simeq 11X_q''|I_{11}| \tag{6.12}$$

$$|V_{13}| \simeq 13X_q''|I_{13}|, \tag{6.13}$$

and thus the salient-pole generator can be considered as a non-salient machine with subtransient reactance equal to the quadrature-axis subtransient reactance. Consequently, the current harmonic levels are the lowest in this case.

By using a non-salient generator with a subtransient reactance equal to the X_d'' of the salient-pole generator, the maximum limit for the harmonic currents can be obtained. On the other hand, the minimum limit for the harmonic currents in a salient-pole machine

can be obtained by using a non-salient generator with its subtransient reactance equal to $X_q^{"}$. Figure 6.6(a) shows the 11th harmonic current levels for a test salient-pole generator (solid lines) when operated at rated power, and the maximum and minimum limits for harmonic currents. The limits are obtained by using non-salient generators with direct-axis or quadrature-axis subtransient reactance values. The results for the salient-pole case are obtained from the unified solution developed in Chapter 5; the direct and quadrature-axis subtransient reactances are 0.2 and 0.367 p.u. respectively. Other parameters for the salient-pole generator are listed in Appendix A1. The firing angles are measured from the ideal sinusoidal commutation voltage behind subtransient reactance. Figure 6.6(b) shows the harmonic voltage levels corresponding to the currents limits. Since the harmonic currents are dependent on the subtransient reactance and the harmonic voltages are dependent on the currents as well as the generator harmonic impedance, the minimum current limit does not always correspond to the maximum voltage limit.

For commutation angles of 30^o or shorter, the harmonic levels reduce with smaller firing angles. However, this trend is not applicable to cases where the commutation angles are longer than 30^o.

6.5.2 Effect of Saliency on Generator Terminal Power Factor

The maximum and minimum limits for commutation angle in direct connected units containing salient-pole generators can also be found by using non-salient generators with appropriate subtransient reactance values as shown in Figure 6.7. In order to keep $\mu < 28^o$, the firing angle should be approximately 10^o or larger when the salient-pole generator acts as a non-salient generator with $X^{"} = X_d^{"}$; 18^o or more when $X^{"} = X_q^{"}$. With reference to Figure 6.8, the corresponding generator terminal power factors for $\alpha = 10^o$ in the case where $X^{"} = X_d^{"}$ and $\alpha = 18^o$ for $X^{"} = X_q^{"}$ case are approximately the same, i.e. 0.96. In practice, the commutation angle would be in between the limits as shown in solid line in Figure 6.7 for the considered salient-pole generator. In this case, the minimum firing angle should be 12.5^o, which also results in a similar generator terminal power factor of 0.96, as shown in Figure 6.8. Thus in the consideration of generator terminal power factor rating, it is not necessary to minimize generator saliency by having full cage damper windings. However full cage damper windings could be recommended due to its positive effect on the generator dynamic response, for instance, to damp oscillations, suppress hunting, provide additional torque for synchronizing generators, etc. [Kimbark 1968].

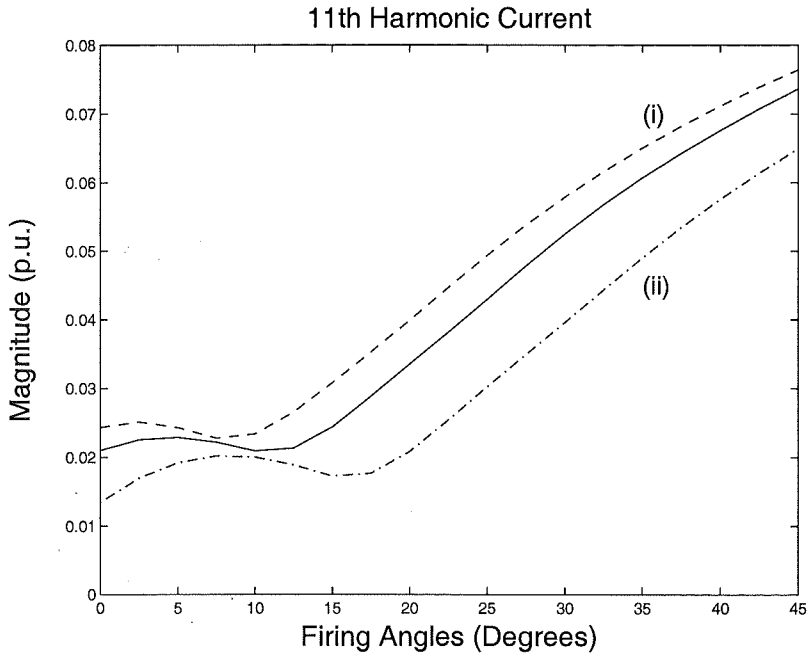

(a)

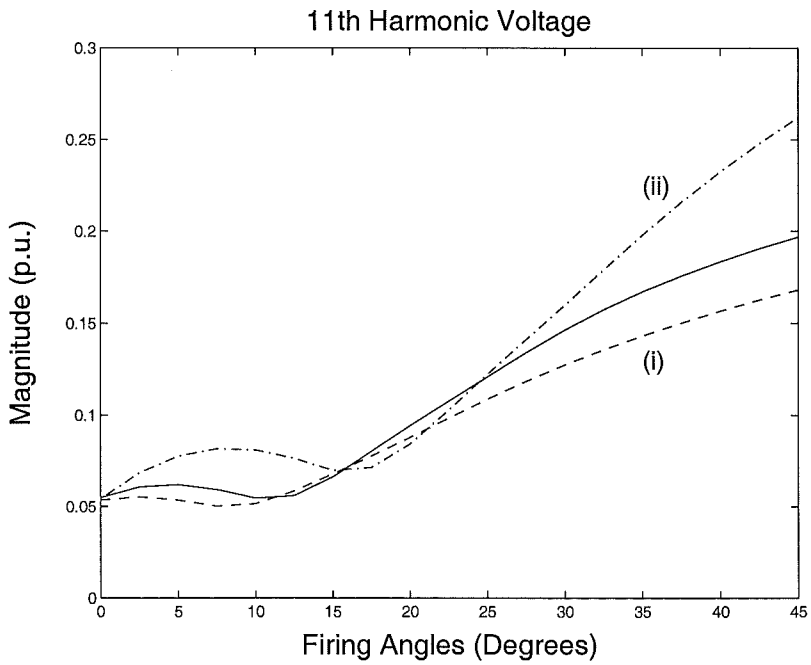

(b)

Figure 6.6 (a) Maximum and minimum limits for the 11th current harmonics of a salient-pole generator in direct connected units; (b) Voltage harmonics corresponded to the current limits. Solid: salient-pole generator, Dashed: non-salient generator with (i): $X" = X_d"$, and (ii) $X" = X_q"$; $X_t = 10\%$.

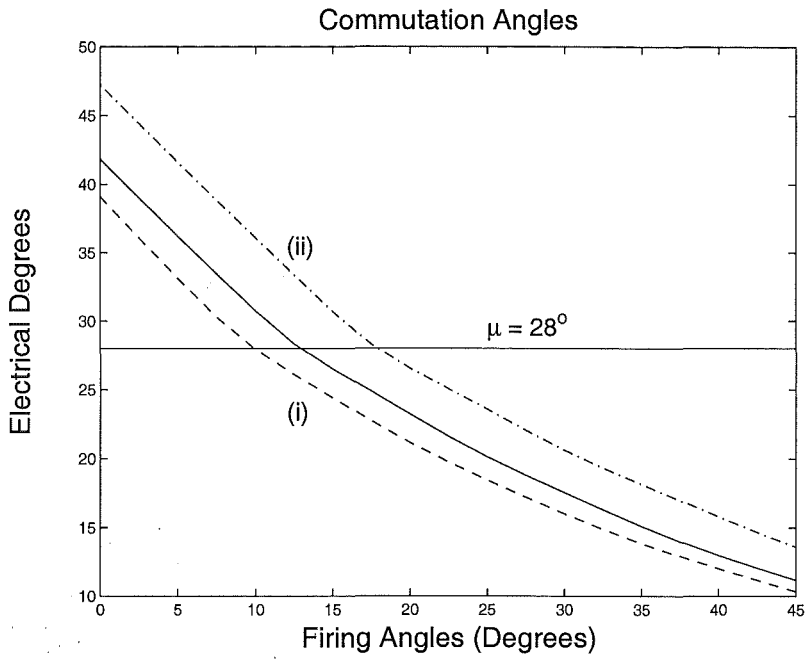

Figure 6.7 Commutation angles limits for salient-pole generators in direct connected units. Solid: salient-pole generator, Dashed: non-salient generator with (i): $X" = X_d" = 0.2$ p.u., and (ii) $X" = X_q" = 0.367$ p.u.; $X_t = 10\%$.

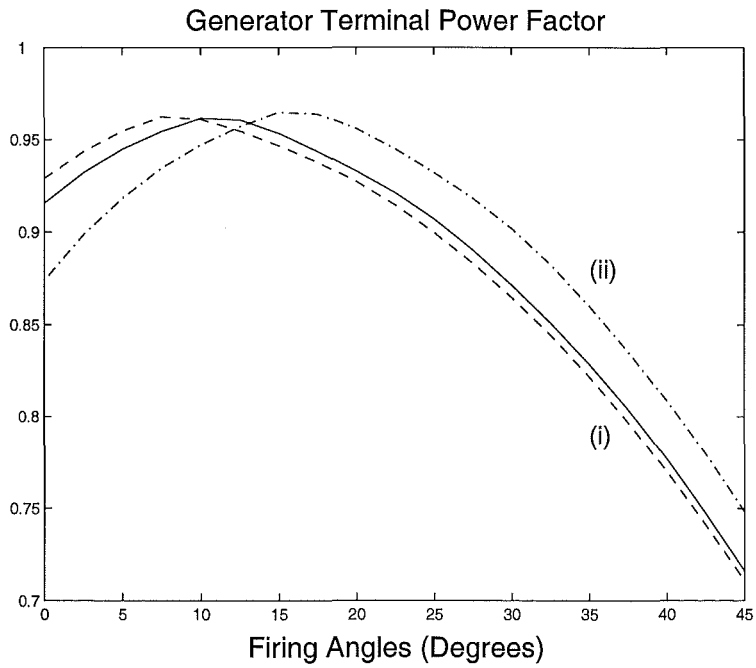

Figure 6.8 Generator terminal power factor ($\cos\phi$) for salient-pole generators. Solid: salient-pole generator, Dashed: non-salient generator with (i): $X" = X_d" = 0.2$ p.u., and (ii) $X" = X_q" = 0.367$ p.u.; $X_t = 10\%$.

6.5.3 Effect of Rotor Angle

With reference to Figure 6.5, the generator harmonic voltages are directly related to the rotor angle, and thus the commutation periods which depend on the terminal voltage distortion are also related to the rotor angle in the presence of saliency. The higher the degree of saliency, the larger the rotor angle effect on the harmonic levels. Figure 6.9 shows the effect of rotor angle on the commutation angle and the 11th harmonic current for various degrees of saliency. The degree of saliency in the subtransient reactances is defined as:

$$S = \frac{X_q'' - X_d''}{X_q'' + X_d''}. \tag{6.14}$$

In this case study, X_d'' and X_q'' are varied so that their average is constant and equal to 0.2835 p.u. to enable the results to be compared with those calculated from the simplified convertor formulae. The dc current order and firing angle are also kept constant and a large smoothing inductor (10H) is used to minimize the effect of the dc ripple. The vertical line indicates the saliency level for a machine with X_d'' and X_q'' equal to 0.2 and 0.367 p.u. respectively. The 5% transformer leakage is obtained when a Group Connection of 2 generators with $X_t = 10\%$ is operated in the unit connected mode, i.e. the output power is approximately half of the total rated power of the group connected unit. The Group Connection implementation is examined in Section 6.6. The firing angle is referenced to the generator terminal voltage so that the firing angle control is effectively independent of rotor angle.

Since the simplified convertor equations use the average of X_d'' and X_q'' in the commutation reactance, the commutation angle and the harmonic levels remain constant regardless of the degree of saliency as long as the average of the subtransient reactance is unchanged. On the other hand, a saliency formulation that does not include the rotor angle effect, e.g. with the rotor angle assumed to be zero, such as by Eggleston *et al.* [1988], can lead to large errors in the solution as also shown in Figure 6.9. For small six-pulse direct connected schemes, the effect of rotor angle is more substantial due to the larger harmonic levels involved in the six-pulse convertor operation. Therefore, it is important that the rotor angle is taken into account in the harmonic solution of direct connected schemes in the presence of saliency.

6.5.4 Effect of Generator Saturation

As examined in Chapter 3, generator saturation produces three main effects on the generator steady state behaviour. Firstly, saturation causes an increase in the dc excitation level, but since the excitation level is not used in the harmonic formulation, this effect can be ignored. Secondly, magnetic saturation produces odd order harmonics due to the

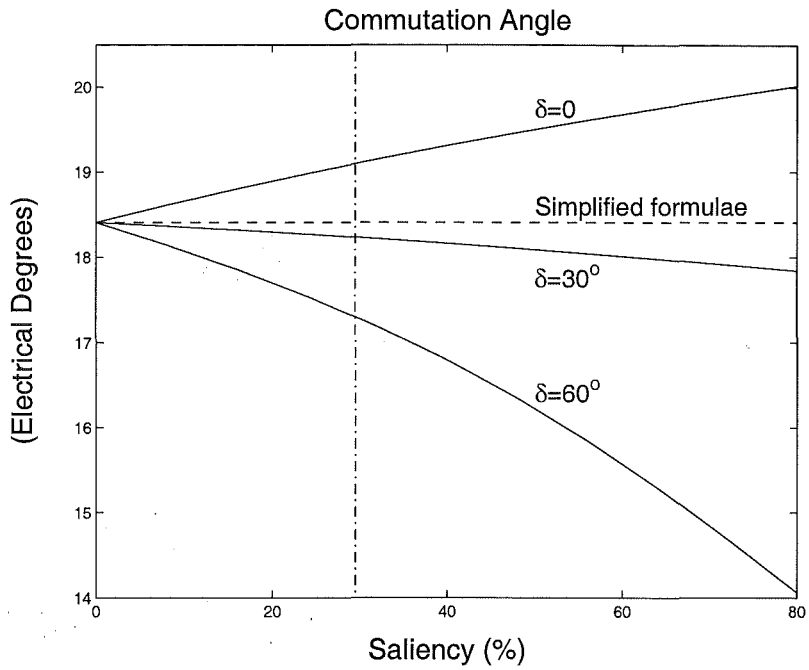

(a)

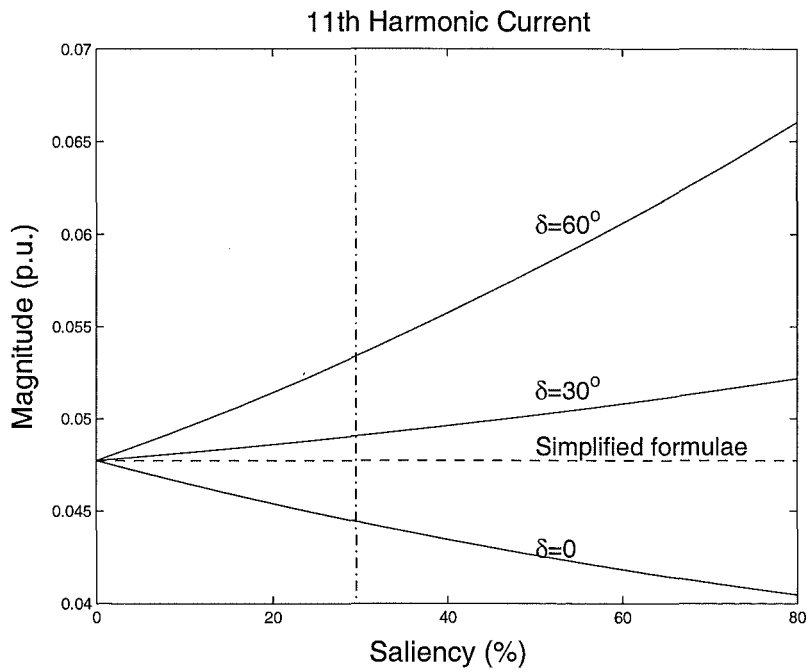

(b)

Figure 6.9 Effect of rotor angle on the commutation angle (a), and on 11th harmonic current level (b) in the presence of generator saliency; $\alpha = 10^o$ referenced to the generator terminal voltage, $X_t = 5\%$. The vertical line indicates the saliency level for a machine with $X_d^{"} = 0.2$ p.u. and $X_q^{"} = 0.367$ p.u.

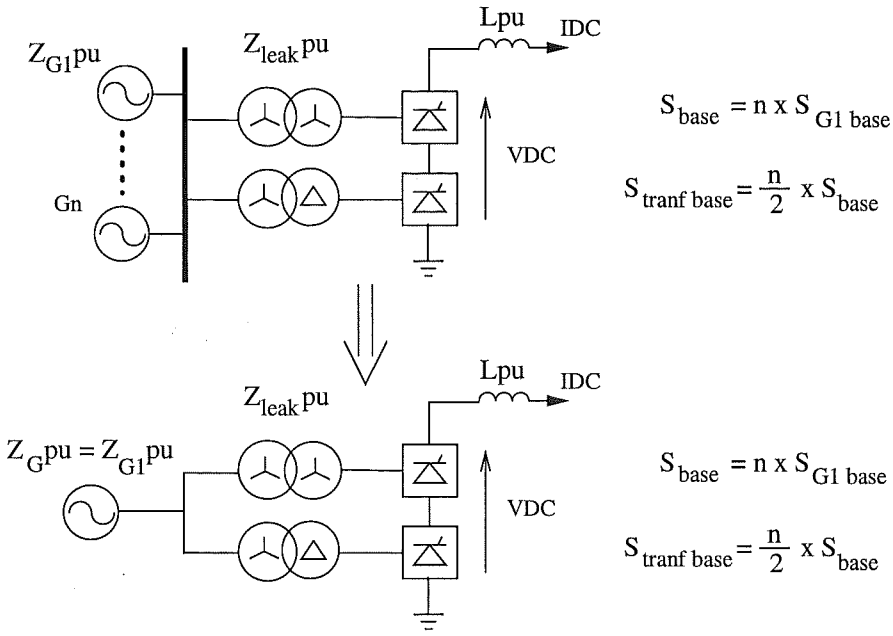

Figure 6.10 Simplification of a Group Connection to the basic Unit Connection for harmonic analysis.

distortion of the air gap flux waves. However it has been shown in Chapter 3 that the harmonics caused by generator saturation are negligible. Thirdly, saturation causes a decrease in generator synchronous reactances which lead to a smaller rotor angle, and thus changes in generator harmonic cross couplings. However since the decrease in rotor angle is in the order of a few electrical degrees for generators operated at full load, the changes in the harmonic levels are small. Moreover as the generator subtransient reactances X_d'' and X_q'' of a synchronous machine with damper windings are associated with fast transient flux that flows mostly in air, they remain constant for a wide range of terminal voltages under saturation conditions. Thus in the context of the harmonic analysis of a Unit Connection containing generators with damper windings, the effect of the generator saturation is insignificant.

6.6 GROUP CONNECTION IMPLEMENTATION

In a Group Connection of n generators, shown in Figure 6.10, the system power base is n times larger than the generator power base, and the convertor transformer nominal power rating is half of the system power base, i.e. $\frac{n}{2}$ times larger than individual generator power rating.

As the generators are connected in parallel, their combined actual impedance is reduced by n times. However since the power base of the system is now n times larger, the impedance base is reduced by a factor of n. Thus the combined per unit generator impedance is the same as the per unit impedance of each generator. Consequently, a Group Connection can be simplified to the basic Unit Connection with no adjustment

Generators	System base (MVA)	Transf. base (MVA)	X_d'' (p.u.)	X_t (p.u.)	I_{dc} (p.u.)
3	300	150	0.2	0.1	1
2	300	150	0.3	0.1	0.67
1	300	150	0.6	0.1	0.33
k	$n\times100$	$\frac{n}{2}\times100$	$\frac{n}{k}\times0.2$	0.1	$\frac{k}{n}\times$ 1
3	300	150	0.2	0.1	1
2	200	100	0.2	0.067	1
1	100	50	0.2	0.033	1
k	$k\times$ 100	$\frac{k}{2}\times100$	0.2	$\frac{k}{n}\times$ 0.1	1

Table 6.2 Adjustment for the generator and convertor parameters of Group Connections operating with a reduced number of generators. Generator base = 100 MVA, transformer rated power = 150 MVA; n, k are the number of nominal generators, and remaining generators respectively.

to the per unit values, as demonstrated in Figure 6.10. The harmonic currents on the primary side of the convertor transformers are shared evenly between the generators, given the assumption that the generators are identical and operated at similar power level, which is normally the case in a Group Connection. Consequently, the harmonic currents in a generator when being connected in a Group Connection are the same as when it is used in a Unit Connection. Note that when calculating the actual harmonic currents flowing in an individual machine, the power rating of the machine is used as the base value instead of the system base.

However when a Group Connection containing n generators is being operated with k generators, the harmonic levels will be affected considerably due to changes in the dc power order and reactances. If the system power base is chosen as n times the generator power base, the combined generator subtransient reactance is increased by $\frac{n}{k}$. The dc output is reduced to $\frac{k}{n}$ while the transformer leakage remains unchanged. The required conversion of the per unit reactances and power order is given in the top half of Table 6.2 for a Group Connection consisting of three 100 MVA generators. The transformers are 150 MVA units with 0.1 p.u. leakage reactance.

Alternatively, the system base can be chosen as k instead of n times generator power base. In this case, the per unit transformer leakage decreases to $\frac{k}{n}$, while the combined generator subtransient reactance, and dc output remain the same in per unit quantity. The conversion in this option, given in the bottom half of Table 6.2, is simpler than the other option since only one parameter which is the per unit transformer leakage reactance is required to be adjusted in the simulations. Consequently, a Group Connection containing n generators when operating with only k generators is equivalent to a Unit Connection with the transformer leakage reactance adjusted by a factor of $\frac{k}{n}$. The system base is chosen as k times the generator base.

6.6.1 Commutation Angle and Generator Power Factor in Group Connections

As the effective per unit transformer leakage and thus commutation reactance decreases with the smaller number of generators, the commutation angles are also reduced, as shown in Figure 6.11(a). This is advantageous in terms of satisfying the overlap angle limit, i.e. the firing angle can be reduced when a Group Connection is being operated with a reduced number of generator while maintaining the overlap angle to less than a set limit. With reference to Figure 6.11(a), the minimum firing angle to satisfy a $\mu = 28^o$ limit can be reduced from 10^o for the nominal 3 generators unit to 2^o in the unit connected mode. However a safe firing angle limit of 10^o to 15^o should be maintained to avoid mis-firing.

The contribution of generator subtransient reactance to the overall commutation reactance is larger when generators are taken out of a Group Connection. This leads to a higher generator terminal power factor for a given firing angle as shown in Figure 6.11(b). For the considered generator, the generator terminal power factor increases from 0.96 in the group connected mode with 3 generators to 0.98 in the unit connected mode for a firing angle of 10^o. Hence the generator power factor rating can be obtained from the group connected mode with the nominal number of generators connected.

6.6.2 Harmonic Content in Group Connections

Upon disconnection of a generating unit, the harmonic current loading in the remaining generators is significantly increased for a given firing angle. For a Group Connection containing 3 generators, the increase in the 11th harmonic current and the current THD is about 0.01 per unit for each generator taken out of service, as shown in Figures 6.12. The parameters of the generator and transformer used are as listed in Table 6.2. The number of generators in a Group Connection is thus an important factor in the calculation of the generator and transformer harmonic ratings. The generator harmonic ratings increase proportionally to the maximum number of generators in a Group Connection. However it is possible to reduce the generator harmonic loading by specifying a smaller nominal firing angle when a Group Connection is operated with fewer than the nominal number of generators, provided that the overlap angle limit and the safe limit for mis-firing are satisfied. Moreover the reduction in the generator fundamental power factor loading can provide extra capacity to accommodate the increase in the generator harmonic current loading. Figure 6.13 shows the harmonic voltage variation with respect to the number of generators in service. Although the increase in the harmonic current loading can be accommodated by the reduction of the generator terminal power factor, the increase in harmonic voltages must be taken into account in the insulation requirement of the generators.

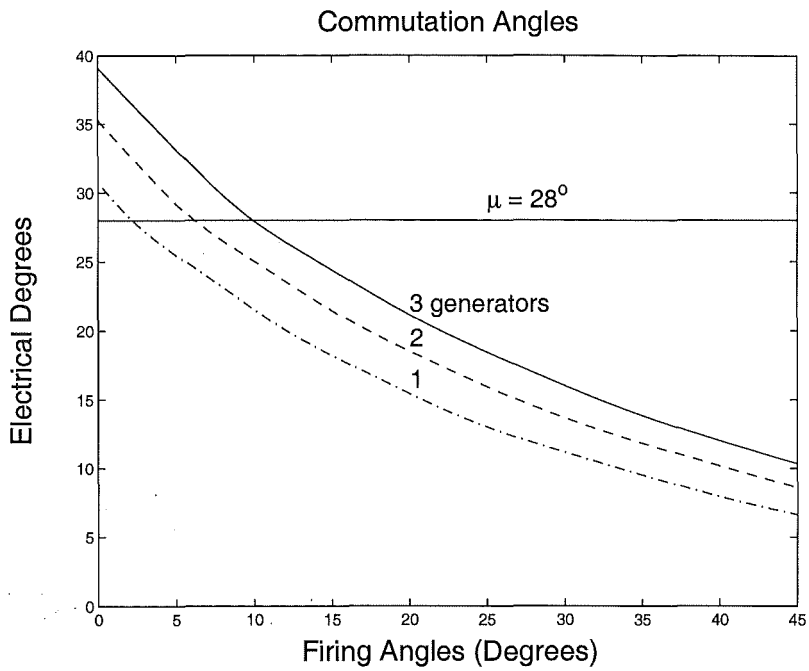

(a)

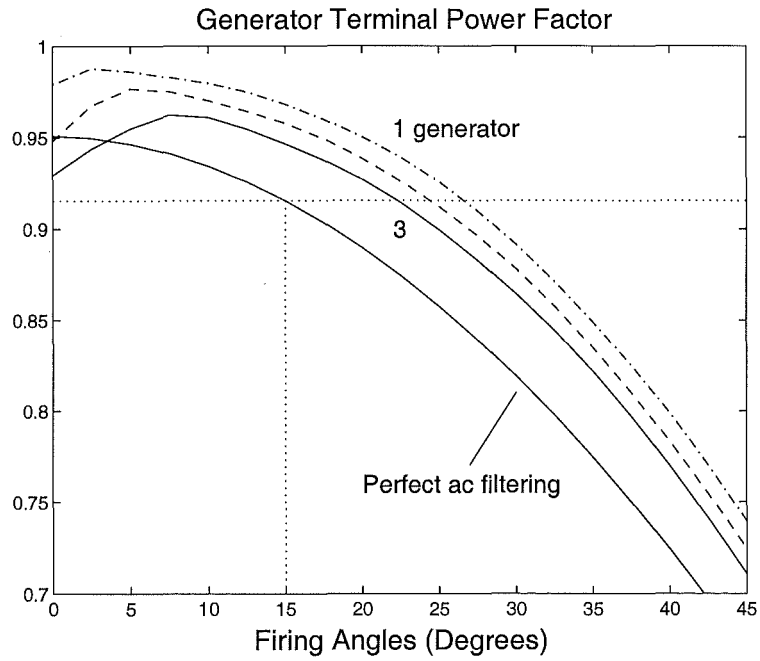

(b)

Figure 6.11 (a) Commutation angle and (b) generator terminal power factor in a Group Connection being operated with various number of generators. $X_t = 10\%$, $X_d'' = 0.2$ p.u.

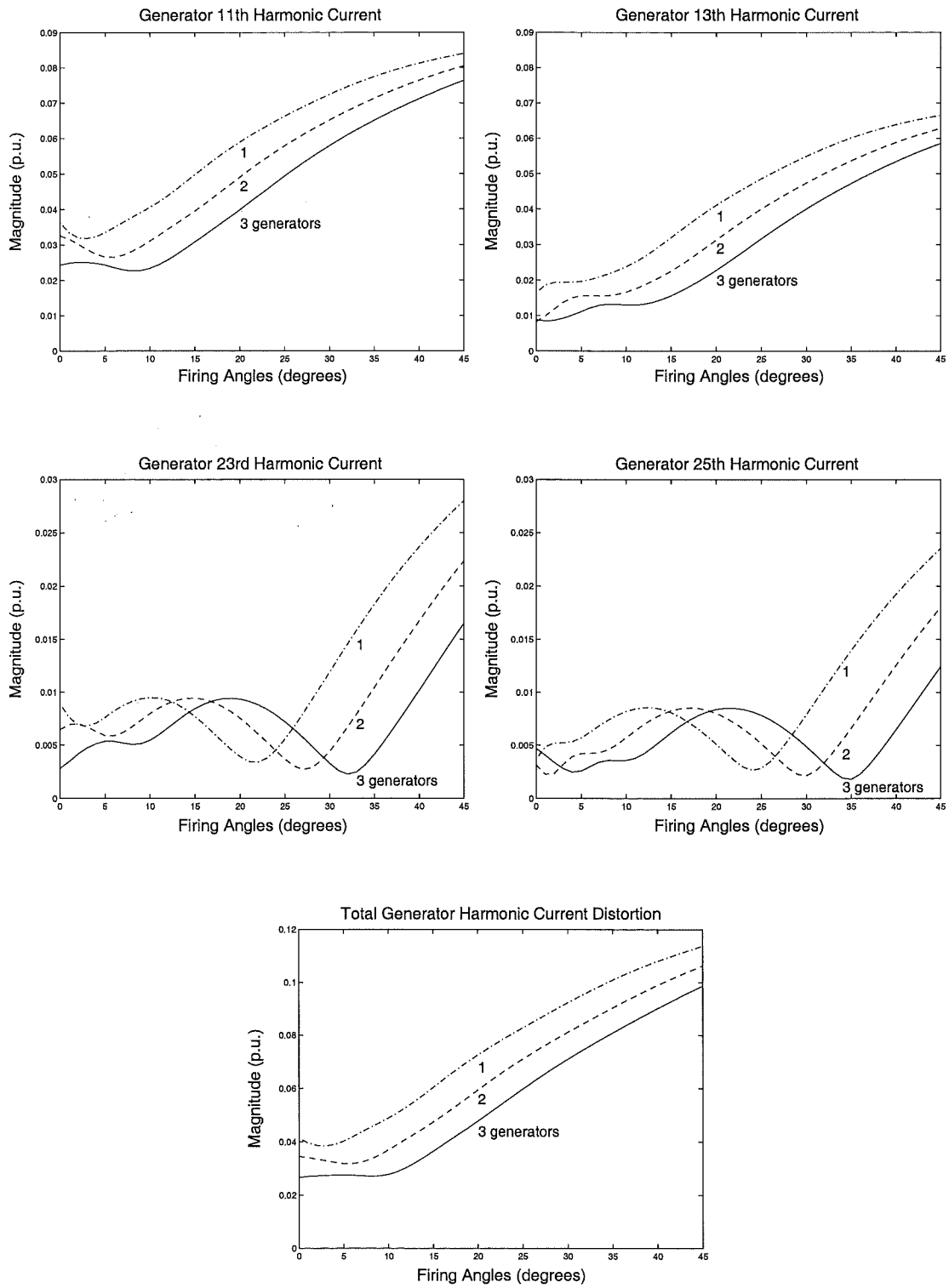

Figure 6.12 Generator harmonic currents in a Group Connection being operated with various number of generators. $X_t = 10\%$, $X^{"} = 0.2$ p.u.

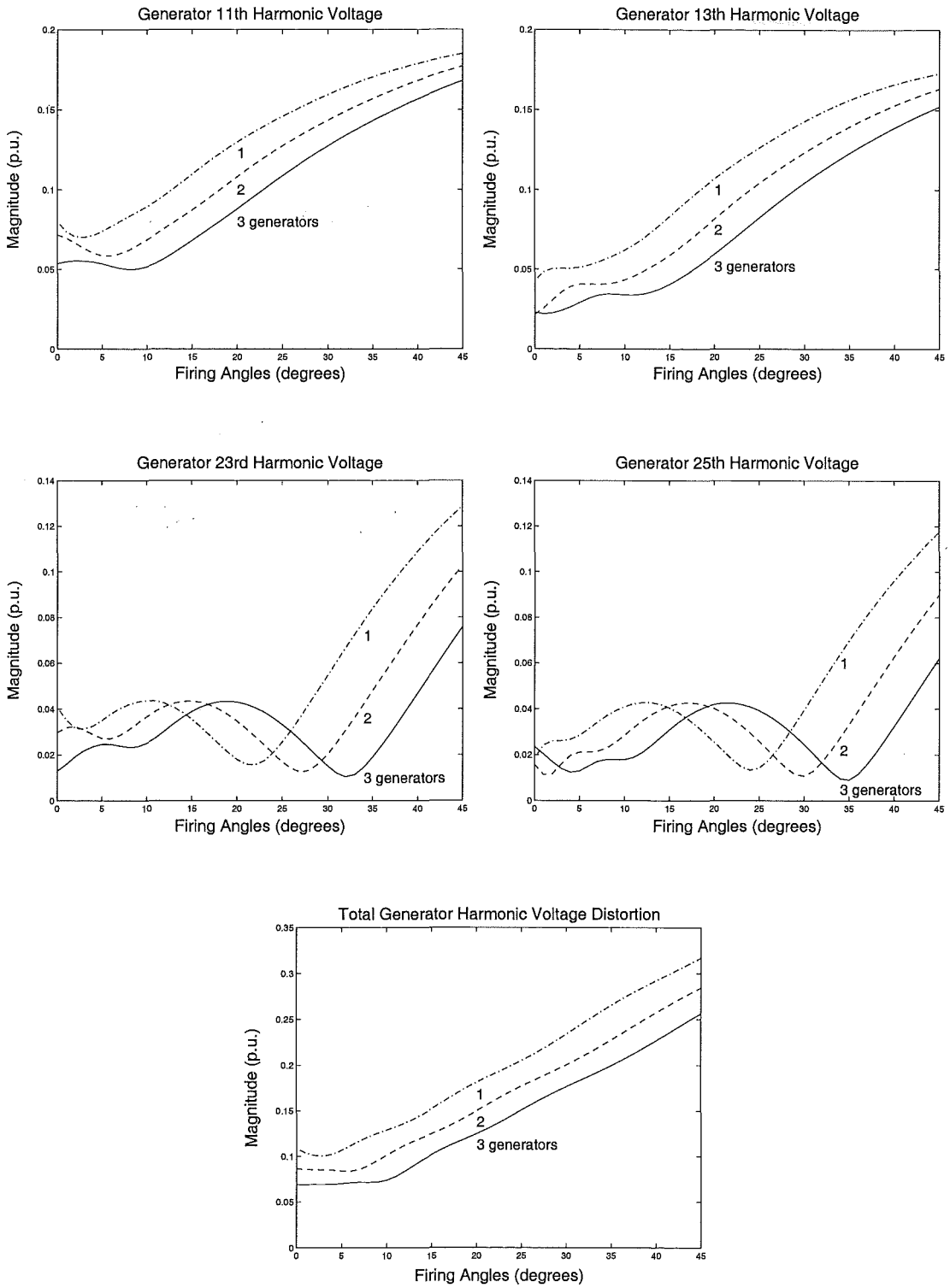

Figure 6.13 Generator harmonic voltages in a Group Connection being operated with various number of generators. $X_t = 10\%$, $X^{"} = 0.2$ p.u.

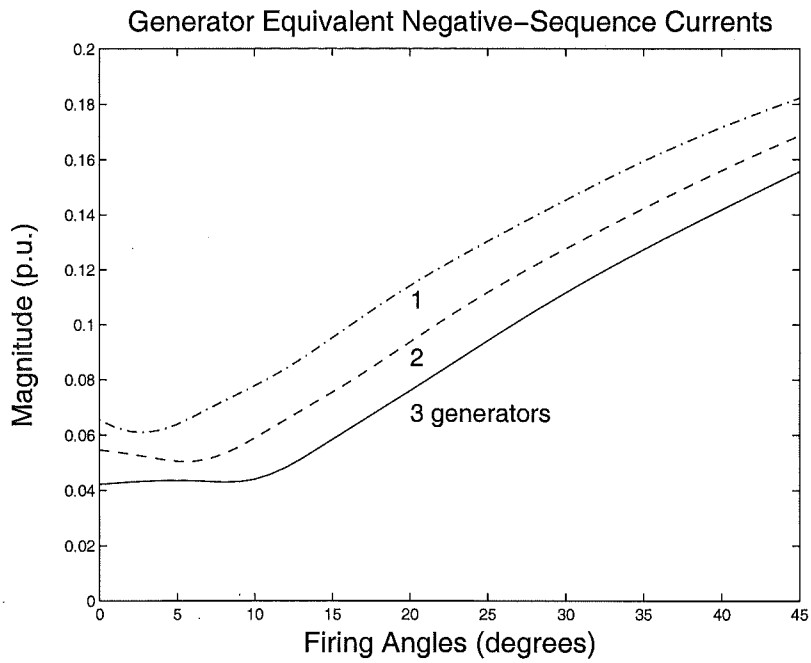

Figure 6.14 Generator equivalent negative-sequence currents for a Group Connection. $X_t = 10\%$, $X" = 0.2$ p.u.

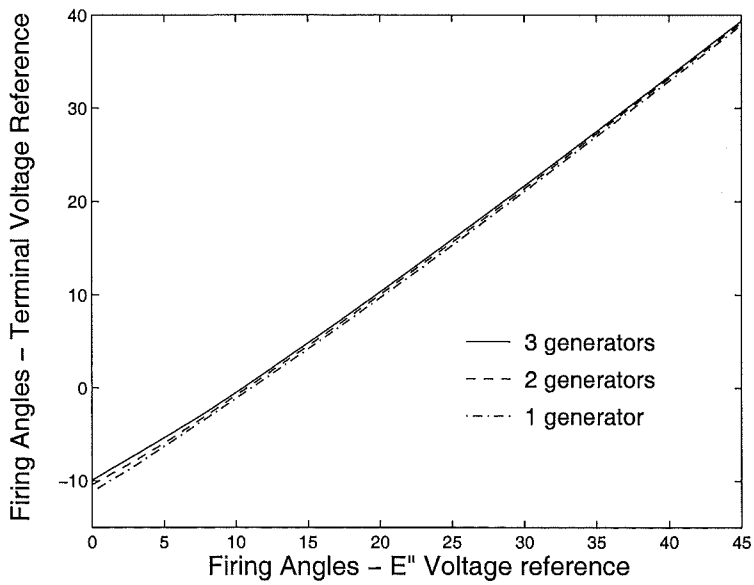

Figure 6.15 Relationship between firing angles referenced to $E"$ and to the generator terminal voltage V for a Group Connection. $X_t = 10\%$, $X" = 0.2$ p.u.

No. of Generators	Nominal firing angle α_{nom} restriction limits				
	$\mu \leq 28^o$ constraint	mis-firing constraint	$\cos\phi \geq 0.915^i$ constraint	$I_{en} \leq 10\%$ constraint	Overall limits
1	$\geq 2^o$	10^o	$\leq 26.6^o$	$\leq 16^o$	$10^o \leq \alpha_{nom} \leq 16^o$
2	$\geq 6^o$	10^o	$\leq 24.5^o$	$\leq 22^o$	$10^o \leq \alpha_{nom} \leq 22^o$
3	$\geq 10^o$	10^o	$\leq 22.5^o$	$\leq 26^o$	$10^o \leq \alpha_{nom} \leq 22.5^o$
No. of Generators	Nominal firing angle α_{nom} restriction limits				
	$\mu \leq 26^o$ constraint	mis-firing constraint	$\cos\phi \geq 0.935^{ii}$ constraint	$I_{en} \leq 10\%$ constraint	Overall limits
1	$\geq 4.4^o$	10^o	$\leq 23.2^o$	$\leq 16^o$	$10^o \leq \alpha_{nom} \leq 16^o$
2	$\geq 8.6^o$	10^o	$\leq 20.2^o$	$\leq 22^o$	$10^o \leq \alpha_{nom} \leq 20.2^o$
3	$\geq 12.7^o$	10^o	$\leq 18^o$	$\leq 26^o$	$12.7^o \leq \alpha_{nom} \leq 18^o$

Table 6.3 Nominal firing angle restriction limits for group connected units imposed by overlap angle, mis-firing, generator power factor and continuous equivalent negative-sequence harmonic loading constraints. X'' =0.2 p.u. and $X_t = 10\%$; (i) Generator terminal power factor for a nominal 15^o firing angle in the presence of perfect ac filtering; (ii) for a 10^o firing angle.

The rotor heating effect caused by convertor loads can be compared with standard specification ratings of generators by using the equivalent continuous negative-sequence current I_{en} [Krishnayya 1973]:

$$I_{en} = \sqrt{(\sum \sqrt{h}(I_{h-1}^2 + I_{h+1}^2))/\sqrt{2}} \tag{6.15}$$

Figure 6.14 shows the variation of equivalent negative-sequence currents with varying delay angle for a Group Connection when being operated with various numbers of generators. In the unit connected mode, the total harmonic loading is typically 10% for a firing angle of 16^o, but increases to about 15% for firing angles of 30^o. As generators are normally designed to sustain an equivalent of 10% continuous negative-sequence current loading, extra capacity for harmonic losses would not be required if the nominal firing angle is carefully selected. In this case, the nominal firing angle should not be more than 16^o, 22^o and 26^o for the unit connected, group connected with 2 and 3 generators mode respectively. The restriction limits of nominal firing angles derived from the overlap angle, generator terminal power factor, continuous equivalent negative-sequence harmonic loading and mis-firing constraints are given in Table 6.3. Provided that the nominal firing angles are kept within the derived limits, practically no extra capacity for generator power factor and harmonic current loading are required in group connected units.

Firing angles referenced to the generator terminal voltages (for control system that

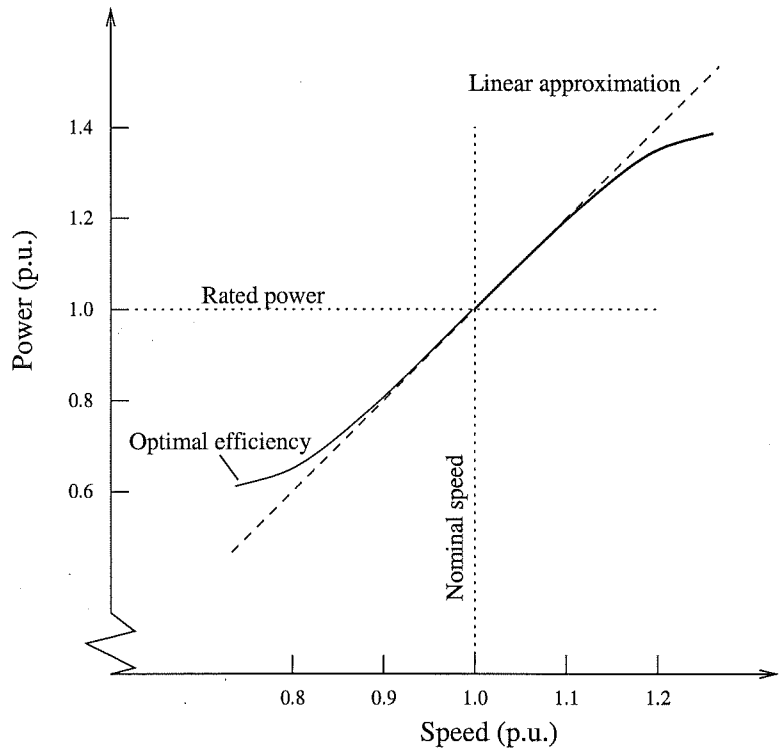

Figure 6.16 Typical hydraulic turbine power-speed characteristic.

uses V as the reference) can be derived from Figure 6.15, which shows the relationship between firing angles referenced to $E"$ and to the generator terminal voltage V. For instance, a 10^o firing angle referenced to $E"$ corresponds to a -1^o firing angle referenced to V; 16^o to 6^o, etc. In per unit quantities, the transformer leakage reduces with fewer generators in service while the dc current order and generator subtransient reactance are unchanged, resulting in smaller commutation period and generator terminal power factor angle. However the phase angle between $E"$ and V only increases slightly with fewer generators since the reduction in power factor angles is small, as indicated by the closeness of the plots shown in Figure 6.15.

6.7 EFFECTS OF ADJUSTABLE SPEED OPERATION

In the absence of ac filters and local loads, generators can be operated with adjustable speed to maximize turbine efficiency. The speed of generators are controlled so that they operate at the optimal efficiency for a machine loading given by the dc power order. A typical hydraulic turbine power-speed characteristic for optimal efficiency is shown in Figure 6.16. Within the $\pm$ 20% speed range the optimal efficiency characteristic can be linearly approximated as indicated by the dotted line.

In theory, the convertor transformers and generators can be designed and rated at any frequency other than the nominal frequency. But this can incur extra cost in the

design process. Alternatively, convertor transformers and generators that are rated at the nominal frequency can be used. Within the interested speed range, the transformer leakage and generator subtransient reactances will vary linearly with speed [CIGRE JWG 14/11-09, 1997]. As a result, the commutation angle is increased with higher speed as illustrated in Figure 6.17(a). The firing angles are referenced to E''. The power base is taken to be rated power at the nominal 50 Hz frequency, and the dc power order is taken from the approximated power-speed characteristic for optimal efficiency as shown in Figure 6.16. However since the intended application of adjustable speed operation is to utilize the generator optimal efficiency in the region where the speed is lower than the nominal, the commutation period in this region is smaller than those at the nominal speed. Thus the overlap angle limit can be taken at the nominal speed.

The generator terminal power factors, shown in Figure 6.17(b), are larger at lower speeds, i.e. less reactive power is required by the convertor. Hence the generator terminal power factor rating can also be taken at the nominal speed.

Figures 6.18 and 6.19 show the ac harmonic current and voltage variation with respect to generator fundamental frequency for various firing angles. The total ac harmonic current loading, indicated by the equivalent continuous negative-sequence current loading, increases as the fundamental frequency reduces due to a reduction in the reactances and subsequently commutation angle. However since the dc power order also reduces with lower speed, the increased harmonic loading is not a problem. On the other hand, the changes in the generator voltage THD is not significant at speed below the nominal speed. Thus generator harmonic ratings can be taken at the nominal speed and rated power output.

6.8 EFFECTS OF DC SIDE RESONANCES

6.8.1 On dc Side Harmonics

The Unit Connection model developed in Chapter 5 is used to investigate the effects of dc system resonances of a test system, shown in Figure 6.20, on the dc and ac harmonic levels. The test system consists of a typical double-tuned filter, smoothing inductor and a dc line. The smoothing inductor, dc filter parameters, generator and transformer parameters are taken from the New Zealand Benmore convertor terminal and are listed in Appendix A2. For simplicity, the dc line is represented by a resistance in series with an inductance. A more detailed dc line representation can be readily incorporated into the Harmonic Domain solution by using its harmonic impedances. The chosen line inductance of 0.2 H corresponds to an overhead dc line of 150 km with typical series line impedance of 1.33 mH/km [1].

[1]The line impedance is obtained from the New Zealand HVdc transmission line

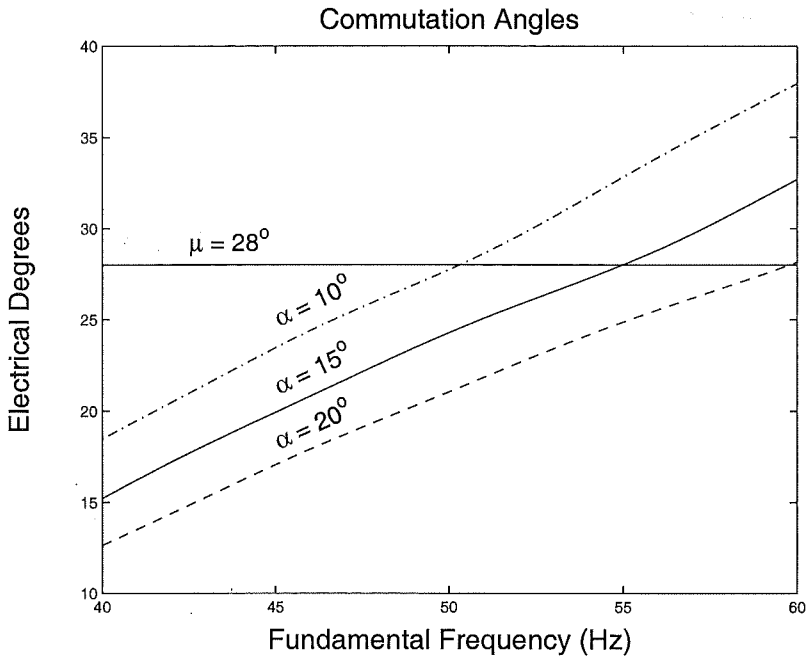

(a)

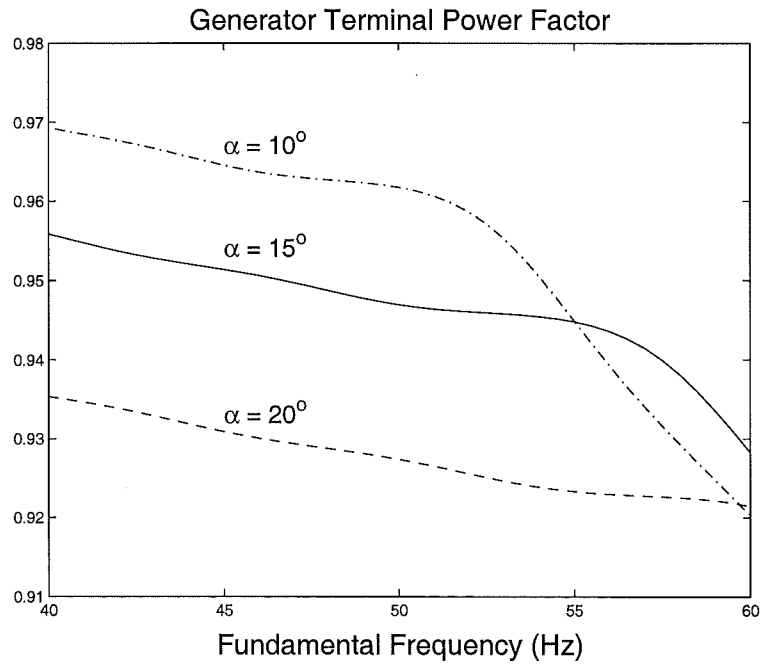

(b)

Figure 6.17 (a) Commutation angle and (b) generator terminal power factor variation with speed for various firing angle. $X_t = 0.1$ p.u., $X_d'' = 0.2$ p.u. at the 50 Hz nominal frequency.

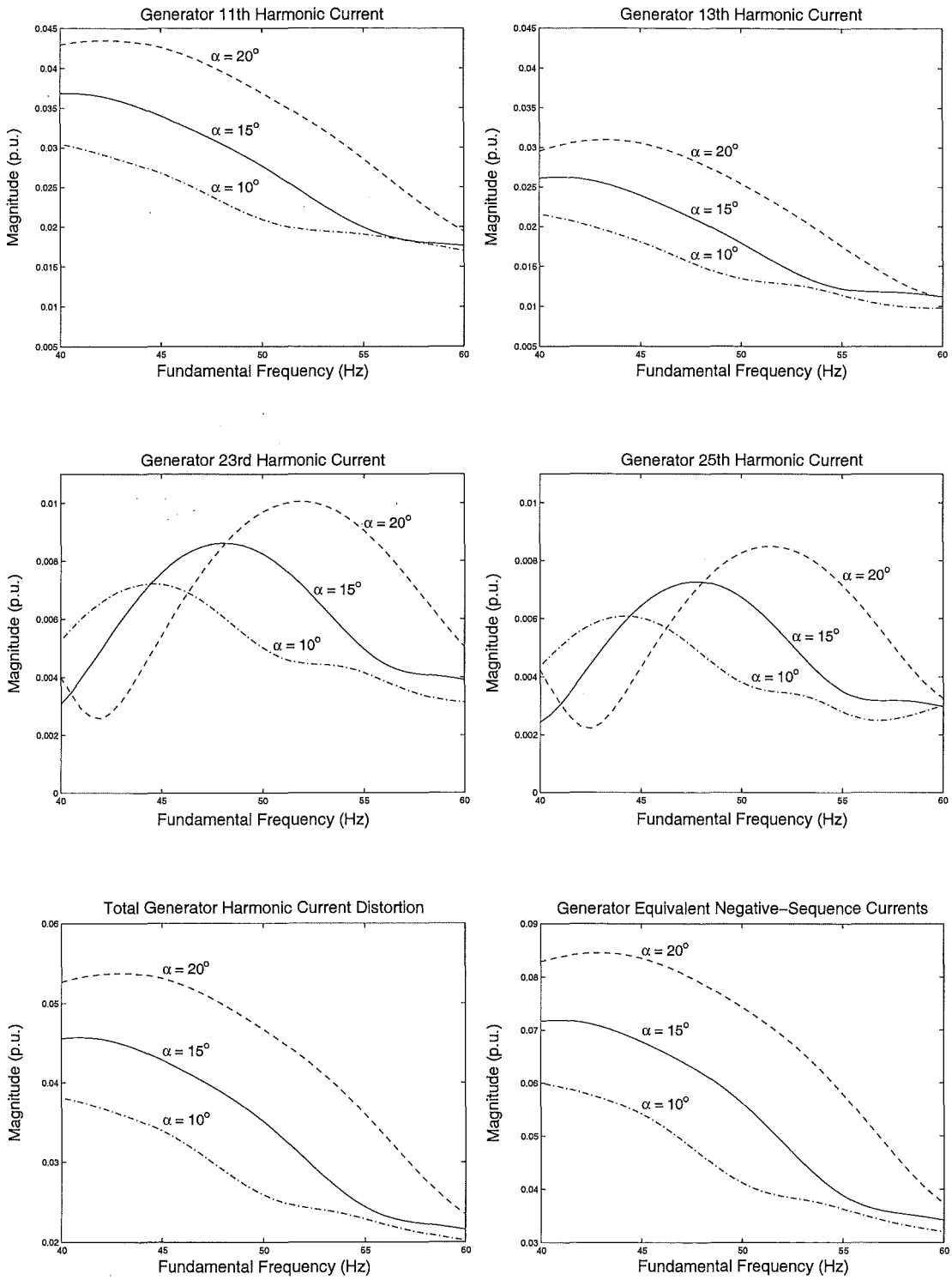

Figure 6.18 Harmonic current variation with speed for various firing angle. $X_t = 0.1$ p.u., $X_d'' = 0.2$ p.u. at the 50 Hz nominal frequency.

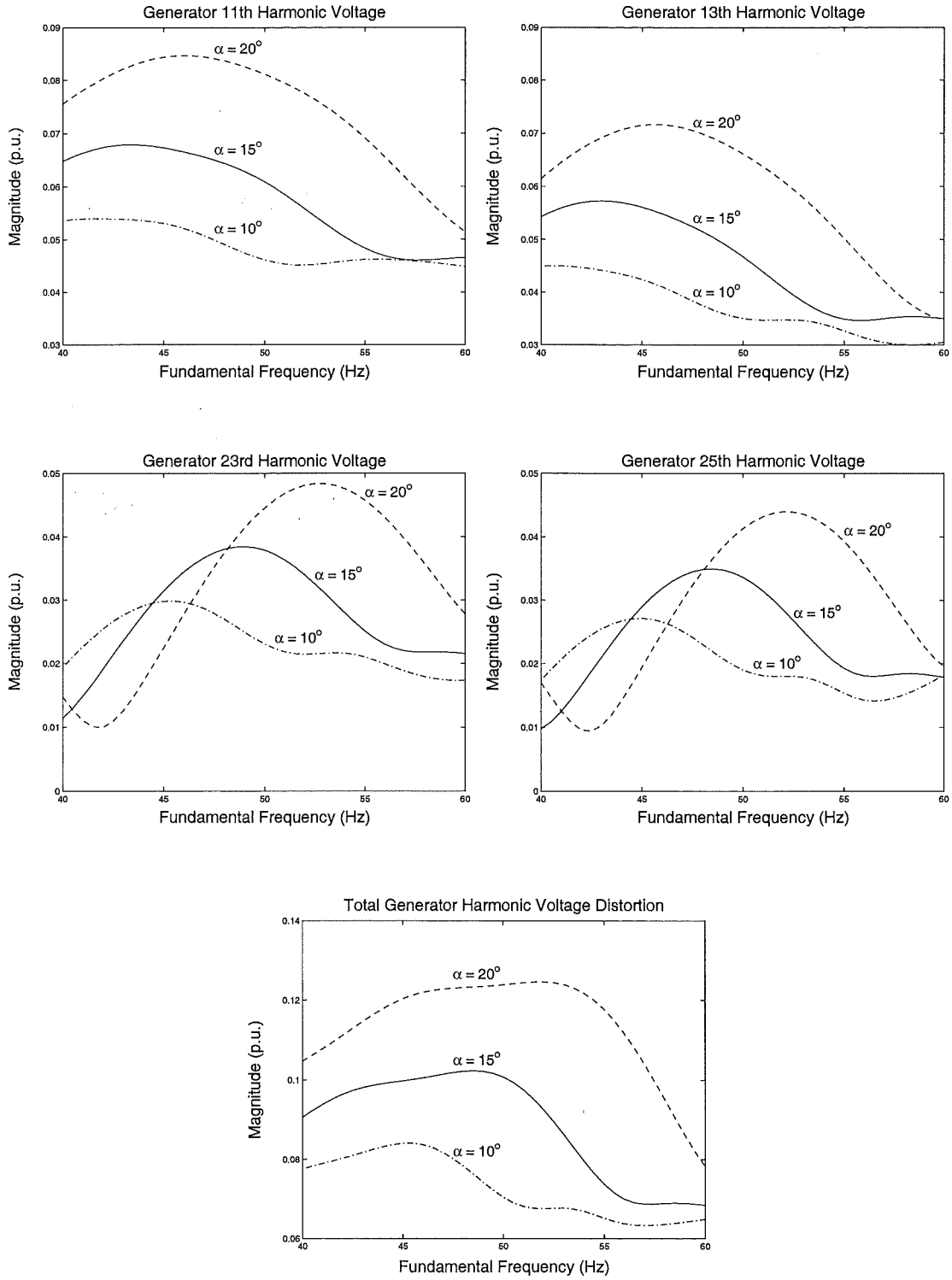

Figure 6.19 Harmonic voltage variation with speed for various firing angle. $X_t = 0.1$ p.u., $X_d'' = 0.2$ p.u. at the 50 Hz nominal frequency.

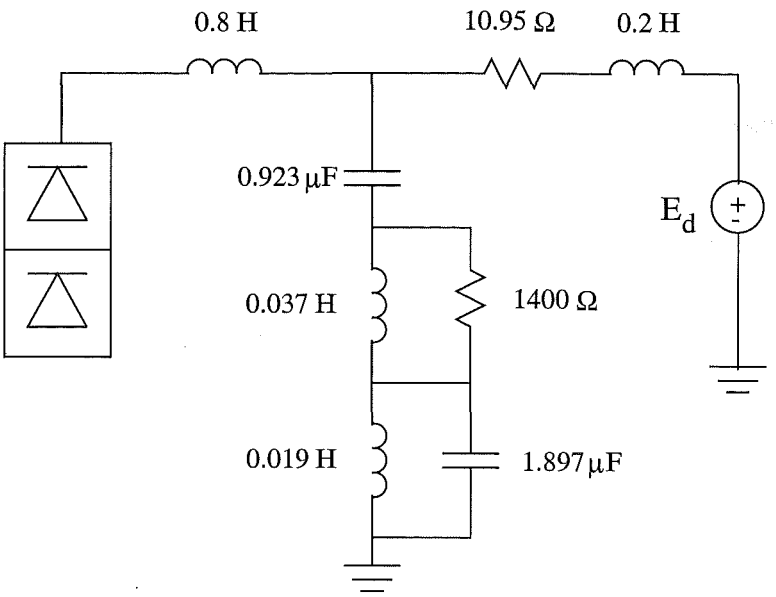

Figure 6.20 A typical dc side configuration with a dc filter, smoothing inductor and a simplified representation of a dc line.

The 12th and 24th dc harmonics are shunted by the low dc filter impedance shown in Figure 6.21(a), where the fundamental frequency is 50 Hz. However new resonance frequencies occur when the dc filter is combined with the smoothing inductance and the dc line impedance as shown in Figure 6.21(b). Parallel resonances occur at 325 and 875 Hz, and series resonances are at 350 and 885 Hz. Of particular importance is the series resonances at which the dc harmonic current ripples are large since the convertor acts as harmonic voltage sources. These large harmonic currents could cause harmonic interference in the dc line, and raise the required ratings of the filter.

The series resonances at 350 and 885 Hz are significantly away from the 12th harmonic (600 Hz) to have any substantial effect on this harmonic in the interested speed range of 35 to 65 Hz. However, they will have significant effects on the 24th, and the 6th as well as the 18th which could exist under unbalanced operation. Considering an unbalance case where the convertor transformer leakage reactance are 11.2 and 11.7% (at the nominal 50 Hz) for the two six-pulse valve groups respectively, Figure 6.22(a) shows the harmonic voltages at the dc filter point for the 6th, 12th, 18th and 24th for a speed range from 35 to 65 Hz in 0.25 Hz steps. At 36.9 Hz fundamental frequency, the 24th harmonic is drastically magnified due to the 885 Hz series resonance. The generators are operated at the optimal efficiency with the approximated power-speed characteristic as depicted in Figure 6.16.

The effects on the 6th and 18th harmonics are more critical as the generator speeds at which the series resonances occur are within the typical ±20% speed variation range of a Unit Connection. For instance, the small 18th voltage harmonic is greatly magnified at about 49 Hz fundamental frequency for this test system. The resonance frequencies

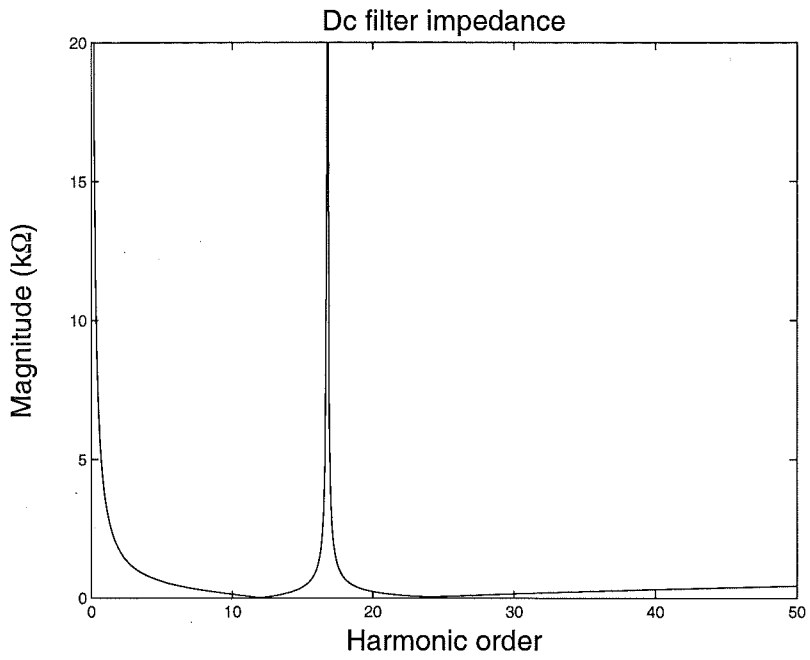

(a)

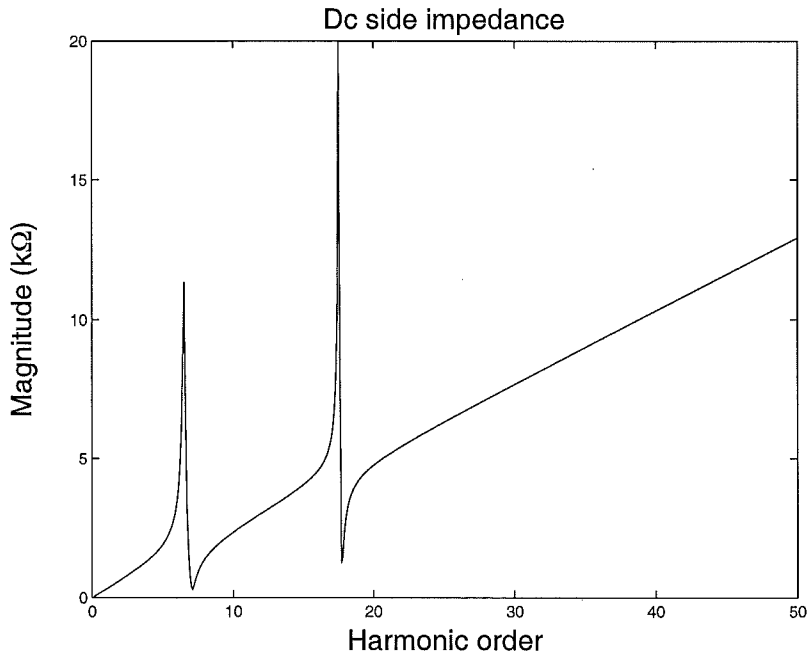

(b)

Figure 6.21 (a) Harmonic impedance of the dc filter. The fundamental frequency is 50 Hz. (b) Harmonic impedances of a dc system consisting of a smoothing inductor (0.8 H), dc filter and a line inductance of 0.2 H.

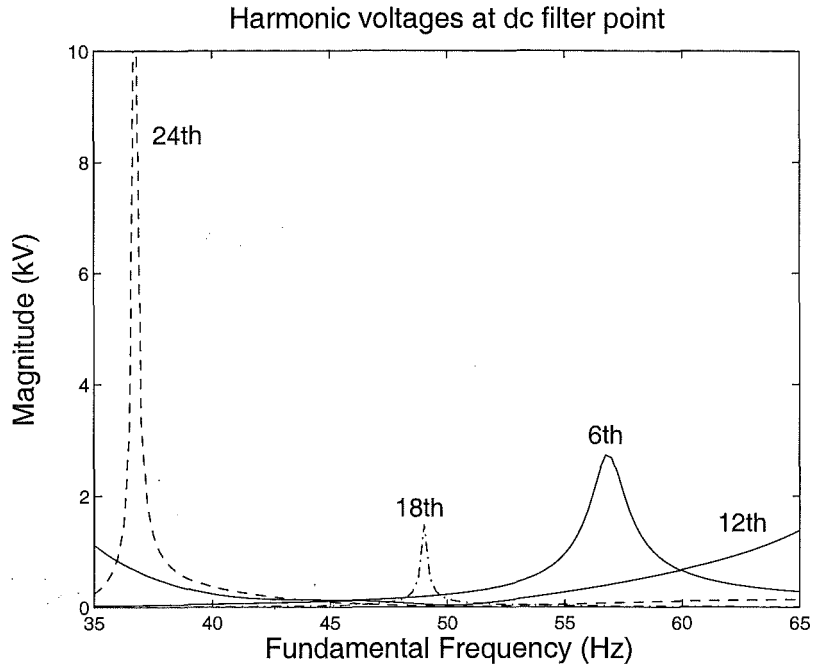

(a) Line inductance = 0.2 H

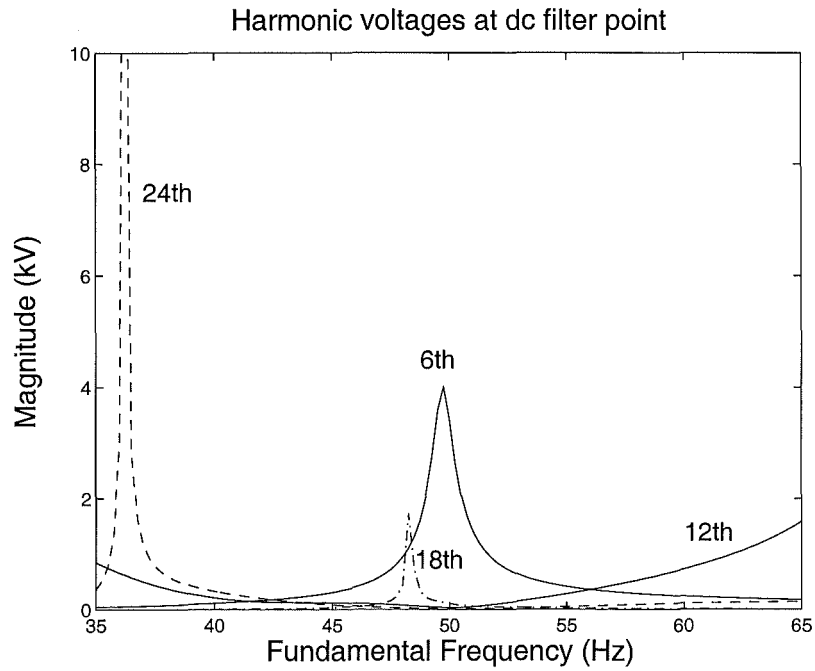

(b) Line inductance = 0.3 H

Figure 6.22 Harmonic voltages at the dc filter point for adjustable speed operation. $\alpha = 20^o$.

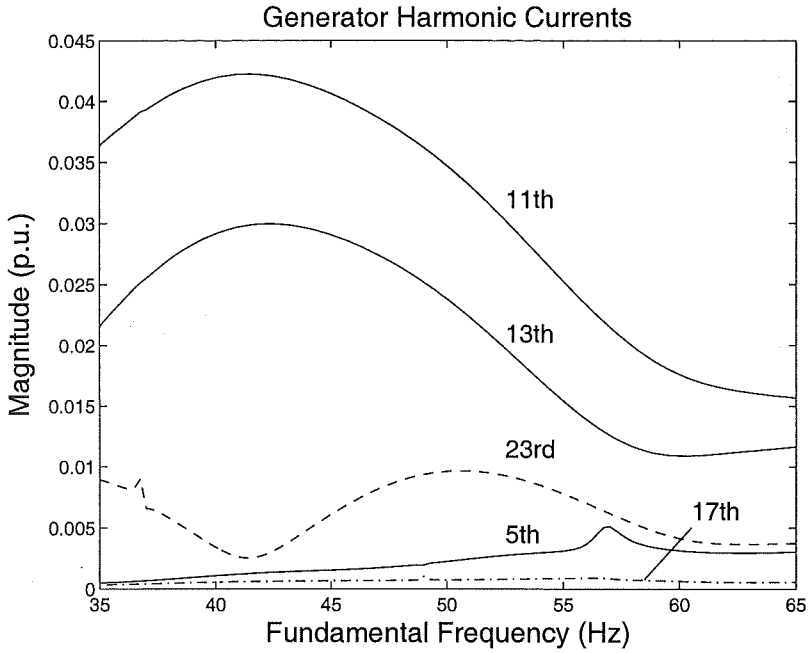

Figure 6.23 Generator current harmonics at different generator speed in the presence of dc side resonances. Line impedance = 0.2 H, $\alpha = 20°$.

of the dc impedances are also varied with the line impedance. Figure 6.22(b) shows the harmonic voltages at the dc filter point for a line inductance of 0.3 H. The magnification of the 6th harmonic voltage now occurs at generator speed of about 49.5 Hz. Thus the conventional tuned dc filter becomes ineffective for the frequencies at which series resonances on the convertor dc side occur.

Alternatively, other filtering schemes have been proposed such as active filters [Zhang *et al.* 1993] [Cheuksun *et al.* 1989], pulse multiplication [Arrillaga *et al.* 1993a] maybe more applicable for adjustable speed operation. Nevertheless, it has been demonstrated that the developed Unit Connection model is a suitable tool for the investigation of dc side resonances regardless of filtering schemes.

6.8.2 On ac Side Harmonics

For dc side resonances at harmonic frequencies, the magnification of dc side harmonic currents at dc resonance frequencies is reflected as spikes on the ac harmonic currents as shown in Figure 6.23. However since the magnitudes of the affected ac harmonic currents are small, the impact of dc resonances on the ac harmonic levels is insignificant. In conventional HVdc schemes, a dc resonance at the fundamental frequency can interact with an ac resonance at the second harmonic caused by ac filter capacitances and ac system impedance. This could result in convertor transformer core saturation instability [Chen *et al.* 1996]. However this is not a problem in direct connected units since ac filters are absent.

6.9 CONCLUSIONS

By choosing the generator terminal voltage instead of the voltage E'' behind generator subtransient reactance as the firing angle reference, the firing control mechanism can be simplified considerably since the generator currents are not required to be included in the firing angle determination. Moreover the existing firing control for conventional HVdc schemes, in which the reference is the generator terminal voltage, can be used for direct connected units with practically no modification.

It has been shown that the rotor angle has a significant effect on the commutation process in the presence of saliency and the close proximity of generators and convertors. Substantial improvement in the accuracy of the harmonic prediction for direct connected units has been obtained by taking into account the position of the rotor. An accurate harmonic solution in the presence of generator saliency can only be obtained by solving the non-linearities in a unified solution since all of the system variables are inter-dependent. However it has been shown that the maximum harmonic current levels in direct connected units containing salient-pole generators can be estimated by using a non-salient generator with its subtransient reactances equal to X_d'' of the salient-pole generator.

The harmonic loading on individual generator when connected in Group Connection is the same as in Unit Connection. However when a Group Connection is being operated with a reduced number of generators, the remaining generators are subjected to large increases in harmonic loadings. This is due to a reduction in the per unit convertor transformer leakage reactance and thus commutating reactance. The total generator harmonic loading in terms of equivalent continuous negative-sequence current is the largest in the unit connected mode and could exceed the normal 10% thermal design rating. However, it has been shown that by keeping the firing angle under a certain limit, which is dependent on power plant parameters, the harmonic loading can be kept under the normal 10% design rating. The range for nominal firing angles in direct connected units are also restricted by the overlap angle, generator terminal power factor, and misfiring constraints. Provided that the nominal firing angles are kept within the imposed limits, practically no extra capacity for generator power factor and harmonic current loading are required in direct connected units.

The generator harmonic content increases as the generator speed reduces. However the increased harmonic loading is not a problem since the dc power order also reduces with lower speed. The generator harmonic ratings can be taken at the nominal speed and rated power output. In the adjustable speed operation, conventional tuned dc filters become ineffective at frequencies where series resonances in the dc system occur, and the harmonic levels on the dc side can be magnified to unacceptable levels at those resonances frequencies. The effect of dc resonances on ac harmonic levels has been found to be insignificant due to the small magnitudes of the affected ac harmonics.

Chapter 7

HARMONIC EVALUATION OF BENMORE CONVERTOR STATION WHEN OPERATED AS A DIRECT CONNECTED UNIT

7.1 INTRODUCTION

The Benmore convertor station of the New Zealand HVdc link occasionally operates as an islanded or group connected system during the maintenance period of the interconnecting transformers, which link the convertor station and the rest of the ac system. In 1993, a set of single-phase harmonic measurements of a direct connected HVdc convertor scheme was collected [Macdonald *et al.* 1995]. While some of the results were of considerable assistance to substantiate the claims of the direct connection, they did not provide accurate harmonic information due to the limitations of the available, at the time, monitoring techniques, i.e. the single phase nature of the test, lack of phase referencing, manual triggering, etc.

Recent advances in harmonic monitoring, and in particular the availability of CHART instrumentation [Continuous Harmonic Analysis in Real Time: Technical Reference 1996], encouraged Trans Power New Zealand Limited to repeat the earlier field test to obtain more reliable information. CHART's improved dynamic range and continuous updating of the fundamental frequency improves the detection of harmonics with small magnitudes, especially the non-characteristic harmonics. Its accurate GPS (Global Positioning System) based time stamping capability and synchronization combined with multi-channel and multi-unit configuration permits the computation of the harmonic phase angles and the signal sequence components at different locations.

This chapter describes the measurement procedures, the setup and configuration of the CHART instrumentation, and the results. The results include the measured waveforms and their harmonic contents in sequence components for a range of dc line current. The harmonic ratings for generators in a Group Connection are also investigated. The measured and calculated firing angles described in this chapter are referenced to the generator terminal voltage since the internal voltage E'' is inaccessible for measurements. The test results are also used to assess the accuracy of the developed harmonic domain Unit Connection models.

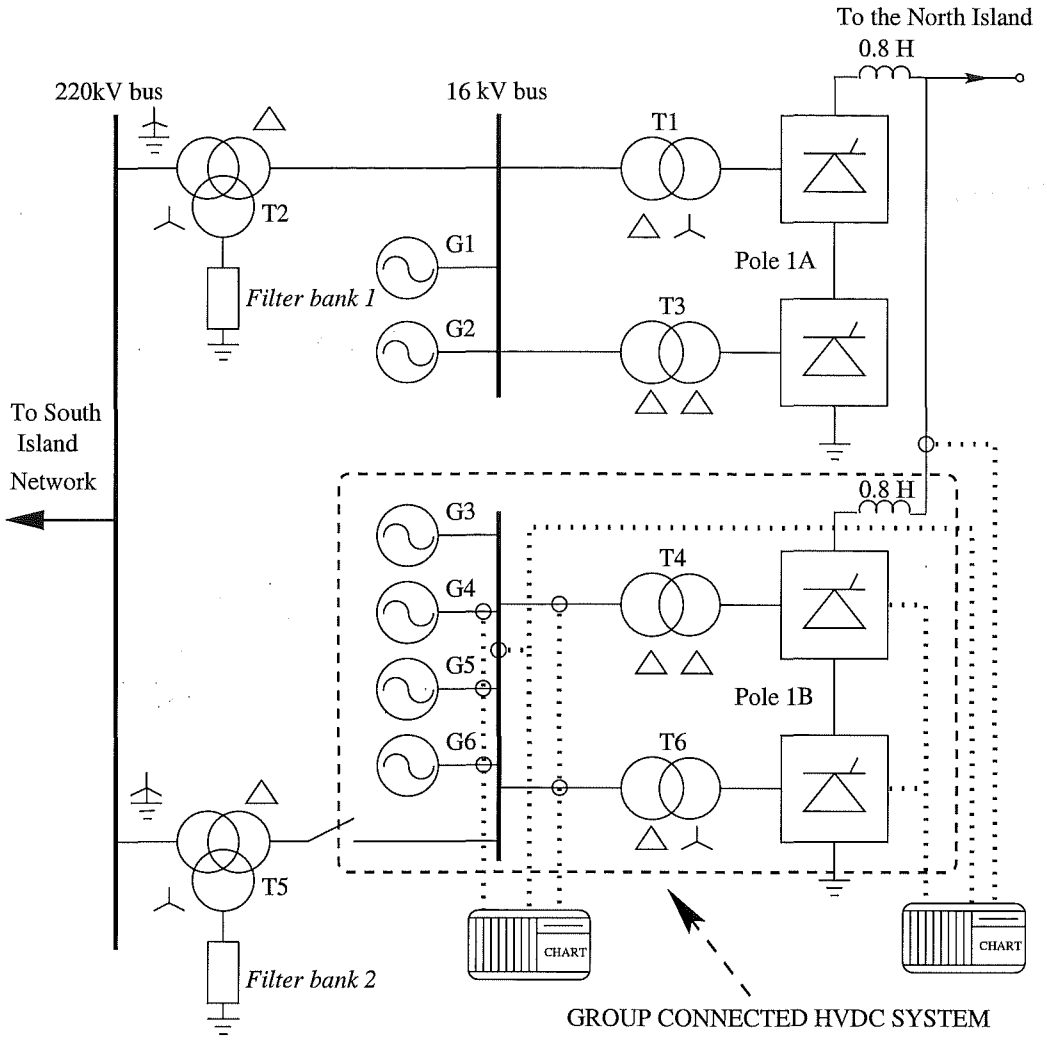

Figure 7.1 Benmore group connection and CHART measurement points.

7.2 TESTING PROCEDURE

By arrangement with Trans Power New Zealand Limited, the Benmore convertor station became available for harmonic tests in group connected mode during a recent maintenance period. The test system, shown in Figure 7.1, involves four generators (G3 to G6) and the convertor group connected to pole-1B. Three-phase measurements were made of the:

- 16 kV bus voltages
- Generator G5 currents
- Convertor transformer T4 and T6 currents

As one of the objectives of the measurements was to provide information for possible validation of the generator harmonic model, three-phase currents of the generator

G5 were recorded. Single-phase measurements of the red-phase currents were made at generators G4 and G6. Pole-1B dc line voltage, current and the firing angles of the valve groups were also recorded.

Due to the geographical separation of the measurement points, two CHART units were used. One unit was placed in the pole-1 dc control room and the other in the power station relay room which are over 200 meters apart. The CHART units were synchronized via GPS satellite, and the red phase 16kV bus voltage was chosen as the harmonic phase angle reference for both units.

CHART adjusts the sampling rate when the fundamental frequency drifts away from its previously measured value so as to maintain exactly the specified number of sampling pulses within a single fundamental cycle throughout the measurement. CHART was programmed to sample and store the signals every three minutes. This would produce several sets of reliable data for each dc current setting, while allowing time for the system to stabilize.

Two types of data were gathered from the waveforms: 256 cycles of 128 sample points and 8 cycles of 1024 sample points. The longer duration intervals provide information on possible sub-synchronous swings and helps determining if the system is stabilized. The higher sampling rate enables the switching instants of the convertor to be resolved accurately.

The pole-1B mercury-arc valve convertor was deblocked and operated as a group connection in the constant current control mode. The dc current was varied from 750 to 1190 amps in approximately 50 amp steps over a four hour period.

7.3 FUNDAMENTAL FREQUENCY VARIATION

The fundamental frequency, computed and recorded for each set of data, varied from 49.0 to 51.2 Hz during the test, as shown in Figure 7.2. The system load restriction required that the dc current be decreased from 1190 to 1016 amps, and then increased from 750 to 950 amps. Due to over compensation of the control system action, the machine speed was faster at heavier loads.

7.4 THREE-PHASE HARMONIC INFORMATION

Figure 7.3 and 7.4 display the 16 kV bus voltages and generator G5 currents as well as their harmonics in sequence components for a dc current setting of 1016 amps (270 MW). The high sampling rate of 51.2 kHz reveals the high frequency ringings of approximately 10 to 15 kHz at the start of commutation periods in the voltage waveforms. This indicates that the total stray capacitance in the circuit is approximately 0.14 to 0.2 nF, given that the smoothing inductance is 0.8 H.

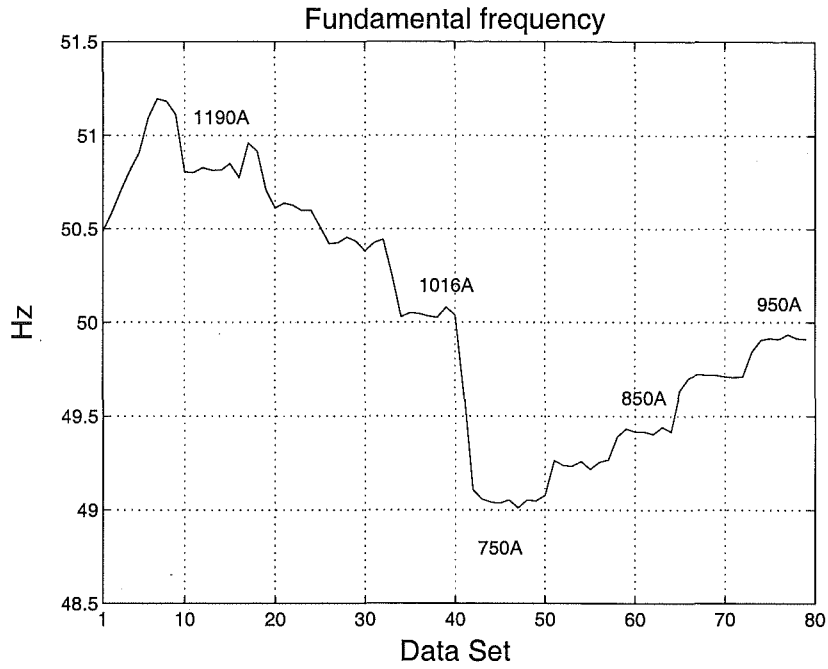

Figure 7.2 Fundamental frequency variation during the test measurement.

The measurement results confirm the rotational sequences of the characteristic harmonics of 12-pulse HVdc operation, ie. the (12n-1)th harmonics are of negative-sequence and the (12n+1)th harmonics are of positive-sequence. Small amounts of the 6-pulse convertor characteristic harmonics, such as the 5th, 7th, etc., caused by slight imbalances among the two 6-pulse valve groups, were also detected.

The measurements show a modest amount of third and smaller amounts of higher triplen zero-sequence voltage harmonics. These must be attributed to generator saturation and space harmonics because the convertor transformers are delta-connected on the generators' side. Thus there is practically no zero-sequence harmonic current path in the group connection configuration. These zero-sequence voltages due to generator saturation and space harmonics would also exist in the conventional operating mode as the interconnecting transformers (T5 and T2) are delta connected onto the generator bus, as shown in Figure 7.1. Figure 7.5 illustrates the variation of the zero sequence voltage harmonics with respect to the 16 kV bus fundamental voltage. In terms of the equipment insulation requirement, the voltage levels are quite small however, and would have little influence on the insulation specification.

On the other hand, the harmonic currents are more serious as they create extra losses in the generator stators. Thus it was decided to obtain the variation of harmonic currents for a range of dc line current. In addition, the availability of multiple data sets should help with the comparison between measurement and simulation results.

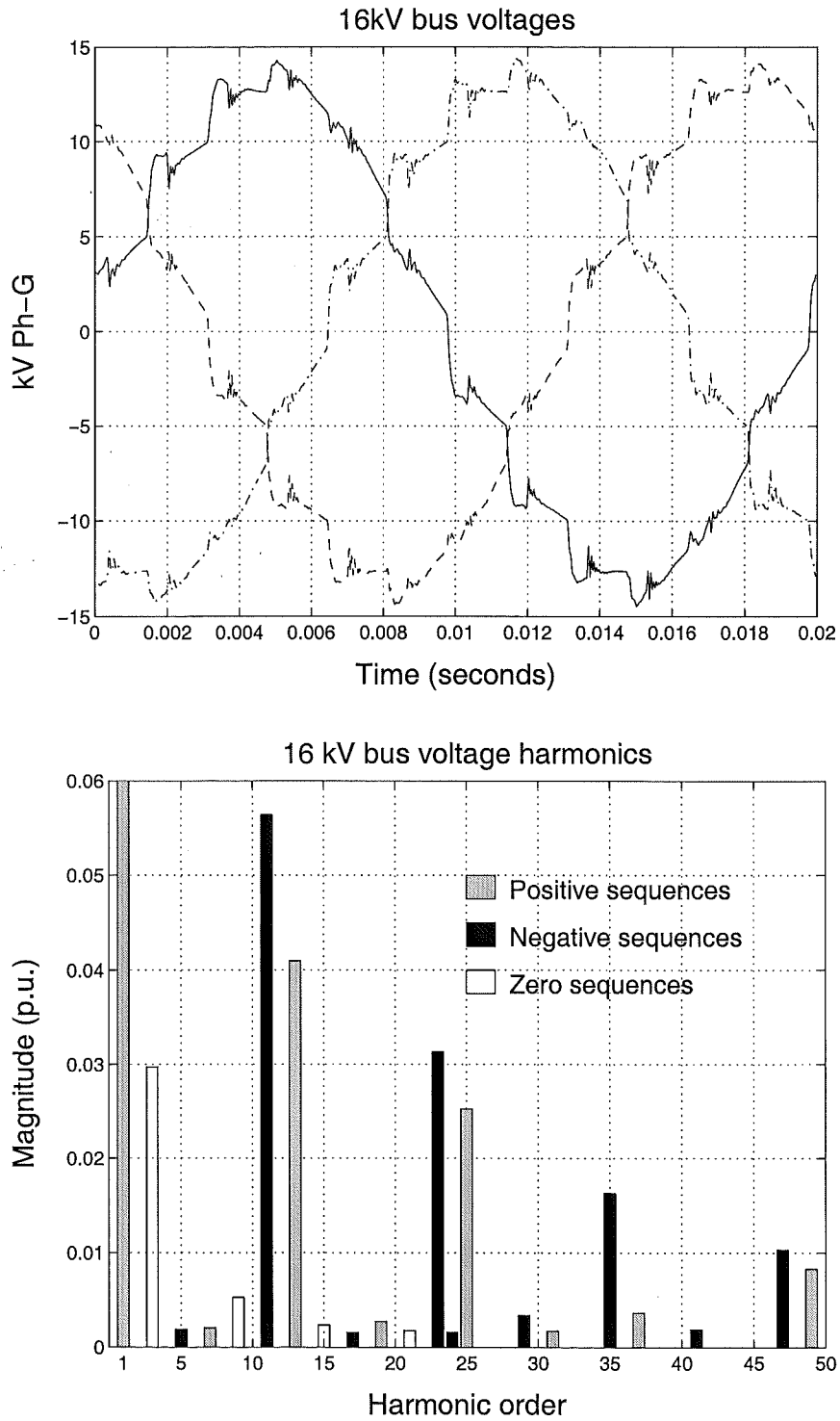

Figure 7.3 Three-phase generator bus voltages and their harmonics in sequence components for a dc current of 1016 amps.

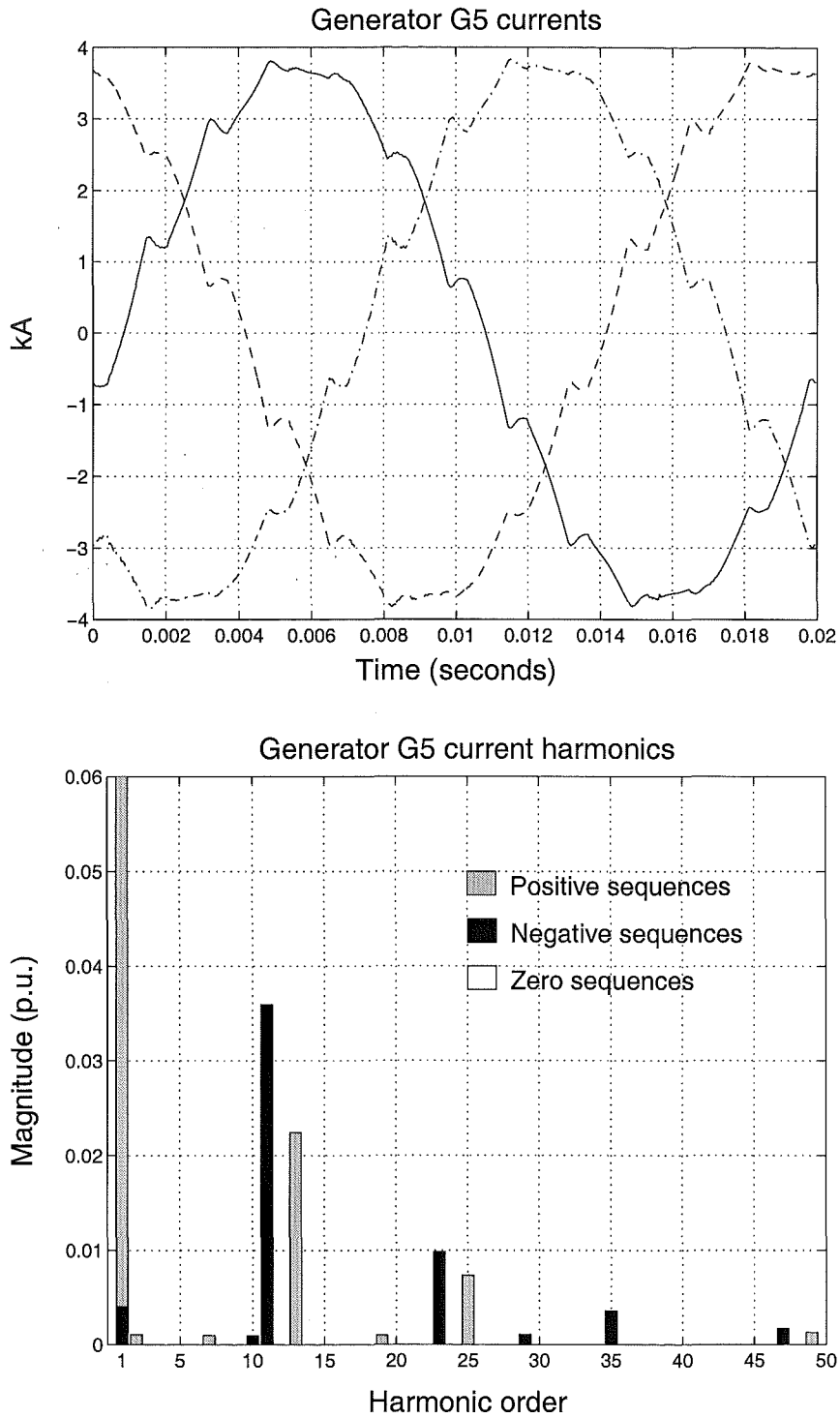

Figure 7.4 Three-phase generator currents and their harmonics in sequence components for a dc current of 1016 amps.

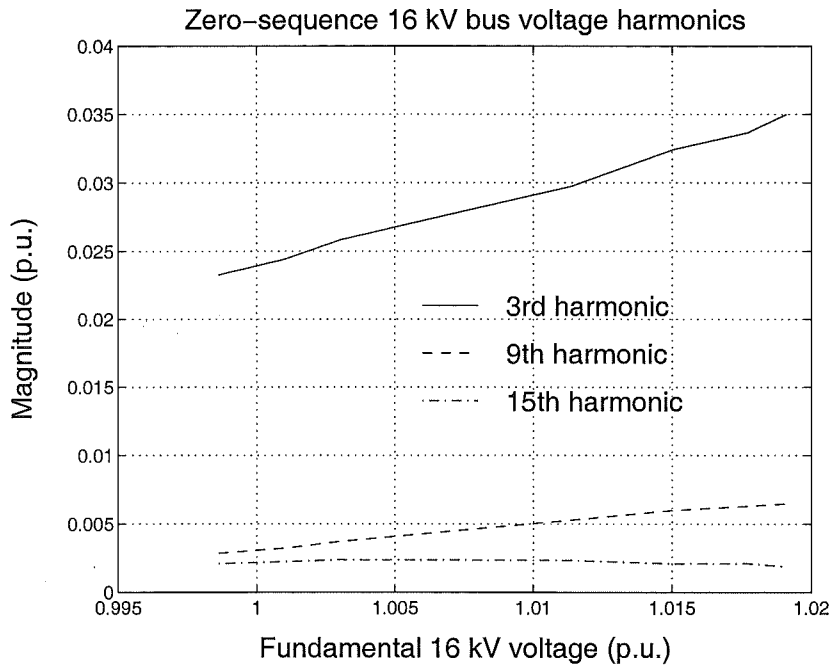

Figure 7.5 Variation of the zero-sequence voltage harmonics with respect to the fundamental 16 kV bus voltage.

7.5 HARMONIC VARIATION WITH DC CURRENT ORDER

7.5.1 DC signals

The dc voltage and current are required for the calculation of the total dc power output, and for the intervalidation with simulation results.

The dc voltage was obtained through a filtered channel, thus containing unreliable harmonic information. However if the dc current harmonics are obtained, the dc voltage harmonics are not required. The voltage level was found to be almost constant at approximately 266 kV for various loads, as shown in Figure 7.6. This is to be expected since the firing angle and the ac terminal voltage magnitude are kept within a narrow band, while the invertor is operated in a minimum gamma control mode, and the line resistance is small.

As dc current harmonics influence the commutation and firing process, it was desirable to obtain the DC current waveform to confirm that the harmonics were small as anticipated. This is clearly the case as illustrated in Figure 7.7 for a dc current order of 1016 Amps. The presence of the 6th, 18th, 30th, etc. harmonics also indicates that there is a slight unbalanced between the two six-pulse valve groups.

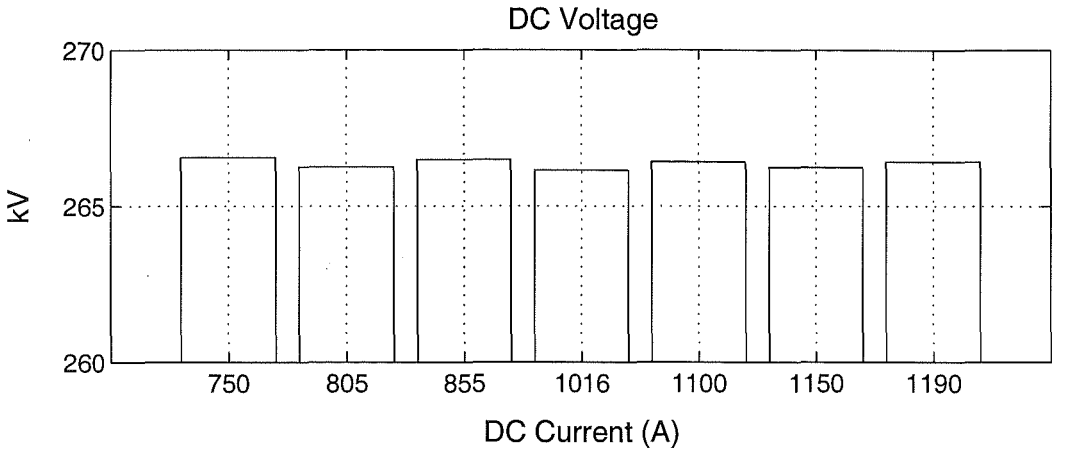

Figure 7.6 DC voltage level for various dc current orders.

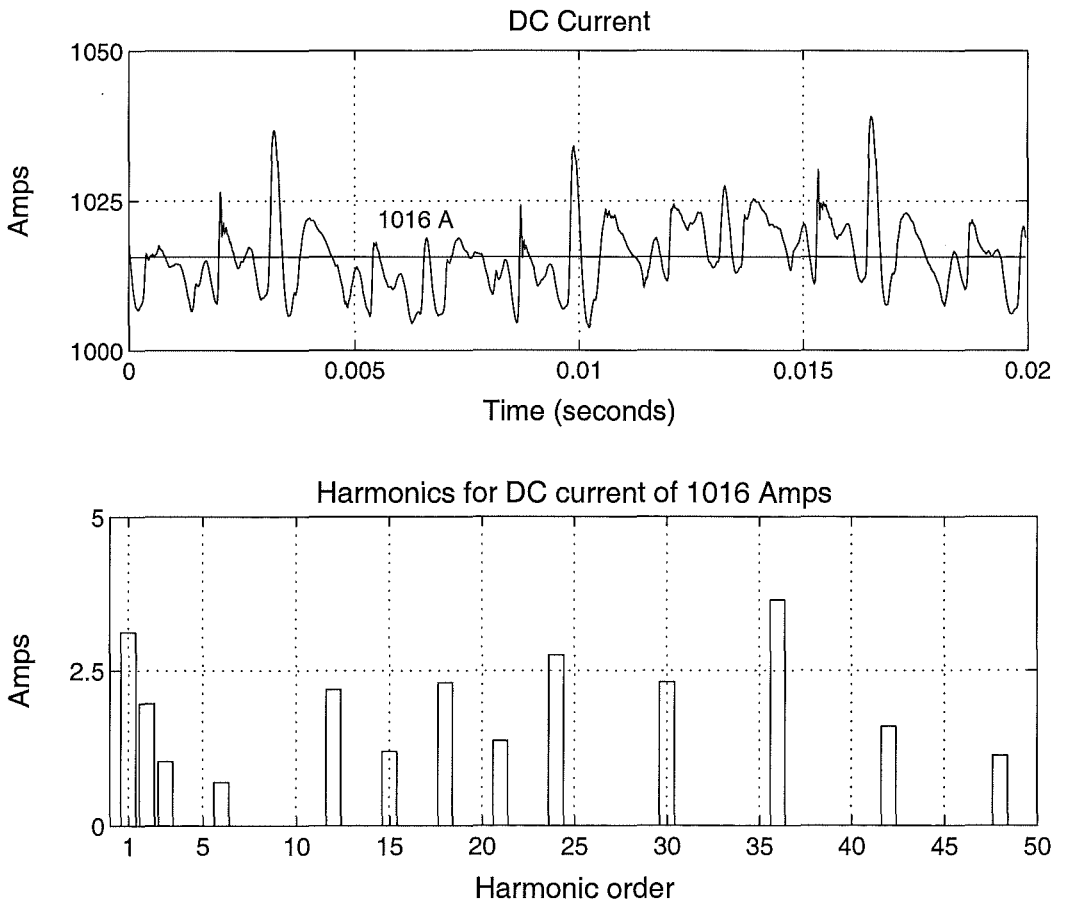

Figure 7.7 DC current and harmonics for the current order of 1016 Amps.

7.5.2 AC harmonics

Since the ideal sinusoidal commutation voltage $E"$ behind generator subtransient reactance is not accessible for measurements, the firing angles have been derived from the crossings of fundamental components of the measured generator terminal voltages. Figure 7.8 shows the derived firing angles, α, commutation angles, μ, and the generator terminal fundamental power factor angles for the tested range of the dc current in pole-1B. It should be noted that the firing angle derived from the crossings of the ideal commutation voltage $E"$ behind subtransient reactance would be larger than those shown since the generator terminal voltage is lagging behind the ideal commutation voltage. Generator terminal voltage waveforms obtained from the test measurement and harmonic domain solution are compared in Figure 7.9 for 11^o firing angle and dc current order of 750 amps. Close agreement in the waveforms is obtained as the firing angle is derived from the generator terminal voltages in both the measurement and unified iterative solution.

Generator current and voltage harmonic variation with respect to dc current order was obtained using the developed Unit Connection model and the firing angle derived from measured waveforms. Relevant information used in the system models is given in Appendix A2. The recorded and simulated harmonic trends, shown in Figure 7.10 and 7.11, are consistent and reasonably close, particularly the 11th and 13th current harmonics, considering the uncertainties in generator parameters and the tolerance of the voltage and current transformers used.

7.6 GENERATOR HARMONIC RATINGS

The possibility of a direct connection was envisaged in the design of the Benmore generators although restrictions were imposed on the nominal power rating (lowered from 112.5 to 102.3 MVA) and on the current harmonic content under such operating conditions. The design ratings as well as the recorded current harmonics at the maximum power output during the test measurements, which include the 1993 single-phase measurement, are listed in Table 7.1. The table shows that none of the design ratings has been exceeded in group connected operation so far. It is observed that the harmonic current levels, particularly the 11th and 13th, were higher when three instead of four generators were used. This increase in harmonic currents is consistent with the Group Connection analysis in Chapter 6, which showed that when a Group Connection is being operated with a reduced number of generators, the remaining generators are subjected to an increase in harmonic loadings.

The Benmore convertor station has not been operated in the unit connected mode. This is partly due to the lack of accurate understanding of the harmonic variation in this operation mode. Using the developed model, harmonic variations in the unit connected

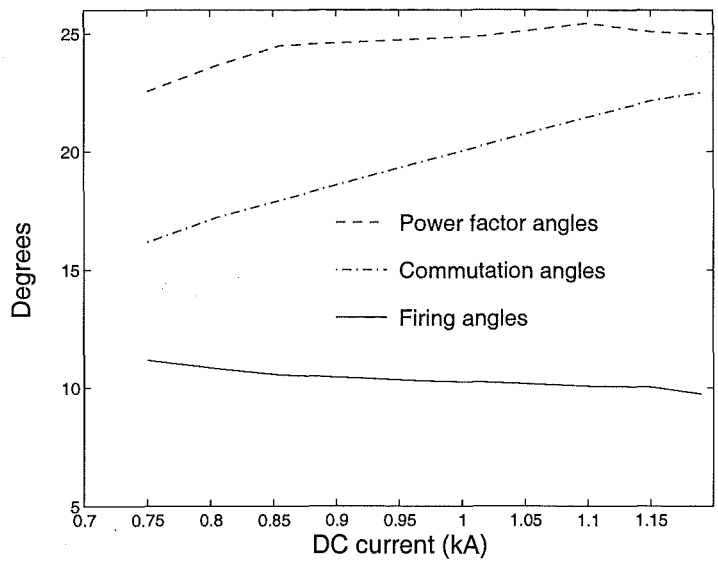

Figure 7.8 Variation of the measured generator terminal power factor angle (lagging), average firing angles (referenced to the measured generator terminal voltage) and commutation angles for a range of dc current.

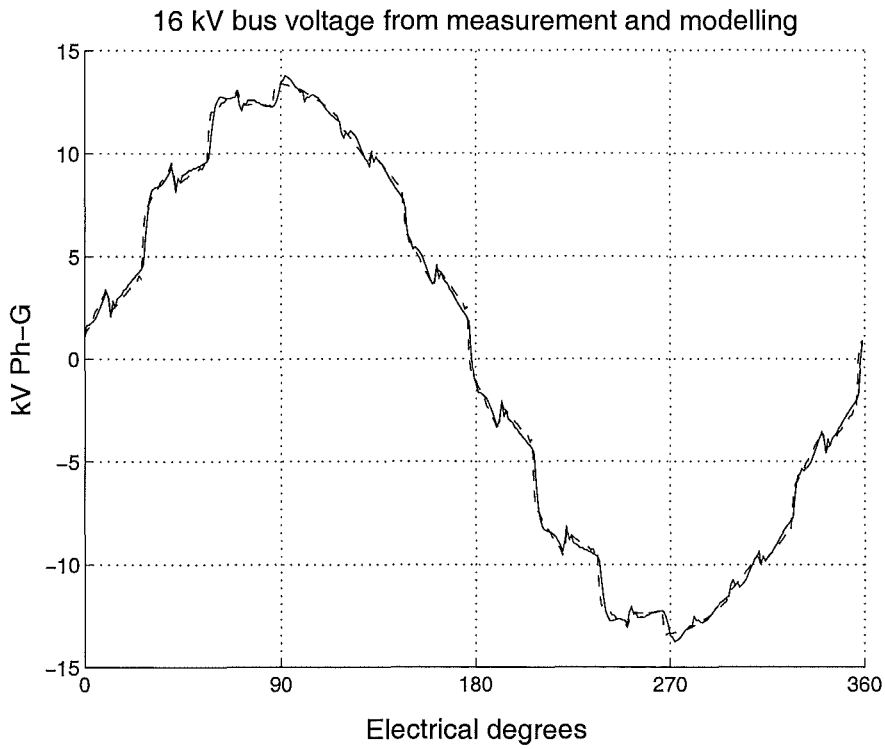

Figure 7.9 Comparison of generator terminal voltage waveforms obtained from the test measurement and harmonic domain solution. *Recorded data = solid, harmonic domain solution = dashed; both reconstructed from 200 harmonics.*

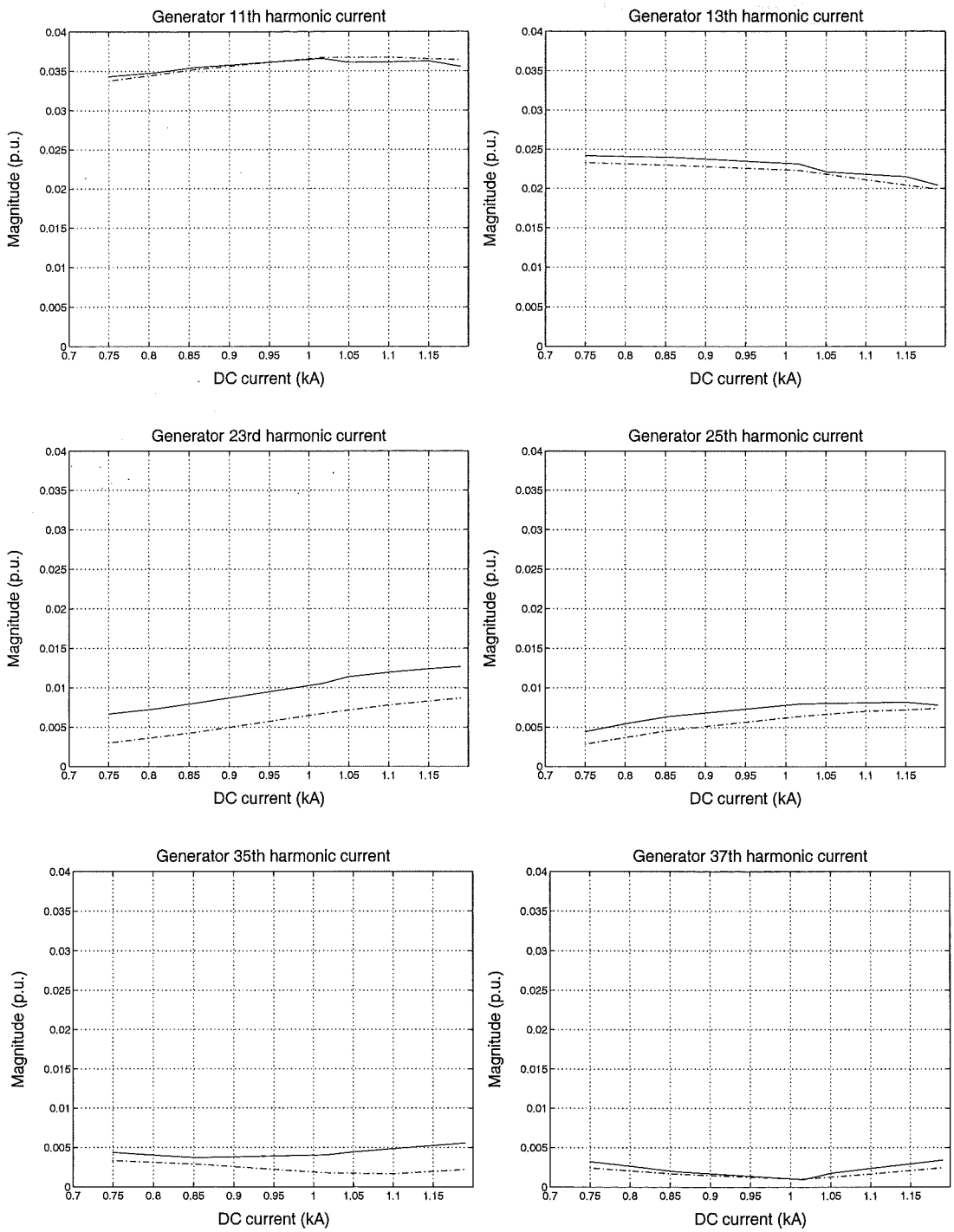

Figure 7.10 Variation of the generator current harmonics for a dc current range; *Recorded data: solid, harmonic domain: dash-dot.*

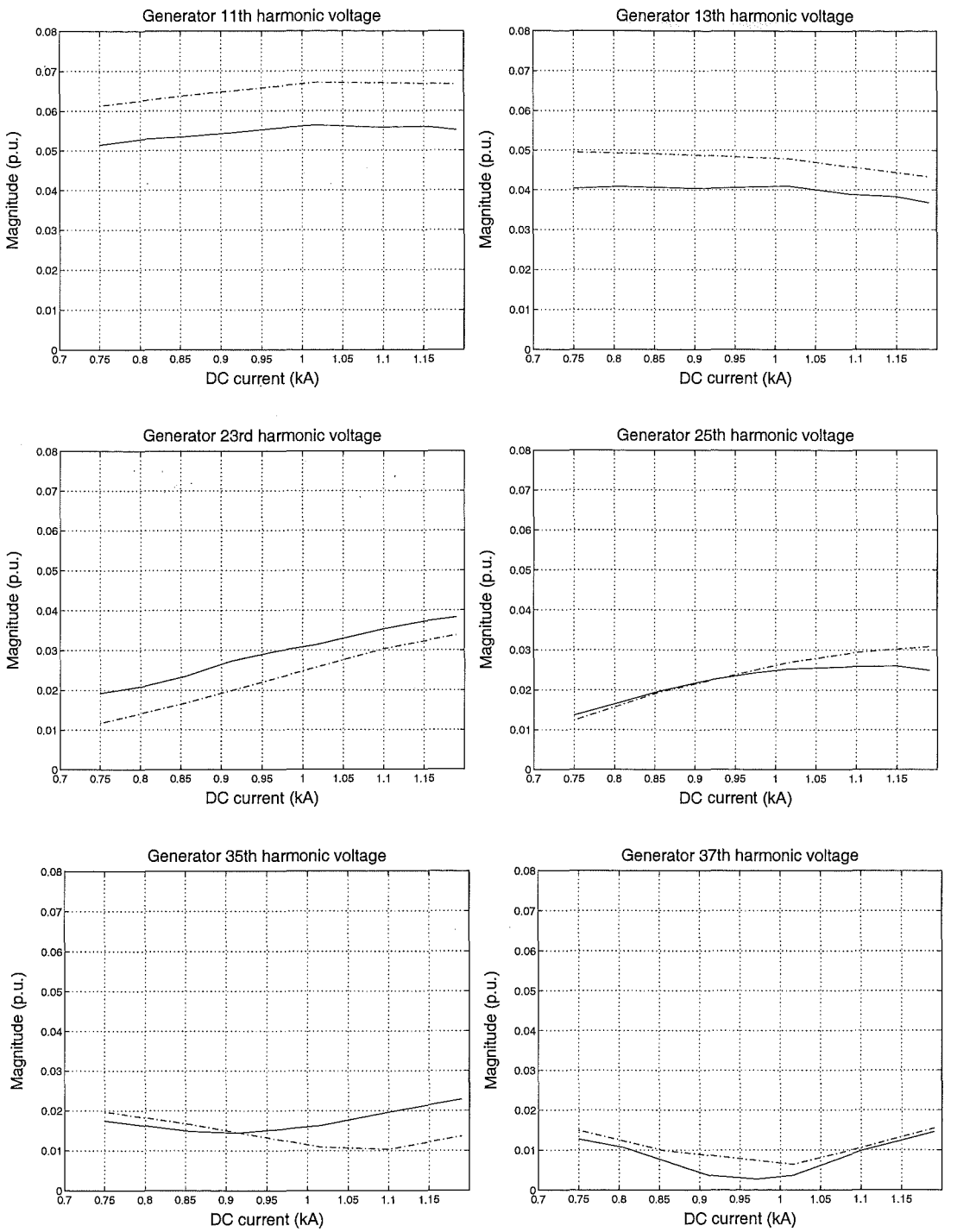

Figure 7.11 Variation of the generator voltage harmonics for a dc current range; *Recorded data: solid, harmonic domain: dash-dot.*

Generator harmonic current	Design ratings (p.u.)	Recorded harmonic currents (p.u.)	
		4 generators (@316 MW)	3 generators* (@212 MW)
11th	0.0744	0.0356	0.0435
13th	0.0595	0.0204	0.0298
23rd	0.0193	0.0127	0.0084
25th	0.0154	0.0078	0.0049

Table 7.1 Generator harmonic ratings for different group connected configuration at the Benmore convertor station; *results from the 1993 measurement.

Gen-erators	System base (MVA)	$X"_d$ (p.u.)	$X"_q$ (p.u.)	$X_{leakage}$ (p.u.)	P_{dc} (MW)
4	409.2	0.1582	0.1728	0.112	360
3	409.2	0.2110	0.2304	0.112	270
2	409.2	0.3164	0.3455	0.112	180
1	409.2	0.6328	0.6911	0.112	90
k	4×102.3	$\frac{4}{k}\frac{102.3}{112.5} \times 0.174$	$\frac{4}{k}\frac{102.3}{112.5} \times 0.19$	0.112	$k \times 90$

Table 7.2 Adjustment of parameters for the Benmore system operating in group connected and unit connected mode. Generator rated power = 102.3 MVA, transformer rated power = 187.5 MVA; k is the number of generators in the group connected mode.

mode can be examined. Simulations were carried out for group connected systems containing 4, 3, 2 or 1 generator. The generators are operated at rated power of 90MW at 50 Hz in all systems. Since the system parameters are changed due to the reduction in the generator power rating for direct connected operation, the modified parameters are listed in Table 7.2.

Figure 7.12(a) shows the variation of commutation angles and generator terminal power factor with respect to firing angles and the number of generating units. Firing angles have been measured from the generator terminal voltages so that they are consistent with the measurement results described in Section 7.5.2. The commutation angles are typically below the 28^o limit provided that the firing angle referenced to V is greater than 2^o for the group connected mode with 4 generators. The generator terminal power factors are also well above the design rating of 0.88. Firing angles referenced to $E"$ can be derived from the relationship between $E"$ referenced and generator terminal voltage V referenced firing angles, as shown in Figure 7.12(b). The phase angle between $E"$ and V only increases slightly with fewer generators since the reduction in power factor angles is small.

The harmonic current variation with respect to the firing angle as well as individual

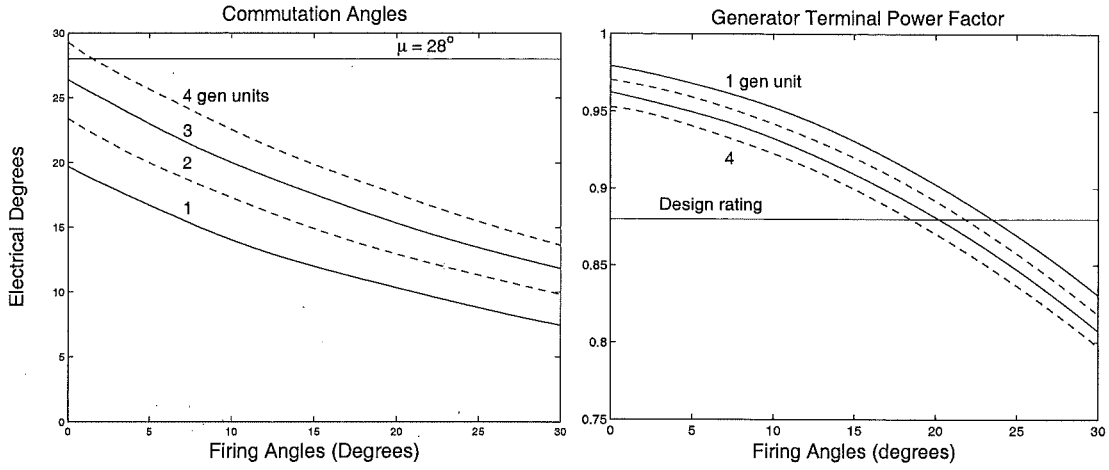

(a)

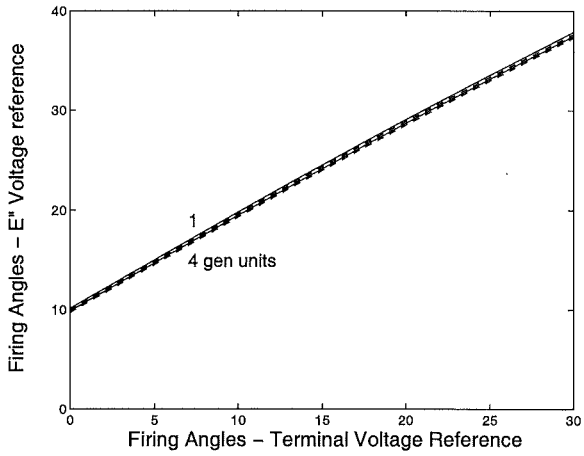

(b)

Figure 7.12 (a) Commutation angle and generator terminal power factor at the rated power output for the Benmore Convertor station operating as group connected units; (b) Relationship between $E^{"}$ referenced and generator terminal voltage V referenced firing angles.

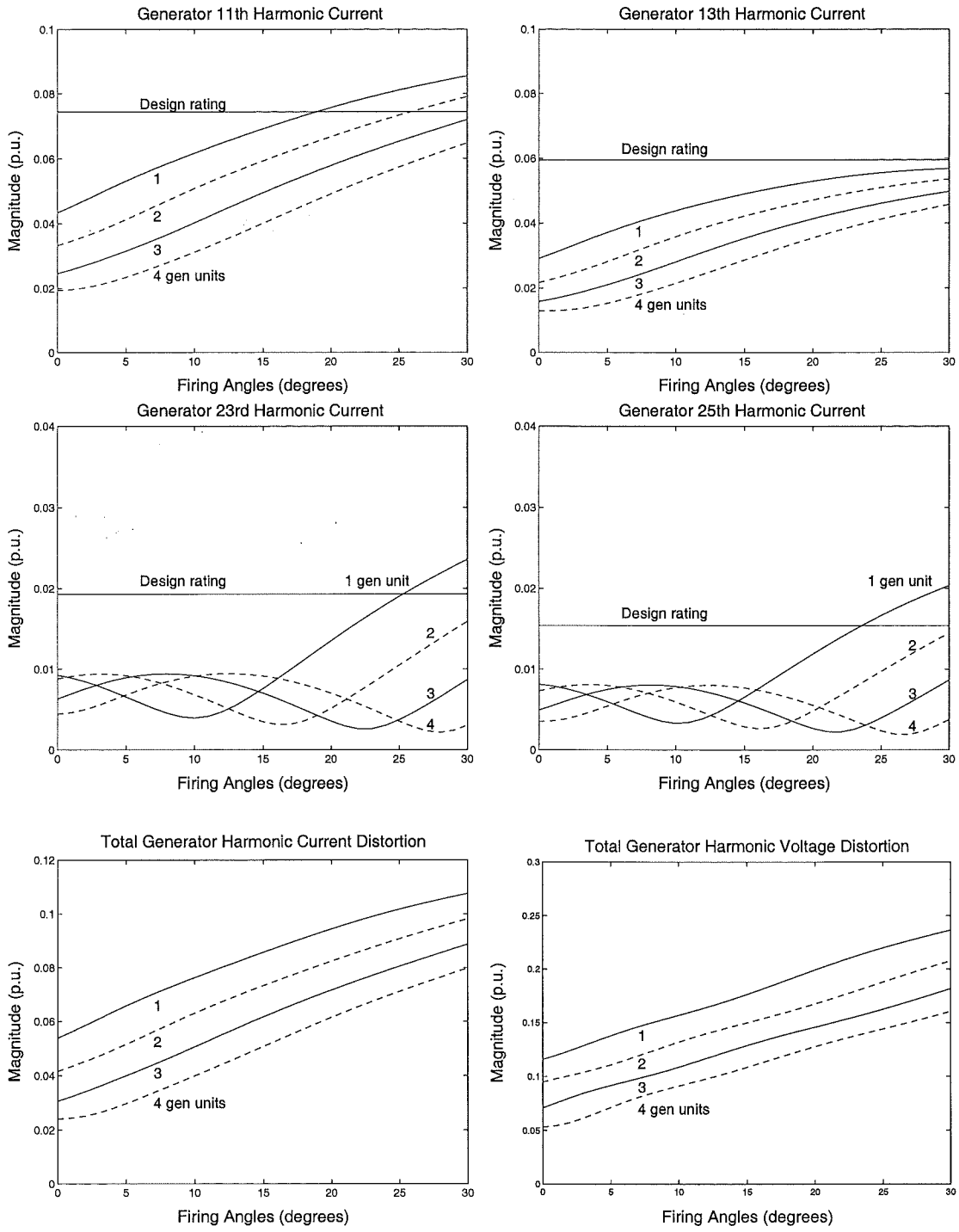

Figure 7.13 Generator harmonic current and voltage levels for the Benmore Convertor station operating as group connected units. Firing angles are referenced to the generator terminal voltage.

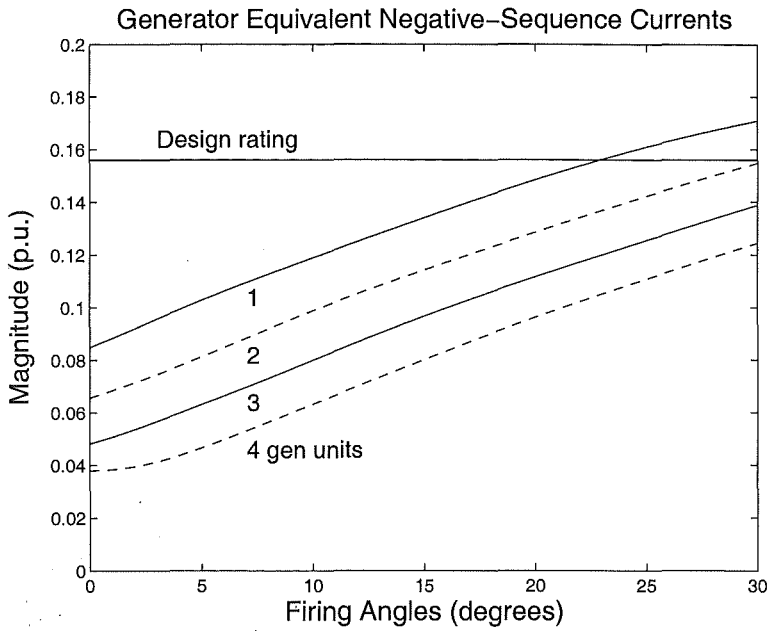

Figure 7.14 Generator equivalent negative-sequence currents for the Benmore Convertor station operating as group connected units.

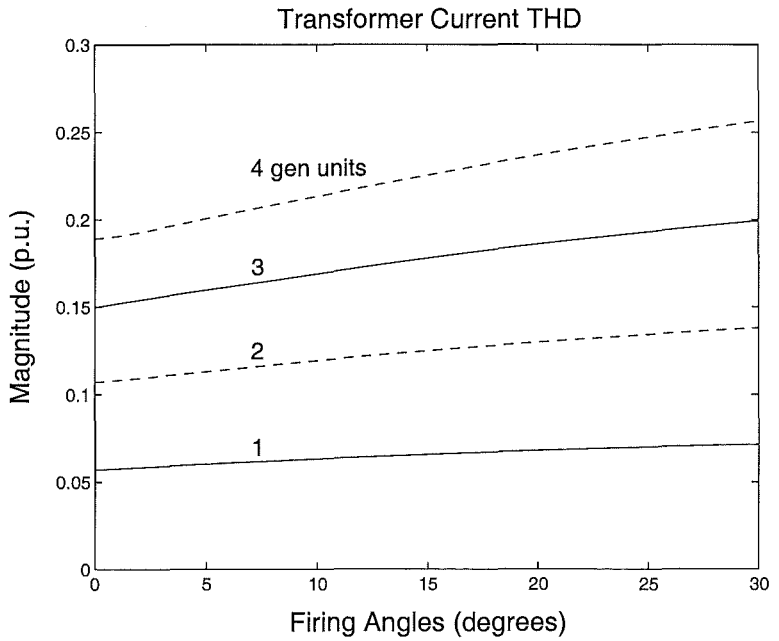

Figure 7.15 Convertor transformer current THD for the Benmore Convertor station operating as group connected units. Transformer power base is 187.5 MVA.

harmonic ratings are plotted in Figure 7.13. Harmonic current levels in the remaining generators increase drastically, as much as 0.01 p.u. in the 11th and 13th harmonic currents, for each generator taken out of service. For a nominal 15^o firing angle, harmonic currents do not exceed the design ratings in any case, although the current harmonic will be close to the limit in the unit connected mode. It should be noted that the harmonic design ratings for Benmore generators are higher than those in typical hydro generators since the 15.6% rated equivalent continuous negative-sequence current harmonic loading of Benmore generators is much higher than the typical 10%, as shown in Figure 7.14.

On the other hand, the convertor transformer harmonic current loading is at the largest when all generators are in service, as shown in Figure 7.15.

7.7 CONCLUSIONS

Detailed three-phase harmonic information of a group connected generator-HVDC convertor scheme has been collected and discussed. The use of CHART improves the detection of harmonics with small magnitudes, and provides confirmation of the harmonic rotational sequences. The high sampling rate of 51.2 kHz enabled accurate derivation of the actual firing instants which has been used in the simulation to improve the harmonic prediction. The results have been used to intervalidate the developed Unit Connection in the harmonic domain model, and close agreements between the measured and simulated results were achieved, particularly the 11th and 13th current harmonics which are the largest and most significant. Besides the validation purpose, the measurement results also provide valuable evidence of the feasibility of the direct connection.

The harmonic current and voltage variation with respect to the number of generators for the Benmore terminal when being operated in group and unit connected mode have been examined. It has been found from the measurement and simulation that the harmonic current levels in the generators increase substantially, as much as 0.01 p.u. in the 11th and 13th harmonic currents, for each generator taken out of service. For a nominal 15^o firing angle, generator harmonic current levels would be below the specified maximum design ratings in all cases, but these come very close to the limits in the unit connected mode. Although the Benmore convertor station has not been operated in the unit connected mode, the simulation results have provided solid evidence of the viability of this mode of operation.

Chapter 8

CONCLUSIONS AND FUTURE WORK

8.1 CONCLUSIONS

The direct connection of generators to HVdc convertors is a flexible and attractive option in which ac harmonic filters, ac switching and protection gear, and a transformation step are dispensed, leading to a more compact HVdc Power Station with substantial savings in capital and operating costs. However the absence of ac filters and the close proximity of generators and convertors lead to strong harmonic interactions in these schemes. Simplified convertor analysis has been found to be inadequate to determine such interactions. Dynamic simulation of the direct connected units to the steady state has been the only acceptable method of harmonic prediction so far. But this is an inefficient approach considering the long time constants of the synchronous generator.

The primary objectives of the research described in this thesis were to develop an accurate and efficient harmonic model of direct connected units as a suitable tool for analysing the harmonic interactions, and to thoroughly investigate the harmonic behaviour of these schemes.

Due to the lack of accurate generator models in the harmonic domain, a synchronous generator model in the form of a harmonically coupled impedance matrix has been developed in Chapter 3. The model takes into account the effects of saturation and the stator-rotor frequency conversion phenomenon due to saliency. The relationship between the generator terminal voltages and currents in the presence of saliency has been expressed in sequence components. The analytical expressions are derived from normally available machine parameters such as direct and quadrature-axis subtransient reactances. Harmonics produced by generator saturation have been shown to be insignificant. The generator harmonic model has been validated against time domain simulations and results from harmonic measurements of the Benmore convertor station when being operated as a group connected unit. The developed analytical model is thus a powerful tool for fast and accurate predictions of the harmonic levels on the generator terminals in the presence of saliency, saturation and distortion.

In the absence of ac harmonic filters at the generator terminal, the ideal sinusoidal commutation voltage moves inside the generator and the commutating reactance consists

of the transformer leakage reactance and generator subtransient reactance. Since generator subtransient reactance varies with rotor angle due to saliency, an iterative solution for the commutation process is necessary. By choosing the generator terminal voltages as *pseudo-commutation voltages*, which can be unbalanced or contain harmonic distortion, the effect of the varying generator subtransient reactance and transformer leakage reactance can be considered separately in the iterative solution. Given the generator terminal voltage as a pseudo-commutation voltage, the convertor harmonic currents can be obtained from the commutation analysis described in Section 4.2, in which the reactances are solely the transformer leakage reactances. The generator terminal voltage harmonics are then updated by injecting the convertor currents into the generator harmonic impedance. Convolution in the harmonic domain is employed to construct the dc voltage and ac currents in terms of the switching angles, ac voltage harmonics and dc current harmonics. Thus the analysis is completely in the harmonic domain.

The harmonic interaction in direct connected units has been described using a set of nonlinear equations. The electrical variables have been chosen to represent physically obtainable signals, such as ac terminal voltages and dc current harmonics, to predict the relationship between these signals. Voltage control, exercised entirely by the generator excitation in the absence of convertor transformer on-load tap-changers, has also been incorporated into the formulation. By decomposing the mixture of real and complex variables into real quantities, the Newton solution can be formulated using real values in positive harmonics only. This enables the harmonic interaction between generators, the convertor switching instants and the dc system to be combined into a unified iterative solution. By exploiting the sparse nature of the Jacobian matrix, the solution has been solved rapidly.

It has been shown that the convergence of the unified solution is greatly improved in comparison with sequential solution methods such as Iterative Harmonic Analysis for such systems. Divergence of Newton's method can occur when the gradient of the iterating function, represented by the Jacobian of partial derivatives, exceeds a certain value. Rigorous analysis has showed that the size of the gradient is directly proportional to the generator subtransient reactance, and inversely proportional to the commutating reactance. For small values of commutating reactance and large subtransient reactances, the magnitudes of the Jacobian elements are large, leading to divergence. Nevertheless, the convergence threshold of the proposed model is small enough and no modification is needed for harmonic analysis of the direct connected units with typical reactance values.

The developed Unit Connection model also serves to intervalidate the time domain simulation, until now the only alternative method of harmonic analysis for direct connected units. Close agreement in ac and dc harmonics has been obtained when a small value of the snubber capacitance value is used in the time domain simulations. The large artificial snubber capacitance normally used in time domain simulations to aid numerical stability does have significant influence on the harmonic levels.

By choosing the generator terminal voltage as the firing angle reference, existing firing control for conventional HVdc schemes can be used for direct connected units with practically no modification. Provided that the nominal firing angles are kept within the restriction limits, imposed by the overlap angle, generator terminal power factor, continuous equivalent negative-sequence harmonic loading, number of generators and mis-firing constraints, practically no extra capacity for generator terminal power factor and harmonic current loading are required in direct connected units. The generator harmonic ratings can be taken at the nominal speed and rated power output.

The effect of rotor angle on the commutation process in the presence of saliency has been shown to be significant in direct connected units. Substantial improvement in the accuracy of the harmonic prediction has been obtained by taking into account the position of the rotor. An accurate harmonic solution in the presence of generator saliency can only be obtained by solving the non-linearities in a unified solution since all of the system variables are inter-dependent. However the harmonic current ratings in direct connected units containing salient-pole generators can be estimated by using a non-salient generator with its subtransient reactances equal to X_d'' of the salient generator.

Detailed three-phase harmonic information of the Benmore convertor station when being operated in the group connected mode was collected and discussed. The test results have provided valuable evidence of the feasibility of direct connection units, and have also been used to assess the accuracy of the harmonic domain models and dynamic simulation techniques. The recorded and simulated harmonic trends are consistent and reasonably close considering the uncertainties in generator parameters, and the tolerance of the voltage and current transformers used. Although the Benmore convertor station has not been operated in the unit connected mode, the simulation results have shown that the harmonic currents would not exceed the design ratings and thus provided solid evidence of the viability of this mode of operation at the station.

8.2 SUGGESTIONS FOR FUTURE WORK

8.2.1 Transformer Saturation Modelling

A transformer model in the Harmonic Domain which takes into account the effect of saturation has been developed [Lisboa 1996]. In order to incorporate this model into the unified solution, three additional variables describing the dc component of magnetising currents are required. The harmonic components of magnetising currents or voltages in each phase can be calculated at each iteration using an FFT, and a curve fitting technique such as cubic splines can be used to represent saturation curves.

8.2.2 Subsynchronous Resonances and Interharmonic Studies

The Harmonic Domain can be extended to include frequencies other than harmonic frequencies to examine possible subsynchronous resonances and interharmonic phenomena. The equations describing machine rotor and mechanical characteristics can be incorporated into a unified solution to examine the combined electrical and mechanical interaction. Changes in the machine inductances, particularly at subsynchronous frequencies, can be readily taken into account at each interested frequency. Moreover, the unified solution method can be used to obtain discrete frequency response characteristics of direct connected units which can then be used to aid the design of the control system.

In the case of HVdc back-to-back connection for systems that have different power frequencies, the Harmonic Domain can be extended to take into account the frequencies resulting from the interaction of all relevant frequencies. As a result, the unified solution method is a powerful tool for analysing not only the harmonic behaviour but also subsynchronous and interharmonic behaviour of HVdc systems.

Appendix A

TEST SYSTEMS DATA

A.1 HWANG'S GENERATOR PARAMETERS

The generator parameters are extracted from a paper by Hwang [1969].

Rating	100	MVA
Voltage	13.8	kV
x_d	1.2	pu
$x_d^{'}$	0.3667	pu
$x_d^{''}$	0.2	pu
x_q	0.8	pu
$x_q^{''}$	0.367	pu
$T_{do}^{'}$	7.64	seconds
$T_{do}^{''}$	0.0633	seconds
$T_{qo}^{''}$	0.132	seconds
R_a	0.005	pu
x_0	0.05	pu

A.2 BENMORE'S GENERATORS AND TRANSFORMERS

Convertor Transformers

Type	Delta-Wye and Delta-Delta
Rating	187.5 MVA
Voltage	16-110 kV
Leakage	11.2 %

Generators

Rating	112.5	MVA
Voltage	16.0	kV

x_d	1.168	pu
$x_d^{'}$	0.264	pu
$x_d^{''}$	0.174	pu
x_q	0.672	pu
$x_q^{''}$	0.19	pu
$T_{do}^{'}$	8.7	seconds
$T_{do}^{''}$	0.087	seconds
$T_{qo}^{''}$	0.132	seconds
x_0	0.0765	pu
R_a	0.0042	pu

For a twelve-pulse unit connection operation, the generator rating is reduced to 102.3 MVA from 112.5 MVA. The generator harmonic current ratings (based on the 102.3 MVA rating) are given as:

Generator harmonic currents	Design ratings
11th	0.0744
13th	0.0595
23rd	0.0193
25th	0.0154
terminal power factor	0.88

Table A.1 Generator harmonic ratings for twelve-pulse group connected operation at the Benmore convertor station.

Generator open circuit saturation curve is given in Figure A.1, which can also be defined by the set of points which is given in Table A.2.

Field current (A)	Terminal line voltage (kV rms)
0	0
100	2.7
200	5.4
300	8.0
400	10.6
500	12.95
600	14.85
700	16.27
800	17.30
900	18.15
1000	18.85
1100	19.40
1200	19.80

Table A.2 Benmore generator open circuit saturation characteristic.

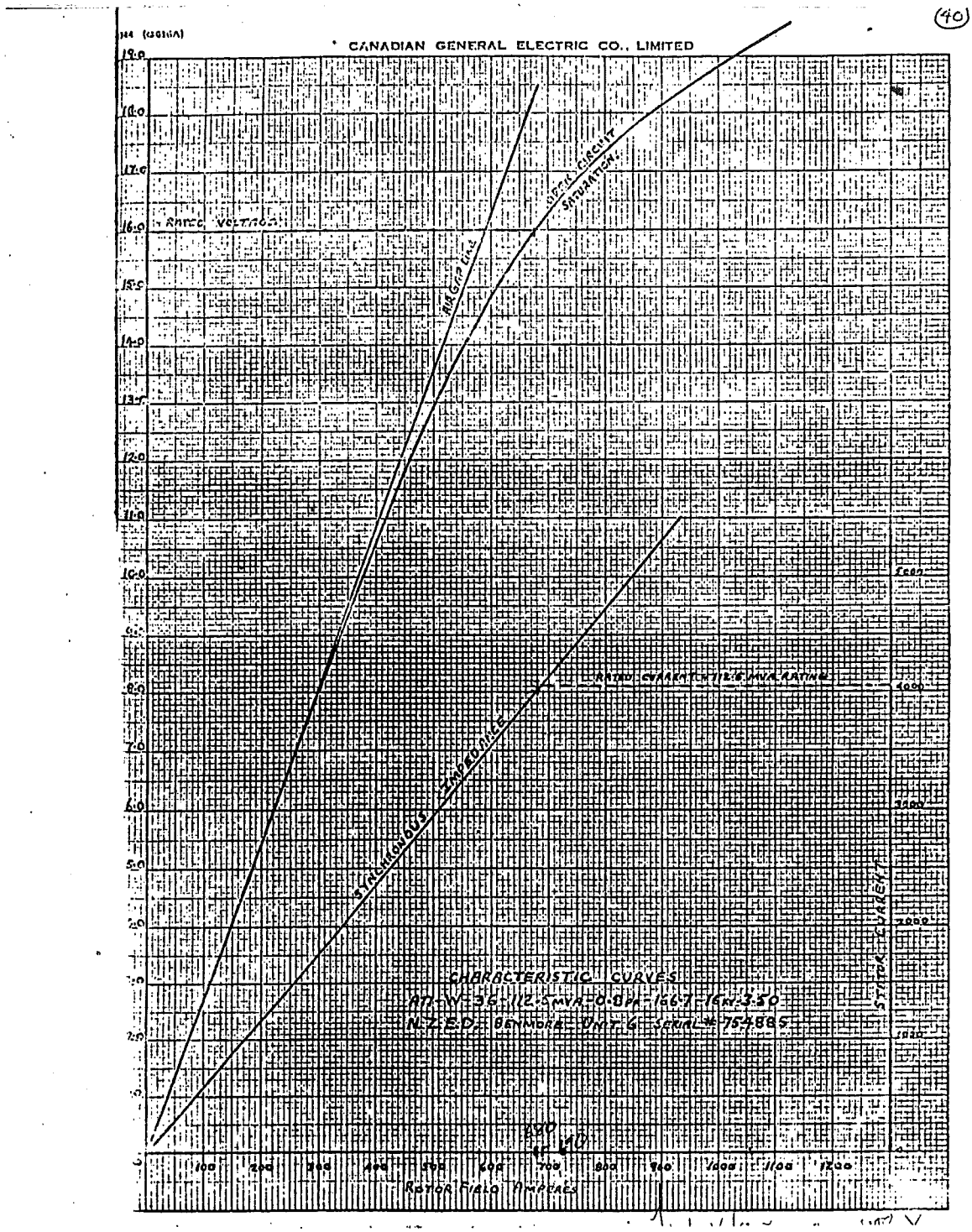

Figure A.1 Benmore generator open circuit saturation curve.

Appendix B

SALIENT-POLE GENERATOR HARMONIC IMPEDANCE CALCULATION FROM MEASURED HARMONIC VOLTAGES AND CURRENTS

This appendix describes the derivation of the self and cross coupling terms of the salient-pole generator impedance from the terminal voltages and currents measured in a HVdc group connected operation. The voltage/current relationship of a characteristic harmonic pair $12n \pm 1$ in the presence of saliency can be expressed by the following complex matrix equation:

$$\begin{bmatrix} V_k \\ V_{k+2} \end{bmatrix} = \begin{bmatrix} Z_{g\,k,k} & Z_{g\,k,k+2} \\ Z_{g\,k+2,k} & Z_{g\,k+2,k+2} \end{bmatrix} \begin{bmatrix} I_k \\ I_{k+2} \end{bmatrix} . \tag{B.1}$$

Substituting the generator harmonic impedance expressions developed in Chapter 3 yields:

$$\begin{bmatrix} V_k \\ V_{k+2} \end{bmatrix} = \begin{bmatrix} R + j\frac{k}{2}(X_d'' + X_q'') & j\frac{k}{2}(X_q'' - X_d'')e^{-j2\delta} \\ j\frac{k+2}{2}(X_q'' - X_d'')e^{j2\delta} & R + j\frac{k+2}{2}(X_d'' + X_q'') \end{bmatrix} \begin{bmatrix} I_k \\ I_{k+2} \end{bmatrix} . \tag{B.2}$$

Equation B.2 is decomposed into four real equations which can then be solved for the four unknown real variables R, X_d'', X_q'', and δ. Decomposing equation B.2 yields:

$$\begin{bmatrix} \mathcal{R}\{V_k\} \\ \mathcal{I}\{V_k\} \\ \mathcal{R}\{V_{k+2}\} \\ \mathcal{I}\{V_{k+2}\} \end{bmatrix} = \begin{bmatrix} A & -B & C & -D \\ B & A & D & C \\ -\frac{k+2}{k}C & -\frac{k+2}{k}D & A & -\frac{k+2}{k}B \\ \frac{k+2}{k}D & -\frac{k+2}{k}C & \frac{k+2}{k}B & A \end{bmatrix} \begin{bmatrix} \mathcal{R}\{I_k\} \\ \mathcal{I}\{I_k\} \\ \mathcal{R}\{I_{k+2}\} \\ \mathcal{I}\{I_{k+2}\} \end{bmatrix} , \tag{B.3}$$

where

$$\begin{aligned} A &= R \\ B &= \frac{k}{2}(X_d'' + X_q'') \\ C &= \frac{k}{2}(X_q'' - X_d'')\sin(2\delta) \\ D &= \frac{k}{2}(X_q'' - X_d'')\cos(2\delta) \end{aligned} \tag{B.4}$$

Rearranging equation B.3 yields:

$$\begin{bmatrix} \mathcal{R}\{V_k\} \\ \mathcal{I}\{V_k\} \\ \mathcal{R}\{V_{k+2}\} \\ \mathcal{I}\{V_{k+2}\} \end{bmatrix} = \begin{bmatrix} \mathcal{R}\{I_k\} & -\mathcal{I}\{I_k\} & \mathcal{R}\{I_{k+2}\} & -\mathcal{I}\{I_{k+2}\} \\ \mathcal{I}\{I_k\} & \mathcal{R}\{I_k\} & \mathcal{I}\{I_{k+2}\} & \mathcal{R}\{I_{k+2}\} \\ \mathcal{R}\{I_{k+2}\} & -\frac{k+2}{k}\mathcal{I}\{I_{k+2}\} & -\frac{k+2}{k}\mathcal{R}\{I_k\} & -\frac{k+2}{k}\mathcal{I}\{I_k\} \\ \mathcal{I}\{I_{k+2}\} & \frac{k+2}{k}\mathcal{R}\{I_{k+2}\} & -\frac{k+2}{k}\mathcal{I}\{I_k\} & \frac{k+2}{k}\mathcal{R}\{I_k\} \end{bmatrix} \begin{bmatrix} A \\ B \\ C \\ D \end{bmatrix}. \tag{B.5}$$

Given the harmonic voltages and currents, the variables A, B, C, D can be found by using equation B.5, subsequently the unknown variables R, X_d'', X_q'', δ can be obtained from equation B.4, i.e.

$$\begin{aligned} R &= A \\ X_d'' &= \frac{B}{k} - \frac{1}{k}\sqrt{C^2 + D^2} \\ X_d'' &= \frac{2B}{k} - X_d'' \\ \delta &= \frac{1}{2}\sin^{-1}\left\{\frac{2C}{k(X_q'' - X_d'')}\right\}. \end{aligned} \tag{B.6}$$

The self and cross-coupling terms of the generator impedance for each pair of characteristic harmonics are then obtained using the impedance expressions in equation B.2

Appendix C

CUBIC SPLINE INTERPOLATION

Cubic spline interpolation has been well documented in literature [Gerald and Wheatly 1985] [Press *et al.* 1992]. This appendix summarizes the cubic spline interpolation formulation with particular application to represent generator or transformer magnetising characteristics.

Given a tabulated function $y_i = f(x_i)$, $i = 1, 2, ...n$, the cubic for the ith interval, which lies between the points (x_i, y_i) and (x_{i+1}, y_{i+1}) is in the form

$$y = A_i(x - x_i)^3 + B_i(x - x_i)^2 + C_i(x - x_i) + D_i \tag{C.1}$$

The slope and curvature, i.e. the first and second derivatives, are required so that the cubics can be fit smoothly from one interval to another. Let S_i and S_{i+1} represent the second derivatives at the point (x_i, y_i) and (x_{i+1}, y_{i+1}) respectively, expressions for the coefficients in equation C.1 can be obtained as:

$$A_i = \frac{S_{i+1} - S_i}{6(x_{i+1} - x_i)} \tag{C.2}$$

$$B_i = \frac{S_i}{2} \tag{C.3}$$

$$C_i = \frac{y_{i+1} - y_i}{x_{i+1} - x_i} - \frac{(x_{i+1} - x_i)}{2S_i + S_{i+1}} \tag{C.4}$$

$$D_i = y_i \tag{C.5}$$

As the slopes of the two cubics that join at (x_i, y_i) are the same, the relationship among the cubics is given by:

$$h_{i-1}S_{i-1} + (2h_{i-1} + 2h_i)S_i + h_iS_{i+1} = 6\left(\frac{y_{i+1} - y_i}{h_i} - \frac{y_i - y_{i-1}}{h_{i-1}}\right) \tag{C.6}$$

where $h_i = x_{i+1} - x_i$. As equation C.6 represents a relationship among three consecutive points, it can only be applied to each internal point, from $i = 2$ to $i = n - 1$. This gives $n - 2$ equations relating the n values of S_i. For a unique solution, two further equations involving S_1 and S_n are needed, and can be obtained when conditions at x_1 and x_n

are specified. To some extent these end conditions are arbitrary. The commonly used choices are:

- Take $S_1 = 0$, $S_n = 0$. This is equivalent to assuming that the end cubics approach linearity at the extremities. This is so-called *natural spline* and frequently used.
- Take $S_1 = S_2$, $S_n = S_{n-1}$. This is equivalent to assuming that the end cubics approach parabolas at their extremities.
- Specify S_1 and S_n so that the first derivatives of end points are equal to the slopes of the unsaturated and saturated region. In doing so, both the saturated and unsaturated regions are represented by straight lines.

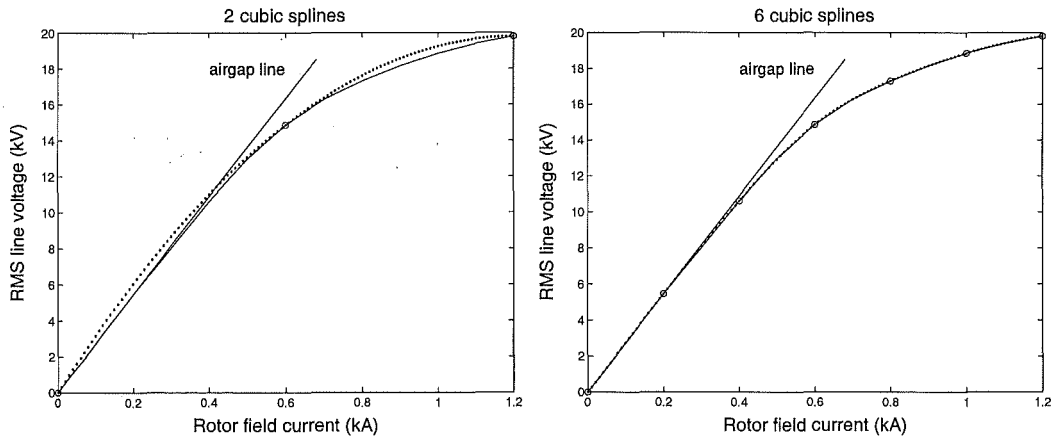

Figure C.1 Cubic spline interpolation of the Benmore generator open circuit characteristic. Solid: manufacturer data, dotted: spline.

Figure C.1 shows a natural cubic pline interpolation on the open circuit characteristic of the Benmore generator. Initially only three points from the tabulated data (obtained from the manufacturer plot) was chosen: the origin, the end and a middle point. With only two cubic splines, a poor agreement was obtained, whereas an almost exact match was obtained using 6 cubic splines.

Appendix D

HARMONIC PHASOR REPRESENTATION

D.1 COMPLEX FOURIER SERIES

A periodic function $f(t)$ can be represented by the Fourier series of trigonometric functions:

$$f(t) = \frac{a_0}{2} + \sum_{k=1}^{\infty} \left[a_k \cos(kwt) + b_k \sin(kwt) \right], \tag{D.1}$$

where

$$\begin{aligned} a_0 &= \frac{1}{\pi} \int_{-\pi}^{\pi} x(wt) d(wt) \\ a_k &= \frac{1}{\pi} \int_{-\pi}^{\pi} x(wt) \cos(kwt) d(wt) \\ b_k &= \frac{1}{\pi} \int_{-\pi}^{\pi} x(wt) \sin(kwt) d(wt), \end{aligned} \tag{D.2}$$

and w is the fundamental angular frequency and k is the harmonic order.

As the sine and cosine functions can be expressed in terms of complex exponential terms, i.e.

$$\begin{aligned} \sin(kwt) &= \frac{e^{jkwt} - e^{-jkwt}}{2j} \\ \cos(kwt) &= \frac{e^{jkwt} + e^{-jkwt}}{2}, \end{aligned} \tag{D.3}$$

the Fourier series in equation D.1 can be expressed in the form of a complex exponential Fourier series as

$$f(t) = \sum_{-\infty}^{\infty} c_k e^{jkwt}, \tag{D.4}$$

where

$$\begin{aligned} c_k &= \frac{1}{2}(a_k - jb_k) \\ c_{-k} &= c_k^* \\ c_0 &= \frac{a_0}{2}. \end{aligned} \tag{D.5}$$

The complex Fourier series expansion is compatible with the Fast Fourier Transform, a method commonly used to determine the harmonic spectrum of time domain waveforms. If frequent transformations from the time domain are not required, harmonic phasors in positive frequency offers several advantages: the redundancy of storing and processing complex conjugate pairs is avoided, the harmonic phasor is compatible with existing power systems analysis method such as the load flow, and it is easy to decompose the phasors into real components that is required in an unified Newton's solution involving a mixture of complex and real number. The Fourier expansion in positive frequency is to be described in the next section.

D.2 POSITIVE FREQUENCY HARMONIC PHASORS

The Fourier expansion can be represented by a series of phase shifted sine terms by substituting

$$a_k \cos(kwt) + b_k \sin(kwt) = d_k \sin(kwt + \psi_k), \tag{D.6}$$

into equation D.1, resulting in

$$f(t) = \sum_{k=0}^{\infty} \mathcal{I}\{\Psi_k e^{jkwt}\}, \tag{D.7}$$

where

$$\begin{aligned} \Psi_k &= d_k e^{\psi_k} \\ d_k &= \sqrt{a_k^2 + b_k^2} \\ \psi_k &= \tan^{-1} \frac{a_k}{b_k}. \end{aligned} \tag{D.8}$$

and Ψ_k being the positive frequency peak value harmonic phasors. The Fourier expansion described by equation D.7 does not contain negative frequency components, and the

phasor at harmonic k is given as:

$$\Psi_k = b_k + ja_k, \tag{D.9}$$

and the dc term becomes

$$\Psi_0 = \frac{a_0}{2}e^{j\pi/2} = j\frac{a_0}{2}. \tag{D.10}$$

When peak value phasors are used, the complex power is given by

$$P + jQ = \frac{1}{2}VI^*. \tag{D.11}$$

D.3 CONVOLUTION OF HARMONIC PHASORS

The multiplication of two time domain waveforms is expressed as a discrete convolution of their Fourier series in the harmonic domain. The convolution of two harmonic phasors of different frequencies will result in harmonic phasors at the sum and difference harmonic orders. Discrete convolution can be explained by first multiplying two sinusoidal waveforms and converted back to phasor form. The time domain multiplication of two phasor A_k and B_m of harmonic orders k and m is:

$$\begin{aligned}|A_k|\sin(kwt+\angle A_k) \times |B_m|\sin(mwt+\angle B_m) \;=\; & \frac{1}{2}|A_k||B_m| \left\{\sin[(k-m)wt + \angle A_k - \angle B_m + \frac{\pi}{2}]\right. \\ & \left. - \sin[(k+m)wt + \angle A_k + \angle B_m + \frac{\pi}{2}]\right\}.\end{aligned} \tag{D.12}$$

Converting to phasor form

$$\begin{aligned}A_k \otimes B_m &= \frac{1}{2}|A_k||B_m| \left[e^{j(\angle A_k - \angle B_m + \frac{\pi}{2})}\Big|_{(k-m)} - e^{j(\angle A_k + \angle B_m + \frac{\pi}{2})}\Big|_{(k+m)}\right] \\ &= \frac{1}{2}\left[\left(|A_k|e^{j\angle A_k}|B_m|e^{-j\angle B_m}e^{j\frac{\pi}{2}}\right)_{k-m} - \left(|A_k|e^{j\angle A_k}|B_m|e^{j\angle B_m}e^{j\frac{\pi}{2}}\right)_{k+m}\right] \\ &= \frac{1}{2}j\left[(A_kB_m^*)_{k-m} - (A_kB_m)_{k+m}\right]\end{aligned} \tag{D.13}$$

If k is less than m, negative harmonics can be avoided by conjugating the difference term. Consequently, the convolution of the two sinusoidal waveforms can be expressed as:

$$A_k \otimes B_m = \begin{cases} \frac{1}{2}j(A_kB_m^*)_{(k-m)} - \frac{1}{2}j(A_kB_m)_{(k+m)} & \textit{if } k \geq m \\ \frac{1}{2}j(A_kB_m^*)^*_{(m-k)} - \frac{1}{2}j(A_kB_m)_{(k+m)} & \textit{otherwise} \end{cases}. \tag{D.14}$$

This expression is readily extended to the discrete convolution of the Fourier Series of two non-sinusoidal periodic waveforms:

$$\begin{aligned} f_a(t)f_b(t) &= \sum_{k=0}^{n} |A_k| \sin(kwt+\angle A_k) \sum_{m=0}^{n} |B_m| \sin(mwt+\angle B_m) \\ &= \sum_{k=0}^{n}\sum_{m=0}^{n} |A_k| \sin(kwt+\angle A_k)|B_m| \sin(mwt+\angle B_m). \end{aligned} \tag{D.15}$$

Rewriting this in terms of phasors as:

$$F_A \otimes F_B = \sum_{k=0}^{n}\sum_{m=0}^{n} A_k \otimes B_m. \tag{D.16}$$

Harmonic phasors of order up to $2n$ are generated by equation D.16 due to the sum terms. Substituting equation D.14 for the convolution of two phasors into D.16 and solving for the lth order component yields:

$$(A \otimes B)_l = \frac{1}{2}j\left[\sum_{k=0}^{n}(A_k B_{k+l}^*)^* + \sum_{k=l}^{n} A_k B_{k-l}^* - \sum_{k=0}^{n} A_k B_{l-k}\right] \quad l > 0, \tag{D.17}$$

$$(A \otimes B)_l = \frac{1}{2}j\left[-2A_0B_0 + \sum_{k=0}^{n} A_k B_k^*\right] \quad l = 0. \tag{D.18}$$

Due to the conjugate terms, the convolution equations are non-analytic in the complex form, but are differentiable by decomposing into real valued components such as in rectangular form.

Appendix E

SIMPLIFIED CONVERTOR COMMUTATION ANALYSIS AND HARMONIC CALCULATION

Assuming balanced and undistorted commutation voltage, ripple free dc current and balanced commutation reactances, the expression for instantaneous commutation current of a six-pulse bridge is [Arrillaga 1983]:

$$i_c = \frac{V_c}{\sqrt{2}X_c}[\cos\alpha - \cos(wt)]. \tag{E.1}$$

where V_c is the phase-to-phase rms voltage and α is the firing angle. The commutation ends when commutation current is equal to dc current, i.e. $i_c = I_{dc}$ at $wt = \alpha + \mu$:

$$I_{dc} = \frac{V_c}{\sqrt{2}X_c}[\cos\alpha - \cos(\alpha + \mu)], \tag{E.2}$$

and thus the commutation angle μ is calculated as:

$$\mu = \cos^{-1}\left(\cos\alpha - \frac{\sqrt{2}X_c I_{dc}}{V_c}\right) - \alpha \tag{E.3}$$

Substituting equation E.2 into E.1, the currents of the incoming and outgoing valves in a six-pulse bridge during commutation, and subsequently phase a current are obtained as:

$$I_a = \frac{I_{dc}(\cos\alpha - \cos wt)}{\cos\alpha - \cos(\alpha + \mu)} \qquad for\ \ \alpha \le wt < \alpha + \mu \tag{E.4}$$

$$I_a = I_{dc} - I_{dc}\frac{\cos\alpha - \cos(wt - 2\pi/3)}{\cos\alpha - \cos(\alpha + \mu)} \qquad for\ \ \alpha + \frac{2\pi}{3} \le wt < \alpha + \frac{2\pi}{3} + \mu \tag{E.5}$$

The rates of changes of incoming and outgoing valve currents are equal since the commutation reactances are balanced.

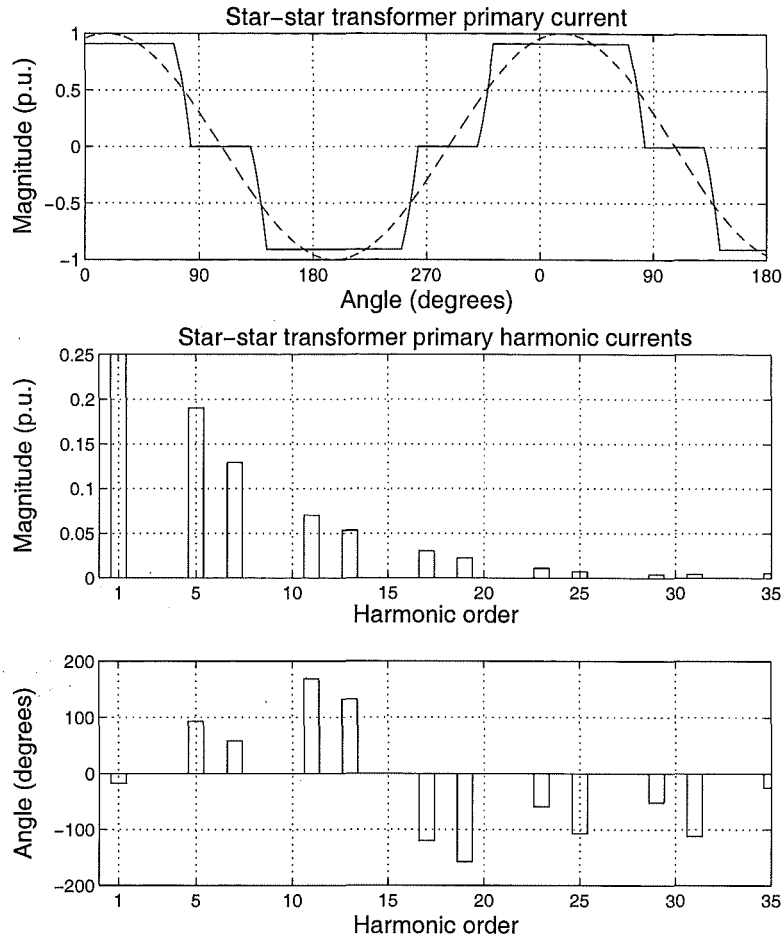

Figure E.1 Star-star transformer primary current and its harmonic content, commutation period is 13 degrees.

The line current is the same as the dc current in between commutations, i.e.

$$I_a = I_{dc} \qquad for \;\; \alpha + \mu \leq wt \leq \frac{2\pi}{3} + \alpha \tag{E.6}$$

The harmonic content can be obtained by integrating the described analytic expressions over one cycle, but this is a complicated process. Alternatively, the waveform can be contructed from α, μ (calculated) and I_{dc}, and an FFT is used to obtain the harmonic information. Therefore, if the commutation voltage, commutation reactance, dc current and firing angle are given, then the commutation angle and the harmonic content can be calculated using the conventional formulation.

Figure E.1 shows the star-star transformer phase a primary current constructed from the dc current and switching instances, and its harmonic content for a case where $\alpha = 10$, $X_c = 0.05$ p.u. and 1 p.u. commutation voltage. The calculated commutation angle is 13^o.

Appendix F

JACOBIAN OF PARTIAL DERIVATIVES

The Jacobian matrix is derived for a six-pulse rectifier attached to a salient-pole generator via star-g/star transformer in this Appendix. The elements of the Jacobian are the partial derivatives of the mismatch functions with respect to the variables that are being solved for by Newton's method. The selected variables are $V_k^a, V_k^b, V_k^c, I_{dk}, \phi_i, \theta_i$, and α_0. In finding the partial derivative of a mismatch function with respect to one of these variables, all other variables are held constant. Figure F.1 shows the construction of the Jacobian for 13 harmonics. The blocks associated with interactions between the dc current harmonics and the ac voltage harmonics comprise the *ac/dc partition*, which is 104 elements square. All other blocks are called switching terms.

The extension to twelve-pulse partial derivatives is relatively straightforward, where the twelve-pulse ac/dc Jacobian partition being the sum of those of the star and delta convertors, minus the identity matrix. The switching terms associated with each group are the same. The derived Jacobian elements have been verified by comparison with the numerical partial derivatives.

As the variables and functions are a mixture of real and complex numbers, decomposition in to real values is required. The basic operations that are extensively used to decompose the complex functions are given in equation F.1 to F.4.

The partial derivatives in real and imaginary components of a function with respect to a variable are given as:

$$\frac{\partial F_V}{\partial V} = \begin{bmatrix} \frac{\partial \mathcal{R}F_V}{\partial \mathcal{R}V} & \frac{\partial \mathcal{R}F_V}{\partial \mathcal{I}V} \\ \frac{\partial \mathcal{I}F_V}{\partial \mathcal{R}V} & \frac{\partial \mathcal{I}F_V}{\partial \mathcal{I}V} \end{bmatrix}, \tag{F.1}$$

when both F_V and V are complex numbers, and reduced to equations F.2 and F.3 when

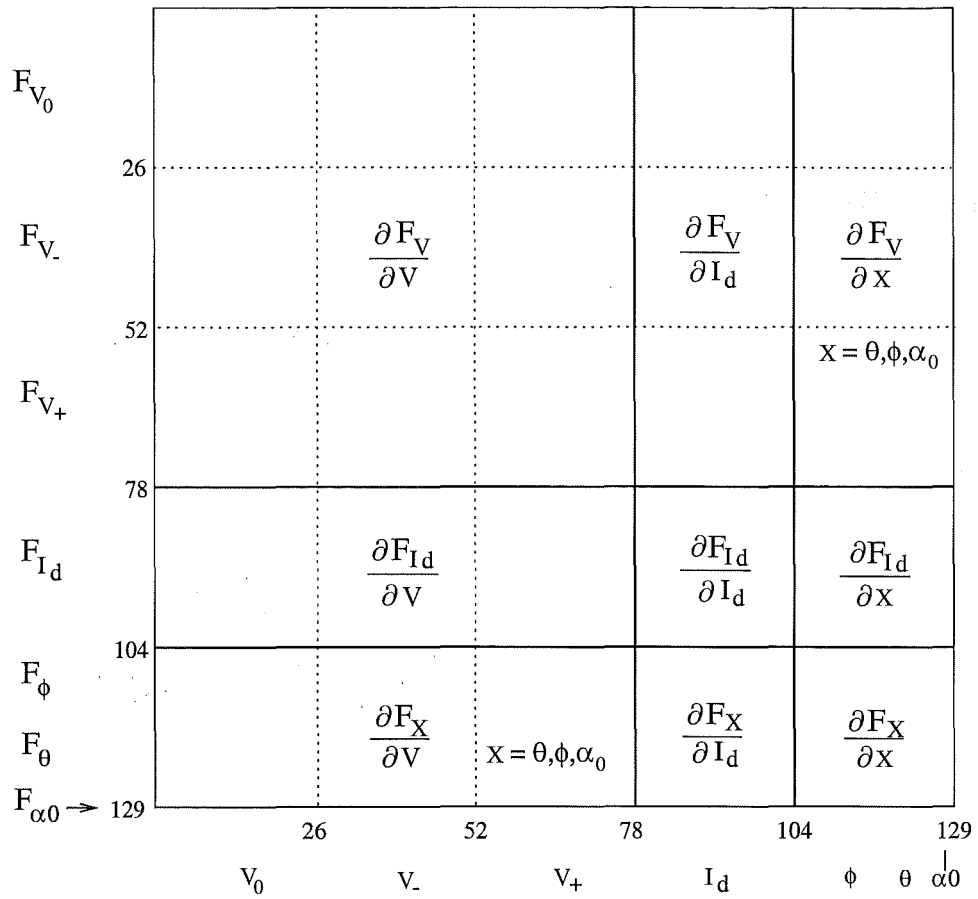

Figure F.1 Partial derivatives in the Jacobian.

one of them is a real number.

$$\frac{\partial F_V}{\partial V} = \begin{bmatrix} \frac{\partial \mathcal{R}F_V}{\partial V} \\ \frac{\partial \mathcal{I}F_V}{\partial V} \end{bmatrix} \qquad V \in \text{real} \tag{F.2}$$

$$\frac{\partial F_V}{\partial V} = \begin{bmatrix} \frac{\partial F_V}{\partial \mathcal{R}V} & \frac{\partial F_V}{\partial \mathcal{R}V} \end{bmatrix} \qquad F_V \in \text{real}. \tag{F.3}$$

The decomposition of an impedance gives a 2×2 matrix, i.e.

$$\begin{bmatrix} \mathcal{R}\{V\} \\ \mathcal{I}\{V\} \end{bmatrix} = \begin{bmatrix} \mathcal{R}\{Z\} & -\mathcal{I}\{Z\} \\ \mathcal{I}\{Z\} & \mathcal{R}\{Z\} \end{bmatrix} \begin{bmatrix} \mathcal{R}\{I\} \\ \mathcal{I}\{I\} \end{bmatrix} \tag{F.4}$$

F.1 VOLTAGE CONTROL EQUATION PARTIAL DERIVATIVES

As the control system frequently deals with filtered signals, only the fundamental voltage crossings are considered in the determination of the average delay angle.

$$F_{\alpha set} \stackrel{\text{def}}{=} \alpha_{set} - \frac{1}{12}\sum_{i=1}^{12}(\theta_i - \gamma_i) = 0\,, \tag{F.5}$$

Differentiating with respect to the selected variables gives:

$$\frac{\partial F_{\alpha set}}{\partial x} = 0, \qquad x \in \{V_k, I_{dk}, \phi_i, \phi_0\} \tag{F.6}$$

$$\frac{\partial F_{\alpha set}}{\partial \theta_i} = -\frac{1}{12} \tag{F.7}$$

For the phase angle, differentiating $\mathcal{I}\{F_{V1\,ps}\} = \mathcal{I}\{V1_{ps}\} = 0$ gives

$$\frac{\partial F_{V1\,ps}}{\partial x} = 0, \qquad x \in \{V_l, I_{dk}, \theta_i, \phi_i, \phi_0\}, l \geq 2 \tag{F.8}$$

$$\frac{\partial \mathcal{I}\{F_{V1\,ps}\}}{\partial \mathcal{I}V_{1\,ps}} = 1 \tag{F.9}$$

$$\frac{\partial \mathcal{R}\{F_{V1\,ps}\}}{\partial \mathcal{R}V_{1\,ps}} = \frac{\partial \mathcal{R}\{F_{V1\,ps}\}}{\partial \mathcal{I}V_{1\,ps}} = \frac{\partial \mathcal{I}\{F_{V1\,ps}\}}{\partial \mathcal{R}V_{1\,ps}} = 0. \tag{F.10}$$

where the subscript $V1\ ps$ denotes the fundamental positive-sequence voltage.

F.2 TERMINAL VOLTAGE PARTIAL DERIVATIVES

The terminal voltage mismatch has been defined as:

$$F_{Vk} \stackrel{\text{def}}{=} V_k - [E]_k + [Z]_{k,k}[I]_k + [Z]_{k,k+2}[I]_{k+2} + [Z]_{k,k-2}[I]_{k-2} = 0. \tag{F.11}$$

Expanding the expression over three phases yields:

$$\begin{bmatrix} F_V^a \\ F_V^b \\ F_V^c \end{bmatrix}_k = \begin{bmatrix} V^a \\ V^b \\ V^c \end{bmatrix}_k - \begin{bmatrix} E^a \\ E^b \\ E^c \end{bmatrix}_k + \begin{bmatrix} Z^{aa} & Z^{ab} & Z^{ac} \\ Z^{ba} & Z^{bb} & Z^{bc} \\ Z^{ca} & Z^{cb} & Z^{cc} \end{bmatrix}_{k,k} \begin{bmatrix} I^a \\ I^b \\ I^c \end{bmatrix}_k$$
$$+ \begin{bmatrix} Z^{aa} & Z^{ab} & Z^{ac} \\ Z^{ba} & Z^{bb} & Z^{bc} \\ Z^{ca} & Z^{cb} & Z^{cc} \end{bmatrix}_{k,k+2} \begin{bmatrix} I^a \\ I^b \\ I^c \end{bmatrix}_{k+2} + \begin{bmatrix} Z^{aa} & Z^{ab} & Z^{ac} \\ Z^{ba} & Z^{bb} & Z^{bc} \\ Z^{ca} & Z^{cb} & Z^{cc} \end{bmatrix}_{k,k-2} \begin{bmatrix} I^a \\ I^b \\ I^c \end{bmatrix}_{k-2}. \tag{F.12}$$

Thus the voltage mismatch for each phase can be written as:

$$\begin{aligned} F_{V_k^\alpha} = V_k^\alpha - E_k^\alpha \; &+ \; Z_{k,k}^{\alpha\alpha} I_k^\alpha + Z_{k,k}^{\alpha\beta} I_k^\beta + Z_{k,k}^{\alpha\gamma} I_k^\gamma \\ &+ \; Z_{k,k+2}^{\alpha\alpha} I_{k+2}^\alpha + Z_{k,k+2}^{\alpha\beta} I_{k+2}^\beta + Z_{k,k+2}^{\alpha\gamma} I_{k+2}^\gamma \\ &+ \; Z_{k,k-2}^{\alpha\alpha} I_{k-2}^\alpha + Z_{k,k-2}^{\alpha\beta} I_{k-2}^\beta + Z_{k,k-2}^{\alpha\gamma} I_{k-2}^\gamma \end{aligned} \tag{F.13}$$

where $[\alpha\ \beta\ \gamma]$ is a permutation of $[a\ b\ c]$. The last six terms in equation F.13 are the saliency terms which require the calculation of currents $k+2$ and $k-2$.

F.2.1 With Respect to ac Voltage Variation

Differentiating equation F.13 with respect to one of the phase voltage in both real and imaginary parts yields

$$\frac{\partial \mathcal{R}\{F_{V_k^\alpha}\}}{\partial \mathcal{R}\{V_m^\delta\}} = \mathcal{R}\left\{ \begin{array}{ll} \sum_{l=k-2,k}^{k+2} \left(Z_{k,l}^{\alpha\alpha} \frac{\partial I_k^\alpha}{\partial \mathcal{R}\{V_m^\delta\}} + Z_{k,l}^{\alpha\beta} \frac{\partial I_k^\beta}{\partial \mathcal{R}\{V_m^\delta\}} + Z_{k,l}^{\alpha\gamma} \frac{\partial I_k^\gamma}{\partial \mathcal{R}\{V_m^\delta\}} \right) & \alpha \neq \delta \text{ or } k \neq m \\ 1 + \sum_{l=k-2,k}^{k+2} \left(Z_{k,l}^{\alpha\alpha} \frac{\partial I_k^\alpha}{\partial \mathcal{R}\{V_m^\delta\}} + Z_{k,l}^{\alpha\beta} \frac{\partial I_k^\beta}{\partial \mathcal{R}\{V_m^\delta\}} + Z_{k,l}^{\alpha\gamma} \frac{\partial I_k^\gamma}{\partial \mathcal{R}\{V_m^\delta\}} \right) & \alpha = \delta \text{ and } k = m \end{array} \right. \tag{F.14}$$

$$\frac{\partial \mathcal{R}\{F_{V_k^\alpha}\}}{\partial \mathcal{I}\{V_m^\delta\}} = \mathcal{I}\left\{ \sum_{l=k-2,k}^{k+2} \left(Z_{k,l}^{\alpha\alpha} \frac{\partial I_k^\alpha}{\partial \mathcal{I}\{V_m^\delta\}} + Z_{k,l}^{\alpha\beta} \frac{\partial I_k^\beta}{\partial \mathcal{I}\{V_m^\delta\}} + Z_{k,l}^{\alpha\gamma} \frac{\partial I_k^\gamma}{\partial \mathcal{I}\{V_m^\delta\}} \right) \right\} \tag{F.15}$$

$$\frac{\partial \mathcal{I}\{F_{V_k^\alpha}\}}{\partial \mathcal{I}\{V_m^\delta\}} = \mathcal{I}\left\{ \begin{array}{ll} \sum_{l=k-2,k}^{k+2} \left(Z_{k,l}^{\alpha\alpha} \frac{\partial I_k^\alpha}{\partial \mathcal{I}\{V_m^\delta\}} + Z_{k,l}^{\alpha\beta} \frac{\partial I_k^\beta}{\partial \mathcal{I}\{V_m^\delta\}} + Z_{k,l}^{\alpha\gamma} \frac{\partial I_k^\gamma}{\partial \mathcal{I}\{V_m^\delta\}} \right) & \alpha \neq \delta \text{ or } k \neq m \\ j + \sum_{l=k-2,k}^{k+2} \left(Z_{k,l}^{\alpha\alpha} \frac{\partial I_k^\alpha}{\partial \mathcal{I}\{V_m^\delta\}} + Z_{k,l}^{\alpha\beta} \frac{\partial I_k^\beta}{\partial \mathcal{I}\{V_m^\delta\}} + Z_{k,l}^{\alpha\gamma} \frac{\partial I_k^\gamma}{\partial \mathcal{I}\{V_m^\delta\}} \right) & \alpha = \delta \text{ and } k = m \end{array} \right. \tag{F.16}$$

$$\frac{\partial \mathcal{I}\{F_{V_k^\alpha}\}}{\partial \mathcal{R}\{V_m^\delta\}} = \mathcal{I}\left\{ \sum_{l=k-2,k}^{k+2} \left(Z_{k,l}^{\alpha\alpha} \frac{\partial I_k^\alpha}{\partial \mathcal{R}\{V_m^\delta\}} + Z_{k,l}^{\alpha\beta} \frac{\partial I_k^\beta}{\partial \mathcal{R}\{V_m^\delta\}} + Z_{k,l}^{\alpha\gamma} \frac{\partial I_k^\gamma}{\partial \mathcal{R}\{V_m^\delta\}} \right) \right\}. \tag{F.17}$$

Subsequently, we need to calculate the partial derivatives of the ac currents with respect to the ac voltage variation, $\frac{\partial I_k^\alpha}{\partial \{V_m^\delta\}}$. As ac currents are functions of $X = [V_k^a, V_k^b, V_k^c, I_{dk}, \phi_i, \theta_i]$, and the switching instants are kept constant, only the effect of phase coltage variation on the sampled commutation currents is required to be considered. This is because the commutation currents are functions of the terminal voltage, whereas currents during "normal" conduction periods are functions of dc current harmonics, which is kept constant.

As there are 6 commutation periods in one cycle:

$$\frac{\partial I_k^\alpha}{\partial \mathcal{R}\{V_m^\delta\}} = \sum_{i=1}^{6} C_{\alpha\delta i} \frac{\partial I_{cik}^s}{\partial \mathcal{R}\{V_m^\delta\}}, \tag{F.18}$$

$$\frac{\partial I_k^\alpha}{\partial \mathcal{I}\{V_m^\delta\}} = \sum_{i=1}^{6} C_{\alpha\delta i} \frac{\partial I_{cik}^s}{\partial \mathcal{I}\{V_m^\delta\}}, \tag{F.19}$$

where I_{ci}^s is the *ith* commutation current I_{ci}, sampled over the commutation period. As there are four commutation period for each cycle of ac current, the coefficient $C_{\alpha\delta i}$ defines whether for the *ith* commutation the phase α current is a function of the phase β terminal voltage. Referring to Table 4.1, C is given as:

$C_{\alpha\delta i}$		δ		
		a	b	c
α	a	[-1, 0, -1, -1, 0, -1]	[0, 0, 1, 0, 0, 1]	[1, 0, 0, 1, 0, 0]
	b	[0, 0, 1, 0, 0, 1]	[0, -1, -1, 0, -1, -1]	[0, 1, 0, 0, 1, 0]
	c	[1, 0, 0, 1, 0, 0]	[0, 1, 0, 0, 1, 0]	[-1, -1, 0, -1, -1, 0]

Table F.1 The coefficient matrix $C_{\alpha\delta i}$ which specifies the dependency among commutation current i, terminal voltage phase, and ac current phase

The commutation current is given by

$$I_{ci}(t) = D + \mathcal{I}\left\{\sum_{k=1}^{n_h} I_{cik} e^{jkwt}\right\}, \tag{F.20}$$

where

$$D = -\mathcal{I}\left\{\sum_{k=1}^{n_h} I_{cik} e^{jk\theta_i}\right\} \tag{F.21}$$

$$I_{cik} = \frac{jkwL_e I_{dk} - V_{ebk}}{jkwL_{eb}}, \tag{F.22}$$

and subscript e and b refer to the phases ending and beginning conduction respectively. Sampling the commutation current requires a convolution with the relevant sampling function:

$$I_{ci}^s = \left[D + \sum_{k=1}^{n_h} I_{ck}\right] \otimes \Psi_{(2i-1)}, \quad \text{for } i = 1, 2, ..., 6. \tag{F.23}$$

Setting $I_{ci0} = D$, expanding the convolution, and taking the kth component yields

$$I_{cik}^{s} = \frac{1}{2}j\left\{\sum_{l=k}^{n_h} I_{cil}\Psi^{*}_{(2i-1)_{l-k}} + \sum_{l=0}^{n_h}(I_{cil}\Psi^{*}_{(2i-1)_{l+k}})^{*} - \sum_{l=0}^{n_h} I_{cil}\Psi_{(2i-1)_{k-l}}\right\}, \quad k > 0. \tag{F.24}$$

Since the commutation circuit is linear, i.e. no couplings between harmonics, changes in the commutation current at harmonic l, i_{cil}, with respect to a voltage at different harmonic m is zero:

$$\frac{\partial I_{cil}}{\partial \mathcal{R}\{V_m^{\delta}\}} = 0 \quad \text{for } l, m \text{ such that } l \neq m \text{ and } l > 0. \tag{F.25}$$

This allows the following partial derivatives to be written:

$$\begin{aligned}\frac{\partial I_{cik}^{s}}{\partial \mathcal{R}\{V_m^{\delta}\}} &= \frac{1}{2}j\left[-\frac{\partial I_{ci0}}{\partial \mathcal{R}\{V_m^{\delta}\}}\Psi_{(2i-1)_k} + \left(\frac{\partial I_{ci0}}{\partial \mathcal{R}\{V_m^{\delta}\}}\Psi^{*}_{(2i-1)_k}\right)^{*}\right. \\ &+ \left.\left(\frac{\partial I_{cim}}{\partial \mathcal{R}\{V_m^{\delta}\}}\Psi^{*}_{(2i-1)_{m+k}}\right)^{*} + \begin{cases} -\frac{\partial I_{cim}}{\partial \mathcal{R}\{V_m^{\delta}\}}\Psi_{(2i-1)_{k-m}}, & m \leq k \\ \frac{\partial I_{cim}}{\partial \mathcal{R}\{V_m^{\delta}\}}\Psi^{*}_{(2i-1)_{m-k}}, & m \geq k \end{cases}\right].\end{aligned} \tag{F.26}$$

Similarly,

$$\begin{aligned}\frac{\partial I_{cik}^{s}}{\partial \mathcal{I}\{V_m^{\delta}\}} &= \frac{1}{2}j\left[-\frac{\partial I_{ci0}}{\partial \mathcal{I}\{V_m^{\delta}\}}\Psi_{(2i-1)_k} + \left(\frac{\partial I_{ci0}}{\partial \mathcal{I}\{V_m^{\delta}\}}\Psi^{*}_{(2i-1)_k}\right)^{*}\right. \\ &+ \left.\left(\frac{\partial I_{cim}}{\partial \mathcal{I}\{V_m^{\delta}\}}\Psi^{*}_{(2i-1)_{m+k}}\right)^{*} + \begin{cases} -\frac{\partial I_{cim}}{\partial \mathcal{I}\{V_m^{\delta}\}}\Psi_{(2i-1)_{k-m}}, & m \leq k \\ \frac{\partial I_{cim}}{\partial \mathcal{I}\{V_m^{\delta}\}}\Psi^{*}_{(2i-1)_{m-k}}, & m \geq k \end{cases}\right].\end{aligned} \tag{F.27}$$

The calculations required to evaluate equations F.26 and F.27 can be approximately halved by using the Cauchy Reimann equations for the partial derivatives of complex functions. For an analytic function:

$$\frac{\partial F(z)}{\partial \mathcal{I}\{z\}} = j\frac{\partial F(z)}{\partial \mathcal{R}\{z\}}, \tag{F.28}$$

and for the complex conjugate of an analytic function

$$\frac{\partial F(z)^{*}}{\partial \mathcal{I}\{z\}} = -j\frac{\partial F(z)^{*}}{\partial \mathcal{R}\{z\}}. \tag{F.29}$$

Consequently, the terms in equation F.27 is obtained by re-arranging the real and imaginary parts of the corresponding terms in equation F.26. The remaining partial

derivatives, $\frac{\partial I_{ci0}}{\partial \mathcal{R}\{V_m^\delta\}}$ and $\frac{\partial I_{cim}}{\partial \mathcal{R}\{V_m^\delta\}}$, are obtained from equations F.21 and F.22:

$$\frac{\partial I_{ci0}}{\partial \mathcal{R}\{V_m^\delta\}} = -j\mathcal{I}\left\{\frac{e^{jk\theta_i}}{jkwL_{eb}}\right\}, \tag{F.30}$$

$$\frac{\partial I_{ci0}}{\partial \mathcal{I}\{V_m^\delta\}} = -j\mathcal{R}\left\{\frac{e^{jk\theta_i}}{jkwL_{eb}}\right\}, \tag{F.31}$$

$$\frac{\partial I_{cim}}{\partial \mathcal{R}\{V_m^\delta\}} = \frac{1}{jkwL_{eb}}. \tag{F.32}$$

It is assumed that phase δ is beginning conduction; phase δ ending conduction is accounted for in the C matrix. This completes the derivation of the partial derivative of terminal voltage mismatch with respect to terminal voltage variation.

F.2.2 With Respect to dc Ripple Current Variation

There are two effects that need to be considered. The ac currents during "normal" conduction periods are functions of dc current harmonics, and the commutation currents are functions of the dc ripples. Differentiate the voltage mismatch with respect to the dc current harmonics yields:

$$\frac{\partial \mathcal{R}\{F_{V_k^\alpha}\}}{\partial \mathcal{R}\{I_{dm}\}} = \mathcal{R}\left\{\sum_{l=k-2,k}^{k+2}\left(Z_{k,l}^{\alpha\alpha}\frac{\partial I_k^\alpha}{\partial \mathcal{R}\{I_{dm}\}} + Z_{k,l}^{\alpha\beta}\frac{\partial I_k^\beta}{\partial \mathcal{R}\{I_{dm}\}} + Z_{k,l}^{\alpha\gamma}\frac{\partial I_k^\gamma}{\partial \mathcal{R}\{I_{dm}\}}\right)\right\} \tag{F.33}$$

$$\frac{\partial \mathcal{R}\{F_{V_k^\alpha}\}}{\partial \mathcal{I}\{I_{dm}\}} = \mathcal{R}\left\{\sum_{l=k-2,k}^{k+2}\left(Z_{k,l}^{\alpha\alpha}\frac{\partial I_k^\alpha}{\partial \mathcal{I}\{I_{dm}\}} + Z_{k,l}^{\alpha\beta}\frac{\partial I_k^\beta}{\partial \mathcal{I}\{I_{dm}\}} + Z_{k,l}^{\alpha\gamma}\frac{\partial I_k^\gamma}{\partial \mathcal{I}\{I_{dm}\}}\right)\right\} \tag{F.34}$$

$$\frac{\partial \mathcal{I}\{F_{V_k^\alpha}\}}{\partial \mathcal{I}\{I_{dm}\}} = \mathcal{I}\left\{\sum_{l=k-2,k}^{k+2}\left(Z_{k,l}^{\alpha\alpha}\frac{\partial I_k^\alpha}{\partial \mathcal{I}\{I_{dm}\}} + Z_{k,l}^{\alpha\beta}\frac{\partial I_k^\beta}{\partial \mathcal{I}\{I_{dm}\}} + Z_{k,l}^{\alpha\gamma}\frac{\partial I_k^\gamma}{\partial \mathcal{I}\{I_{dm}\}}\right)\right\} \tag{F.35}$$

$$\frac{\partial \mathcal{I}\{F_{V_k^\alpha}\}}{\partial \mathcal{R}\{I_{dm}\}} = \mathcal{I}\left\{\sum_{l=k-2,k}^{k+2}\left(Z_{k,l}^{\alpha\alpha}\frac{\partial I_k^\alpha}{\partial \mathcal{R}\{I_{dm}\}} + Z_{k,l}^{\alpha\beta}\frac{\partial I_k^\beta}{\partial \mathcal{R}\{I_{dm}\}} + Z_{k,l}^{\alpha\gamma}\frac{\partial I_k^\gamma}{\partial \mathcal{R}\{I_{dm}\}}\right)\right\} \tag{F.36}$$

The phase currents are composed of commutation currents and the dc current sampled on the ac side:

$$I^\alpha = \sum_{i=1}^{6}[E_i^\alpha I_{ci} \otimes \Psi_{2i-1}] + I_d \otimes \Psi^\alpha \,. \tag{F.37}$$

E_i^α, listed in Table F.2, is a coefficient matrix that specifies how the commutation currents contribute to each of the phase currents, and Ψ^α is the phase α dc current compound sampling function.

E_i^α		α		
		a	b	c
i	1	1	0	-1
	2	0	-1	1
	3	-1	1	0
	4	1	0	-1
	5	0	-1	1
	6	-1	1	0

Table F.2 Coefficient matrix E_i^α defining the contribution of the commutation currents to each phase current. i is the commutation number.

Differentiating the kth component of equation F.37 with respect to $\mathcal{R}\{I_{dm}\}$ gives:

$$\frac{\partial I_k^\alpha}{\partial \mathcal{R}\{I_{dm}\}} = \frac{\partial\{\sum_i [E_i^\alpha I_{ci} \otimes \Psi_{2i-1}]\}_k}{\partial \mathcal{R}\{I_{dm}\}} + \frac{\partial\{I_d \otimes \Psi_\alpha\}_k}{\partial \mathcal{R}\{I_{dm}\}} . \tag{F.38}$$

The first term is similar to the differential with respect to voltage already derived in the previous section, as a variation in I_{dm} affects only I_{cim} and I_{ci0}. Expanding the convolution in the first term, selecting the kth component, and differentiating yields

$$\begin{aligned}\frac{\partial\{\sum_i [E_i^\alpha I_{ci} \otimes \Psi_{2i-1}]\}_k}{\partial \mathcal{R}\{I_{dm}\}} = \frac{1}{2} j \sum_i E_i^\alpha \Bigg[& - \frac{\partial I_{ci0}}{\partial \mathcal{R}\{I_{dm}\}} \Psi_{(2i-1)_k} \\ & + \left(\frac{\partial I_{ci0}}{\partial \mathcal{R}\{I_{dm}\}} \Psi^*_{(2i-1)_k} \right)^* + \left(\frac{\partial I_{cim}}{\partial \mathcal{R}\{I_{dm}\}} \Psi^*_{(2i-1)_{m+k}} \right)^* \\ & + \begin{cases} -\frac{\partial I_{cim}}{\partial \mathcal{R}\{I_{dm}\}} \Psi_{(2i-1)_{k-m}} & m \le k \\ \frac{\partial I_{cim}}{\partial \mathcal{R}\{I_{dm}\}} \Psi^*_{(2i-1)_{m-k}} & m \ge k \end{cases} \Bigg] . \end{aligned} \tag{F.39}$$

Expanding the convolution in the second term of equation F.38 gives the kth component of the sampled dc current:

$$I_d^{s\alpha}{}_k = \frac{1}{2} j \left\{ \sum_{l=k}^{n_h} I_{dl} \Psi^{\alpha *}_{l-k} + \left(\sum_{l=0}^{n_h} I_{dl} \Psi^{\alpha *}_{l+k} \right)^* - \sum_{l=0}^{n_h} I_{dl} \Psi^\alpha_{k-l} \right\} \quad k > 0, \tag{F.40}$$

where $I_{dk}^{s\alpha}$ is the phase α sample of the dc current. This equation can be differentiated to give:

$$\frac{\partial\{I_d \otimes \Psi^\alpha\}_k}{\partial \mathcal{R}\{I_{dm}\}} = \frac{1}{2} j \, \Psi^\alpha_{k+m} + \frac{1}{2} j \begin{cases} -\Psi^\alpha_{k-m} & m \le k \\ \Psi^{\alpha *}_{m-k} & m \ge k \end{cases} . \tag{F.41}$$

Applying the above analysis for variations in the imaginary part of I_{dm} gives

$$\frac{\partial\{\sum_i[E_i^\alpha I_{ci}\otimes\Psi_{2i-1}]\}_k}{\partial\mathcal{I}\{I_{dm}\}} = \frac{1}{2}j\sum_i E_i^\alpha\Bigg[-\frac{\partial I_{ci0}}{\partial\mathcal{I}\{I_{dm}\}}\Psi_{(2i-1)_k} + \left(\frac{\partial I_{ci0}}{\partial\mathcal{I}\{I_{dm}\}}\Psi^*_{(2i-1)_k}\right)^* + \left(\frac{\partial I_{cim}}{\partial\mathcal{I}\{I_{dm}\}}\Psi^*_{(2i-1)_{m+k}}\right)^* + \begin{cases} -\frac{\partial I_{cim}}{\partial\mathcal{I}\{I_{dm}\}}\Psi_{(2i-1)_{k-m}} & m\le k \\ \frac{\partial I_{cim}}{\partial\mathcal{I}\{I_{dm}\}}\Psi^*_{(2i-1)_{m-k}} & m\ge k \end{cases}\Bigg]. \tag{F.42}$$

and

$$\frac{\partial\{I_d\otimes\Psi^\alpha\}_k}{\partial\mathcal{I}\{I_{dm}\}} = \frac{1}{2}j(j\Psi^{\alpha*}_{k+m})^* + \frac{1}{2}j\begin{cases} -j\Psi^\alpha_{k-m} & m\le k \\ j\Psi^{\alpha*}_{m-k} & m\ge k \end{cases}. \tag{F.43}$$

These equations are then substituted into an equation analogous to equation F.38 and hence into equations F.34 and F.36. The remaining derivatives, $\frac{\partial I_{ci0}}{\partial\mathcal{R}\{I_{dm}\}}$ and $\frac{\partial I_{cim}}{\partial\mathcal{R}\{I_{dm}\}}$, are obtained from equations F.21 and F.22:

$$\frac{\partial I_{ci0}}{\partial\mathcal{R}\{I_{dm}\}} = -j\mathcal{I}\left\{\frac{L_e e^{jk\theta_i}}{L_{eb}}\right\}, \tag{F.44}$$

$$\frac{\partial I_{ci0}}{\partial\mathcal{I}\{I_{dm}\}} = -j\mathcal{R}\left\{\frac{L_e e^{jk\theta_i}}{L_{eb}}\right\}, \tag{F.45}$$

$$\frac{\partial I_{cim}}{\partial\mathcal{R}\{I_{dm}\}} = \frac{L_e}{L_{eb}}. \tag{F.46}$$

F.2.3 With Respect to end of Commutation Variation

A variation in the end of commutation angle, ϕ_h, affects the $(2h{-}1)th$ and $2hth$ sampling functions. This affects all harmonics of the ac side sampled commutation currents, and dc current. Combining these two effects into the phase current variation, and injecting into the ac system yields the variation in the terminal voltage mismatch:

$$\frac{\partial\mathcal{R}\{F_{V_k}^\alpha\}}{\partial\phi_h} = \mathcal{R}\left\{\sum_{l=k-2,k}^{k+2}\left(Z^{\alpha\alpha}_{k,l}\frac{\partial I^\alpha_k}{\partial\phi_h} + Z^{\alpha\beta}_{k,l}\frac{\partial I^\beta_k}{\partial\phi_h} + Z^{\alpha\gamma}_{k,l}\frac{\partial I^\gamma_k}{\partial\phi_h}\right)\right\}, \tag{F.47}$$

$$\frac{\partial\mathcal{I}\{F_{V_k}^\alpha\}}{\partial\phi_h} = \mathcal{I}\left\{\sum_{l=k-2,k}^{k+2}\left(Z^{\alpha\alpha}_{k,l}\frac{\partial I^\alpha_k}{\partial\phi_h} + Z^{\alpha\beta}_{k,l}\frac{\partial I^\beta_k}{\partial\phi_h} + Z^{\alpha\gamma}_{k,l}\frac{\partial I^\gamma_k}{\partial\phi_h}\right)\right\}. \tag{F.48}$$

Differentiating the kth component of equation F.37 with respect to ϕ_h:

$$\frac{\partial I_k^\alpha}{\partial \phi_h} = \frac{\partial\{\sum_i [E_i^\alpha I_{ci} \otimes \Psi_{2i-1}]\}_k}{\partial \phi_h} + \frac{\partial\{I_d \otimes \Psi^\alpha\}_k}{\partial \phi_h} . \tag{F.49}$$

A variation in ϕ_h affects only the sampling of the hth commutation current in the first term of equation F.49. Expanding only this convolution of the summation yields:

$$I_{chk}^s = \frac{1}{2} j E_h^\alpha \left\{ \sum_{l=k}^{n_h} I_{chl} \Psi^*_{(2h-1)_{l-k}} + \sum_{l=0}^{n_h} \left(I_{chl} \Psi^*_{(2h-1)_{l+k}} \right)^* - \sum_{l=0}^{n_h} I_{chl} \Psi_{(2h-1)_{k-l}} \right\} \quad k > 0. \tag{F.50}$$

Differentiating this gives

$$\frac{\partial\{\sum_i [E_i^\alpha I_{ci} \otimes \Psi_{2i-1}]\}_k}{\partial \phi_h} = \frac{1}{2} j E_h^\alpha \left\{ \sum_{l=k}^{n_h} I_{chl} \frac{\partial \Psi^*_{(2h-1)_{l-k}}}{\partial \phi_h} + \sum_{l=0}^{n_h} \left(I_{chl} \frac{\partial \Psi^*_{(2h-1)_{l+k}}}{\partial \phi_h} \right)^* - \sum_{l=0}^{n_h} I_{chl} \frac{\partial \Psi_{(2h-1)_{k-l}}}{\partial \phi_h} \right\} \quad k > 0, \tag{F.51}$$

where

$$\frac{\partial \Psi_{(2h-1)_m}}{\partial \phi_h} = -\frac{\partial \Psi_{2hm}}{\partial \phi_h} = \frac{1}{\pi} [\sin(m\phi_h) + j \cos(m\phi_h)]. \tag{F.52}$$

The compound sampling function in the second term of equation F.49 is affected by variation in four of the six end of commutation angles. This is because the transfer of dc current to the ac side is defined by two conduction periods per cycle; the beginning and end of each conduction period corresponding to an end of commutation angle. The effect of a variation in ϕ_h therefore depends upon whether it corresponds to the beginning or end of a positive or negative conduction period for phase α. This information is already collated as the coefficient matrix E_i^α.

A similar analysis to the above for the second term of equation F.49 results in

$$\frac{\partial\{I_d \otimes \Psi^\alpha\}_k}{\partial \phi_h} = -\frac{1}{2} j E_h^\alpha \left\{ \sum_{l=k}^{n_h} I_{dl} \frac{\partial \Psi^*_{2hl-k}}{\partial \phi_h} + \sum_{l=0}^{n_h} \left(I_{dl} \frac{\partial \Psi^*_{2hl+k}}{\partial \phi_h} \right)^* - \sum_{l=0}^{n_h} I_{dl} \frac{\partial \Psi_{2hk-l}}{\partial \phi_h} \right\} \quad k > 0, \tag{F.53}$$

Since the compound sampling function is a sum of constituent sampling functions, it has been replaced in the partial derivative by the only term which is a function of ϕ_h. This is then substituted back into equation F.49 to give the required partial derivative.

F.2.4 With Respect to Firing Instant Variation

The transfer of dc current to the ac side of the convertor is defined entirely with reference to the end of commutation angles. The effect of a variation in the firing instants on the phase currents can therefore be obtained by analysing just the sampling of the commutation currents. The partial derivative of the ac voltage mismatch with respect to a firing angle variation is:

$$\frac{\partial \mathcal{R}\{F_{V_k^\alpha}\}}{\partial \theta_h} = \mathcal{R}\left\{ \sum_{l=k-2,k}^{k+2} \left(Z_{k,l}^{\alpha\alpha} \frac{\partial I_k^\alpha}{\partial \theta_h} + Z_{k,l}^{\alpha\beta} \frac{\partial I_k^\beta}{\partial \theta_h} + Z_{k,l}^{\alpha\gamma} \frac{\partial I_k^\gamma}{\partial \theta_h} \right) \right\}. \tag{F.54}$$

Since the ac side sampled dc current is not a function of θ_h

$$\begin{aligned} -\frac{\partial I_k^\alpha}{\partial \theta_h} = \frac{\partial \left\{ \sum_{i=1}^{6} E_i^\alpha I_{ci}^s \right\}_k}{\partial \theta_h} &= \frac{\partial \left\{ \sum_{i=1}^{6} E_i^\alpha I_{ci}^s \otimes \Psi_{(2i-1)} \right\}_k}{\partial \theta_h} \\ &= \frac{\partial \left\{ E_h^\alpha I_{ch}^s \otimes \Psi_{(2h-1)} \right\}_k}{\partial \theta_h}. \end{aligned} \tag{F.55}$$

Noting that a change in θ_h affects I_{ch0} and $\Psi_{(2h-1)}$. Applying the product rule to the expansion of the convolution leads to

$$\begin{aligned} \frac{\partial I_k^\alpha}{\partial \theta_h} = & -\frac{1}{2} j E_h^\alpha \left[\sum_{l=k}^{n_h} I_{chl} \frac{\partial \Psi^*_{(2h-1)_{l-k}}}{\partial \theta_h} + \sum_{l=0}^{n_h} \left(I_{chl} \frac{\partial \Psi^*_{(2h-1)_{l+k}}}{\partial \theta_h} \right)^* \right. \\ & \left. - \frac{\partial I_{ch0}}{\partial \theta_h} \Psi_{(2h-1)_k} + \left(\frac{\partial I_{ch0}}{\partial \theta_h} \Psi^*_{(2h-1)_k} \right)^* - \sum_{l=0}^{n_h} I_{chl} \frac{\partial \Psi_{(2h-1)_{k-l}}}{\partial \theta_h} \right]. \end{aligned} \tag{F.56}$$

This completes the analysis of the terminal voltage mismatch equation partial derivatives as there is no dependence upon α_0, the only remaining variable.

F.3 DIRECT CURRENT PARTIAL DERIVATIVES

The direct current partial derivatives are obtained by a process analogous to that used in obtaining the terminal voltage partial derivatives. The dc voltage partial derivatives are obtained and then applied to the dc system admittance to calculate the direct current differential. The direct current mismatch equation is

$$F_{Ik} = I_{dk} - V_{dk}Y_{dk} = 0. \tag{F.57}$$

Finding the partial derivatives of this equation is therefore mainly concerned with V_{dk}, which is a function of all the convertor variables except α_0.

F.3.1 With Respect to ac Voltage Variation

Differentiating equation F.57 with respect to terminal voltage yields

$$\frac{\partial \mathcal{R}\{F_{Ik}\}}{\partial \mathcal{R}\{V_m^\delta\}} = \mathcal{R}\left\{-Y_{dk}\frac{\partial V_{dk}}{\partial \mathcal{R}\{V_m^\delta\}}\right\}, \tag{F.58}$$

$$\frac{\partial \mathcal{R}\{F_{Ik}\}}{\partial \mathcal{I}\{V_m^\delta\}} = \mathcal{R}\left\{-Y_{dk}\frac{\partial V_{dk}}{\partial \mathcal{I}\{V_m^\delta\}}\right\}, \tag{F.59}$$

$$\frac{\partial \mathcal{I}\{F_{Ik}\}}{\partial \mathcal{R}\{V_m^\delta\}} = \mathcal{I}\left\{-Y_{dk}\frac{\partial V_{dk}}{\partial \mathcal{R}\{V_m^\delta\}}\right\}, \tag{F.60}$$

$$\frac{\partial \mathcal{I}\{F_{Ik}\}}{\partial \mathcal{I}\{V_m^\delta\}} = \mathcal{I}\left\{-Y_{dk}\frac{\partial V_{dk}}{\partial \mathcal{I}\{V_m^\delta\}}\right\}. \tag{F.61}$$

V_{dk} is given by

$$V_{dk} = \frac{1}{2}j\sum_{i=1}^{12}\left\{\sum_{l=k}^{n_h} V_{dil}\Psi^*_{i\,l-k} + \sum_{l=0}^{n_h}\left(V_{dil}\Psi^*_{i\,l+k}\right)^* - \sum_{l=0}^{n_h} V_{dil}\Psi_{ik-l}\right\}, \quad k > 0. \tag{F.62}$$

The only terms in this equation which are a function of V_m^δ are the twelve pre-convolved dc voltage phasors V_{dil}. There are three equations which define the twelve pre-convolved dc voltage phasors:

$$V_{d,normal_l} = V_l^+ - V_l^- - jwk(L^+ + L^-)I_{dl} \tag{F.63}$$

for a 'normal' conduction interval,

$$V_{d,commutation_l} = \frac{L_e V_l^b + L_b(V_l^e - jwkL_eI_{dl})}{L_e + L_b} - V_l^o - jkwL_oI_{dl} \tag{F.64}$$

for a commutation on the positive dc rail, and

$$V_{d,commutation_l} = V_l^o - jkwL_oI_{dl} - \frac{L_eV_l^b + L_b(V_l^e - jlwL_eI_{dl})}{L_e + L_b} \tag{F.65}$$

for a commutation on the negative rail. Differentiating these three equations with respect to V_m^δ gives 36 possible values for $\frac{\partial V_{dil}}{\partial V_m^\delta}$ according to the sample number i and the phase of δ. The required partial derivatives are summarized in table F.3 by reference to the partial derivatives of equations F.63, F.64, and F.65, where:

$$\begin{aligned} \frac{\partial V_{dil}}{\partial \mathcal{R}\{V_l^+\}} &= 1 \\ \frac{\partial V_{dil}}{\partial \mathcal{R}\{V_l^-\}} &= -1 \end{aligned} \tag{F.66}$$

for a 'normal' conduction interval,

$$\begin{aligned} \frac{\partial V_{dil}}{\partial \mathcal{R}\{V_l^e\}} &= \frac{L_b}{L_b + L_e} \\ \frac{\partial V_{dil}}{\partial \mathcal{R}\{V_l^b\}} &= \frac{L_e}{L_b + L_e} \\ \frac{\partial V_{dil}}{\partial \mathcal{R}\{V_l^o\}} &= -1 \end{aligned} \tag{F.67}$$

for a commutation on the positive dc rail, and

$$\begin{aligned} \frac{\partial V_{dil}}{\partial \mathcal{R}\{V_l^e\}} &= -\frac{L_b}{L_b + L_e} \\ \frac{\partial V_{dil}}{\partial \mathcal{R}\{V_l^b\}} &= -\frac{L_e}{L_b + L_e} \\ \frac{\partial V_{dil}}{\partial \mathcal{R}\{V_l^o\}} &= 1 \end{aligned} \tag{F.68}$$

for a commutation on the negative rail. The Cauchy Reimann equations can be used to give the partial derivative with respect to the imaginary part of the voltage variation as j times that listed above.

The partial derivatives in equations F.66, F.67, and F.68 are then substituted into

sample (i)	DC Voltage derivatives					
	b	e	o	+	-	eqn
1	A	C	B			F.67
2				A	B	F.66
3	C	B	A			F.68
4				A	C	F.66
5	B	A	C			F.67
6				B	C	F.66
7	A	C	B			F.68
8				B	A	F.66
9	C	B	A			F.67
10				C	A	F.66
11	B	A	C			F.68
12				C	B	F.66

Table F.3 Construction of dc voltage partial derivatives.

the partial derivatives of equation F.62, which are given below:

$$\frac{\partial V_{dk}}{\partial \mathcal{R}\{V_m^\delta\}} = \frac{1}{2} j \sum_{i=1}^{12} \left[\left(\frac{\partial V_{dim}}{\partial \mathcal{R}\{V_m^\delta\}} \Psi^*_{i\,m+k} \right)^* + \left\{ \begin{array}{ll} -\frac{\partial V_{dim}}{\partial \mathcal{R}\{V_m^\delta\}} \Psi_{ik-m} & m \leq k \\ \frac{\partial V_{dim}}{\partial \mathcal{R}\{V_m^\delta\}} \Psi^*_{i\,m-k} & m \geq k \end{array} \right] , k > 0, \tag{F.69}$$

$$\frac{\partial V_{dk}}{\partial \mathcal{I}\{V_m^\delta\}} = \frac{1}{2} j \sum_{i=1}^{12} \left[\left(\frac{\partial V_{dim}}{\partial \mathcal{I}\{V_m^\delta\}} \Psi^*_{i\,m+k} \right)^* + \left\{ \begin{array}{ll} -\frac{\partial V_{dim}}{\partial \mathcal{I}\{V_m^\delta\}} \Psi_{ik-m} & m \leq k \\ \frac{\partial V_{dim}}{\partial \mathcal{I}\{V_m^\delta\}} \Psi^*_{i\,m-k} & m \geq k \end{array} \right] , k > 0. \tag{F.70}$$

This completes the derivation of the partial derivative of dc current mismatch equation with respect to terminal voltage.

F.3.2 With Respect to dc Ripple Current Variation

Apart from being the most significant term in the dc current mismatch equation, the dc ripple affects the commutation currents, and also causes a voltage drop through the commutating reactance. These last two effects mean that the dc voltage is a function of the dc current ripple. It is therefore necessary to obtain partial derivatives of the dc voltage harmonics in a similar manner to that undertaken already for the derivative with

respect to terminal voltage. Differentiating the dc current mismatch equation gives:

$$\frac{\partial \mathcal{R}\{F_{Ik}\}}{\partial \mathcal{R}\{I_{dm}\}} = \mathcal{R}\left\{\begin{array}{ll} -Y_{dk}\frac{\partial V_{dk}}{\partial \mathcal{R}\{I_{dm}\}} & k \neq m \\ 1 - Y_{dk}\frac{\partial V_{dk}}{\partial \mathcal{R}\{I_{dm}\}} & k = m \end{array}\right., \tag{F.71}$$

$$\frac{\partial \mathcal{R}\{F_{Ik}\}}{\partial \mathcal{I}\{I_{dm}\}} = \mathcal{R}\left\{-Y_{dk}\frac{\partial V_{dk}}{\partial \mathcal{I}\{I_{dm}\}}\right\}, \tag{F.72}$$

$$\frac{\partial \mathcal{I}\{F_{Ik}\}}{\partial \mathcal{I}\{I_{dm}\}} = \mathcal{I}\left\{\begin{array}{ll} -Y_{dk}\frac{\partial V_{dk}}{\partial \mathcal{I}\{I_{dm}\}} & k \neq m \\ j - Y_{dk}\frac{\partial V_{dk}}{\partial \mathcal{I}\{I_{dm}\}} & k = m \end{array}\right., \tag{F.73}$$

$$\frac{\partial \mathcal{I}\{F_{Ik}\}}{\partial \mathcal{R}\{I_{dm}\}} = \mathcal{I}\left\{-Y_{dk}\frac{\partial V_{dk}}{\partial \mathcal{R}\{I_{dm}\}}\right\}. \tag{F.74}$$

Differentiating equation F.62 with respect to $\mathcal{R}\{I_{dm}\}$ yields

$$\frac{\partial V_{dk}}{\partial \mathcal{R}\{I_{dm}\}} = \frac{1}{2}j\sum_{i=1}^{12}\left[\left(\frac{\partial V_{dim}}{\partial \mathcal{R}\{I_{dm}\}}\Psi^*_{i\,m+k}\right)^* + \left\{\begin{array}{ll} -\frac{\partial V_{dim}}{\partial \mathcal{R}\{I_{dm}\}}\Psi_{ik-m} & m \leq k \\ \frac{\partial V_{dim}}{\partial \mathcal{R}\{I_{dm}\}}\Psi^*_{i\,m-k} & m \geq k \end{array}\right.\right], k > 0. \tag{F.75}$$

Similarly,

$$\frac{\partial V_{dk}}{\partial \mathcal{I}\{I_{dm}\}} = \frac{1}{2}j\sum_{i=1}^{12}\left[\left(\frac{\partial V_{dim}}{\partial \mathcal{I}\{I_{dm}\}}\Psi^*_{i\,m+k}\right)^* + \left\{\begin{array}{ll} -\frac{\partial V_{dim}}{\partial \mathcal{I}\{I_{dm}\}}\Psi_{ik-m} & m \leq k \\ \frac{\partial V_{dim}}{\partial \mathcal{I}\{I_{dm}\}}\Psi^*_{i\,m-k} & m \geq k \end{array}\right.\right], k > 0. \tag{F.76}$$

The partial derivatives $\frac{\partial V_{dim}}{\partial \mathcal{I}\{I_{dm}\}}$ are obtained from equations F.63, F.64, and F.65:

$$\frac{\partial V_{dim}}{\partial \mathcal{R}\{I_{dm}\}} = -jkw(L_+ + L_-) \tag{F.77}$$

during normal conduction, and

$$\frac{\partial V_{dim}}{\partial \mathcal{R}\{I_{dm}\}} = jkw\left[L_o + \frac{L_e L_b}{L_e + L_b}\right] \tag{F.78}$$

during any commutation. The imaginary partial derivatives are then obtained by the Cauchy Reimann equations. The correct phase subscripts can be obtained from Table F.3. This completes the linearized dependence of the dc mismatch upon dc ripple variation.

F.3.3 With Respect to end of Commutation Variation

The effect of variation in the end of commutation angle ϕ_h is limited solely to the sampling of relevant dc voltage sections. This is best explained with reference to the following equation for the dc voltage:

$$V_d = \frac{1}{2} j \sum_{i=1}^{12} V_{di} \otimes \Psi_i \,. \tag{F.79}$$

In this equation, only two of the twelve Ψ_i are functions of ϕ_h. Table F.4 shows that Ψ_{2h} and Ψ_{2h-1} are functions of ϕ_h. Equation F.62 can therefore be differentiated to yield:

$$\begin{aligned}\frac{\partial V_{dk}}{\partial \phi_h} = \frac{1}{2} j \Bigg\{ & \sum_{l=0}^{n_h} V_{d(2h-1)_l} \frac{\partial \Psi_{2hk-l}}{\partial \phi_h} - \sum_{l=k}^{n_h} V_{d(2h-1)_l} \left(\frac{\partial \Psi_{2hl-k}}{\partial \phi_h} \right)^* \\ & - \sum_{l=0}^{n_h} \left[V_{d(2h-1)_l} \left(\frac{\partial \Psi_{2hl-k}}{\partial \phi_h} \right)^* \right]^* - \sum_{l=0}^{n_h} V_{d(2h)_l} \frac{\partial \Psi_{2hk-l}}{\partial \phi_h} \\ & + \sum_{l=k}^{n_h} V_{d(2h)_l} \left(\frac{\partial \Psi_{2hl-k}}{\partial \phi_h} \right)^* + \sum_{l=0}^{n_h} \left[V_{d(2h)_l} \left(\frac{\partial \Psi_{2hl-k}}{\partial \phi_h} \right)^* \right]^* \Bigg\}\end{aligned} \tag{F.80}$$

sample (i)	a_i	b_i
1	θ_1	ϕ_1
2	ϕ_1	θ_2
3	θ_2	ϕ_2
4	ϕ_2	θ_3
5	θ_3	ϕ_3
6	ϕ_3	θ_4
7	θ_4	ϕ_4
8	ϕ_4	θ_5
9	θ_5	ϕ_5
10	ϕ_5	θ_6
11	θ_6	ϕ_6
12	ϕ_6	θ_1

Table F.4 Limits of convertor states for use in sampling functions.

Differentiating the dc ripple mismatch equation F.57 yields:

$$\frac{\partial \mathcal{R}\{F_{Ik}\}}{\partial \phi_h} = \mathcal{R}\left\{-Y_{dk}\frac{\partial V_{dk}}{\partial \phi_h}\right\}, \tag{F.81}$$

and

$$\frac{\partial \mathcal{I}\{F_{Ik}\}}{\partial \phi_h} = \mathcal{I}\left\{-Y_{dk}\frac{\partial V_{dk}}{\partial \phi_h}\right\}. \tag{F.82}$$

Substituting equation F.80 into F.81 and F.82 gives the required partial derivative of dc ripple mismatch with respect to end of commutation.

F.3.4 With Respect to Firing Instant Variation

The partial derivatives of dc ripple mismatch with respect to firing angle are obtained in an exactly similar manner. The result is:

$$\frac{\partial \mathcal{R}\{F_{Ik}\}}{\partial \theta_h} = \mathcal{R}\left\{-Y_{dk}\frac{\partial V_{dk}}{\partial \theta_h}\right\}, \tag{F.83}$$

and

$$\frac{\partial \mathcal{I}\{F_{Ik}\}}{\partial \theta_h} = \mathcal{I}\left\{-Y_{dk}\frac{\partial V_{dk}}{\partial \theta_h}\right\}., \tag{F.84}$$

where

$$\begin{aligned}\frac{\partial V_{dk}}{\partial \theta_h} = \frac{1}{2}j \Bigg\{ & \sum_{l=0}^{n_h} V_{d(2h-2)_l}\frac{\partial \Psi_{2hk-l}}{\partial \theta_h} - \sum_{l=k}^{n_h} V_{d(2h-2)_l}\left(\frac{\partial \Psi_{2hl-k}}{\partial \theta_h}\right)^* \\ & - \sum_{l=0}^{n_h}\left[V_{d(2h-2)_l}\left(\frac{\partial \Psi_{(2h-1)_{l-k}}}{\partial \theta_h}\right)^*\right]^* - \sum_{l=0}^{n_h} V_{d(2h-1)_l}\frac{\partial \Psi_{(2h-1)_{k-l}}}{\partial \theta_h} \\ & + \sum_{l=k}^{n_h} V_{d(2h-1)_l}\left(\frac{\partial \Psi_{(2h-1)_{l-k}}}{\partial \theta_h}\right)^* + \sum_{l=0}^{n_h}\left[V_{d(2h-1)_l}\left(\frac{\partial \Psi_{(2h-1)_{l-k}}}{\partial \theta_h}\right)^*\right]^* \Bigg\}\end{aligned} \tag{F.85}$$

F.4 END OF COMMUTATION MISMATCH EQUATION PARTIAL DERIVATIVES

The end of commutation mismatch is the current in the phase that is commutating off, at the end of the commutation. This current should be zero, and is given by:

$$F_{\phi_i} = \mathcal{I}\left\{ j(I_{d0} - D) + \sum_{k=1}^{n_h} F_{\phi ik} e^{jk\phi_i} \right\} = 0, \tag{F.86}$$

for a commutation on the positive rail, where

$$D = -\mathcal{I}\left\{ \sum_{k=1}^{n_h} I_{cik} e^{jk\theta_i} \right\} \tag{F.87}$$

$$F_{\phi ik} = I_{dk} - I_{cik} \tag{F.88}$$

$$I_{cik} = \frac{jkwL_e I_{dk} - V_k^{eb}}{jkwL_{eb}}. \tag{F.89}$$

The end of commutation mismatch equation is therefore a function of all the variables except the average delay angle α_0. A commutation on the negative rail is accounted for by substituting $-I_{dm}$ in the above equations for I_{dm}.

F.4.1 With Respect to ac Voltage Variation

Differentiating equation F.86 with respect to an arbitrary voltage phase and harmonic yields:

$$\frac{\partial F_{\phi_i}}{\partial \mathcal{R}\{V_m^\delta\}} = \mathcal{I}\left\{ -\frac{\partial D}{\partial \mathcal{R}\{V_m^\delta\}} - \frac{\partial I_{cim}}{\partial \mathcal{R}\{V_m^\delta\}} e^{jm\phi_i} \right\}, \tag{F.90}$$

and

$$\frac{\partial F_{\phi_i}}{\partial \mathcal{I}\{V_m^\delta\}} = \mathcal{R}\left\{ -\frac{\partial D}{\partial \mathcal{I}\{V_m^\delta\}} - \frac{\partial I_{cim}}{\partial \mathcal{I}\{V_m^\delta\}} e^{jm\phi_i} \right\}. \tag{F.91}$$

The partial derivatives in these equations are obtained from equations F.87 to F.89

as

$$\frac{\partial D}{\partial \mathcal{R}\{V_m^\delta\}} = \frac{1}{jmw(L_e+L_b)}e^{jk\theta_i}, \tag{F.92}$$

$$\frac{\partial I_{cim}}{\partial \mathcal{R}\{V_m^\delta\}} = \frac{-1}{jmw(L_e+L_b)}, \tag{F.93}$$

$$\frac{\partial D}{\partial \mathcal{I}\{V_m^\delta\}} = \frac{j}{jmw(L_e+L_b)}e^{jk\theta_i}, \tag{F.94}$$

$$\frac{\partial I_{cim}}{\partial \mathcal{I}\{V_m^\delta\}} = \frac{-j}{jmw(L_e+L_b)}, \tag{F.95}$$

It is assumed in the above analysis that V_m^δ corresponds to a phase ending conduction. Multiplying by -1 gives the required partial derivative for the case that V_m^δ corresponds to a phase beginning conduction.

F.4.2 With Respect to dc Ripple Current Variation

The analysis is similar to that for ac phase voltage variation. Differentiating equation F.86 yields:

$$\frac{\partial F_{\phi_i}}{\partial \mathcal{R}\{I_{dm}\}} = \mathcal{I}\left\{-\frac{\partial D}{\partial \mathcal{R}\{I_{dm}\}} - \frac{\partial I_{cim}}{\partial \mathcal{R}\{I_{dm}\}}e^{jm\phi_i}\right\}, \tag{F.96}$$

and

$$\frac{\partial F_{\phi_i}}{\partial \mathcal{I}\{I_{dm}\}} = \mathcal{R}\left\{-\frac{\partial D}{\partial \mathcal{I}\{I_{dm}\}} - \frac{\partial I_{cim}}{\partial \mathcal{I}\{I_{dm}\}}e^{jm\phi_i}\right\}. \tag{F.97}$$

The partial derivatives in these equations are obtained from equations F.87 to F.89 as

$$\frac{\partial D}{\partial \mathcal{R}\{I_{dm}\}} = \frac{L_e}{L_e+L_b}e^{jk\theta_i}, \tag{F.98}$$

$$\frac{\partial I_{cim}}{\partial \mathcal{R}\{I_{dm}\}} = \frac{-L_e}{L_e+L_b}, \tag{F.99}$$

$$\frac{\partial D}{\partial \mathcal{I}\{I_{dm}\}} = \frac{jL_e}{L_e+L_b}e^{jk\theta_i}, \tag{F.100}$$

$$\frac{\partial I_{cim}}{\partial \mathcal{I}\{I_{dm}\}} = \frac{-jL_e}{L_e+L_b}. \tag{F.101}$$

This analysis assumes that the commutation is on the positive rail. A similar analysis holds for a commutation on the negative rail, but with $-I_{dm}$ substituted into equation F.86.

F.4.3 With Respect to end of Commutation Variation

This partial derivative gives the effect on the 'residual' commutating-off current at the end of the commutation, if the end of commutation is moved. It is obtained simply by differentiating equation F.86 with respect to ϕ_i to give

$$\frac{\partial F_{\phi i}}{\partial \phi_i} = \mathcal{I}\left\{\sum_{k=1}^{n_h} jkF_{\phi ik}e^{jk\phi_i}\right\}. \tag{F.102}$$

F.4.4 With Respect to Firing Instant Variation

The dc offset to the commutation, D, is a function of the firing instant, and so the only effect of θ_i on F_{ϕ_i} is through D. Differentiating the expression for D, equation F.87, gives the required partial derivative.

$$\frac{\partial F_{\phi i}}{\partial \theta_i} = \mathcal{I}\left\{-\sum_{k=1}^{n_h} jkI_{ck}e^{jk\theta_i}\right\}. \tag{F.103}$$

F.5 FIRING INSTANT MISMATCH EQUATION PARTIAL DERIVATIVES

For the implemented constant current controller, the firing instant mismatch is not a function of the ac terminal voltage. This is because the firing order is obtained solely from monitoring the dc current. This also means that the firing mismatch is not a function of the end of commutation instants. The firing instant mismatch is a function only of the dc ripple, the firing angle, and the average firing order. The firing mismatch equation is:

$$F_{\theta i} = \mathcal{I}\left\{ j(\alpha_0 + \zeta_i - \theta_i) + \sum_{k=1}^{n_k} \alpha_{ik} e^{jk\theta_i} \right\} = 0, \tag{F.104}$$

where

$$\alpha_{ik} = \frac{G}{1 + jkwT}\left(P + \frac{1}{jkwT_I}\right) I_{dk}. \tag{F.105}$$

The partial derivatives are readily obtained as:

$$\frac{\partial F_{\theta i}}{\partial \alpha_0} = 1, \tag{F.106}$$

$$\frac{\partial F_{\theta i}}{\partial \theta_i} = \mathcal{I}\left\{ -j + \sum_{k=1}^{n_h} jk\theta_i \alpha_{ik} e^{jk\theta_i} \right\}, \tag{F.107}$$

$$\frac{\partial F_{\theta i}}{\partial \mathcal{R}\{I_{dk}\}} = \mathcal{I}\left\{ \sum_{k=1}^{n_h} \frac{\partial \alpha_{ik}}{\partial I_{dk}} e^{jk\theta_i} \right\}, \tag{F.108}$$

$$\frac{\partial F_{\theta i}}{\partial \mathcal{I}\{I_{dk}\}} = \mathcal{R}\left\{ \sum_{k=1}^{n_h} \frac{\partial \alpha_{ik}}{\partial I_{dk}} e^{jk\theta_i} \right\}, \tag{F.109}$$

where

$$\frac{\partial \alpha_{ik}}{\partial I_{dk}} = \frac{G}{1 + jkwT}\left(P + \frac{1}{jkwT_I}\right). \tag{F.110}$$

F.6 AVERAGE DELAY ANGLE PARTIAL DERIVATIVES

The average delay angle, α_0, is obtained by requiring that the average dc voltage, when applied to the dc system, should result in the current order. Thus α_0 is a control variable, required for the case of constant current control. The mismatch equation is:

$$F_{\alpha 0} = \mathcal{I}\left\{I_{dk} - (V_{d0} - V_{dc})Y_{d0}\right\}, \tag{F.111}$$

where V_{dc} represents a dc voltage source, and

$$V_{d0} = \frac{1}{2} j \sum_{i=1}^{12} \left\{ \sum_{l=0}^{n_h} V_{dil} \Psi_{il}^{*} \right\}. \tag{F.112}$$

Thus $F_{\alpha 0}$ is a function of all the convertor variables, with the exception of α_0 itself. Analysis of the partial derivatives of equation F.111 is similar to that for the partial derivatives of the dc ripple mismatch.

F.6.1 With Respect to ac Voltage Variation

Differentiating the mismatch equation F.111 with respect to an arbitrary phase and harmonic of ac voltage yields

$$\frac{\partial F_{\alpha 0}}{\partial \mathcal{R}\{V_m^{\delta}\}} = \mathcal{I}\left\{ -Y_{d0} \frac{\partial V_{d0}}{\partial \mathcal{R}\{V_m^{\delta}\}} \right\}, \tag{F.113}$$

$$\frac{\partial F_{\alpha 0}}{\partial \mathcal{I}\{V_m^{\delta}\}} = \mathcal{I}\left\{ -Y_{d0} \frac{\partial V_{d0}}{\partial \mathcal{I}\{V_m^{\delta}\}} \right\}. \tag{F.114}$$

Differentiating equation F.112 yields

$$\frac{\partial V_{d0}}{\partial \mathcal{R}\{V_m^{\delta}\}} = \frac{1}{2} j \sum_{i=1}^{12} \left(\frac{\partial V_{dim}}{\partial \mathcal{R}\{V_m^{\delta}\}} \Psi_{im}^{*} \right), \tag{F.115}$$

and

$$\frac{\partial V_{d0}}{\partial \mathcal{I}\{V_m^{\delta}\}} = \frac{1}{2} j \sum_{i=1}^{12} \left(\frac{\partial V_{dim}}{\partial \mathcal{I}\{V_m^{\delta}\}} \Psi_{im}^{*} \right), \tag{F.116}$$

which when substituted back into equations F.113 and F.114 give the required partial derivatives. The remaining partial derivatives, $\frac{\partial V_{dim}}{\partial \mathcal{R}\{V_m^{\delta}\}}$ etc, have already been obtained in equations F.63, F.64, and F.65, and by reference to Table F.3.

F.6.2 With Respect to dc Ripple Current Variation

Variation in the dc ripple affects the dc voltage samples in a similar manner to that of a variation in the terminal voltage above. Differentiating the mismatch equation F.111 with respect to an arbitrary phase and harmonic of dc current ripple yields

$$\frac{\partial F_{\alpha 0}}{\partial \mathcal{R}\{I_{dm}\}} = \mathcal{I}\left\{-Y_{d0}\frac{\partial V_{d0}}{\partial \mathcal{R}\{I_{dm}\}}\right\}, \tag{F.117}$$

$$\frac{\partial F_{\alpha 0}}{\partial \mathcal{I}\{I_{dm}\}} = \mathcal{I}\left\{-Y_{d0}\frac{\partial V_{d0}}{\partial \mathcal{I}\{I_{dm}\}}\right\}. \tag{F.118}$$

Differentiating equation F.112 yields

$$\frac{\partial V_{d0}}{\partial \mathcal{R}\{I_{dm}\}} = \frac{1}{2}j\sum_{i=1}^{12}\left(\frac{\partial V_{dim}}{\partial \mathcal{R}\{I_{dm}\}}\Psi^*_{i\,m}\right), \tag{F.119}$$

and

$$\frac{\partial V_{d0}}{\partial \mathcal{I}\{I_{dm}\}} = \frac{1}{2}j\sum_{i=1}^{12}\left(\frac{\partial V_{dim}}{\partial \mathcal{I}\{I_{dm}\}}\Psi^*_{i\,m}\right), \tag{F.120}$$

which when substituted back into equations F.117 and F.118 give the required partial derivatives. The remaining partial derivatives, $\frac{\partial V_{dim}}{\partial \mathcal{R}\{I_{dm}\}}$ etc, have already been obtained in equations F.77 and F.78.

F.6.3 With Respect to end of Commutation Variation

The effect of a variation in the end of commutation is to modify the sampling of the dc voltage sections in equation F.112. Differentiating equation F.111 with respect to ϕ_h yields

$$\frac{\partial F_{\alpha 0}}{\partial \phi_h} = \mathcal{I}\left\{-Y_{d0}\frac{\partial V_{d0}}{\partial \phi_h}\right\}. \tag{F.121}$$

This requires the partial derivative $\frac{\partial V_{d0}}{\partial \phi_h}$. Differentiating equation F.112 yields

$$\frac{\partial V_{d0}}{\partial \phi_h} = \frac{1}{2}j\left\{\sum_{l=1}^{n_h} V_{d(2h-1)_l}\frac{\partial \Psi^*_{(2h-1)_l}}{\partial \phi_h} + \sum_{l=1}^{n_h} V_{d(2h)_l}\frac{\partial \Psi^*_{(2h)_l}}{\partial \phi_h}\right\}, \tag{F.122}$$

where use has been made of Table F.4 to determine the only two sampling functions that are affected by ϕ_h.

F.6.4 With Respect to Firing Instant Variation

The effect of a change in the firing angle on the average delay angle mismatch equation is similar to that for a change in the end of commutation angle. The sampling of the dc voltage sections is modified, and this changes the average dc voltage. The analysis carried out above for the end of commutation variation is also valid in this case, with only the two affected sampling functions, as determined from Table F.4 being different. The result is that

$$\frac{\partial F_{\alpha 0}}{\partial \theta_h} = \mathcal{I}\left\{-Y_{d0}\frac{\partial V_{d0}}{\partial \theta_h}\right\}, \tag{F.123}$$

where

$$\frac{\partial V_{d0}}{\partial \theta_h} = \frac{1}{2}j\left\{\sum_{l=1}^{n_h} V_{d(2h-2)_l}\frac{\partial \Psi^*_{(2h-2)_l}}{\partial \theta_h} + \sum_{l=1}^{n_h} V_{d(2h-1)_l}\frac{\partial \Psi^*_{(2h-1)_l}}{\partial \theta_h}\right\}. \tag{F.124}$$

This completes the derivation of the partial derivatives required for the Jacobian matrix, as the average delay angle mismatch equation is not a function of the average delay angle.

Appendix G

PUBLISHED PAPERS

N.Q. Dinh and J. Arrillaga, Direct Connections of generators and HVDC converters, *Proc. Third New Zealand Conference of Postgraduate Students in Engineering and Technology*, July, 1996, New Zealand, pp. 313-18.

N.Q. Dinh and J. Arrillaga, Generator Modelling in the Harmonic Domain, *Proc. International Power Engineering Conference*, May, 1997, Singapore, pp. 804-08.

N.Q. Dinh, J. Arrillaga, A.R. Wood, S. Chen, W. Enright, B.C. Smith and Z. Du, Harmonic Evaluation of Benmore Converter Station When Operated as a Group Connected Unit, *IEEE Transactions on Power Delivery*, Vol 12, No 4, Oct, 1997, pp. 1730-35.

N.Q. Dinh, J. Arrillaga and B.C. Smith, A Steady-state model of direct connected generator-HVDC convertor units in the Harmonic Domain, accepted for publication in the Proc. IEE Generation, Transmission and Distribution.

REFERENCES

11/14-09, C.J.W.G. (1993), 'Hvdc unit connected generators', *ELECTRA*, Vol. 149, August.

11/14-09, C.J.W.G. (1997), *Guide for Preliminary Design and specification of Hydro Stations with HVDC Unit Connected generators.*

36.05.02/14.03.03, C.J.T.F. (1996), 'Ac system modelling for ac filter design - an overview of impedance modelling', *ELECTRA*, No. 164, February, pp. 133–151.

ARRILLAGA, J. (1983), *High Voltage Direct Current Transmission*, Vol. 6, Peter Peregrinus Ltd., London, UK.

ARRILLAGA, J., WATSON, N., EGGLESTON, J. AND CALLAGHAN, C. (1987), 'Comparison of steady state and dynamic models for the calculation of ac/dc system harmonics', *IEE Proceedings Pt. C*, Vol. 134, No. 1, January, pp. 31–37.

ARRILLAGA, J., YONGE, L., CRIMP, C. AND VILLABLANCA, M. (1993a), 'Harmonic elimination by dc ripple reinjection in generator-converter units operating at variable speeds', *IEE Proceedings-C*, Vol. 140, No. 1, August, pp. 57–64.

ARRILLAGA, J., CAMACHO, J., MACDONALD, S. AND ARNOLD, C. (1993b), 'Operating characteristics of unit and group connected generator-hvdc converter schemes', *IEE Proceedings-C*, Vol. 140, No. 6, November, pp. 503–8.

BLONDEL, A. (1923), 'The two-reaction method for study of oscillatory phenomena in coupled alternators', *Revue generale de I'electricite*, Vol. 13, February, pp. 235–51.

BROYDEN, C. (1965), *Mathematics of Computation*, Vol. 19. pp. 557-93.

BURDEN, R.L., FAIRES, J.D. AND REYNOLDS, A. (1981), *Numerical Analysis*, PWS Publishers, Boston, Massachusetts, second ed.

CALLAGHAN, C. AND ARRILLAGA, J. (1990), 'Convergence criteria for iterative harmonic analysis and its application to static convertors', *ICHPS IV*, October, pp. 38–43.

CALVERLEY, T.E., OTTAWAY, C.H. AND TUFNELL, D.H.A. (1973), 'Concept of a unit generator converter transmission system', *IEE Conference on High Voltage dc and ac Transmission.*

CHEN, S., WOOD, A.R. AND ARRILLAGA, J. (1996), 'Hvdc convertor core saturation instability; a frequency domain analysis', *IEE Proc. Pt C*, Vol. 143, No. 1, January, pp. 75–81.

CHEUKSUN, W., MOHAN, N., WRIGHT, S. AND MORTENSEN, X. (1989), 'Feasibility study of ac and dc side active filters for hvdc converter terminals', *IEEE Trans. on Power Delivery*, Vol. 4, pp. 2067–75.

CLARKE, E. (1950), *Circuit Analysis of AC Power Systems*, Vol. 2, John Wiley & Sons, London.

(1996), *Continuous Harmonic Analysis in Real Time: Technical Reference*, CHART Instrument Limited, New Zealand.

DOHERTY, R. AND NICKLE, C. (1926), 'Synchronous machines 1: An extension of blondel's two-reaction theory', *AIEE Transactions*, Vol. 45, pp. 927–42.

DOMMEL, H. (1969), 'Digital computer solution of electromagnetic transients in single and multiphase networks', *IEEE Trans. on Power Apparatus and Systems*, Vol. PAS-88, No. 4, April, pp. 388–399.

DOMMEL, H., CHIU, B. AND MEYER, W. (1980), 'Analysing transients in a.c./d.c. systems with the bpa electromagnetic transients program', *IEEE Conference Publication 205, on Thyristor and Variable Static Equipment for a.c. and d.c. Transmission*, pp. 109 – 113.

EGGLESTON, J. (1985), *Harmonic Modelling of Transmission Systems Containing Synchronous Machines and Static Convertors*, PhD thesis, University of Canterbury, New Zealand.

EGGLESTON, J.F., ARRILLAGA, J. AND SEMLYEN, A. (1988), 'Analysis of the harmonic distortion resulting from the interaction between synchronous machine and hvdc convertors', *IEEE Trans. on Power Delivery*, Vol. 3, No. 1, January, pp. 325–332.

GERALD, C. AND WHEATLY, P.O. (1985), *Applied numerical analysis*, Addison-Wesley, third ed.

GOLE, A., FERNANDO, I., IRWIN, G. AND NAYAK, O. (1997), 'Modelling of power electronic apparatus: Additional interpolation issues', *International Conference on Power Systems Transients Proceedings*, June, pp. 23–28.

HARLEY, R.G., LIMEBEER, D.J.N. AND CHIRRICOZZI, E. (1980), 'Comparative study of saturation methods in synchronous machine models', *IEE Proc., Pt. B*, Vol. 127, No. 1, January, pp. 1–7.

HWANG, H. (1969), 'Unbalanced operation of three-phase machines with damper circuits', *IEEE Trans. on Power Apparatus and Systems*, Vol. PAS-88, No. 11, November, pp. 1585–93.

KILGORE, L. (1935), 'Effects of saturation on machine reactances', *AIEE Trans.*, Vol. 54, May, pp. 545–50. Disc., v.56, 903-4, July, 1937.

KIMBARK, E.W. (1968), *Power system stability: Synchronous machines*, Dover Publications, Inc., New York, New York, NY, USA.

KIMBARK, E.W. (1971), *Direct Current Transmission*, Vol. 1, John Wiley and Sons, Inc.

KRISHNAYYA, P. (1973), 'Stresses on generators and transformers of block and double-block connections proposed for hvdc power station infeed.', *IEE conf. on 'High voltage dc and/or ac power transmission', Publication no. 107*, pp. 279–286.

LARSON, E., BAKER, D. AND MACIVER, J. (1989), 'Low order harmonic interaction on ac/dc systems', *IEEE Transactions on Power Delivery*, Vol. 4, No. 1, January, pp. 493–501.

LEE, C. (1961), 'Saturation harmonics of polyphase induction machines', *AIEE Trans.*, Vol. Part III, No. 80, October, pp. 597–603.

LISBOA, M.L.V. (1996), *Three-phase three-limb transformer models in the Harmonic Domain*, PhD thesis, University of Canterbury, New Zealand.

MACDONALD, S., ENRIGHT, W., ARRILLAGA, J. AND O'BRIEN, M. (1995), 'Harmonic measurements from a group connected generator hvdc converter scheme', *IEEE Transactions on Power Delivery*, Vol. 10, No. 4, October, pp. 1937–43.

MCPHERSON, G. AND LARAMORE, R.D. (1990), *An Introduction to Electrical Machines and Transformers*, Wiley.

MEDINA, A. AND ARRILLAGA, J. (1994), 'Analysis of transformer-generator interaction in the harmonic domain', *IEE Proc.-Gener. Transm. Distrib.*, Vol. 141, No. 1, January, pp. 38–46.

NAIDU, M. AND MATHUR, R. (1989), 'Evaluation of unit connected, variable speed, hydropower station for hvdc power transmission', *IEEE Transactions on Power Systems*, Vol. 4, No. 2, May, pp. 668–676.

NARAIN, H.G. (1996), 'High-voltage dc transmission: A power electronics workhorse', *IEEE Spectrum*, April, pp. 63–72.

PARK, R. (1929), 'Two-reaction theory of synchronous machines-p.1, generalized method of analysis', *AIEE Trans.*, Vol. 48, July, pp. 716–30.

PRESS, W., TEUKOLSKY, S., VETTERLING, W. AND FLANNERY, B. (1992), *Numerical Recipes in FORTRAN*, Cambridge University Press, New York, New York, second ed.

REEVE, J. AND BARON, J. (1971), 'Harmonic interaction between hvdc convertors and ac power systems', *IEEE Transactions on Power Apparatus and Systems*, Vol. 90, No. 6, pp. 2785–2793.

SANKAR, S. (1991), *Dynamic Simulation of AC/DC systems with reference to convertor control and unit connection*, PhD thesis, University of Canterbury, New Zealand.

SAY, M.G. (1983), *Alternating Current Machine*, Longman Scientific & Technical, UK, fifth ed.

SEMLYEN, A., ACHA, E. AND ARRILLAGA, J. (1988), 'Newton-type algorithms for the harmonic phasor analysis of non-linear power circuits in periodical steady state with special reference to magnetic non-linearities', *IEEE Trans. on Power Delivery*, Vol. 3, No. 3, July, pp. 1090–1097.

SMITH, B.C., WATSON, N.R., WOOD, A.R. AND ARRILLAGA, J. (1995), 'Steady state model of the ac/dc convertor in the harmonic domain', *IEEE Proc.-Gener. Transm. Distrib.*, Vol. 142, No. 2, March, pp. 109–118.

SMITH, B.C., WATSON, N.R., WOOD, A.R. AND ARRILLAGA, J. (1996), 'Newton solution for the steady-state interation of ac/dc systems', *IEEE Proc.-Gener. Transm. Distrib.*, Vol. 143, No. 2, March, pp. 200–210.

UHLMAN, E. (1975), *Power Transmission by Direct Current*, Springer-Verlag.

VALCARCEL, M. AND MAYORDOMO, J. (1993), 'Harmonic power flow for unbalanced systems', *IEEE PES winter meeting 93 WM 061-2 PWRD.*

WOOD, A.R. AND ARRILLAGA, J. (1995), 'Hvdc convertor waveform distortion - a frequency domain analysis', *IEE proceedings Pt C*, Vol. 142, No. 1, January, pp. 88–96.

WOODFORD, D., GOLE, A. AND MENZIES, R. (1983), 'Digital simulation of dc links and ac machines', *IEEE Trans. on Power Apparatus and Systems*, Vol. PAS-102, No. 6, June, pp. 1616–1623.

XIA, D. AND HEYDT, G. (1982), 'Harmonic power flow studies, part i and ii', *IEEE Trans on Power Apparatus and Systems*, Vol. PAS 101, No. 6, pp. 1257–70.

XU, W.W., MARTI, J.R. AND DOMMEL, H.W. (1990), 'Multiphase harmonic load flow solution technique', *IEEE PES winter meeting 90WM 098-4 PWRS.*

XU, W.W., DOMMEL, H.W. AND MARTI, J.R. (1991), 'A synchronous machine model for three-phase harmonic analysis and emtp initialization', *IEEE Trans. on Power Systems*, Vol. 6, No. 4, November, pp. 1530–1538.

XU, W.W., DRAKOS, J.E., MANSOUR, Y. AND CHANG, A. (1994), 'A three-phase converter model for harmonic analysis of hvdc systems', *IEEE Trans. on Power Delivery*, Vol. 9, No. 3, July, pp. 1724–1730.

YACAMINI, R. AND DE OLIVEIRA, J.C. (1980), 'Harmonics in multiple convertor systems: a generalised approach.', *IEE Proceedings Pt.B*, Vol. 127, No. 2, March, pp. 96–106.

YACAMINI, R. AND DE OLIVEIRA, J.C. (1986), 'Comprehensive calculation of convertor harmonics with system impedances and control representation', *IEE Proceedings Pt. B*, Vol. 133, No. 2, March, pp. 95–102.

ZAGRADISNIK, I. AND HRIBERNIK, B. (1988), 'Influence of anisotropy of magnetic material on the saturation harmonics in the three-phase induction motor', *IEEE Trans. on Magetics*, Vol. 24, No. 1, January, pp. 491–494.

ZHANG, W., ASPLUND, G., ABERG, A., JONSSON, U. AND LOOF, O. (1993), 'Active dc filter for hvdc system - a test installation in the konti-skan dc link at lindome converter station', *IEEE Trans on Power Delivery*, Vol. 8, No. 3, July.

ZLATEV, Z. (1991), *Computational Methods for General Sparse Matrices*, Kluwer Academic Publishers, Netherlands.

ZOLLENKOPF, K. (1970), 'Bi-factorisation basic computational algorithm and programming techniques', *Conference on large sets of sparse linear equations.*